Role of Electrotonic Coupling in the Olivocerebellar System

Ruben Simon van der Giessen

Role of Electrotonic Coupling in the Olivocerebellar System

De rol van electrotone koppeling in het olivocerebellaire systeem

Proefschrift

ter verkrijging van de graad van doctor aan de
Erasmus Universiteit Rotterdam
op gezag van de Rector Magnificus
Prof.dr. S.W.J.Lamberts
en volgens besluit van het College voor Promoties.

De openbare verdediging zal plaatsvinden op
woensdag 5 december 2007 om 13.45 uur

door

Ruben Simon van der Giessen

geboren te Hendrik Ido Ambacht.

ERASMUS UNIVERSITEIT ROTTERDAM

Promotiecomissie

Promotor:	Prof.dr. C.I. de Zeeuw
Overige leden:	Dr. C.R.W. Hansel
	Dr. J.C. Holstege
	Dr. T.J.H. Ruigrok
Copromotor:	Dr. M.T.J. de Jeu

Voor Abraham Wit

Disce ut semper victurus
Vive ut cras moriturus

TABLE OF CONTENTS

Chapter 1

Chapter 2

Expression and distribution of connexins in the Olivocerebellar system

Chapter 3

Consequences of a lack of Connexin36 on olivary neurons at the cellular electrophysiological level

Chapter 4

Consequences of a lack of Connexin36 on olivary neurons at the systems level

Chapter 5

CHAPTER 1

GENERAL INTRODUCTION

1.1 GENERAL INTRODUCTION

1.1.1 Motor control and the olivocerebellar system

Motor behavior is the active output that regulates our interaction with the environment. This motor behavior is commanded by primary motor neurons in the motor cortex that send signals to muscles via lower motoneurons in the brainstem and spinal cord. Besides brain areas that directly command voluntary muscle activity, parallel systems like the cerebellum and basal ganglia modify the activity of the upper motor neurons and thus coordinate motor behavior (Figure 1A). Although the cerebellum and basal ganglia appear to influence the same cortical areas, they project to the cortex via different parts of the thalamus and have different functions.
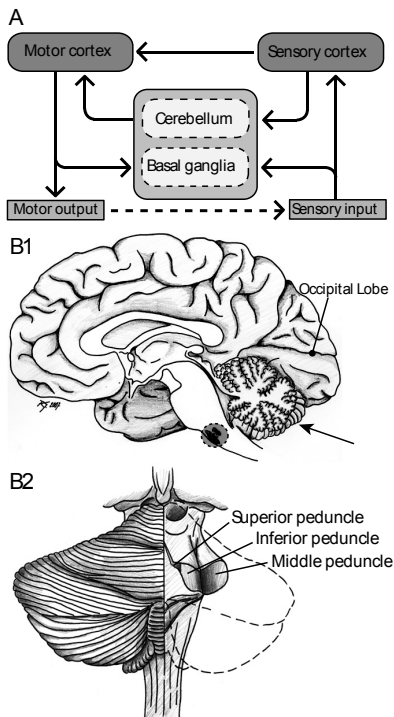
Figure 1. General features of the cerebellum.

A. A schematic diagram shows the parallel arrangement of the cerebellum and basal ganglia with regard to the sensory and motor cortex. Both cerebellum and basal ganglia receive sensory input and motor output which are used to give information that adjusts the motor output. **B1.** A sagittal view of a human brain. The olivocerebellar system is represented by the cerebellum and the inferior olive. The cerebellum is located beneath the occipital lobe (the arrow indicates the cerebellum), The inferior olive is located in the ventral part of the brainstem (indicated by the dashed circle). **B2.** Dorsal view of the cerebellum. The dashed area shows connections of the cerebellum that are normally covered by the cerebellum itself. The cerebellar peduncles consists of the superior, inferior and middle peduncle containing efferent and afferent pathways.

Furthermore, the output of the cerebellum has an excitatory effect whereas that of the basal ganglia has an inhibitory effect upon upper motor neurons (Jueptner and Weiller, 1998). The cerebellum is linked to the motor cortex, which relays its information to muscles that give rise to motor performance. It also receives peripheral sensory input and information from the sensory cortex. The cerebellum integrates these two pathways and its output is directed to the motor cortex (Figure 1A).

The cerebellum therefore receives constant feedback about position and proprioception during movements. Because of this parallel arrangement, dysfunctions of the cerebellum do not result in paralysis or loss of muscle strength but rather in disorders of fine movement, equilibrium, coordination and posture. Furthermore, cerebellar lesions can also abolish motor learning (Thach et al., 1992). Although the inferior olive represents a part of the olivocerebellar system, it provides major sensory input to the cerebellum. Some diseases have even been exclusively ascribed to the inferior olive. In diseases like essential tremor, palatal myoclonus and olivopontocerebellar atrophy (OPCA) the inferior olive may play a key role (Deuschl and Elble, 2000; Haller et al., 2006; Nitschke et al., 2001; Welsh et al., 1998; Wenning et al., 1996). Since the cerebellum plays a main role as a comparator in the integration of sensory information and motor output, it is important to understand how the olivocerebellar system does accomplish this complex task.

1.2 Anatomy and physiology of the olivocerebellar system

1.2.1 Macroscopic organization of the olivocerebellar system

The cerebellum (=little brain (Lat.)) is located in the posterior cranial fossa under the occipital part of the cerebrum (Figure 1B1). It is connected to the dorsal part of the brain stem by three pairs of tracts. These tracts contain major pathways from and to the cerebellum (Figure 1B2). Briefly, the superior cerebellar peduncle (or brachium conjunctivum) contains projections from the cerebellar nuclei to several areas (i.e. inferior olive, red nucleus), the middle cerebellar peduncle (or brachium pontis) contains axons from the pontine nuclei projecting to the cerebellar cortex and the inferior cerebellar peduncle (or restiform body); which forms the major input from the brainstem to the cerebellum (containing olivo-cerebellar fibers).

Although the cerebellum comprises only ten percent of the total volume of the brain, it contains around 70 percent of all neurons (Herculano-Houzel and Lent, 2005; Le Strange et al., 2004). This high number of neurons is achieved by the presence of many convolutions called folia (=leaves (Lat.)) at the surface of the cerebellum. The basic cerebellar circuit is quite constant throughout the cerebellum and is organized in functional modules (Figure 2A, left panel). These modules are composed of one or more parasagittally arranged bands of Purkinje cells that project to a specific part of the cerebellar nuclei.

These cerebellar nuclei project to an area of the contralateral inferior olive.

Climbing fibers that originate from this contralateral inferior olivary subnucleus projects back to same Purkinje cells and cerebellar nuclei, thereby creating a cerebellar loop (Figure 2A, right panel). These olivo-cortico-nuclear modules have been suggested to represent functional cerebellar units (Garwicz, 2000) and each module is involved in a specific task.
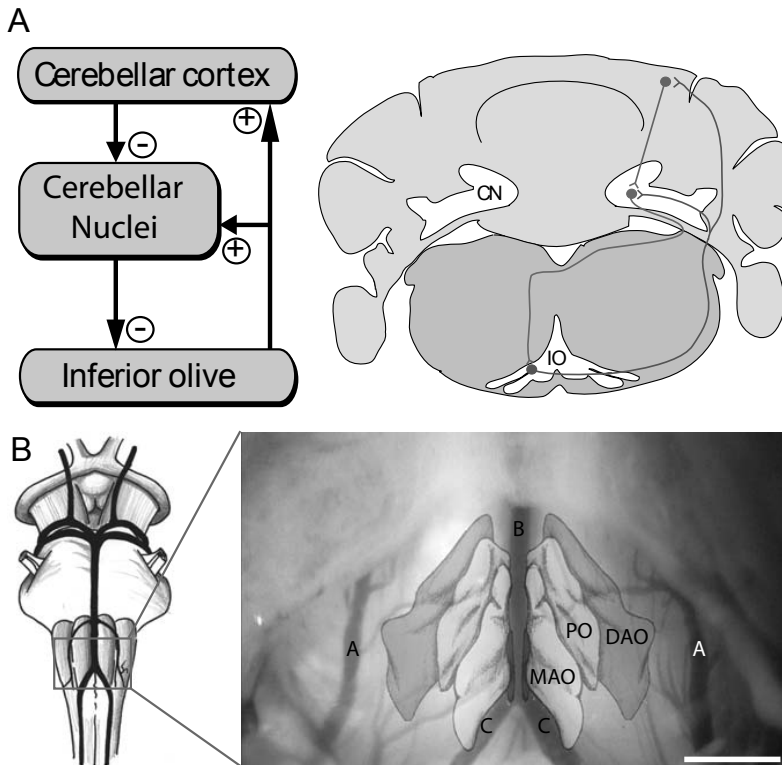
Figure 2. Anatomy of the cerebellar module and the inferior olive in detail.

A. A simplified scheme of a cerebellar module (left panel). Notice the output of the inferior olive is excitatory and the output of both cerebellar cortex and cerebellar nucleus are inhibitory. A coronal brain section (right panel) shows the climbing fiber projection from the inferior olive that travels to the contralateral side and gives off collaterals while it projects to the Purkinje cells in the cerebellar cortex. The Purkinje cell projects to the cerebellar nuclei neuron that receives the same climbing fiber projection. Furthermore, the olivary neuron receives input from the same cerebellar nuclei neuron to which its climbing fiber is projected. This structural organization of the olivocerebellar system common is known as the cerebellar module. **B.** Ventral view of the brainstem showing the main artery system. A higher magnification shows the brainstem after a ventral approach surgery and tracheotomy. The inferior olive is depicted in the photograph in order to show its position in the ventral brainstem. A, Posterior Inferior Cerebellar Artery (PICA); B, Basal artery; C, Vertebral arteries; MAO, Medial accessory olive; PO, Principal olive; DAO, Dorsal accessory olive. Scale bar, 1 mm.

The uniform structure of the olivocerebellar system, suggests that the basic neural computation performed is similar in the entire cerebellum for movement functions as well as autonomic functions and some studies even suggest cognitive functions (Thach, 1997).

1.2.2 The Inferior olive

The inferior olivary complex is located in the ventral part of the brainstem and consists of different subnuclei. It can be divided into three major subdivisions: the principal olive and two accessory olives (dorsal and medial; see Figure 2B). Only the minority of olivary neurons are interneurons (<0.1%) and some studies have indeed reported a low density of GABA-immunoreactive neurons (Walberg and Ottersen, 1989). Olivary neurons have an oval shaped cell body with a diameter of 15-20 µm, a distinctive nucleolus and give rise to a single axon. Each axon ramifies into several climbing fibers. An olivary neuron gives rise to only one climbing fiber which innervates about ten Purkinje cells (Sugihara, 2005). Based on morphology, two types of olivary neurons can be distinguished: Type I neurons have sparsely branched, spiny dendrites radiating away from the soma and this creates a large dendritic range. This type is only found in the medial accessory olive. The main type of neuron has a highly branched dendritic arbor. These dendrites make loops as they tend to circle back toward the soma. This category of olivary neurons were classified as Type II. This type can be found in the principle olive, dorsal accessory olive and medial accessory olive (Scheibel and Scheibel, 1955). Foster and Peterson in 1986 even further subdivided this form in Type IIa as being a transitional form and Type IIb as the tightly branched form. The dendrites of every olivary neuron are confined to the inferior olive complex and neurons at the edge of the nucleus are especially affected by this restriction (Foster & Peterson, 1986).

Electrical communication among olivary neurons was first suggested in 1955 by Scheibel and Scheibel. Using the well-known technique of Golgi, they described "a relatively small area available on neuron somata for terminals and their apparent scarcity on the more peripheral portions of the dendritic tree". Through this observation they suggested the existence of "ephaptic" action (Scheibel and Scheibel, 1955). In 1974 electrotonic junctions were first described in the inferior olive with use of electron microscopy together with electrophysiological measurements (Llinás et al., 1974; Sotelo et al., 1974). More recently, other studies showed that the density of gap junctions in the inferior olive is one of the highest in all brain areas and that it is the main pathway of direct communication between these neurons (Condorelli et al., 2000; De Zeeuw et al., 2003; De Zeeuw et al., 1995).
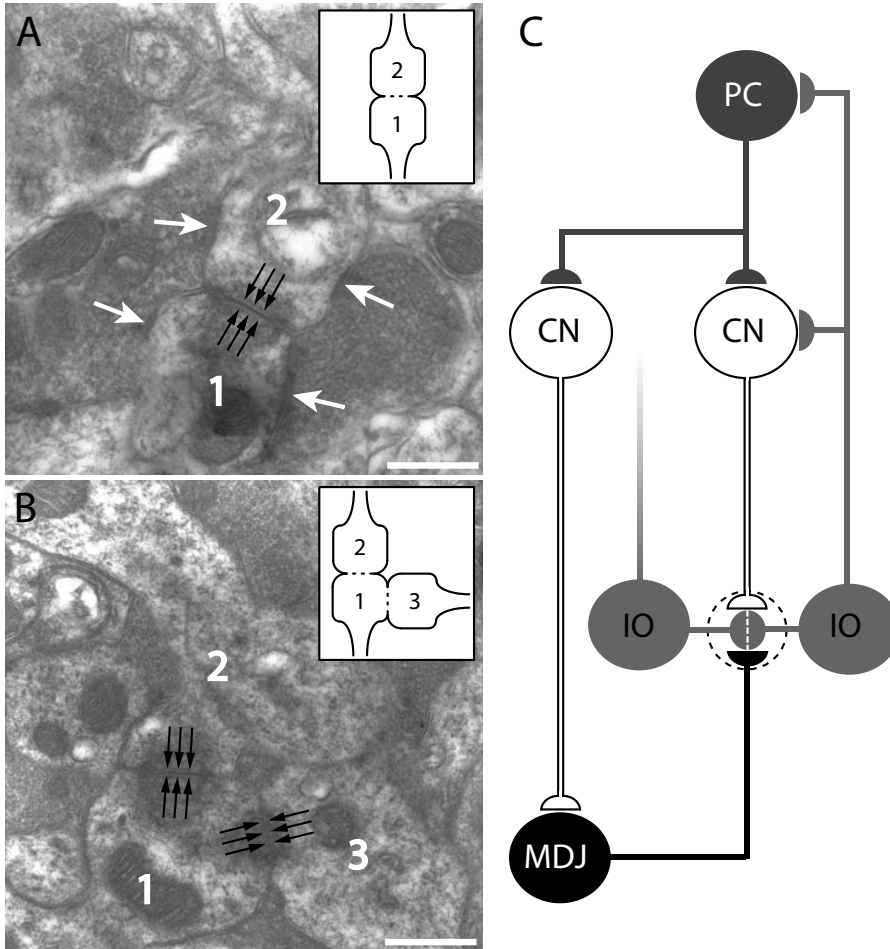
Figure 3. Organization of the glomerulus in the inferior olive. A. Ultrastructural micrograph showing a olivary glomerulus. A glomerulus consists of two opposing dendrites (1 and 2) with a gap junction (black arrows). The inset show the schematic organization of the glomerulus. The core of these dendritic spines is surrounded by terminals (white arrows). **B.** Some glomeruli in the inferior olive in some cases even contain multiple gap junctions (black arrows) thereby connecting multiple dendritic spines (1,2 and 3). This demonstrates the high degree of coupling that is present in the glomeruli. See also the inset with a schematic organization. Scale bars in A and B, 500 nm. **C.** A simplified scheme showing the origin of the terminals which project to the glomerulus. The cerebellar nuclei neurons project either directly or via the mesodiencephalic junction to the glomerulus. The direct projection of the cerebellar nuclei is inhibitory on the glomerulus while the indirect pathway is excitatory.

Dendritic spines of olivary cells are characterized by their unusually long spine necks that support grouping of spine heads of different olive cells. Between these dendritic spines that cluster together gap junctions are formed. Five to six of these grouped spine heads are surrounded by several sheaths of glia cells, which are called a glomerulus (Figure 3A).

Almost all spines are located within glomeruli. In most of the cases two spines and in some cases even three spines are linked with gap junctions within the glomerulus therefore the olivary cells are intensively coupled (Figure 3B).

BOX 1

Harmaline, a naturally occurring ß-carboline alkaloid, is a reversible monoamine oxidase inhibitor that stimulates the brain by inhibiting the metabolism of serotonin and other monoamines. Harmaline is found in the seeds (3%) of the plant *Peganum harmala* also known as Syrian Rue. When injected systemically, it increases the excitability and firing of neurons in the inferior olive. Although harmaline strongly affects the entire inferior olive, it is noteworthy that after application no rhythmic discharge at the frequency is detected in the eye movements (Batini et al., 1981). Furthermore, 2-deoxyglucose and c-fos labeling studies showed that the dorsal cap of Kooy is not active after harmaline injections (Bernard et al., 1984, Oldenbeuving et al., 1999). A harmaline-induced tremor occurs rapidly (5-10 min) after injection and the severity and frequency are dose-dependent. This harmaline tremor shares several characteristics with essential tremor. For example the olivocerebellar system plays a major role underlying both harmaline-induced tremor and essential tremor. Both tremors are around the same frequency range (4-12 Hz) and therefore, harmaline is used often as a model for this disease. Essential tremor (ET), the most common movement disorder, is a progressive and often inheritable disorder usually beginning before the age of 50. It is characterized by involuntary rhythmical oscillations of a body part resulting from either alternating or synchronous contractions of opposing muscles. Tremor is essentially the only symptom present, although, subtle gait abnormalities may be present when the legs are affected. Weakness in muscle power is not a primary symptom although tremor can in fact produce weakness by reducing the strength of contraction. The tremor is classically present in posture however it may be exacerbated by action and is present at rest. It most often occurs in the hands and arms but may also affect the head, voice, tongue and legs. The tremor is invariably worsened with stress, fatigue, and stimulant medications and is significantly improved by small amounts of alcohol. Electrophysiological studies are consistent with a central source of tremorgenic oscillation. The inferior olive and cerebellum have been shown implicated by PET studies.

Dendritic spines in the glomerulus receive a combined inhibitory and excitatory input. The inhibitory input is derived from the cerebellar nuclei shows pleiomorphic vesicles and symmetric synapses. The excitatory input that is obtained from the mesodiencephalic junction demonstrates round vesicles and asymmetric synapses (de Zeeuw et al., 1988).

Electrophysiological properties

Action potentials of olivary neurons show an initial sharp peak followed by a prolonged after-depolarizing potential (ADP) and a long lasting after hyperpolarizing potential (AHP). The ADP lasts for 10-15 ms and has several small wavelets on top. Its termination is rather abrupt and merges directly into the AHP. This AHP has an overall duration of 150-200 ms (Llinás and Yarom, 1981a). Afferents to the inferior olive are mainly from sensory nuclei such as the trigeminal nucleus.

Although olivary cells (mainly dorsal accessory olivary cells) are very sensitive to sensory stimulation, they respond with a single action potential (usually with a latency of 15-30 ms). During maintained stimuli no sustained discharge has been observed. Additionally, in half of all olivary neurons stimuli of different body part converge (Cook and Wiesendanger, 1976). Another unusual feature is the extremely low firing frequency of olivary neurons. Olivary neurons discharge a single spike around once or twice per second, even in awake animals (Armstrong, 1974; Armstrong & Rawson, 1979; Crill, 1970). The low frequency range of climbing fibers stands in contrast to the high frequency range of parallel fiber activity (Thach, 1967). After application of chemical excitants, such as Harmaline (See Box 1), only a maximal olivary firing of 8 to 10 Hz might be reached (de Montigny and Lamarre, 1973; Lamarre et al., 1971; Llinás and Volkind, 1973).

Olivary neurons also oscillate their membrane potential. *In vitro* olivary cells oscillate their membrane potential at a frequency range between 4 to 10 Hz with an amplitude range from 3 to 10 mV. Early *in vitro* studies (80's) exhibited spontaneous subthreshold oscillations in only 10% of the slice preparations (Llinás and Yarom, 1986). Most cells in these slices oscillated. More recent studies reported silent olivary neurons which started oscillating only after gross electrical stimulation of the slice (Bal and McCormick, 1997). Slice treatment with a cold sucrose solution increased the amount of oscillating cells dramatically. It was suggested that the higher occurrence of subthreshold oscillations that was found with this treatment was due to an enhancement of the viability of slices (Devor and Yarom, 2002). Therefore a valid question still remains whether these *in vitro* studies exactly resemble the *in vivo* condition. The subthreshold oscillations are generated mainly by calcium channels since oscillations disappear after application of calcium blockers and remain unaffected by sodium blockers. Olivary neurons indeed express high amounts of calcium-channels such as T-type, P/Q-type and L-type channels (Hillman et al., 1991; Llinás and Yarom, 1981b). Besides the high-threshold- and low-threshold calcium-channels, the I_h-current is also important in generating subthreshold oscillations. Several studies have suggested that gap junction coupling not only mediates synchrony, but that it is also required for the generation of these subthreshold oscillations (Loewenstein et al., 2001; Manor et al., 1997). Interestingly, the time course of the development of membrane potential oscillations coincides with the morphological appearance of gap junctions (P10-15) in the inferior olive (Bleasel and Pettigrew, 1992). In this thesis we investigated whether subthreshold oscillations in inferior olivary neurons depend on electrotonic coupling between the olivary neurons or not.
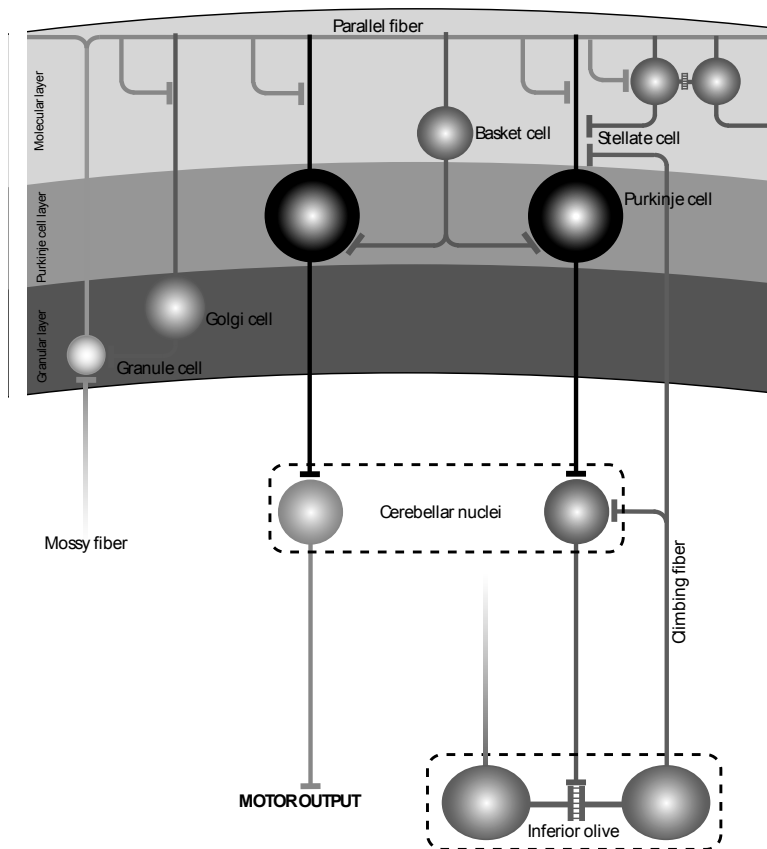
Figure 4. A detailed scheme of the olivocerebellar system. The scheme shows the three layers of the cerebellar cortex and the main interneurons that are present in these layers. Note the gap junctions between stellate cells and the excitatory output of the cerebellar nuclei neurons to the motor output. Two types of cerebellar nuclei neurons can project either to motor output brain areas or back to the same olivary subnucleus (called the closed loop).

1.2.3 Cerebellar cortex

The basic neuronal circuitry of the olivocerebellar system involves the cerebellar cortex, cerebellar nuclei and the inferior olive. In the cerebellar cortex Purkinje cells are arranged as a monolayer, separating the outer molecular layer from the inner granular layer (Figure 4). These cells play a central role since they are the only output from the cerebellar cortex. Purkinje cells are GABAergic and therefore the entire output of the cerebellar cortex is inhibitory. Purkinje cells have a large dendritic tree that is orientated in the sagittal plane (Ramon y Cayal, 1909; Marr, 1969). The terminal part of the dendrite is covered with

numerous spines, which forms small excitatory synapses with the parallel fibers that travel perpendicular through the sagittal plane and originate from granule cells (Pichitpornchai et al., 1994). The granule cells are the major component of the granular layer. They have round or oval cell bodies, with a diameter of 5-8 μm. The unmyelinated thin axon of the granule cells ascends vertically in the molecular layer, where it bifurcates in two branches (T-shape) running parallel to the axis of the folium in opposite directions. Granule cells receive their input from mossy fibers. These fibers originate from many parts of the central nervous system such as the spinal cord, lateral reticular nucleus and pontine nuclei. Their terminals end in the granular layer, making an enlarged ending called a rosette. This rosette is part of a complex synaptic globular arrangement enclosed in a few sheets of glial membranes, called the glomerulus. A single rosette makes synapses with approximately 100 different granule cell dendrites. Additionally, the rosette may also stimulate descending dendrites of Golgi cells. Local interneurons in the cerebellar cortex modulate the activity of Purkinje cells. Basket cells are located in the inner one-third part of the molecular layer with a ratio of one per six Purkinje cells. They give off descending collaterals that surround the Purkinje cell soma, forming a basket-like structure. Additionally, stellate cells are located in the outer two-thirds of the molecular layer (Leto et al., 2006). They have a small soma and make inhibitory synapses with the Purkinje cell dendrites outside the basket. The Purkinje cell also receives numerous inputs from a single climbing fiber that originates from the inferior olive. From 1978, it is known that all climbing fibers arise from the inferior olive (Courville et al. 1978; Desclin 1974). Specific sets of olivary neurons project to longitudinal strips of Purkinje cells on the contralateral side of the cerebellar cortex. A single ascending climbing fiber winds around the proximal part of the dendritic tree of the Purkinje cell. This unique connection between climbing fiber and Purkinje cell is the most powerful excitatory synapse in the brain.

Individual spikes produces a large excitatory post synaptic potentials (EPSPs) of about 10 ms that always trigger the generation of an action potential called a complex spike (Thach et al. 1967). The complex spike shows a fast sodium spike followed by a slow component that consists of a plateau phase with spikelets (Schmolesky et al., 2002). This slow component is mediated by voltage-gated calcium channels that facilitate, due to the multiple synaptic contacts of the climbing fiber, a strong depolarization of the Purkinje cell. This influx of calcium ions induces an intracellular cascade which results in long lasting changes in the synaptical strength. Intracellular calcium levels determine whether the synaptic strength is decreased and these concentrations depend on the exact timing of climbing fiber and

parallel fiber activity within a certain window (Coesmans et al., 2004).

Since the inferior olive provides climbing fibers to all parts of the cerebellar cortex, it is therefore likely that the inferior olive has a common function in cerebellar processing. All Purkinje cells project to the cerebellar nuclei. These neurons in turn receive besides inhibitory input from the Purkinje cells also excitatory input from both mossy fiber and climbing fiber collaterals. Modulation of the level of excitation is determined by the Purkinje cell output.

1.2.4 Cerebellar Nuclei

All cerebellar nuclei neurons receive GABAergic input from Purkinje cells, however, the cerebellar nuclei can be divided into two populations of neurons. The first group consists of large non-GABAergic neurons that provide an input to subcortical premotor areas in the brain such as red nucleus, thalamus and superior colliculus (called the open loop). In this way, these neurons are the final cells of the olivocerebellar system to influence motor behavior. The other group consist of small GABAergic neurons that terminate into glomeruli of the inferior olive (Teune et al., 1998; Uusisaari et al., 2007). This is part of the closed loop. Although, this nucleo-olivary pathway gives an inhibitory effect on olivary cells after a tonic discharges. It has been proposed that this large GABAergic transmission causes a shunting effect on these strategically positioned gap junctions. In this concept the nucleo-olivary pathway is involved in the dynamic coupling of olivary cells by temporarily bypassing the current flow between olivary cells (Angaut and Sotelo, 1989; Llinás et al., 1974; Sotelo et al., 1986).

Earlier studies showed a similar mechanism in pharyngeal motoneurons of the mollusk, *Navanax inermis* that are also electrically coupled and tend to fire synchronously. However, stimulation of the pharyngeal nerve reduced the coupling between these cells. The loss of coupling appeared to be due to inhibitory synapses along the pathway connected to the neurons, an increase in conductance shunted the electrotonic spreading. Under these circumstances, the neurons could be activated asynchronously by other excitatory inputs (Spira and Bennett, 1972). Using the same mechanism, the cerebellar nuclei could be involved in the formation of dynamic clusters that can recruit or withdraw cells from the oscillating ensembles by coupling and uncoupling mechanisms in the many glomeruli in the olive. Since the inferior olive provides a major input to the cerebellum but also receives feedback information from the cerebellar nuclei there are many theories on the function of the inferior olive within the cerebellar circuit.

1.3 Main hypotheses on the Olivocerebellar system

1.3.1 Motor learning hypothesis

In 1969 David Marr proposed the hypothesis entitled "*A Theory of Cerebellar Cortex*" in which a detailed theory is put forward on the role of the cerebellum in learning motor skills (Marr, 1969). This hypothesis stated that only the parallel fiber to Purkinje cell synapse was modifiable. In this theory the inferior olive provides the cerebellum information about the occurring movement by small adjustments the movement can be optimized (motor learning). This early hypothesis was further modified by Albus and Ito, who postulated that the climbing fibers existed solely to modify the strength of the parallel fiber-Purkinje cell synapse (Ito, 1972; Ito, 1989). Their theories directly connected the inferior olive to motor learning. The climbing fiber signal can trigger an enhancement (when absent it leads to depression) of parallel fiber synapses and in this way the climbing fiber system teaches Purkinje cells which of their 150,000 parallel fibers should influence the output. The motor learning hypothesis was further adapted by Thompson to explain the learning during eyeblink conditioning. During eyeblink conditioning the signal that is associated with the unconditioned stimulus is conducted through the inferior olive (Mauk et al., 1986; Thompson et al., 1997). Other studies showed that olivary neurons are quite sensitive to sensory input. Stimuli, like a corneal air puff, during eyeblink conditioning could also be considered as error events or unexpected events. The theory based upon these findings suggests that olivary neurons signal the occurrence of movement errors and in this way the inferior olive functions as an error detector or detector of unexpected events (Andersson and Armstrong, 1987). Supported by this hypothesis it was further proposed that climbing fibers specifically signal these motor performance errors to Purkinje cells, to subsequently change their output in order to improve motor performance (Kawato and Gomi, 1992).

1.3.2 Timing hypothesis

Another hypothesis proposed is that the inferior olive is directly involved in the coordination of movement rather then modification and storage of information in the cerebellar cortex. The hypothesis was based on the fact that olivary neurons are electrically coupled via dendro-dendritic gap junctions through which subthreshold oscillation or action potentials can pass. This electrotonic coupling permits olivary cells to fire coherently as a synchronized oscillatory ensemble. In this way the climbing fibers act as a pacemaker producing a significant and rhythmic modulation of the motor systems as movement proceeds.

Because subthreshold oscillations can be synchronized between olivary cells, olivary spikes can also be synchronized or a specific rhythmic pattern can be generated. These synchronized firing patterns can be used for specific movements that are coded by a population of cells in temporal manner (Welsh, 2002). In this way clusters of olivary neurons can provide sensory information based on a rhythmic temporal pattern made by subthreshold oscillations. Additionally, the oscillations can generate windows of opportunity for firing, a gating mechanism. Through these windows subthreshold oscillations determine when sensory input can pass through the climbing fibers or not (Devor and Yarom, 2002; Lang et al., 2006).

1.3.3 Alternative hypotheses

Although one of the most significant functions of the olivocerebellar system is to coordinate movements, its involvement has been reported in several aspects of cognition (Bugalho et al., 2006; Gordon, 2007; Schmahmann, 2004). Therefore, the inferior olive also may play a role in cognition as part of the olivocerebellar system. For example, in autism patients, the altered shape of the inferior olive is one of the most common disturbances of their brain anatomy (Palmen et al., 2004). Additionally, experiments with classical eyeblink conditioning demonstrated that the inferior olive is necessary to learn sequences of stimuli presented at intervals in the range of 250-500 ms. A disruption of the inferior olive reduces the stimulus processing speed on this time scale, this decrease in processing speed at 250-500 ms is also impaired in children with autism (Welsh et al., 2005). Therefore it is thought that social and communication cues pass by too fast for autistic children to process, which makes them appear socially or emotionally detached.

Although all these hypotheses are somewhat different, they share the common concept that the precise timing of climbing fiber discharge is critical to their function and it relates directly to some aspect of movement. In case of the motor learning hypothesis, climbing fiber discharges are assumed to be generated by detection of some specific motor-related event. The timing between complex spike and simple spike can modulate the strength of the parallel fiber transmission. And in the movement timing hypothesis, the intrinsic properties of the inferior olive itself are assumed to control the timing of climbing fiber activity and thereby the timing of the movement.

1.4 Gap junctions

1.4.1 Gap junctions properties

Gap junctions are protein complexes made up of several connexins that allow intercellular passage of signaling molecules and ions. By interconnecting multiple cells gap junctions can form a large network of directly communicating cells (See box 2). Each connexin protein has four transmembrane domains, which are highly conserved between the different kinds of connexins (Figure 5A). The N- and C-terminus (intracellular domains) are the most variable in amino acid sequence among the different connexins (Duffy et al., 2002).

> **BOX 2**
>
> The Italian Camillo Golgi (1844-1926) studied the histological properties of the nervous system. In 1873, he developed a revolutionary staining technique, still in use and named after him (Golgi staining or impregnation), which allowed for the first time a clear visualization of a nerve cell body with all its processes. Golgi was convinced that the nervous system consisted of one large network (the reticular theory). The Spanish Santiago Ramón y Cajal (1852-1934) improved his staining-technique. Using this method, Cajal became the main supporter of the 'neuron theory', which correctly interpreted the nervous system as composed of anatomically and functionally distinct cells. According to Ramón y Cajal the nervous system consisted of millions of nerve cells that receive electrical input via axons of other neurons. In 1906 Golgi and Ramón y Cajal shared the Nobelprize for Physiology and Medicine because of their revolutionary studies. In his acceptance speech Camillo Golgi defended the reticular theory that was proposed by Josef von Gerlach in 1871 and was also supported by other "reticularists", whereas Ramón y Cajal talked about his theory that nerve cells contact each other via little currents. It was the latter theory that eventually became generally accepted. Another defender of the new theory was "neuronist" Heinrich Wilhelm von Waldeyer, who in 1891 used the term "neuron" to refer to nerve cells, postulated the neuron doctrine (Lopez-Munoz et al., 2006). The neuron doctrine is the concept that neurons are the basic fundamental and individually functional units of the nervous system. The consolidation of the neuron theory came with the electron microscopy in 1954. This technique demonstrated the individuality of neurons thereby confirming the neuronal independence.
>
> While the neuron doctrine has remained a central tenet of modern neuroscience, several studies have challenged this view and suggest that the constricted boundaries of this doctrine need to be expanded toward the reticular theory. One of those expansions to the reticular theory is the existence of electrical synapses in the brain. These electrical synapses, also known as gap junctions, allow neurons to form a continuous syncytium not only during the first stages of embryonic development but also in the adult brain. This suggests that rather than functioning as an individual entity, in some brain areas large ensembles of neurons may be active together as a network.

After insertion into the plasma membrane the docking of two connexons located in opposing membranes leads to gap junction plaque formation (Figure 5B). These gap junction aggregates can be visualized with the use of scanning electron microscopy and show a characteristic view of two adjacent membranes that are lined up with a extracellular gap

of 3-4 nm wide (Figure 5C). Gap junction proteins attach to proteins of the cytoplasmic cytoskeleton, which can be seen as electron-dense deposits at both sides of the membranes (specially in neuronal gap junctions as oppose to glial gap junctions).

Among these proteins is ZO-1 that has been identified associating with for instance Connexin36. ZO-1 has been identified as a tight junction-associated protein (Stevenson et al., 1986) that interacts with the C-terminus of Connexin36 and may play a role in determining the size of the gap junction plaque (Hunter et al., 2003; Li et al., 2004). Although, it is still unknown whether these gap junction-associated proteins are located at the dendritic spines when gap junction channels are absent. Neurons in the brain mainly form gap junctions with other neurons.

Though, there have been reports about gap junctions between neurons and glial cells, however this is usually only weak coupling (Söhl et al., 2005). Gap junctions not only allow exchange of ions and thereby can synchonize electrical activity, they also provide a exchange pathway for traffic of metabolites and second messengers such as Ca^{2+}, ATP and cAMP among neurons (Rozental et al., 2000).

1.4.2 Connexin protein family

The nomenclature of connexin proteins is determined by their approximate molecular weight in kilodaltons (Beyer et al., 1990; Rozental et al., 2000). Generally, gap junctions are found in nearly every cell type except mature skeletal muscle, spermatozoa and erythrocytes. Liver and heart specifically express an abundance of gap junctions (Dermietzel and Spray, 1993). Thus far, connexins comprise of a family of at least 20 members in the murine genome and 21 connexin genes in the human genome (Rozental et al., 2000; Söhl and Willecke, 2003; Willecke et al., 2002). Only ten of these connexins are expressed in the nervous system (Figure 6). Whereas neurons themselves only express Cx30.2, Cx36, Cx45 and Cx57. The other connexins are expressed in glia cells, like oligodendrocytes and astrocytes. Besides their neuronal expression, Cx30.2 and Cx45 also have been found in cardiomyocytes. Connexin57 is only expressed in horizontal cells of the retina and therefore Connexin36 deserves specific attention because it is exclusively neuronal and brain specific. Although the expression of Connexin36 in excitable ß-cells of the pancreas (Degen et al., 2004) seems to contradict the brain specificity, the presence of Connexin36 and other neuronal gene transcripts is correlated by the absence of a transcription factor named neuron-restrictive silencer factor/repressor element silencing transcription factor (NRSF/REST).

This transcription factor normally silences neuronal gene expression in non-neuronal tissues (Martin et al., 2003). Apparently, the β-cells of the pancreas is derived from neuronal precursors and shares neuronal properties such as expression of Connexin36.

1.4.3 General properties of Connexin36

Connexin36 is one of the major connexins expressed in neurons (Condorelli et al., 1998; Söhl et al., 1998). Connexin36 has been found in many brain areas such as thalamus, hippocampus, basal ganglia, cerebral cortex, olfactory bulb, brainstem and retina. Especially, Connexin36 was found to be highly expressed in the inferior olive (Condorelli et al., 2000).
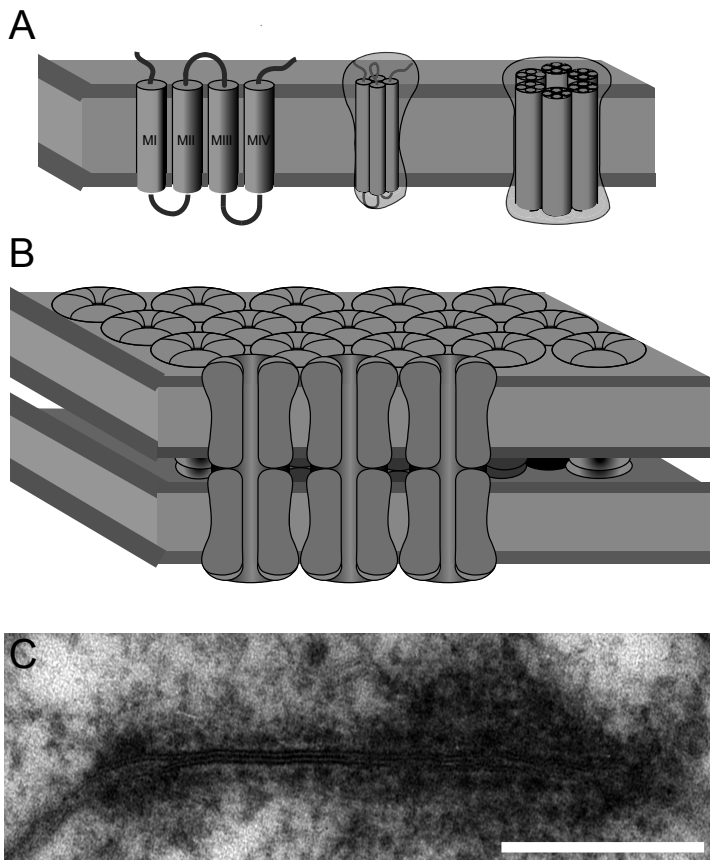
Figure 5. The formation of gap junctions. A. Connexin proteins consist of four transmembrane domains. Six connexin proteins assemble to form a connexon or hemichannel. **B.** A schematic transection of a membrane with a gap junction. Connexons of opposing membranes cluster together and generate functional gap junction channels. **C.** An ultrastructural micrograph showing a typical olivary gap junction. The gap junction is identified by two membranes that approach each other with a distance of approximately 3-4 nm. This plaque is enclosed by electron dense material formed by gap junction-associated proteins that is characteristic for olivary gap junctions.
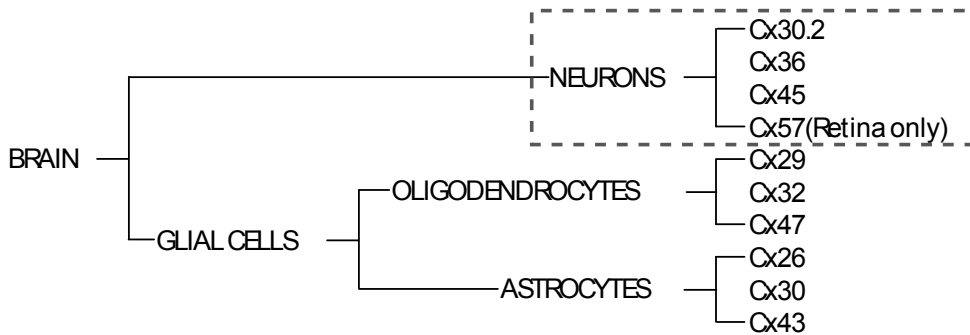
Figure 6. A dendrogram of the connexin family in the brain. Thus far the connexin family includes at least 20 members, ten of those are expressed in the brain. Note that neurons only expressed four types of connexins (indicated by dashed box). Connexin36 is the only neuron-specific connexin protein and only neurons in the retina express Connexin57.

Many textbooks describe that connexin proteins have a non-specific permeability to molecules smaller than 1 kiloDalton (kDa). However, this property depends on the specific connexin composition and can therefore vary between cells. It is unknown what exact maximum molecular weight can pass through Connexin36 gap junctions, yet several studies have shown that Connexin36 gap junctions are at least permeable for Lucifer yellow, a fluorescent anionic dye of approximately 457 Dalton (De Zeeuw et al., 2003; Srinivas et al., 1999). Additionally, connexin proteins exhibit a large range of single channel conductances from 10 to 300 pS (Veenstra et al., 1994). Characterization of the electrophysiological properties of Connexin36, however, shows a unitary conductance of 10-15 pS and a weak voltage sensitivity (Srinivas et al., 1999). Connexin36 has one of the lowest voltage sensitivities and one of the smallest unitary conductances of all connexin isoforms (Söhl et al., 2005). Since Connexin36 is neuron specific, the hypothesis is that expression of connexin proteins with low unitary conductance allow neurons to achieve a more precise control of the extent of electrical coupling (by varying number of channels) than connexins with higher unitary conductances. Another way of manipulating the size and properties of electrical coupling can be achieved by composing gap junction from different connexin-types. Connexons composed of similar connexins are called homomeric connexons, whereas heteromeric connexons consist of different connexins. Gap junctions formed by corresponding connexons are defined as homotypic channels, whereas heterotypic channels consist of different connexons. The number of possible interactions between various connexins therefore markedly increases the complexity of gap junctions. Connexin45 for instance has a large voltage sensitivity and an average single channel conductance (32±8 pS) compared with other connexin isoforms (Moreno et al., 1995).

By forming different heterotypic channels a large range of gap junction properties can be generated. However, it is unclear, whether brain areas with high degree of electrical coupling such as the inferior olive also co-express different connexins. The majority of connexins have been shown to be phosphoproteins. Connexin36, for example, has recently been shown to be modulated by Calmodulin-dependent protein kinase II (CamKII), Casein kinase II (CKII) and Protein kinase A (PKA) (Urschel et al., 2006). This phosphorylation may be involved in a uncoupling mechanism by means of closing channels, internalization or degradation of the gap junctions (Laird, 2005).

The closing of gap junction channels can also be influenced by several other factors such as acidification or transjunctional voltage. Different types of substances can also block gap junctional coupling like long-chain alcohols (such as heptanol and octanol), halothane, ethrane, glycyrrhetinic acid derivatives, oleamide derivatives (carbenoxolone) and arachidonic acid metabolites (Burt and Spray, 1989; Christ et al., 1999; Leznik and Llinás, 2005; Ohba et al., 2007; Sagar and Larson, 2006; Wentlandt et al., 2006). Recently, Quinine derivatives were found to block specifically Connexin36 junctional currents in a reversible and concentration-dependent manner (Cruikshank et al.2004, Srinivas et al.2001). Since Connexin36 has low voltage sensitivity and a small unitary conductance, the closing of these gap junction channels occurs mainly through either phosphorylation (Urschel et al., 2006) or pharmacological effects.

1.4.4 Connexin expression in the olivocerebellar system

Several parts of the olivocerebellar system have been reported to show evidence of gap junctions like the vestibular nuclei (Korn et al., 1973), inferior olive (Sotelo et al., 1974) and cerebellar cortex (Mann-Metzer and Yarom, 1999). For the inferior olive, which has the highest density of electrical coupling in the brain, the exact composition of the gap junctions is still unknown. Since only four kinds of connexins expressed by neurons, the number of connexin-types found in gap junctions of the inferior olive can also be limited to four. This thesis will describe the specific connexins that are involved in the formation of olivary gap junctions. Other parts of the olivocerebellar system such as cerebellar nuclei and cerebellar cortex have also been shown to be coupled electrophysiologically (Mann-Metzer and Yarom, 1999), however morphological evidence has not yet been demonstrated.

1.5 Scope of thesis

An important role of the olivocerebellar system is involved in fine-tuning of movements. The inferior olive, as a part of this circuit, plays a key role because it provides one of the major sensory inputs to the cerebellar cortex. Olivary neurons show several distinct properties such as low firing rates, subthreshold oscillations and a high degree of gap junctional coupling. The present study describes these properties in the inferior olive in order to elucidate their role within the olivocerebellar system. To obtain more insight on the function of gap junctions in the inferior olive, we investigated different mouse mutants that lack a gap junction protein. Chapter 2 describes the two major gap junction-proteins expressed by neurons in the olivocerebellar system. Although several studies have shown electrophysiological evidence of electrotonic coupling in the olivocerebellar system, the exact distribution of connexins in the olivocerebellar system remains unknown. Chapter 2.1 specifically examines the expression of Connexin36 in the olivocerebellar system while Chapter 2.2 describes the expression and distribution of Connexin45. Furthermore, this chapter characterizes the contribution of Connexin45 in the olivocerebellar system during adulthood with special emphasis on the gap junctions in the inferior olive. The general aim of these studies is to investigate the exact connexin composition in the olivary gap junctions. Thus far, the presence of gap junctions and their precise composition in the inferior olive was unclear. Chapter 3 shows the consequences of a lack of Connexin36 in olivary neurons. In Chapter 3.1 the interaction between subthreshold oscillations and gap junctions *in vitro* was investigated, while the general firing properties and oscillatory activity of olivary neurons *in vivo* were studied in Chapter 3.2. In Chapter 4 the role of Connexin36 on the behavioral level is further investigated. General motor performances but also specific conditioning tasks such as eyeblink conditioning and the Erasmusladder were studied in Connexin36 knockout and wildtype mice. Additionally, electrophysiological data shows the alterations in mice lacking Connexin36 gap junctions. In Chapter 5, we discuss the role the olivary neurons with regard to timing and control during movements and their specific properties. Based on the findings described in this thesis we will provide a model of how olivary neurons could function within a network.

REFERENCES

Andersson, G., and Armstrong, D. M. (1987). Complex spikes in Purkinje cells in the lateral vermis (b zone) of the cat cerebellum during locomotion. J Physiol *385*, 107-134.

Angaut, P., and Sotelo, C. (1989). Synaptology of the cerebello-olivary pathway. Double labelling with anterograde axonal tracing and GABA immunocytochemistry in the rat. Brain Res *479*, 361-365.

Bal, T., and McCormick, D. A. (1997). Synchronized oscillations in the inferior olive are controlled by the hyperpolarization-activated cation current I(h). J Neurophysiol *77*, 3145-3156.

Batini, C., Bernard, J. F., Buisseret-Delmas, C., Conrath-Verrier, M., and Horcholle-Bossavit, G. (1981). Harmaline-induced tremor. II. Unit activity correlation in the interposito-rubral and oculomotor systems of cat. Exp Brain Res *42*, 383-391.

Bernard, J. F., Buisseret-Delmas, C., Compoint, C., and Laplante, S. (1984). Harmaline induced tremor. III. A combined simple units, horseradish peroxidase, and 2-deoxyglucose study of the olivocerebellar system in the rat. Exp Brain Res *57*, 128-137.

Beyer, E. C., Paul, D. L., and Goodenough, D. A. (1990). Connexin family of gap junction proteins. J Membr Biol *116*, 187-194.

Bleasel, A. F., and Pettigrew, A. G. (1992). Development and properties of spontaneous oscillations of the membrane potential in inferior olivary neurons in the rat. Brain Res Dev Brain Res *65*, 43-50.

Bugalho, P., Correa, B., and Viana-Baptista, M. (2006). [Role of the cerebellum in cognitive and behavioural control: scientific basis and investigation models]. Acta Med Port *19*, 257-267.

Burt, J. M., and Spray, D. C. (1989). Volatile anesthetics block intercellular communication between neonatal rat myocardial cells. Circ Res *65*, 829-837.

Christ, G. J., Spektor, M., Brink, P. R., and Barr, L. (1999). Further evidence for the selective disruption of intercellular communication by heptanol. Am J Physiol *276*, H1911-1917.

Coesmans M, Weber JT, De Zeeuw CI, Hansel C. (2004). Bidirectional parallel fiber plasticity in the cerebellum under climbing fiber control. Neuron 44(4):691-700.

Condorelli, D. F., Belluardo, N., Trovato-Salinaro, A., and Mudo, G. (2000). Expression of Cx36 in mammalian neurons. Brain Res Brain Res Rev *32*, 72-85.

Condorelli, D. F., Parenti, R., Spinella, F., Trovato Salinaro, A., Belluardo, N., Cardile, V., and Cicirata, F. (1998). Cloning of a new gap junction gene (Cx36) highly expressed in mammalian brain neurons. Eur J Neurosci *10*, 1202-1208.

Courville, J., F. Faraco-Cantin, et al. (1974). "A functionally important feature of the distribution of the olivo-cerebellar climbing fibers." Can J Physiol Pharmacol 52(6): 1212-7.

de Montigny, C., and Lamarre, Y. (1973). Rhythmic activity induced by harmaline in the olivo-cerebello-bulbar system of the cat. Brain Res *53*, 81-95.

Desclin, J. C. (1974). "Histological evidence supporting the inferior olive as the major source of cerebellar climbing fibers in the rat." Brain Res 77(3): 365-84.

De Zeeuw, C. I., Chorev, E., Devor, A., Manor, Y., Van Der Giessen, R. S., De Jeu, M. T., Hoogenraad, C. C., Bijman, J., Ruigrok, T. J., French, P., *et al.* (2003). Deformation of network connectivity in the inferior olive of connexin 36-deficient mice is compensated by morphological and electrophysiological changes at the single neuron level. J Neurosci *23*, 4700-4711.

De Zeeuw, C. I., Hertzberg, E. L., and Mugnaini, E. (1995). The dendritic lamellar body: a new neuronal organelle putatively associated with dendrodendritic gap junctions. J Neurosci *15*, 1587-1604.

de Zeeuw, C. I., Holstege, J. C., Calkoen, F., Ruigrok, T. J., and Voogd, J. (1988). A new combination of WGA-HRP anterograde tracing and GABA immunocytochemistry applied to afferents of the cat inferior olive at the ultrastructural level. Brain Res *447*, 369-375.

Degen, J., Meier, C., Van Der Giessen, R. S., Söhl, G., Petrasch-Parwez, E., Urschel, S., Dermietzel, R., Schilling, K., De Zeeuw, C. I., and Willecke, K. (2004). Expression pattern of lacZ reporter gene representing Connexin36 in transgenic mice. J Comp Neurol *473*, 511-525.

Dermietzel, R., and Spray, D. C. (1993). Gap junctions in the brain: where, what type, how many and why? Trends Neurosci *16*, 186-192.

Deuschl, G., and Elble, R. J. (2000). The pathophysiology of essential tremor. Neurology *54*, S14-20.

Devor, A., and Yarom, Y. (2002). Generation and propagation of subthreshold waves in a network of inferior olivary neurons. J Neurophysiol *87*, 3059-3069.

Duffy, H. S., Delmar, M., and Spray, D. C. (2002). Formation of the gap junction nexus: binding partners for connexins. J Physiol Paris *96*, 243-249.

Garwicz, M. (2000). Micro-organisation of cerebellar modules controlling forelimb movements. Prog Brain Res *124*, 187-199.

Gordon, N. (2007). The cerebellum and cognition. Eur J Paediatr Neurol.

Haller, S., Winkler, D. T., Gobbi, C., Lyrer, P., Wetzel, S. G., and Steck, A. J. (2006). Prominent activation of the putamen during essential palatal tremor: a functional MR imaging case study. AJNR Am J Neuroradiol *27*, 1272-1274.

Herculano-Houzel, S., and Lent, R. (2005). Isotropic fractionator: a simple, rapid method for the quantification of total cell and neuron numbers in the brain. J Neurosci *25*, 2518-2521.

Hillman, D., Chen, S., Aung, T. T., Cherksey, B., Sugimori, M., and Llinás, R. R. (1991). Localization of P-type calcium channels in the central nervous system. Proc Natl Acad Sci U S A *88*, 7076-7080.

Hunter, A. W., Jourdan, J., and Gourdie, R. G. (2003). Fusion of GFP to the carboxyl terminus of connexin43 increases gap junction size in HeLa cells. Cell Commun Adhes *10*, 211-214.

Ito, M. (1972). Neural design of the cerebellar motor control system. Brain Res *40*, 81-84.

Ito, M. (1989). Long-term depression. Annu Rev Neurosci *12*, 85-102.

Jueptner, M., and Weiller, C. (1998). A review of differences between basal ganglia and cerebellar control of movements as revealed by functional imaging studies. Brain *121 (Pt 8)*, 1437-1449.

Kawato, M., and Gomi, H. (1992). A computational model of four regions of the cerebellum based on feedback-error learning. Biol Cybern *68*, 95-103.

Korn, H., Sotelo, C., and Crepel, F. (1973). Electronic coupling between neurons in the rat lateral vestibular nucleus. Exp Brain Res *16*, 255-275.

Laird, D. W. (2005). Connexin phosphorylation as a regulatory event linked to gap junction internalization and degradation. Biochim Biophys Acta *1711*, 172-182.

Lamarre, Y., de Montigny, C., Dumont, M., and Weiss, M. (1971). Harmaline-induced rhythmic activity of cerebellar and lower brain stem neurons. Brain Res *32*, 246-250.
Lang, E. J., Sugihara, I., and Llinás, R. (2006). Olivocerebellar modulation of motor cortex ability to generate vibrissal movements in rat. J Physiol *571*, 101-120.

Le Strange, E., Saeed, N., Cowan, F. M., Edwards, A. D., and Rutherford, M. A. (2004). MR imaging quantification of cerebellar growth following hypoxic-ischemic injury to the neonatal brain. AJNR Am J Neuroradiol *25*, 463-468.

Leto, K., Carletti, B., Williams, I. M., Magrassi, L., and Rossi, F. (2006). Different types of cerebellar GABAergic interneurons originate from a common pool of multipotent progenitor cells. J Neurosci *26*, 11682-11694.

Leznik, E., and Llinás, R. (2005). Role of gap junctions in synchronized neuronal oscillations in the inferior olive. J Neurophysiol *94*, 2447-2456.

Li, X., Olson, C., Lu, S., Kamasawa, N., Yasumura, T., Rash, J. E., and Nagy, J. I. (2004). Neuronal Connexin36 association with zonula occludens-1 protein (ZO-1) in mouse brain and interaction with the first PDZ domain of ZO-1. Eur J Neurosci *19*, 2132-2146.

Llinás, R., Baker, R., and Sotelo, C. (1974). Electrotonic coupling between neurons in cat inferior olive. J Neurophysiol *37*, 560-571.

Llinás, R., and Volkind, R. A. (1973). The olivo-cerebellar system: functional properties as revealed by harmaline-induced tremor. Exp Brain Res *18*, 69-87.

Llinás, R., and Yarom, Y. (1981a). Electrophysiology of mammalian inferior olivary neurones *in vitro*. Different types of voltage-dependent ionic conductances. J Physiol *315*, 549-567.

Llinás, R., and Yarom, Y. (1981b). Properties and distribution of ionic conductances generating electroresponsiveness of mammalian inferior olivary neurones *in vitro*. J Physiol *315*, 569-584.

Llinás, R., and Yarom, Y. (1986). Oscillatory properties of guinea-pig inferior olivary neurones and their pharmacological modulation: an *in vitro* study. J Physiol *376*, 163-182.

Loewenstein, Y., Yarom, Y., and Sompolinsky, H. (2001). The generation of oscillations in networks of electrically coupled cells. Proc Natl Acad Sci U S A *98*, 8095-8100.

Lopez-Munoz, F., Boya, J., and Alamo, C. (2006). Neuron theory, the cornerstone of neuroscience, on the centenary of the Nobel Prize award to Santiago Ramon y Cajal. Brain Res Bull *70*, 391-405.

Mann-Metzer, P., and Yarom, Y. (1999). Electrotonic coupling interacts with intrinsic properties to generate synchronized activity in cerebellar networks of inhibitory interneurons. J Neurosci *19*, 3298-3306.

Manor, Y., Rinzel, J., Segev, I., and Yarom, Y. (1997). Low-amplitude oscillations in the inferior olive: a model based on electrical coupling of neurons with heterogeneous channel densities. J Neurophysiol *77*, 2736-2752.

Marr, D. (1969). A theory of cerebellar cortex. J Physiol *202*, 437-470.

Martin, D., Tawadros, T., Meylan, L., Abderrahmani, A., Condorelli, D. F., Waeber, G., and Haefliger, J. A. (2003). Critical role of the transcriptional repressor neuron-restrictive silencer factor in the specific control of Connexin36 in insulin-producing cell lines. J Biol Chem *278*, 53082-53089.

Mauk, M. D., Steinmetz, J. E., and Thompson, R. F. (1986). Classical conditioning using stimulation of the inferior olive as the unconditioned stimulus. Proc Natl Acad Sci U S A *83*, 5349-5353.

Moreno, A. P., Laing, J. G., Beyer, E. C., and Spray, D. C. (1995). Properties of gap junction channels formed of connexin 45 endogenously expressed in human hepatoma (SKHep1) cells. Am J Physiol *268*, C356-365.

Nitschke, M. F., Krüger, G., Bruhn, H., Klein, C., Gehrking, E., Wessel, K., Frahm, J., and Vieregge, P. (2001). Voluntary palatal tremor is associated with hyperactivation of the inferior olive: a functional magnetic resonance imaging study. Mov Disord *16*, 1193-1195.

Ohba, Y., Kanao, Y., Morita, N., Fujii, E., Hohrai, M., Takatsuji, M., Hirose, H., Miura, D., Watari, A., Yutsudo, M.*, et al*. (2007). Oleamide derivatives suppress the spontaneous metastasis by inhibiting connexin 26. Int J Cancer *121*, 47-54.

Oldenbeuving, A. W., L. M. Eisenman, et al. (1999). "Inferior olivary-induced expression of Fos-like immunoreactivity in the cerebellar nuclei of wild-type and Lurcher mice." Eur J Neurosci 11(11): 3809-22.

Palmen, S. J., van Engeland, H., Hof, P. R., and Schmitz, C. (2004). Neuropathological findings in autism. Brain *127*, 2572-2583.

Pichitpornchai, C., Rawson, J. A., and Rees, S. (1994). Morphology of parallel fibres in the cerebellar cortex of the rat: an experimental light and electron microscopic study with biocytin. J Comp Neurol *342*, 206-220.

Ramon y Cayal, S. (1909). Histologie du Systeme Nerveux de l'Homme et des Vertebres, Maloine.

Rozental, R., Giaume, C., and Spray, D. C. (2000). Gap junctions in the nervous system. Brain Res Brain Res Rev *32*, 11-15.

Sagar, G. D., and Larson, D. M. (2006). Carbenoxolone inhibits junctional transfer and upregulates Connexin43 expression by a protein kinase A-dependent pathway. J Cell Biochem *98*, 1543-1551.

Scheibel, M. E., and Scheibel, A. B. (1955). The inferior olive; a Golgi study. J Comp Neurol *102*, 77-131.

Schmahmann, J. D. (2004). Disorders of the cerebellum: ataxia, dysmetria of thought, and the cerebellar cognitive affective syndrome. J Neuropsychiatry Clin Neurosci *16*, 367-378.

Schmolesky MT, Weber JT, De Zeeuw CI, Hansel C (2002). The making of a complex spike: ionic composition and plasticity. Ann N Y Acad Sci 978:359-390.

Söhl, G., Degen, J., Teubner, B., and Willecke, K. (1998). The murine gap junction gene Connexin36 is highly expressed in mouse retina and regulated during brain development. FEBS Lett *428*, 27-31.

Söhl, G., Maxeiner, S., and Willecke, K. (2005). Expression and functions of neuronal gap junctions. Nat Rev Neurosci *6*, 191-200.

Söhl, G., and Willecke, K. (2003). An update on connexin genes and their nomenclature in mouse and man. Cell Commun Adhes *10*, 173-180.

Sotelo, C., Gotow, T., and Wassef, M. (1986). Localization of glutamic-acid-decarboxylase-immunoreactive axon terminals in the inferior olive of the rat, with special emphasis on anatomical relations between GABAergic synapses and dendrodendritic gap junctions. J Comp Neurol *252*, 32-50.

Sotelo, C., Llinás, R., and Baker, R. (1974). Structural study of inferior olivary nucleus of the cat: morphological correlates of electrotonic coupling. J Neurophysiol *37*, 541-559.

Spira, M. E., and Bennett, M. V. (1972). Synaptic control of electrotonic coupling between neurons. Brain Res *37*, 294-300.

Srinivas, M., Rozental, R., Kojima, T., Dermietzel, R., Mehler, M., Condorelli, D. F., Kessler, J. A., and Spray, D. C. (1999). Functional properties of channels formed by the neuronal gap junction protein Connexin36. J Neurosci *19*, 9848-9855.

Stevenson, B. R., Siliciano, J. D., Mooseker, M. S., and Goodenough, D. A. (1986). Identification of ZO-1: a high molecular weight polypeptide associated with the tight junction (zonula occludens) in a variety of epithelia. J Cell Biol *103*, 755-766.

Sugihara, I. (2005). Microzonal projection and climbing fiber remodeling in single olivocerebellar axons of newborn rats at postnatal days 4-7. J Comp Neurol *487*, 93-106.

Teune, T. M., van der Burg, J., de Zeeuw, C. I., Voogd, J., and Ruigrok, T. J. (1998). Single Purkinje cell can innervate multiple classes of projection neurons in the cerebellar nuclei of the rat: a light microscopic and ultrastructural triple-tracer study in the rat. J Comp Neurol *392*, 164-178.

Thach, W. T. (1997). Context-response linkage. Int Rev Neurobiol *41*, 599-611.

Thach, W. T., Goodkin, H. P., and Keating, J. G. (1992). The cerebellum and the adaptive coordination of movement. Annu Rev Neurosci *15*, 403-442.

Thompson, R. F., Bao, S., Chen, L., Cipriano, B. D., Grethe, J. S., Kim, J. J., Thompson, J. K., Tracy, J. A., Weninger, M. S., and Krupa, D. J. (1997). Associative learning. Int Rev Neurobiol *41*, 151-189.

Urschel, S., Hoher, T., Schubert, T., Alev, C., Söhl, G., Worsdorfer, P., Asahara, T., Dermietzel, R., Weiler, R., and Willecke, K. (2006). Protein kinase A-mediated phosphorylation of Connexin36 in mouse retina results in decreased gap junctional communication between AII amacrine cells. J Biol Chem *281*, 33163-33171.

Uusisaari, M., Obata, K., and Knopfel, T. (2007). Morphological and electrophysiological properties of GABAergic and non-GABAergic cells in the deep cerebellar nuclei. J Neurophysiol *97*, 901-911.

Veenstra, R. D., Wang, H. Z., Beyer, E. C., Ramanan, S. V., and Brink, P. R. (1994). Connexin37 forms high conductance gap junction channels with subconductance state activity and selective dye and ionic permeabilities. Biophys J *66*, 1915-1928.

Welsh, J. P. (2002). Functional significance of climbing-fiber synchrony: a population coding and behavioral analysis. Ann N Y Acad Sci *978*, 188-204.

Welsh, J. P., Ahn, E. S., and Placantonakis, D. G. (2005). Is autism due to brain desynchronization? Int J Dev Neurosci *23*, 253-263.

Welsh, J. P., Chang, B., Menaker, M. E., and Aicher, S. A. (1998). Removal of the inferior olive abolishes myoclonic seizures associated with a loss of olivary serotonin. Neuroscience *82*, 879-897.

Wenning, G. K., Tison, F., Elliott, L., Quinn, N. P., and Daniel, S. E. (1996). Olivopontocerebellar pathology in multiple system atrophy. Mov Disord *11*, 157-162.

Wentlandt, K., Samoilova, M., Carlen, P. L., and El Beheiry, H. (2006). General anesthetics inhibit gap junction communication in cultured organotypic hippocampal slices. Anesth Analg *102*, 1692-1698.

Willecke, K., Eiberger, J., Degen, J., Eckardt, D., Romualdi, A., Güldenagel, M., Deutsch, U., and Söhl, G. (2002). Structural and functional diversity of connexin genes in the mouse and human genome. Biol Chem *383*, 725-737.

Chapter 2

Specific expression and distribution of connexins in the Olivocerebellar system

Chapter 2.1

Expression Pattern of lacZ Reporter Gene Representing Connexin36 in Transgenic Mice

JOACHIM DEGEN[1], CAROLA MEIER[2], RUBEN S. VAN DER GIESSEN[3], GORAN SÖHL[1], ELISABETH PETRASCH-PARWEZ[2], STEPHANIE URSCHEL[1], ROLF DERMI-ETZEL[2], KARL SCHILLING[4], CHRIS I. DE ZEEUW[3], AND KLAUS WILLECKE[1]

[1]*Institute of Genetics, Division of Molecular Genetics, University of Bonn, D-53117 Bonn, Germany*
[2]*Department of Neuroanatomy and Molecular Brain Research, Institute of Anatomy, Ruhr-University Bochum, D-44801 Bochum, Germany*
[3]*Department of Neuroscience, Erasmus MC, 3000 DR Rotterdam, The Netherlands*
[4]*Department of Anatomy, University of Bonn, D-53115 Bonn, Germany*

ABSTRACT

Previous studies showed that targeted deletion of the Connexin36 (Cx36) gene in the mouse genome leads to visual transmission defects, weakened synchrony of rhythmic inhibitory potentials in the neocortex, and disruption of γ-frequency network oscillations. We have generated transgenic mice in which a reporter protein consisting of the exon1 coded N-terminal part of Cx36 fused to (ß-galactosidase (N36-ß-gal) is expressed instead of Cx36. Here, we have used these mice for a detailed analysis of the reporter gene expression. By (ß-gal staining of adult retina, we found expression of the lacZ reporter gene in the ganglion cell layer, in two rows of the inner nuclear layer, and in the photoreceptor layer. In the brain, (ß-gal staining was present in γ-aminobutyric acid (GABA)ergic neurons of the cerebellar nuclei, in non-GABAergic neurons of the inferior olive, in mitral cells of the olfactory bulb, and in parvalbumin-positive cells of the cerebral cortex. Outside the central nervous system, N36-ß-gal signals were detected in insulin producing ß-cells of the pancreas and in the medulla of the adrenal gland of adult Cx36+/del[LacZ] mice. This expression pattern suggests that Cx36 fulfills functional roles not only in several types of neurons in the retina and central nervous system but also in excitable cells of the pancreas and adrenal gland.

INTRODUCTION

Gap junctions allow direct diffusional exchange of small molecules between adjacent cells by docking of two hemichannels (connexons), each of which is composed of six connexin protein subunits. The connexin multigene family comprises at least 19 members in the mouse and 20 members in the human genome (Eiberger et al., 2001). Targeted deletion of distinct connexin genes in the mouse leads to defects in development or dysfunctions of adult organs, including the heart, liver, lens, and cochlea, some of which resemble pathological conditions in patients with inherited mutations of the corresponding orthologous connexin genes (cf. Willecke et al., 2002). Connexin36 (Cx36) (Condorelli et al., 1998; Söhl et al., 1998) has been demonstrated to be expressed in interneurons of the retina (Feigenspan et al., 2001), in nerve cells of various parts of the central nervous system (Belluardo et al., 2000; Condorelli et al., 2000; Rash et al., 2000; Venance et al., 2000), as well as in ß-cells of the pancreas (Serre-Beinier et al., 2000) and chromaffin cells in adrenal slices (Martin et al., 2001). In the eye, targeted deletion of Cx36 coding DNA in the mouse genome was described to decrease

the ß-wave in the electroretinogram (Güldenagel et al., 2001), whereas the mice showed normal eye movements with a minor increase in the latency of optokinetic signals (Kistler et al., 2002) and an elimination of rod-mediated, on-center responses at the ganglion cell level (Deans et al., 2002). Additionally, the synchrony of rhythmic inhibitory potentials in the neocortex was impaired in Cx36-deficient mice (Deans et al., 2001), and γ-frequency network oscillations in neuronal networks of the hippocampus were disrupted (Hormuzdi et al., 2001; Buhl et al., 2003). Furthermore, Cx36 deletion reduced high-frequency network oscillations (ripples) and pathological network discharges in hippocampal slices (Maier et al., 2002). However, no morphologic abnormalities corresponding to these functional changes were identified so far in Cx36-deficient mice (Buhl et al., 2003). Previously, in situ hybridization and Northern blot analyses have been carried out to localize Cx36 transcripts (see above). Furthermore, Feigenspan et al. (2001) applied confocal microscopy to verify Cx36 protein expression in retinal AII amacrine cells, which were identified based on their characteristic morphology after injection of neurobiotin and subsequently immunolabeled with anti-bodies to Cx36. Deans et al. (2001) verified Cx36 expression in subtypes of neocortical γ-aminobutyric acid (GABA)ergic interneurons by investigation of transgenic mice in which the Cx36 coding region was replaced by the ß-galactosidase coding lacZ gene and internal ribosome entry site (IRES)-controlled placental alkaline phosphatase (PLAP). By double staining for ß-galactosidase and parvalbumin or somatostatin, they were further able to document Cx36 expression in fast spiking (parvalbuminpositive) and low-threshold spiking (somatostatinpositive) neurons. Hormuzdi et al. (2001) localized Cx36 transcripts in GABAergic interneurons by means of single-cell reverse transcriptase polymerase chain reaction (RT-PCR) and in situ hybridization. Despite the various methods employed, our knowledge of cellular Cx36 protein expression is still limited. For example, various Cx36 antibodies described turned out to be partly nonspecific (Meier et al., 2002).

To analyze the function of Cx36 in individual tissues and cell types, conditional ablation in these cells would be desirable. Such an approach could help to circumvent compensatory mechanisms that might occur in general in Cx36-deficient mice (De Zeeuw et al., 2003). Thus, we have flanked exon2 of the Cx36 gene with two loxP sites, i.e., recognition sites of the Cre-recombinase. The floxed Cx36 (Cx36 fl) was constructed such that upon Cre-mediated deletion a lacZ reporter gene sequence would be placed under control of the Cx36 promoter (Cx36 del[LacZ]). The resulting genomic sequence was predicted to code for a functional fusion protein comprising the N-terminal part of Cx36 and ß-galactosidase (N36-ß-gal).

For hitherto unknown reasons, the floxed Cx36 allele was not expressed in these mice, thus precluding experiments of cell type-specific deletion. However, the ß-galactosidase activity of the lacZ reporter gene generated upon Cre-mediated re-combination was faithfully expressed and thus provided a useful tool to identify those cells in which the Cx36 gene is normally expressed.

Here, we report results obtained by mating the floxed Cx36 animals with mice in which the Cre-recombinase was ubiquitously expressed under control of the phosphoglycerate kinase (PGK) promoter. Together with in situ hybridization and immunofluorescence and immunohistochemical analyses, the N36-ß-gal detection by ß-galactosidase histochemistry allowed us to analyze Cx36 expression in different areas of the brain, in the retina, and in the pancreas and adrenal gland of adult heterozygous Cx36 del[LacZ] mice.

MATERIALS AND METHODS

All mice used for this study were kept under standard housing conditions with a 12-hour/12-hour dark-light cycle and with food and water ad libitum.

Cloning of targeting vector

The targeting vector was cloned by using a 9.8-kb fragment containing the mouse genomic Cx36 locus of pCx36 (Güldenagel et al., 2001). The final targeting construct (pJD1-LacZ) contained two homologous regions: 5' up-stream a 1.3-kb NheI/XbaI fragment and 3' downstream a 5.5-kb BbrPI/XhoI fragment. In the 5' part of the down-stream homologous region, a blunted Asp718I/BamHI 3.5-kb fragment from pSV-LacZ (Promega, Madison, WI) containing the coding region of ß-galactosidase was ligated to a blunted HindIII/BamHI 200-bp fragment of pCx36 containing the splice acceptor site of Cx36. Between the upstream homologous region and the modified downstream homologous region, several sequence sections were flanked by two loxP sites: a 310-bp eukaryotic spacer-fragment (KpnI/EcoRI from a plasmid containing the coding region of hCx30.2; unpublished results) used for a polymerase chain reaction (PCR)-mediated selection of homologous recombined ES cell clones, a 1.25-kb HindIII/BbrPI fragment containing the splice acceptor site ahead of exon2 of Cx36, a 150-bp SalI/EcoRI fragment harboring a SV40poly(A) signal, and a 1.95-kb Ecl136II/ SalI PGK-neomycin selection marker flanked by two frt sites (Meyers et al., 1998). The final targeting vector was analyzed after restriction mapping by partial sequencing at the AGOWA sequencing service (Berlin, Germany).

The functions of loxP and frt sites within the pJD1-LacZ vector were verified after transformation of Cre or Flp recombinase expressing E. coli bacteria (Buchholz et al., 1996). Splicing and activity of the fusion protein N36-ß-gal (25 N-terminal amino acids of Cx36 fused to the ß-galactosidase reporter protein) were tested by cloning the 4.5-kb SmaI/NcoI fragment of pJD1-LacZ/Cre into the expression vector pBEHpac18 (Horst et al., 1991). This vector was transiently transfected in HeLa cells (Teubner et al., 2000). Cells were fixed 3 days later and stained for ß-gal activity (results not shown). The function of the floxed Cx36 was tested by immunofluorescence analysis of HeLa cells after transient transfection of the vector pBEHpac18 including a SmaI/EcoRV fragment of pJD1-LacZ (data not shown).

Cell culture and screening of ES cell clones

DNA (300 pg) of the targeting vector pJD1-LacZ was linearized by NotI digestion and transfected by electroporation (800 V, 3 pF) in feeder-independent HM-1 embryonic stem (ES) cells (Magin et al., 1992). Cell culture and selection of transfected colonies were performed according to Theis et al. (2000) using 350 pg G418 (Sigma, St. Louis, MO) per ml of medium. Genomic DNA of G418-resistant ES cell clones was prepared and processed for PCR analysis using a 5' upstream primer external to the targeting vector (Cx36t-USP; 5'-CTACTTAAGGGCGGATTAGAGGCG, Güldenagel et al., 2001) and a spacer fragment-specific downstream primer (DSP Spacer1 5'-GAGTGAATTGTACCGGATGTGTGG). PCR conditions were as follows: 95°C for 15 minutes, 40 cycles with 95°C for 30 seconds, 66°C for 45 seconds, 72°C for 1.30 minutes, and finally 72°C for 10 minutes. PCR was carried out on a Peltier PTC200 thermocycler (Biozym, Oldendorf, Ger-many) using Taq DNA polymerase (Promega). The resulting amplicon had an estimated size of 1.6 kb. For genomic Southern blot hybridization, DNA from PCR-positive clones was digested with KpnI (exernal probe) or XbaI (internal probe) electrophoretically separated on 0.7% agarose gels, blotted onto Hybond N+ membranes (Amersham Biosciences, Bucks, UK), and fixed by ultraviolet (UV) crosslinking. A 860-bp XhoI/HindIII fragment (Güldenagel et al., 2001) served as an external hybridization probe; the internal probe was a 722-bp SmaI/ PstI exon1/intron-specific fragment. Hybridization was performed under stringent conditions (two washes in 0.1% sodium dodecyl sulfate [SDS] in 0.5X SSC at 60°C for 15 minutes) using Quick Hyb hybridization solution (Stratagene, La Jolla, CA) according to the manufacturer's instructions. After KpnI digestion and hybridization to the external probe, the Cx36 wild-type allele had an estimated size of 8.5 kb compared with 15 kb of the targeted Cx36 allele. After an XbaI digestion and hybridization with the internal probe, both alleles had an estimated size of 1.6 kb.

Generation and genotyping of Cx36del[LacZ] mice

Homologous recombined ES cell clones were prepared for injection into C57BL/6 blastocysts as described by Theis et al. (2000). Blastocyst injection resulted in the birth of coat-color chimeric mice, which were subsequently crossed with C57BL/6 mice. Agouti offspring were checked for germline transmission of the mutated allele (Cx36 fl), using tail DNA for PCR analysis. Mice heterozygous for the Cx36 fl allele were mated with hACTB:FLPe mice (Rodriguez et al., 2000), resulting in offspring deficient for the frt site-flanked PGK neomycin selection cassette (Cx36 fldN) due to Flp/frt-mediated deletion (Andrews et al., 1985). Mice heterozygous for the Cx36 fl or Cx36 fldN allele were interbred with PGK-Cre mice (Lallemand et al., 1998). Half of this offspring were heterozygous for the Cx36del[LacZ] allele in which the loxP site-flanked region was deleted from the targeted locus. In these mice, the Cx36 del[LacZ] allele led to expression of a functional N36-β-gal protein, which allowed identification of cells in which the Cx36 exon2-containing coding region had been replaced by the coding region of β-galactosidase. All heterozygous mice were further crossed back to the C57BL/6 mouse strain.

RT-PCR analysis

Mice of defined genotype, verified by PCR analysis of DNA from tail-tip biopsies, were sacrificed by cervical dislocation. Brains were quickly dissected and homogenized in 5 ml TRIzol (Invitrogen, Carlsbad, CA). Total RNA was isolated according to the manufacturer's protocol. Two micrograms of total RNA were reverse transcribed by using oligo-dT primers and AMV reverse transcriptase (Gibco-BRL) as described in the manufacturer's protocol. One hundred nanograms of this cDNA was used to perform PCR reactions using the RedTaq PCR-mix (Sigma) and the following Cx36 intron spanning primers: the Cx36 upstream primer was 5'-TACTGCCCAGTCTTTGTCTGCTGC, and the Cx36 downstream primer 5'-CACACCATTATGATCT-GGAAGACC. The PCR was performed at 95°C for 5 minutes, 40 cycles at 95°C for 5 minutes, 55°C for 1 minute, 72°C for 2 minutes, and finally 72°C for 10 minutes. Probes were separated on 1.5% agarose gel, and amplicons were visualized by ethidium bromide staining. Gels were scanned by using ImageMaster (Amersham Biosciences, Freiburg, Germany).

Immunoprecipitation and immunoblotting

Mouse eyes were dissected on ice, and retinae were immediately frozen in liquid nitrogen and stored at -70°C until further use. The tissue was solubilized in RIPA buffer (10 mM NaH_2PO_4/Na_2HPO_4, 0.1% SDS, 1% Triton X-100, 0.1% sodium deoxycholate, 40 mM sodium

fluoride) supplemented with protease inhibitor cocktail 1X Complete (Roche, Mannheim, Germany) at a final concentration of 20 µg/µl. Samples were incubated for 20 minutes on ice. Every 5 minutes, they were sonicated for 20 seconds. Lysates were centrifuged at 13,000 rpm for 30 minutes at 4˚C, and supernatants were precleared by incubation with 40 pl sepharose CL4B beads (Amersham Biosciences) at 4˚C for 30 minutes. The protein concentration of the precleared supernatants was determined by using the bicinchoninic acid protein assay (Sigma), and aliquots were diluted in RIPA buffer. For immunoprecipitation, rabbit Cx36 antibodies (Zytomed, Berlin, Ger-many) were incubated with 10 µl protein A sepharose beads (Amersham Biosciences) for 30 minutes at 4˚C. Then 250 pl of lysate (350 pg of protein) were added to the beads and incubated at 4˚C for 4 hours. The beads were washed three times in RIPA washing buffer (10 mM NaH_2PO_4/Na_2HPO_4, 1 M NaCl, 10 mM EDTA, 40 mM sodium fluoride, 0.2% Triton X-100) and once in distilled water. The pellet was resuspended in 15 pl SDS-polyacrylamide gel electrophoresis (PAGE) loading buffer, and the supernatant was loaded on 2% SDS-polyacrylamide gels. Separated proteins were transferred to 0.45 pm polyvinylidene difluoride membranes (Millipore, Bedford, MA) by blotting in transfer buffer (25 mM Tris, 192 mM glycine, pH 8.3, in 20% [v/v] methanol/H_2O). Membranes were incubated in blocking solution (20 mM Tris, pH 7.4, 150 mM NaCl, 0.1% Tween 20 [TBS-Tween], and 5% skim milk powder) at RT for 2 hours and then incubated with Cx36 antibody (1:500) at 4˚C overnight. After incubation with primary antibody, membranes were washed for 1 hour in blocking solution, followed by incubation with anti-rabbit horseradish peroxidase-conjugated secondary antibodies (Dianova, Hamburg, Germany) diluted 1:12,000 in blocking solution at room temperature (RT) for 1 hour. Blots were washed twice in TBS-Tween and once in TBS and then incubated for 2 minutes with ECL chemiluminescence reagents (Amersham Biosciences).

In situ hybridization

Adult Cx36+/del[LacZ] mice and matched controls were deeply anesthetized with Nembutal (75 mg/kg, i.p.), and brains were carefully removed, frozen on dry ice, and stored at -80˚C. Fourteen-micrometer sections were cut on a cryostat, mounted on poly-lysine–coated glass slides, and stored at -80˚C. For in situ hybridizations, slides were fixed for 5 minutes in 4% paraformaldehyde and acetylated in 1.4% triethanolamine and 0.25% acetic anhydride. Sections were then prehybridized for 1 hour in buffer containing 50% formamide, 5x SSC, 5x Denhardt's solution, 250 pg/ml yeast tRNA (Sigma), and 500 pg/ml acid-alkali cleaved salmon testis DNA (Sigma). Hybridization was performed overnight at 65˚C in prehybridiza-

tion buffer containing 100 ng/ml digoxigenin (DIG)-UTP labeled cRNA probes. Probes were generated using a DIG RNA labeling kit (Roche) according to the manufacturer's instructions. Sense and antisense probes generated to the full-length coding sequence of Cx36, and the full-length coding sequence of lacZ reporter gene were then hydrolyzed in 40 mM $NaHCO_3$, 60 mM Na_2CO_3 for 25 minutes at 60°C to generate fragments of ~300 bases. Following hybridization, sections were washed in 0.2X SSC at 65°C, blocked in 0.1 M Tris-HCl, pH 7.5, 0.15 M NaCl, and 10% heat inactivated sheep serum (Sigma) for 1 hour at room temperature. Alkaline phosphatase conjugated digoxigenin antibodies (Roche) were added to the sections at a dilution of 1:5,000 in 0.1 M Tris-HCl, pH 7.5, 0.15 M NaCl, 1% heat-inactivated sheep serum and incubated overnight at 4°C. Following washing of the sections, color reactions were performed in 0.1 M Tris-HCl, pH 9.5, 0.1 M NaCl, 50 mM $MgCl_2$, 2 mM Levamisole (Sigma), 0.35 mg/ml nitro-blue tetrazolium (Roche), and 0.18 mg/ml 5-bromo-4-chloro-3-indolylphosphate (Roche). Reactions were terminated once an intense reaction product had developed (after ~18 hours), counterstained in 0.1% Fast red, dehydrated, and mounted in Permount (Fisher, Fair Lawn, NJ).

ß-galactosidase staining, histological, and Cx36 immunohistochemical analyses

Adult Cx36 del[LacZ] mice and adequate controls were deeply anesthetized with either Hypnodil and Nembutal or Rompun (0.2%) and Ketavet (0.5%) (10 ml/kg). For cryosectioning, animals were transcardially perfused with saline (20 mM phosphate buffer, 0.9% NaCl, pH 7.4) and 4% paraformaldehyde in 0.1 M phosphate buffer. Brains were cryoprotected in 30% sucrose in PBS and embedded in 11% gelatin or 2% agarose in PBS. Other organs were frozen on dry ice and embedded in Tissue-Tec (Sakura, Zoeterwoude, The Netherlands). Twelve to 20-µm-thick slices were prepared by using a cryostat (MICROM HM 500 OM), and 400-pm slices were cut from brains embedded in 2% agarose with a vibratome (Leica VT1000S). To analyze the expression of the reporter protein N36-ß-gal, sections were fixed for 5 minutes in 0.2% glutaraldehyde in 0.1 M Na-phosphate buffer (pH 7.4) containing 1.25 mM $CaCl_2$ and 2 mM EGTA. Sections were washed three times in the same buffer supplemented with 0.1% Triton X-100 and incubated overnight with X-gal staining solution (buffer as before, supplemented with 5 mM $K_3[Fe(CN)_6]$, 5 mM $K_4[Fe(CN)_6]$, and 0.1% X-Gal [5-bromo-4-chloro-3-indolyl-ß-galactosidase]) at 37°C overnight. Subsequently, the 20-µm sections were stained with 0.1% eosin and mounted with Entellan (Merck, Darmstadt, Germany). Vibratome sections were photographed with a digital camera (Leica DC 150) combined with a binocular (Leica MS 5). Cryosections were documented by using an axiophot (Zeiss) equipped with the axiocam color HR (Zeiss).

For immunohistochemical analysis of Cx36 in combination with β-gal staining, brains were dissected, cut into frontal brain blocks, covered in tissue freezing medium (Leica, Nussloch, Germany), and frozen in 8% methylcyclohexan in 2-methylbutane (v/v; -60°C). Cryosections of 14 μm thickness, mounted on Superfrost Plus slides (Merck), were heat dried for 1 hour at 40°C prior to fixation. For simultaneous detection of Cx36 protein and N36-β-gal expression, sections were fixed in -20°C cold ethanol for 10 minutes, rinsed three times in Ca^{2+}, Mg^{2+}-free PBS (BioWhittaker Europe, Verviers, Belgium; PBS-), and preincubated in blocking buffer (10% normal goat serum and 0.1% Triton X-100 in PBS-) for 1 hour. Polyclonal Cx36 antibodies (Teubner et al., 2000) were diluted in blocking buffer, and sections were incubated at RT for 16 hours. Samples were then rinsed three times for 10 min in PBS-, followed by a 30-minute blocking step in 0.2% BSA in PBS-. Incubation with secondary antibodies (Alexa Fluor™ 488 goat anti-rabbit, Molecular Probes, Leiden, Netherlands) was performed at a 1:4,000 dilution in blocking buffer at RT for 2 hours, followed by three washes in PBS- (5 minutes each). Sections were then postfixed in 4% paraformaldehyde in 100 mM phosphate buffer, pH 7.4, (4% PFA) for 15 minutes and subsequently rinsed in PBS-. Sections were washed in 2 mM MgCl2, 0.01% sodium deoxycholate, and 0.02% Nonidet P-40 in PBS-(LacZ buffer), followed by incubation in 0.1% X-Gal, 5 mM potassium ferricyanide, and 5 mM potassium ferrocyanide in lacZ buffer at 37°C for 6 hours. Afterwards, sections were rinsed three times in PBS- (5 minutes each), post-fixed in 4% PFA for 10 minutes, and washed again in PBS- (three times 5 minutes). Sections were finally rinsed in water and subsequently mounted by using the ProLong Antifade Kit (Molecular Probes).

Fluorescence was documented by using confocal imaging microscopy (Zeiss LSM510 META inverted confocal microscope). Data were collected as single planes, documenting 488-nm fluorescence as well as Nomarski optics by using a multitrack scanning module. All data were exported as TIFF files into Adobe Photoshop 7.0 (Adobe, San Jose, CA) for documentation.

For immunostaining of neuronal marker proteins, brains of adult Cx36+/del[LacZ] mice and control animals were cryoprotected, embedded in TissueTek, and sectioned as described above. Immunohistochemical analyses were performed as described by Maxeiner et al. (2003), by using the following antibodies (dilution and supplier in parentheses): anti-parvalbumin (clone Parv-19, 1:100; Sigma) and anti-insulin (clone K36aC10, 1:100; Sigma). The glutamic acid decarboxylase (GAD) staining was performed as described by Oertel et al. (1981).

Semithin sections

Adult mice were deeply anesthetized using ketamine (Ketolar 50 mg/100 g body weight) and transcardially perfused with a solution of 2.5% glutaraldehyde and 1.5% formaldehyde in 0.1 M sodium phosphate buffer, pH 7.4, at 38°C for 30 minutes. Fixation was followed by a 10-minute perfusion with 0.15 M sucrose in 0.1 M phosphate buffer, pH 7.4, at room temperature. The brains were dissected, embedded in 2% agarose dissolved in the previous buffer, coronally cut into 2-mm slices, postfixed in 4% osmium tetroxide, dehydrated in ethanol, and embedded in araldite. Slices containing the inferior olivary nuclei, the cerebellum, and the olfactory bulb were prepared for semithin sectioning, series of which were stained in a 1% toluidine blue solution.

RESULTS

Construction of the targeting vector and generation of transgenic mice

To generate conditional Cx36 deficient mice, we flanked exon2 of Cx36 by two loxP-sites. We also inserted a PGK-neomycin selection cassette, flanked by two frt sites, into the targeting vector pJD1-LacZ (Figure 1A). The resulting strain of transgenic mice (Cx36 fl) was interbred with mice ubiquitously expressing the Flp-recombinase (Rodriguez et al., 2000), in order to obtain mice, in which the PGK-neomycin selection cassette was excised from the genome (designated Cx36 fldN mice; Figure 1A). In both Cx36 fl and Cx36 fldN mice, only the recombined Cx36, but not the inserted reporter gene, was expected to be expressed. Alternatively, in mice originating from crosses of Cx36 fl or Cx36 fldN mice with animals ubiquitously expressing the Cre-recombinase under control of regulatory elements of the PGK promoter (PGK-Cre; Lallemand et al., 1998), exon2 of Cx36 (in Cx36 fldN animals) or exon2 and the selection cassette (in Cx36 fl animals) were expected to be excised; these animals were therefore designated Cx36 del[LacZ] (Figure 1A). Successful recombination of the different genotypes expected was verified by PCR (Figure 1B) and Southern blot analysis (Figure 1C). Regarding Cx36 del[LacZ] mice, a functional reporter fusion protein was expressed under regulatory elements of the Cx36 promoter to mimic Cx36 expression after excision of the Cx36 coding region on exon2. This endogenously expressed reporter protein comprised the Cx36 N-terminus encoded by exon1 and the inframe cloned ß-galactosidase protein (reporter protein N36-ß-gal).
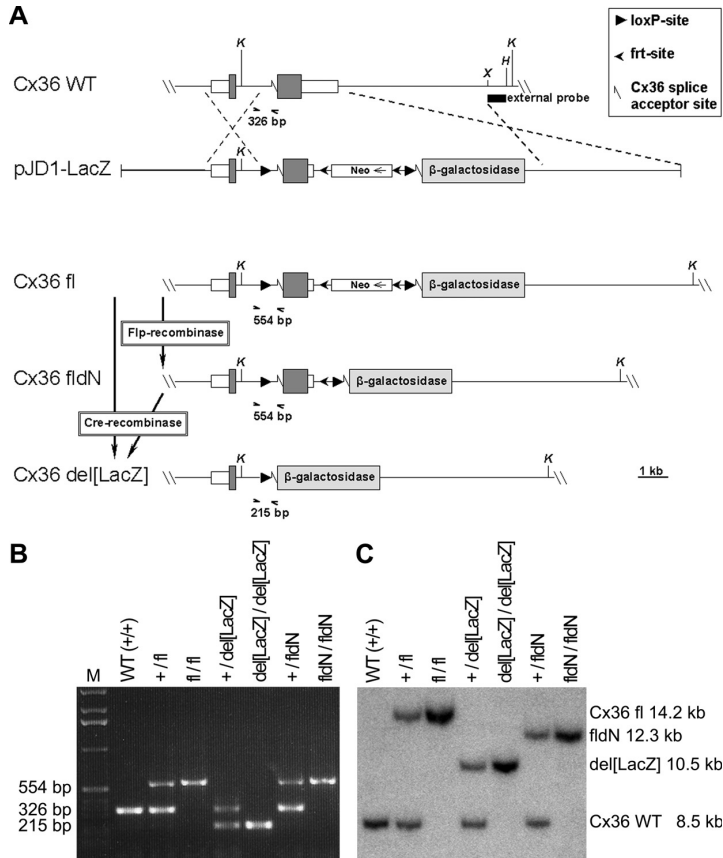
Figure 1. Targeting scheme of the floxed Connexin36 allele before and after recombination. A. The vector pJD1-LacZ was transfected in HM1 mouse ES cells, checked by PCR and Southern blot analysis for homologous recombination (data not shown), and injected in C57BL/6 blastocysts. In this floxed Cx36 allele (Cx36 fl) the frt-sites flanked selection cassette can be deleted with Flp-recombinase activity (Cx36 fldN). After Cre-recombinase activity, either the loxP-flanked exon2 of Cx36 (shaded box) in case of the Cx36 fldN allele or exon2 and the frt-flanked selection cassette in case of the Cx36 fl allele are deleted, resulting in generation of the Cx36 del[LacZ] allele. In mice carrying this allele, the reporter gene β-galactosidase is accordingly expressed under the control of Cx36 regulatory elements as a fusion protein of the exon1 coded N-terminal part of Cx36 and the β-galactosidase (N36-β gal). The black bar indicates the sequence of the external probe used for Southern blot hybridization. K, KpnI; X, XhoI; H, HindIII. **B.** Tail-tip DNA was used for PCR analysis to discriminate different genotypes of the recombined Cx36 allele. A 554-bp amplicon represents the Cx36 fl or Cx36 fldN allele, a 326-bp amplicon indicates the wild-type allele, and a 215-bp amplicon shows the presence of the Cx36 del[LacZ] allele. **C.** The expected fragments after KpnI digestion and Southern blot hybridization of DNA using the external probe (see A). +, Cx36 wild-type allele; fl, floxed Cx36 (Cx36 fl); del [LacZ], deleted Cx36 exon2 after Cre-recombinase activity and N36-β-gal expression; fldN, floxed Cx36 after Flp-recombinase activity without frt-flanked PGK-neomycin cassette; M, 1-kb ladder standard (Gibco-BRL).

Thus, N36-β-gal expression from this recombined transgene labeled sites of normal Cx36 expression after deletion of Cx36 exon2.
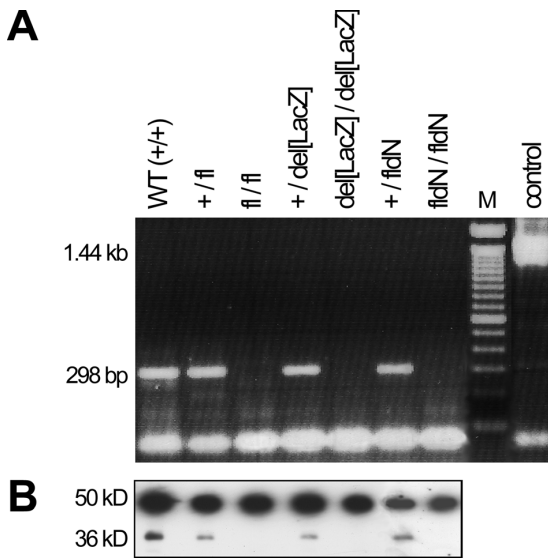
Figure 2. Expression analysis of the recombined Cx36 allele using RT-PCR and immunoprecipitation. A. RT-PCR analysis of total mRNA from whole brain of adult mice using intron spanning primers for Cx36. Only a 298-bp amplicon reflecting the transcript of the Cx36 wild-type allele was found, indicating that the transgene and its recombination-induced variant of Cx36 were not expressed. **B.** Immunoprecipitation using protein lysate from whole retinae of adult mice with polyclonal antibodies to the Cx36 protein. Only in mice harboring at least one wild-type allele could Cx36 protein be detected. Control for RT-PCR, 1 ng of plasmid DNA pCx36 including the intron sequences; +, Cx36 wild-type allele; fl, floxed Cx36 allele (Cx36 fl); del[LacZ], deleted Cx36 allele after Cre-recombinase activity; fldN, floxed Cx36 allele with deleted selection marker after Flprecombinase activity; M, 100-bp ladder standard (Gibco-BRL).

Cx36 transcript and protein are not expressed in Cx36 floxed mice

Transcription and protein expression of the floxed Connexin36 alleles were analyzed by RT-PCR (Figure 2A) and immunoprecipitation (Figure 2B), respectively. Neither recombined Cx36 mRNA nor Cx36 protein could be detected in homozygous Cx36 fl or Cx36 fldN mice. In contrast, we consistently detected a 298-bp amplicon upon RT-PCR analysis and a protein signal with an apparent molecular mass of about 36 kDa upon immunoprecipitation of material from mice carrying a single Cx36 wild-type allele, regardless of the exact genotype of these animals. Therefore, we concluded that Cx36 is not expressed from the recombined ("floxed") Cx36 locus under *in vivo* conditions and that these animals in fact correspond to functional knockout mice. Thus, both conditional Cx36 fl and Cx36 fldN mouse strains are not suitable as conditional Cx36-deficient mice. Nevertheless, the expression pattern of the N36-β-gal reporter protein within the strain Cx36 del-[LacZ] closely mirrored that of previously described Cx36 mRNA and protein distribution (Condorelli et al., 2000; Deans et al., 2001 and 2002). Therefore these Cx36 del-[LacZ] mice were used to analyze the cell type-specific expression of Cx36 as well as to explore its coexpression with other proteins.

Expression of the lacZ reporter gene in adult Cx36+/del[LacZ] mice

Neuronal tissues. In the retina, N36-ß-gal activity was detected as four distinct rows of blue signals located in three different layers (Figure 3). Intense ß-gal staining was prominent in the ganglion cell layer. In the inner nuclear layer, N36-ß-gal–positive somata of cells were distributed in two sublayers at its internal and external border. A fourth row of moderate N36-ß-gal staining was observed in the external part of the outer nuclear layer, at the region linking the outer segments of photoreceptor cells with their somata. This localization points to a lower level of Cx36 expression in certain mouse photoreceptor cells.

Our reporter gene analysis suggested that Cx36 is abundantly expressed in the central nervous system (CNS), including the spinal cord, the olivocerebellar system, several brainstem nuclei, the thalamus, the hippocampus, and the olfactory system. In the olivocerebellar system, N36-ß-gal positive cells were prominent in the inferior olive as well as in the deep cerebellar nuclei of adult Cx36+/del[LacZ] mice.
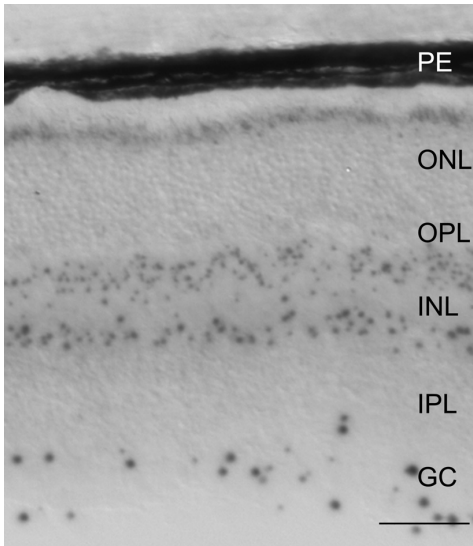
Figure 3. N36-ß-gal expression in the retina of adult Cx36+/del[LacZ] mice. Cryosection of the whole eye from adult Cx36+/del[LacZ] mice, stained with ß-gal and counterstained with eosin. Punctated rows of N36-ß-gal–positive cells are prominent in the ganglion cell layer (GCL) and in two lines of the inner nuclear layer (INL) and are relatively faint in the layer of the outer photoreceptor segments adjacent to the outer nuclear layer (ONL). PE, pigment epithelium; ONL, outer nuclear layer; OPL, outer plexiform layer; INL, inner nuclear layer; IPL, inner plexiform layer; GC, ganglion cell layer. Scale bar = 20 µm.

To demonstrate the reliability of expression analysis by mapping of N36-ß-gal activity, the expression pattern of the reporter gene transcript was compared with that of the Cx36 transcript. As expected, both lacZ and Cx36 transcripts were expressed in corresponding areas in olivary (Figure 4A–D) and cerebellar nuclei (Figure 4E,F). Thus, N36-ß-gal activity was documented after processing of 400-µm vibratome sections that showed expression in different nuclei of the inferior olive, including the cap of Kooy and the ß-subnucleus (Figure 5A). To check further the reliability of reporter gene-driven ß-gal expression as an indicator of cognate Cx36 expression, we compared the simultaneous expression of Cx36 protein and

N36-ß-gal activity in adult Cx36+/del[LacZ] mice, combining immunohistochemical detection of Cx36 protein with histochemistry for N36-ß-gal activity. Because ß-gal protein usually shows a cytoplasmatic and perinuclear localization (Maxeiner et al., 2003), whereas Cx36 protein typically localizes to cell membranes,
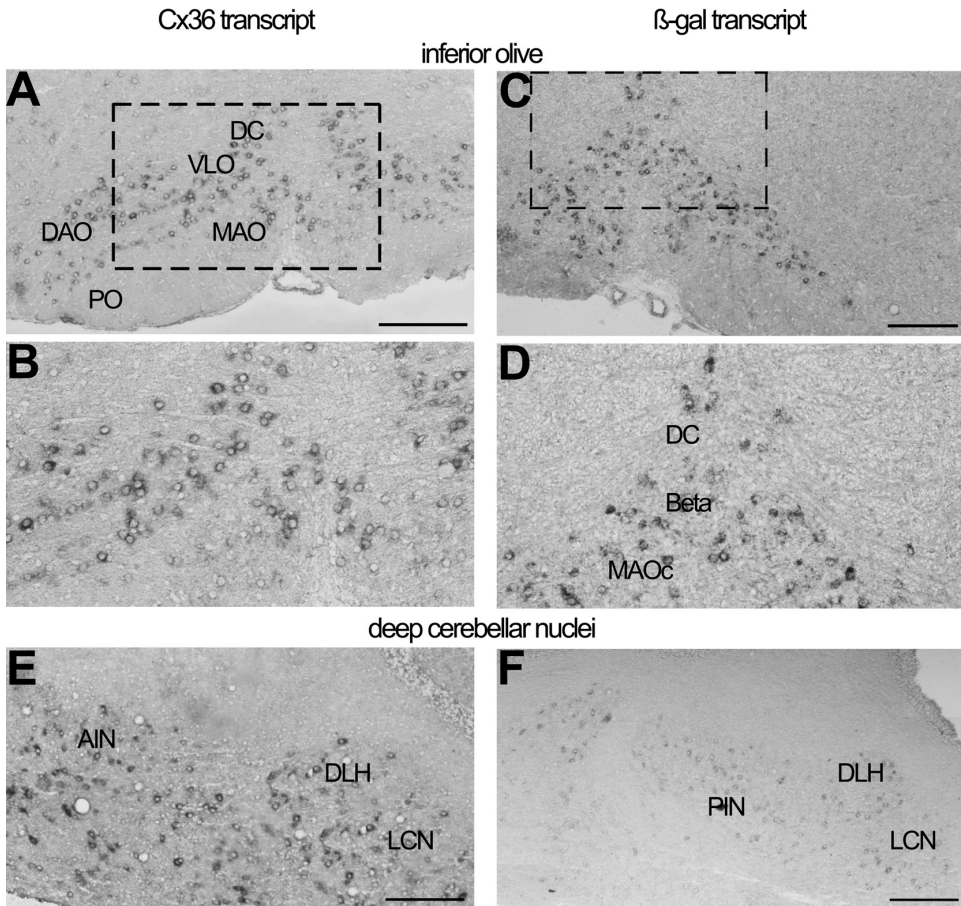
**Figure 4. Distribution of mRNA coding for Cx36 and ß-gal in the inferior olive and in deep cerebellar nuclei of Cx36+/del[LacZ] mice using in situ hybridization. A.** Inferior olive following in situ hybridization (DIG labeling) with an antisense probe directed against Cx36 mRNA. **B.** Higher power view of the area boxed in A. **C.** The inferior olive following *in situ* hybridization with an antisense probe directed to ß-gal mRNA. **D.** Higher magnification view of the area boxed in C. For comparison, the dorsal cap and medial accessory olive were included in micrographs A and C, although *in situ* hybridization showed labeling in all nuclei of the inferior olive for Cx36 and LacZ transcripts. **E,F.** Labeling of deep cerebellar nuclei following in situ hybridization with an anti-sense probe directed against Cx36 mRNA (E) or ß-gal (F). Abbreviations: AIN, anterior interposed nucleus; DLH, dorsal lateral hump; DLP, dorsolateral protuberance; LCN, lateral cerebellar nucleus; MCN, medial cerebellar nucleus; PIN, posterior interposed nucleus. Scale bar = 100 µm. Abbreviations: Beta, beta subnucleus; DAO, dorsal accessory olive; DC, dorsal cap; MAO, medial accessory olive; MAOc, medial accessory nucleus group C; PO, principal olive; VLO, ventrolateral outgrowth.

we expected labeling of different subcellular compartments by applying both methods in parallel. To correlate ß-gal staining and immunodetection of Cx36 protein, we focused on those areas of the CNS where morphology and projection of Cx36-expressing cells are well established (cf. Condorelli et al., 2000; De Zeeuw et al., 2003). In the nuclear complex of the inferior olive, Cx36 protein and N36-ß-gal were shown to be coexpressed in the cap of Kooy (IOK, Figure 5C,D), whereas in the principal nucleus of the inferior olive, only Cx36 protein but no N36-ß-gal reaction product was detected (Figure 5F,G).
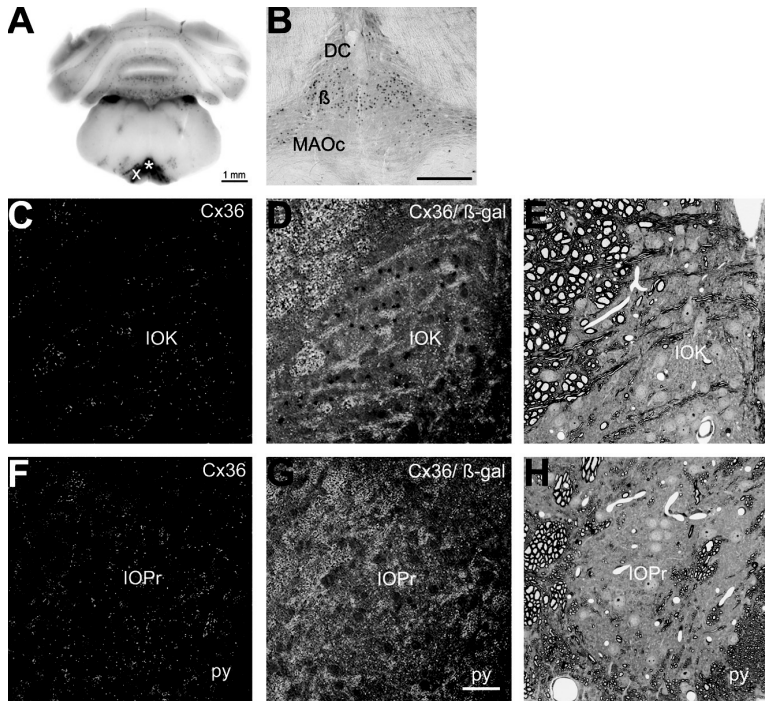
Figure 5. ß-Galactosidase staining and Cx36 immunoreactivity in the cap of Kooy (IOK) and the principal nucleus (IOPr) of the inferior olive. A. Overview showing a strong blue staining of the N36-ß-gal reaction product in a 400-µm vibratome section comprising the inferior olive. The cap of Kooy is marked by an asterisk (*) and the principal nucleus by an x. **B.** Combined staining on sections for glutamic acid decarboxylase (GAD) and N36-ß-gal indicated that blue-stained areas are not GAD-positive. ß, beta subnucleus; DC, dorsal cap; MAOc, medial accessory nucleus group C. **C,D,F,G.** Double staining for Cx36 immunoreactivity and N36-ß-gal activity documented by fluorescent and Nomarski optics in a cryosection. In the cap of Kooy (IOK), a specific punctate Cx36 immunostaining is present (C), and many dark blue spots of N36-ß-gal reaction products are observed in the same nuclear region as shown in the merged image (D). The nuclear area of the cap of Kooy including some traversing myelinated fibers is shown in the semithin section of the corresponding area (E). In the principal nucleus (IOPr), specific punctate Cx36 immunostaining could be detected (F); however, the merged image (G) demonstrates the presence of immunoreactivity, but no N36-ß-gal staining. Fine structure of the principal nucleus adjacent to the pyramidal tract (py) is documented in a semithin section of the corresponding area (H). Scale bar = 200 µm in B; 20 µm in G (applies to C–H).
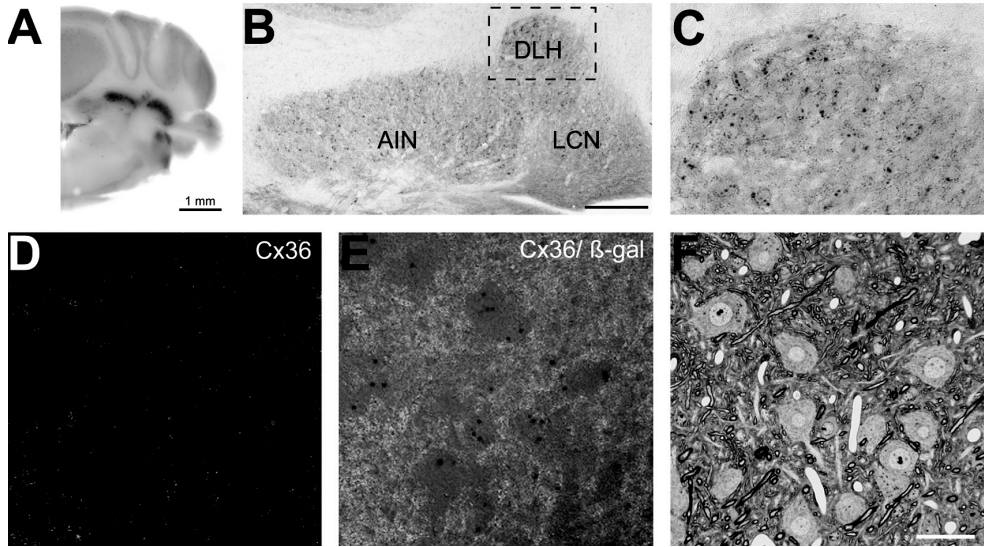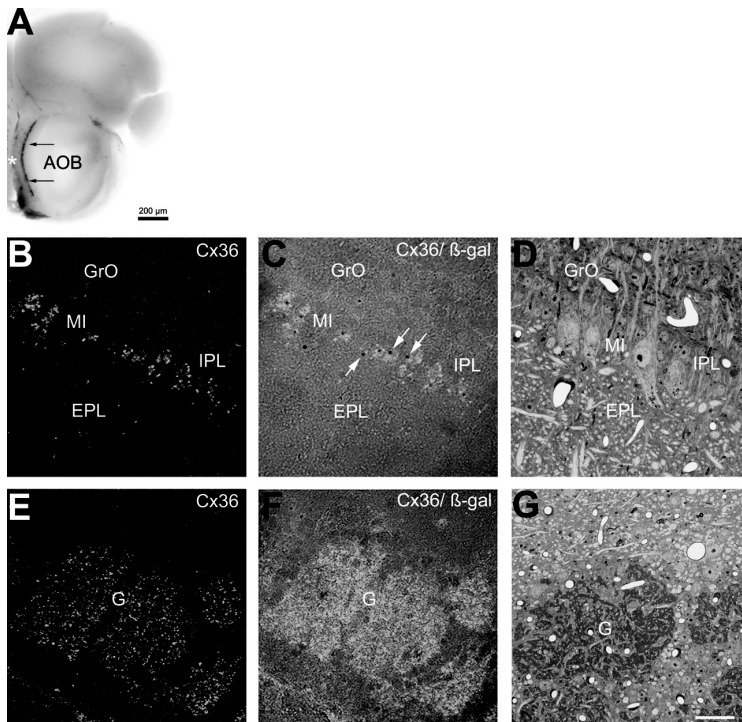
Figure 6. ß-Galactosidase staining and Cx36 immunofluorescence in the cerebellar nuclei. A. Overview, showing the strong blue signals of the N36-ß-gal reaction product in a 400-µm vibratome section through various cerebellar nuclei. The lateral cerebellar nucleus is marked by an x. **B.** Combined staining for glutamic acid decarboxylase (GAD) and N36-ß-gal indicates that blue-stained structures are also GAD-positive. **C.** Area of higher magnification, boxed in B, showing GAD-positive terminals on the soma of the N36-ß-gal-expressing neurons. AIN, anterior interposed nucleus; DLH, dorsal lateral hump; LCN, lateral cerebellar nucleus. **D,E.** Double staining of Cx36 immunoreactivity (D) and N36-ß-gal reaction product in the lateral cerebellar nucleus documented by a merged image of fluorescence and Nomarski optics (E) of cryosections. It exhibits no specific Cx36 immunostaining but several blue spots of the N36-ß-gal reaction product, which are visualized in large neurons. Fluorescence is located outside the neurons, as evident from a semithin section of the corresponding area (F) is due to nonspecific staining of myelin. Scale bar = 200 µm in B; 20 um in F (applies to D-F).

The specificity of these immunopositive signals, obtained with well-characterized antibodies to Cx36 (Meier et al., 2002), was verified by using sections of homozygous Cx36-deficient mice (Cx36del[LacZ]/del[LacZ]) as controls (data not shown). By comparison with the corresponding semithin sections (Figure 5E), blue N36-ß-gal staining (Figure 5D) was assigned to neurons of the IOK, and the absence of N36-ß-gal reaction product (Figure 5G) was shown not to be confined to any specific cellular structure of the IOPr (Figure 5H). Given the functional relationship between the inferior olive and the cerebellum, expression analysis was also performed on cerebellar nuclei. In 400-µm vibratome and 20-µm sections of the cerebellum, N36-ß-gal staining was very intense in the deep cerebellar nuclei (Figure 6A). To clarify the neuronal subtype expressing N36-ß-gal in the deep cerebellar nuclei of adult Cx36+/del[LaZ] mice, we performed GAD-staining (Figure 6B,C) to visualize GABAergic neurons.

GAD-positive structures were also positive for N36-ß-gal staining, pointing to the expression of Cx36 in GABAergic neurons. We also investigated whether the observed N36-ß-gal activity also related to translation of native Cx36 protein. In the lateral cerebellar nucleus, representing the results of all cerebellar nuclei, a large number of blue stained cells but no Cx36 immunosignals were detected, suggesting that Cx36 is at least transcribed (Figure 4E) but presumably not translated within this cerebellar area (Figure 6D,E).

Figure 7. ß-Galactosidase staining and Cx36 immunofluorescence in the mitral cell layer and the glomerular layer of the accessory olfactory bulb. A. Overview of a 400-µm vibratome section of the accessory olfactory bulb (AOB) indicates the localization of the dark blue N36-ß-gal staining in the mitral cell layer (black arrows) and the glomerular layer, marked by an asterisk (*). **B,C.** Double staining of a cryosection showing the mitral cell layer (MI) containing Cx36 immunoreactivity (B) and N36-ß-gal reaction product as documented by a merged image of fluorescent and Nomarski optics (C). The immunoreactivity exhibits a punctate Cx36 immunolabeling, frequently out-lining the plasma membrane of large mitral cells. N36-ß-gal reaction product (white arrows) is mainly restricted to the mitral cells, shown in C. The granule cell layer (GrO), internal plexiform layer (IPL), and external plexiform layer (EPL) are immunonegative. **D.** The corresponding semithin section allows precise identification of the accessory olfactory bulb layers. **E,F.** In the glomerular layer, a dense punctate Cx36 immunostaining (E) was detected in the glomeruli (G) but no N36-(3-gal reaction (F). Some immunonegative neurons adjacent to the glomeruli exhibit N36-ß-gal reaction product. The semi-thin section of the glomerular layer shows the fine structure of the area (G). Scale bar = 20 µm in G (applies to B-G).

Cortex | Reticular thalamic nucleus
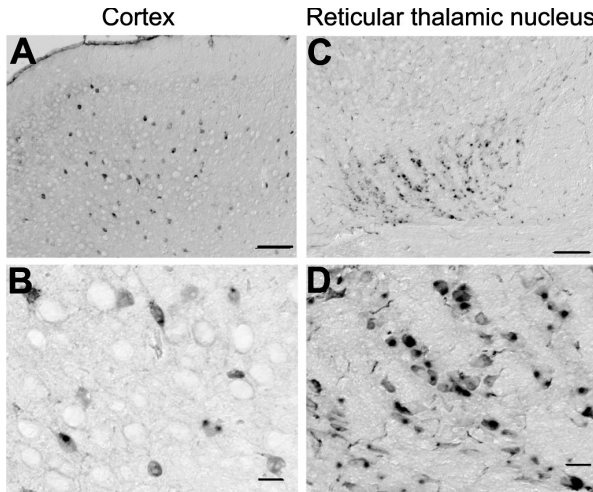
Figure 8. Immunohistochemical analysis of cells expressing N36-ß-gal with antibodies directed to parvalbumin in different regions of the brain. A. In the cortex, about 50% of parvalbumin-positive cells (brown) also express N36-ß-gal reaction product (blue), and all N36-ß-gal-expressing cells are parvalbumin-positive. B: Higher power view of A. C: This concordance between expression of parvalbumin and N36-ß-gal is also apparent in the reticular thalamic nucleus. D: Higher power view of C. Scale bar = 100 µm in A,C; 20 µm in B,D.

By comparison with the corresponding semithin section (Figure 6F), the blue N36-ß-gal product (Figure 6E) can be assigned to large neuronal cell bodies. Taken together, Cx36 protein was shown to be localized in all olivary nuclei, although differently expressed, but not in neurons of the deep cerebellar nuclei, whereas the N36-ß-gal reporter protein was present in many but not all nuclei of the inferior olive but in all deep cerebellar nuclei. In the olfactory system, numerous N36-ß-gal–positive cells were found in the main and accessory olfactory bulb, in the mitral cell layer (MI), and in the outermost part of the external plexiform layer (EPL) upon analysis of 400-µm vibratome sections (Figure 7A). Combined analysis of immunofluorescence and ß-gal staining (Figure 7B,C) demonstrated that in the MI, Cx36 immunoreactivity co-localized with the N36-ß-gal blue staining (Figure 7C).
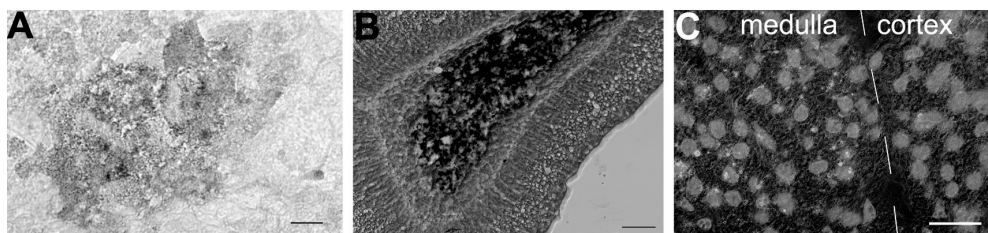
Figure 9. Analysis of Cx36 expression in the pancreas and the adrenal gland. A. Cryosection of the pancreas from an adult Cx36+/del[LacZ] mouse stained for ß-gal activity and counterstained using monoclonal antibodies to insulin, visualized by the immunohistochemical DAB reaction. The cellular cluster demonstrates coexpression of the N36-ß-gal reporter protein and insulin in insulin-secreting ß-cells of the endocrine pancreas. **B.** Section of the adrenal gland from an adult Cx36+/del[LacZ] mouse stained for ß-gal activity and counterstained with eosine. The N36-ß-gal reaction product in the medulla of the adrenal gland indicates expression of Cx36. **C.** Immunofluorescence analysis with antibodies to the Cx36 protein (green) and counterstaining of the nuclei with Hoechst (blue). Cx36-expressing cells are restricted to the medulla, whereas cortical cells are not immunostained. Scale bar = 20 µm in A,C; 100 µm in B.

By comparison with semithin sections of the corresponding area, the blue signals of the N36-ß-gal reaction product (Figure 7C) were assigned to large mitral cells (Figure 7D). Whereas the MI consists mainly of mitral cells and a few granule cells, the EPL contains van Gehuchten cells as well as tufted cells. In the glomerular layer of the olfactory bulb, strong Cx36 immunoreactivity was found (Figure 7E) but no blue signals, indicative of N36-ß-gal fusion protein (Figure 7F). Ultrastructural details of the glomerular layer are shown in Figure 7G. N36-ß-gal reaction product was also observed in several other areas of the brain. Within the forebrain, labeling was particularly prominent in structures related to the olfactory system such as the piriform cortex, the nucleus of the lateral olfactory tract, which is considered an anterior part of the amygdala (Shipley et al., 1996), the nucleus corticalis amygdalae, and the medial amygdaloid nucleus. Numerous N36-ß-gal–positive cells were also observed in areas of the brainstem involving the vestibular nuclei and the dorsal cochlear nucleus. More anteriorly, the superior olivary nucleus and the medial nucleus of the trapezoid body contained many N36-ß-gal–positive cells.

Finally, in more caudal parts of the brainstem, moderate numbers of positive cells were located in the lateral parts of the medulla and in the region containing the spinal nucleus of the trigeminal nerve (data not shown). Whereas N36-ß-gal–positive nuclei were only rarely seen throughout deeper layers of the cortex (Figure 8A,B), more strongly labeled cells could be identified in the cingulate gyrus. In the hippocampal formation, only a few labeled cells were seen within the pyramidal cell layer of the CA2 and CA3 subfields (data not shown), which is in contrast to previous in situ hybridization analysis obtained in rat brain (Condorelli et al., 1998). Furthermore, the dentate gyrus was completely devoid of labeling. Only a few N36-ß-gal–positive nuclei were found throughout the striatum and in various parts of the thalamus like the nucleus anteromedialis, the nucleus reuniens thalami, and the nucleus reticularis thalami (Landisman et al., 2002; Figure 8C,D). Numerous positive cells were located in the mamillary nuclei, in particular in the medial mamillary nucleus, and in what was tentatively identified as the supramamillary nucleus. Frequent N36-ß-gal–positive cells were also obvious within the triangular and the medial septal nuclei and the nucleus of the anterior commissure. Within the midbrain, the nucleus nervi abducentis was prominently labeled. Some N36-ß-gal–labeled cells were also seen in the molecular layer of the cerebellar cortex, predominantly in the vermal part of the caudal lobes (data not shown). As demonstrated above, blue-stained cells were present in the lateral cerebellar nucleus. Similarly, the nucleus cuneatus lateralis contained N36-ß-gal–positive cells.

Colocalization studies with the marker parvalbumin, known to be expressed in in-

terneurons, were performed in regions previously described to show Cx36 expression (Priest et al., 2001). In the cortex, many of parvalbuminpositive neurons were stained blue (Figure 8A,B). Interestingly, not all parvalbumin-positive neurons showed N36-β-gal expression, but all N36-β-gal cells coexpressed parvalbumin. In the reticular thalamic nucleus (see also Figure 8C,D) most of the parvalbumin-positive neurons showed N36-β-gal staining.

Non-neuronal tissues. Additionally, N36-β-gal staining was detected in excitable tissues outside the CNS of adult Cx36+/del[LacZ] mice. In the adult pancreas, blue clusters of N36-β-gal staining were visible in cells morphologically resembling endocrine β-islets. Colocalization of β-gal reaction product with the immunohistochemical detection of the hormone insulin confirmed the presence of Cx36 in β-cells of endocrine pancreatic island (Figure 9A). Furthermore, strong N36-β-gal staining was detected in the medulla of the adrenal gland (Figure 9B), where the hormone adrenaline is produced. Immunofluorescence analysis of adrenal glands showed that Cx36 protein was present in medullary cells (Figure 9C), clearly separated from cells of the adjacent adrenal cortex.

DISCUSSION

Absence of functional expression of the floxed Cx36 allele

Contrary to our experimental strategy, RT-PCR and immunoprecipitation analysis unexpectedly revealed that neither the recombined Cx36 transcript nor Cx36 protein was expressed in the retina when exon2 of Cx36 was flanked in our transgenic mice by two loxP sites (Cx36 fl and Cx36 fldN). This phenomenon is apparently independent of the presence of the strong PGK promoter driving the expression of the neomycin selection cassette. One possible explanation for the transcriptional silence of the recombined Cx36 allele in mice could be the shortening of the 3' untranslated region (3' UTR) in the transgenic construct from 1.14 kb to a residual 200 bp. Alternatively, the substitution of an endogenous 174 bp XbaI/HindIII fragment by a spacer sequence of 410 bp including one loxP site could have caused transcriptional inactivation of the Cx36 transgene. However, functional expression of Cx36 was not disturbed by these modifications when parts of the targeting vector pJD1-LacZ were tested by transient transfections in HeLa cells (data not shown). Obviously, the omitted sequences may have a negative impact on gene regulation in neurons and thus prevent expression of the altered Cx36 allele. A putative transcription enhancing element might be located on the excised part of

the intron or the 3' UTR might play an important role in stabilizing the Cx36 mRNA, which may not be required in HeLa cells. However, independent of the functional Cx36 expression, the N36-ß-gal reporter protein in Cx36 del[LacZ] animals was found to be ex-pressed in neural tissues in which Cx36 had already been described (Condorelli et al., 1998, 2000; Serre-Beinier et al., 2000; Deans et al., 2001, 2002) and allowed additional, novel insights into the expression pattern of the Cx36 gene.

Cx36 expression in the CNS

Retina. After ß-gal staining of the adult retina of Cx36 del[LacZ] mice, three intense and one moderate row of blue-stained cells were detected. Spare blue dots in the ganglion cell layer suggested Cx36 expression in α-ganglion cells, as deduced from their location and number. In the inner nuclear layer (INL), two distinct rows of N36-ß-gal–positive cells were observed. In the INL, Cx36 expression had already been described in AII amacrine cells and certain sub-types of bipolar cells (Feigenspan et al., 2001; Mills et al., 2001; Deans et al., 2002) but was excluded from horizontal cells (Deans and Paul, 2001). In this study we confirmed recent findings that Cx36 is likely to be expressed in different subtypes of bipolar cells. Further-more, the fourth row of faint N36-ß-gal staining between the outer nuclear layer (ONL) and the outer photoreceptor segments suggested that Cx36 expression occurs in photoreceptor cells. This seems plausible, because gap junctions between mouse rod photoreceptors have already been visualized by electron microscopy (Tsukamoto et al., 2001) without identifica-tion of the ex-pressed connexin. Most recently, Deans et al. (2002) implied Cx36 expression in mouse rod photoreceptor cells after ß-gal immunofluorescence analysis. The Cx36 del[LacZ] mice might help to discriminate between rods and cones in future studies. Only reporter gene assays allowed the identification of Cx36 expression in mouse photoreceptor cells, because *in situ* hybridization (Condorelli et al., 1998) as well as immunofluorescence analysis (Gül-denagel et al., 2000) had not been sensitive enough to detect Cx36 expression in these cells. *Brain. In situ* hybridization in adult rat brains showed prominent Cx36 expression in the olfacto-ry bulb, inferior olive, cerebellar nuclei, cerebral cortex, and hippocampus (Condorelli et al., 1998) and to a minor extent in other thalamic subfields of rat and human (reviewed in Condorelli et al., 2000). Further investigations using freeze-fracture replica immunogold labeling (FRIL) in the gray matter of adult rats confirmed the presence of Cx36 protein in ultrastructurally de-fined gap junctions between neurons of the brain and of spinal cord (Rash et al., 2000, 2001).

In the present study, we mainly focused on the N36-ß-gal and Cx36 expression pat-tern in the olivocerebellar system, because there were some differences between the ex-

pression profile of Cx36 and the reporter gene analyzed. Both transcripts coding for Cx36 and the N36-ß-gal reporter were coexpressed in all the different nuclei of the inferior olive in heterozygous Cx36+/del[LacZ] mice. This was also the case for the Cx36 protein and N36-ß-gal reaction product except for the principal nucleus (IOPr) and parts of the dorsal accessory olive (DAO), which lacked the N36-ß-gal reaction product but showed Cx36 immunoreactivity. In the cerebellum, this situation was found to be reversed, because all the different subnuclei stained blue for N36-ß-gal but showed no specific Cx36 immunosignals. It is tempting to speculate that Cx36 protein is synthesized in neurons of the deep cerebellar nuclei and then subsequently transported along their axons to neurons of the inferior olive. However, there are some caveats with regard to this hypothesis:

1.   It cannot be ruled out that the deletion of some genomic sequences in the recombined Cx36 allele disrupts splicing or translation of the N36-ß-gal reporter mRNA, at least in the principal olivary nucleus, although its successful transcription was documented by corresponding in situ hybridizations. Additionally, due to the loss of the original Cx36-related 3' UTR, the stability of the N36-ß-gal mRNA could be severely impaired.

2.   As pointed out before, colocalization of Cx36 protein and N36-ß-gal fusion protein in neurons could not be expected. After translation, Cx36 protein is thought to be transported into cellular subcompartments, mainly into dendrites, but possibly also into axon terminals to establish electrical synapses (Zoidl and Dermietzel, 2002). Although N36-ß-gal fusion protein includes the whole N-terminal part of Cx36, suggested to contain the signal peptide for subcellular transport (Zoidl et al., 2002), it is not transported but instead localized in the perinuclear region.

Thus, it is conceivable that coexpression of Cx36 protein and the N36-ß-gal reporter protein occurs in certain subfields or nuclei, but some blue-stained neurons project to different subfields where the Cx36 protein could consequently be detected. This is obviously the case for the cerebellar nuclei: neurons project to various nuclei in the inferior olive. There, the absence of Cx36 immunofluorescence signals, in contrast to blue-stained neuronal cell bodies, may be explained by the transport of Cx36 protein to the inferior olive. If Cx36 is transported to the various olivary nuclei, this would be explain why all cerebellar nuclei express Cx36 and N36-ß-gal reporter transcripts, whereas no Cx36-immunopositive signals were found. In the hippocampus of adult Cx36+/del[LacZ] mice, only a few cells express N36-ß-gal. This corresponds well to the recent findings that only GABAergic interneurons express Cx36 in the hippocampus (Hormuzdi et al., 2001). These results are at variance with the prominent Cx36 *in situ* signal in the CA3 pyramidal cell layer of adult rat (Condorelli et al., 1998) and

with the staining of the ß-gal reporter gene seen also in the pyramidal cell layer of the CA3 region in mice at postnatal day 15 (Deans et al., 2001). The first observations could be explained by species differences between rat and mouse but the second is likely to be due to an overstaining of 400-µm vibratome sections (Deans et al., 2001) resulting in the accumulation of ß-gal reaction product in the CA3 pyramidal cell layer. We obtained similar results by overstaining of 400-µm sections from adult mouse brains; however, 14-µm sections revealed expression of Cx36 only in some interspersed neurons within the CA3 pyramidal cell layer. In this case, ß-gal staining in thicker sections might have led to an overestimation of Cx36 expression in principal cells of the hippocampus. Results obtained by combined *in situ* hybridization immunohistochemistry (Belluardo et al., 2000) and double immunohistochemistry (Priest et al., 2001) showed that approximately 50–55% of parvalbumin-labeled neurons in the rat mature cerebral cortex were double labeled for Cx36. The numbers of colocalized neurons fit well with our observation of N36-ß-gal staining colocalized with immunodetection of parvalbumin in the adult cortex of Cx36+/del[LacZ] mice. In the cortex, nearly half of parvalbumin-positive cells were stained blue, indicating that about 50% of the parvalbumin-positive neurons express Cx36 (Figure 8A,B), but all N36-ß-gal expressing cells were parvalbumin-positive. The reduced synchrony of rhythmic inhibitory potentials (Deans et al., 2001) might be caused by the absence of Cx36 protein in these parvalbumin-positive GABAergic interneurons in the neocortex.

Cx36 expression outside the CNS

It has been suggested that endocrine cells require signals from neighboring cells as well as from their extracellular environment to coordinate normal physiological responses (Meda et al., 1982, 1986; Morand et al., 1996). Furthermore, cell communication via gap junctions is hypothesized to have a significant role in differentiation, endocrine cell growth, and hormone response (cf. Munari-Silem and Rousset, 1996; Oyoyo et al., 1997). In sections of the pancreas from adult Cx36+/del[LacZ] mice, we colocalized cell clusters of strong N36-ß-gal expression with immunoreactivity to insulin, confirming previous reports that Cx36 was expressed in endocrine pancreatic ß-cell islets (Serre-Beinier et al., 2000). Calabrese et al. (2001) further described the inability to secrete insulin after reduction of Cx36 expression in cultured MIN6 cells. The expression levels of three other connexins, Cx26, Cx32, and Cx43, were studied in different endocrine and exocrine glands (Meda et al., 1993). Cx32 and Cx26 were described to be present in exocrine glands, whereas Cx43 and Cx26 were found in endocrine glands. Gap

junctions were shown to be abundant in the zonae fasciculata (ZF) and reticularis (ZR) of the adrenal gland cortex; however, only a few plaques were found in cells of the zona glomerulosa (ZG). Immunohistochemical analysis demonstrated Cx43 as the major connexin expressed in the cortex of the adrenal gland (Murray and Pharrams, 1997; Davis et al., 2002). Martin et al. (2001) showed by RT-PCR analysis that neural crest cell-derived chromaffin cells coexpressed Cx36 and, contrary to other results (see above), Cx43. Communication via gap junctions in the adrenal gland may be important for efficient release of catecholamines from secretory cells of the adrenal medulla, which are functionally equivalent to the postgangliotic neurons of the sympathetic nervous system. The possible function of Cx36 in hormone-secreting cells (pancreas and adrenal gland) as well as in neurons, where it forms electrical synapses, especially in different parts of the limbic system, suggests that the behavior of Cx36-deficient mice should be analyzed.

In conclusion, our lacZ reporter gene analysis has shown that Cx36 is expressed not only in certain neurons but also in endocrine excitable cells of the pancreas and adrenal gland. Thus it should be worthwhile to study the cell type-specific functions of Cx36 in appropriate transgenic mice in which the Cx36 coding DNA can be conditionally deleted.

ACKNOWLEDGMENTS

REFERENCES

Andrews BJ, Proteau GA, Beatty LG, and Sadowski PD. 1985. The FLP recombinase of the 2 micron circle DNA of yeast: interaction with its target sequences. Cell 40:795–803.

Belluardo N, Mudo G, Trovato-Salinaro A, Le Gurun S, Charollais A, Serre-Beinier V, Amato G, Haefliger JA, Meda P, Condorelli DF. 2000. Expression of Connexin36 in the adult and developing rat brain. Brain Res 865 AB:121–138.

Buchholz F, Angrand PO, Stewart AF. 1996. A simple assay to determine the functionality of Cre or FLP recombination targets in genomic manipulation constructs. Nucleic Acids Res 24:3118–3119.

Buhl DL, Harris KD, Hormuzdi SG, Monyer H, Buzsaki G. 2003. Selective impairment of hippocampal gamma oscillations in connexin-36 knock-out mouse *in vivo*. J Neurosci 23:1013–1018.

Calabrese A, Güldenagel M, Charollais A, Mas C, Caton D, Bauquis J, Serre-Beinier V, Caille D, Söhl G, Teubner B, Le Gurun S, Trovato-Salinaro A, Condorelli DF, Haefliger JA, Willecke K, Meda P. 2001. Cx36 and the function of endocrine pancreas. Cell Commun Adhes 8:387–391.

Condorelli DF, Parenti R, Spinella F, Trovato SA, Belluardo N, Cardile V, Cicirata F. 1998. Cloning of a new gap junction gene (Cx36) highly expressed in mammalian brain neurons. Eur J Neurosci 10:1202–1208.

Condorelli DF, Belluardo N, Trovato-Salinaro A, Mudo G. 2000. Expression of Cx36 in mammalian neurons. Brain Res Brain Res Rev 32:72–85.

Davis KT, Prentice N, Gay VL, Murray SA. 2002. Gap junction proteins and cell-cell communication in the three functional zones of the adrenal gland. J Endocrinol 173:13–21.

De Zeeuw CI, Chorev E, Devor A, Manor Y, Van Der Giessen RS, De Jeu MT, Hoogenraad CC, Bijman J, Ruigrok TJ, French P, Jaarsma D, Kistler WM, Meier C, Petrasch-Parwez E, Dermietzel R, Söhl G, Güldenagel M, Willecke K, Yarom Y. 2003. Deformation of network connec-

tivity in the inferior olive of connexin 36-deficient mice is compensated by morphological and electrophysiological changes at the single neuron level. J Neurosci 23:4700–4711.

Deans MR, Gibson JR, Sellitto C, Connors BW, Paul DL. 2001. Synchronous activity of inhibitory networks in neocortex requires electrical synapses containing Connexin36. Neuron 31:477–485.

Deans MR, Paul DL. 2001. Mouse horizontal cells do not express connexin26 or Connexin36. Cell Commun Adhes 8:361–366.

Deans MR, Volgyi B, Goodenough DA, Bloomfield SA, Paul DL. 2002. Connexin36 is essential for transmission of rod-mediated visual signals in the mammalian retina. Neuron 36:703–712.

Eiberger J, Degen J, Romualdi A, Deutsch U, Willecke K, Söhl G. 2001. Connexin genes in the mouse and human genome. Cell Commun Adhes 8:163–165.

Feigenspan A, Teubner B, Willecke K, Weiler R. 2001. Expression of neuronal Connexin36 in AII amacrine cells of the mammalian retina. J Neurosci 21:230-239.

Güldenagel M, Söhl G, Plum A, Traub O, Teubner B, Weiler R, Willecke K. 2000. Expression patterns of connexin genes in mouse retina. J Comp Neurol 18:193–201.

Güldenagel M, Ammermuller J, Feigenspan A, Teubner B, Degen J, Söhl G, Willecke K, Weiler R. 2001. Visual transmission deficits in mice with targeted disruption of the gap junction gene Connexin36. J Neurosci 21:6036–6044.

Hormuzdi SG, Pais I, LeBeau FE, Towers SK, Rozov A, Buhl EH, Whittington MA, Monyer H. 2001. Impaired electrical signaling disrupts gamma frequency oscillations in connexin 36-deficient mice. Neuron 31:342–344.

Horst M, Harth N, Hasilik A. 1991. Biosynthesis of glycosylated human lysozyme mutants. J Biol Chem 266:13914-13919.

Kistler WM, De Jeu MT, Elgersma Y, Van Der Giessen RS, Hensbroek R, Luo C, Koekkoek SK, Hoogenraad CC, Hamers FP, Güldenagel M, Söhl G, Willecke K, De Zeeuw CI. 2002. Analysis of Cx36 knockout does not support tenet that olivary gap junctions are required for complex spike synchronization and normal motor performance. Ann NY Acad Sci 978:391–404.

Lallemand Y, Luria V, Haffner-Krausz R, Lonai P. 1998. Maternally ex-pressed PGK-Cre transgene as a tool for early and uniform activation of the Cre site-specific recombinase. Transgenic Res 7:105–112.

Landisman CE, Long MA, Beierlein M, Deans MR, Paul DL, Connors BW. 2002. Electrical synapses in the thalamic reticular nucleus. J Neurosci 22:1002–1009.

Magin TM, McWhir J, Melton DW. 1992. A new mouse embryonic stem cell line with good germ line contribution and gene targeting frequency. Nucleic Acids Res 20:3795–3796.

Maier N, Güldenagel M, Söhl G, Siegmund H, Willecke K, Draguhn A. 2002. Reduction of high-frequency network oscillations (ripples) and pathological network discharges in hippocampal slices from connexin 36- deficient mice. J Physiol 541:521–528.

Martin AO, Mathieu MN, Chevillard C, Guerineau NC. 2001. Gap junctions mediate electrical signaling and ensuring cytosolic Ca2+ in-creases between chromaffin cells in adrenal slices: a role in catecholamine release. J Neurosci 21:5397–405.

Maxeiner S, Krüger O, Schilling K, Traub O, Urschel S, Willecke K. 2003. Spatiotemporal transcription of connexin45 during brain development results in neuronal expression in adult mice. Neuroscience 119:689–700.

Meda P, Kohen E, Kohen C, Rabinovitch A, Orci L. 1982. Direct communication of homologous and heterologous endocrine islet cells in culture. J Cell Biol 92:221–226.

Meda P, Santos RM, Atwater I. 1986. Direct identification of electrophysiologically monitored cells within intact mouse islets of Langerhans. Diabetes 35:232–236.

Meda P, Pepper MS, Traub O, Willecke K, Gros D, Beyer E, Nicholson B, Paul D, Orci L. 1993. Differential expression of gap junction connexins in endocrine and exocrine glands. Endocrinology 133:2371–2378.

Meier C, Petrasch-Parwez E, Habbes HW, Teubner B, Güldenagel M, Degen J, Söhl G, Willecke K, Dermietzel R. 2002. Immunohistochemical detection of the neuronal Connexin36 in the mouse central nervous system in comparison to Connexin36-deficient tissues. Histochem Cell Biol 117:461–471.

Meyers EN, Lewandoski M, Martin GR. 1998. An Fgf8 mutant allelic series generated by Cre- and Flp-mediated recombination. Nat Genet 18:136– 141.

Mills SL, O'Brien JJ, Li W, O'Brien J, Massey SC. 2001. Rod pathways in the mammalian retina use connexin 36. J Comp Neurol 436:336–350.

Morand I, Fonlupt P, Guerrier A, Trouillas J, Calle A, Remy C, Rousset B, Munari-Silem Y. 1996. Cell-to-cell communication in the anterior pituitary: evidence for gap junction-mediated exchanges between endocrine cells and folliculostellate cells. Endocrinology 137:3356–3367.

Munari-Silem Y and Rousset B. 1996. Gap junction-mediated cell-to-cell communication in endocrine glands—molecular and functional aspects: a review. Eur J Endocrinol 135:251– 264.

Murray SA, Pharrams SY. 1997. Comparison of gap junction expression in the adrenal gland. Microsc Res Tech 36:510–519.

Oertel WH, Schmechel DE, Mugnaini E, Tappaz ML, Kopin IJ. 1981. Immunocytochemical localization of glutamate decarboxylase in rat cerebellum with a new antiserum. Neuroscience 6:2715–2735.

Oyoyo UA, Shah US, Murray SA. 1997. The role of alpha1 (connexin-43) gap junction expression in adrenal cortical cell function. Endocrinology 138:5385–5397.

Priest CA, Thompson AJ, Keller A. 2001. Gap junction proteins in inhibitory neurons of the adult barrel neocortex. Somatosens Mot Res 18: 245–252.

Rash JE, Staines WA, Yasumura T, Patel D, Furman CS, Stelmack GL, Nagy JI. 2000. Immunogold evidence that neuronal gap junctions in adult rat brain and spinal cord contain connexin-36 but not connexin-32 or connexin-43. Proc Natl Acad Sci USA 97:7573–7578.

Rash JE, Yasumura T, Davidson KG, Furman CS, Dudek FE, Nagy JI. 2001. Identification of cells expressing Cx43, Cx30, Cx26, Cx32 and Cx36 in gap junctions of rat brain and spinal cord. Cell Commun Adhes 8:315–320.

Rodriguez CI, Buchholz F, Galloway J, Sequerra R, Kasper J, Ayala R, Stewart AF, Dymecki SM. 2000. High-efficiency deleter mice show that FLPe is an alternative to Cre- loxP. Nat Genet 25:139–140.

Serre-Beinier V, Le Gurun S, Belluardo N, Trovato-Salinaro A, Charollais A, Haefliger JA, Condorelli DF, Meda P. 2000. Cx36 preferentially connects beta-cells within pancreatic islets. Diabetes 49:727–734.

Shipley MT, McLean JH, Zimmer LA, Ennis M. 1996. The olfactory system. In Integrated systems of the CNS, part III, Cerebellum, basal ganglia, olfactory system. Amsterdam: Elsevier.

Söhl G, Degen J, Teubner B, Willecke K. 1998. The murine gap junction gene Connexin36 is highly expressed in mouse retina and regulated during brain development. FEBS Lett 428:27–31.

Teubner B, Degen J, Söhl G, Güldenagel M, Bukauskas FF, Trexler EB, Verselis VK, De Zeeuw CI, Lee CG, Kozak CA, Petrasch-Parwez E, Dermietzel R, Willecke K. 2000. Functional expression of the murine connexin 36 gene coding for a neuron-specific gap junctional protein. J Membr Biol 176:249–262.

Theis M, Magin TM, Plum A, Willecke K. 2000. General or cell type-specific deletion and replacement of connexin-coding DNA in the mouse. Methods 20:205–218.

Tsukamoto Y, Morigiwa K, Ueda M, Sterling P. 2001. Microcircuits for night vision in mouse retina. J Neurosci 21:8616–8623.

Venance L, Rozov A, Blatow M, Burnashev N, Feldmeyer D, Monyer H. 2000. Connexin expression in electrically coupled postnatal rat brain neurons. Proc Natl Acad Sci USA 97:10260–10265.

Willecke K, Eiberger J, Degen J, Eckardt D, Romualdi A, Güldenagel M, Deutsch U, Söhl G. 2002. Structural and functional diversity of connexin genes in the mouse and human genome. Biol Chem 383: 725–737.

Zoidl G, Meier C, Petrasch-Parwez E, Zoidl C, Habbes HW, Kremer M, Srinivas M, Spray DC, Dermietzel R. 2002. Evidence for a role of the N-terminal domain in subcellular localization of the neuronal Connexin36 (Cx36). J Neurosci Res 15:448–45.

Zoidl G, Dermietzel R. 2002. On the search for the electrical synapse: a glimpse at the future. Cell Tissue Res 310:137–142.

CHAPTER 2.2

Spatiotemporal Distribution of Connexin45 in the Olivo-cerebellar System

RUBEN S. VAN DER GIESSEN[1], STEPHAN MAXEINER[2], PIM J. FRENCH[1,3], KLAUS WILLECKE[2], AND CHRIS I. DE ZEEUW[1]

[1]Department of Neuroscience, Erasmus MC, 3000 DR Rotterdam, The Netherlands

[2]Institut für Genetik, Abteilung Molekulargenetik, Universität Bonn, D-53117 Bonn, Germany

[3]Department of Neurology, Erasmus MC, 3000 DR Rotterdam, The Netherlands

ABSTRACT

The olivocerebellar system is involved in the transmission of information to maintain sensory motor coordination. Gap junctions have been described in various types of neurons in this system, including the neurons in the inferior olive that provide the climbing fibers to Purkinje cells. While it is well established that Connexin36 is necessary for the formation of these neuronal gap junctions, it is not clear whether these electrical synapses can develop without Connexin45. Here we describe the development and spatiotemporal distribution of Connexin45 in relation to that of Connexin36 in the olivocerebellar system. During development Connexin45 is expressed in virtually all neurons of the inferior olive and cerebellar nuclei. During later postnatal development and adulthood there is a considerable overlap of expression of both connexins in subpopulations of all main olivary nuclei and cerebellar nuclei as well as in the stellate cells in the cerebellar cortex. Despite this prominent expression of Connexin45, ultrastructural analysis of neuronal gap junctions in null-mutants of Connexin45 showed that their formation appears normal in contrast to that in knockouts of Connexin36. These morphological data suggest that Connexin45 may play a modifying role in widely distributed, coupled neurons of the olivocerebellar system, but that it is not essential for the creation of its neuronal gap junctions.

INTRODUCTION

Gap junctions are protein complexes made up of several Connexins (Cx) that allow intercellular passage of signaling molecules or mono/divalent ions. Six connexin proteins cluster together to form a connexon or hemichannel and the docking of two hemichannels located in opposing membranes leads to the generation of functional gap junctions between neighboring cells (Kumar and Gilula, 1996). Homomeric connexons are composed of similar connexins, whereas heteromeric connexons consist of different connexins. Gap junctions formed by corresponding connexons are defined as homotypic channels, whereas heterotypic channels consist of different connexons. The number of possible interactions between various connexins therefore markedly increases the complexity of gap junctions. Specific connexin compositions result in different functional properties. For example, differences in permeability, affinity (Weber et al., 2004), and coupling asymmetry (Bevans et al., 1998; Bukauskas et al., 2002) have been described. The connexin family includes at least 20 members in the murine genome and 21 connexin genes in the human genome (Willecke et al., 2002).

Only 10 of these connexin genes are expressed in the nervous system. While Cx57 appears to be specifically expressed in horizontal cells in the retina (Hombach et al., 2004), Cx26, Cx29, Cx30, C32, Cx43, and Cx47 have been found to be expressed in astrocytes and oligodendrocytes in the brain (Theis et al., 2005). Cx32 and Cx43 were originally suggested to be expressed by neurons in the central nervous system (Theis et al., 2003), but analysis of transgenic mice with connexin-specific markers indicated that these outcomes were probably incorrect (Nelles et al., 1996; Theis et al., 2003; Duan et al., 2004). It wasn't until the late 1990s that Condorelli et al. (1998) cloned, guided by the distribution of dendritic lamellar bodies that can be associated with dendrodendritic gap junctions (De Zeeuw et al., 1995), the first truly neuronal connexin (Cx36) (see also Söhl et al., 1998). Indeed, the absence of Cx36 results in neurons in nonfunctional "gap junction-like" structures with an abnormal wide distance between the two adjacent membranes, whereas in glia cells it does not affect the ultrastructure of their gap junctions (De Zeeuw et al., 2003). More recently, another connexin was also found to be expressed in neurons, without being expressed in astrocytes and oligodendrocytes: Cx45 (Condorelli et al., 2003; Maxeiner et al., 2003; Söhl et al., 2004). At present, it is unclear, however, whether Cx45 is coexpressed with Cx36 by the same neurons, and if so, whether Cx45 and Cx36 are expressed during the same developmental stages.

In addition, it remains to be elucidated whether Cx45 is also necessary for the formation of neuronal gap junctions. One of the best areas to tackle these questions is the inferior olive, since here the density of neuronal gap junctions is probably higher than any other brain region (De Zeeuw et al., 1995), because here gap junctions can be readily identified under the electron microscope (Sotelo et al., 1974; De Zeeuw et al., 1989), and because here Cx36 is virtually ubiquitously expressed (Belluardo et al., 2000; De Zeeuw et al., 2003; Degen et al., 2004). Olivary neurons are coupled through gap junctions, which are located between dendritic spines within glomeruli. These coupled spines receive both an inhibitory GABAergic input from the hindbrain and a non-GABAergic excitatory input from various areas providing ascending and descending projections to the olive (De Zeeuw et al., 1989, 1998). Apart from the inferior olive, the olivocerebellar system may also show the formation of gap junctions in both cerebellar nuclei and cerebellar cortex, because in these regions Cx36 is also prominently expressed (Degen et al., 2004). However, neuronal gap junctions have not been demonstrated yet at the electron microscopic level in these areas. Thus, to further uncover the spatiotemporal distribution of Cx45 in the olivocerebellar system and to explore the possible role of this connexin in the formation of its neuronal gap

junctions, we investigated Cx45 transgenic mouse mutants for LacZ labeling, applied *in situ* hybridization and reverse transcriptase polymerase chain reaction (RT-PCR) analysis using Cx45 probes in wildtypes, and examined all three major parts of the olivocerebellar system, i.e., the inferior olive, cerebellar nuclei, and cerebellar cortex at the electron microscopy level in both Cx45 null mutants and wildtype littermates. Since our first global studies of Cx45 indicated that its role may be particularly relevant during early postnatal development (Maxeiner et al., 2003), special emphasis was put on its distribution during this stage.

MATERIALS AND METHODS

In situ hybridization

Mice at ages of postnatal days (P)1, P8, P14, and P21 were anesthetized with Nembutal (75 mg/kg, i.p.) and brains were carefully removed, frozen on dry ice, and stored at –80°C. Fourteen-μm sections were cut on a cryostat, mounted on polylysine-coated glass slides, and stored at –80°C. Slides were fixed in 4% paraformaldehyde (5 minutes), acetylated in 1.4% triethanolamine, 0.25% acetic anhydride, and prehybridized (1 hour) in buffer (pH 7.4) containing 50% formamide, 5X SSC, 5X Denhardt's, 250 pg/ml yeast tRNA (Sigma, St. Louis, MO), and 500 pg/ml acid-alkali cleaved salmon testis DNA (Sigma). *In situ* hybridization was performed essentially as described by De Zeeuw et al. (2003). Briefly, sections were incubated overnight at 65°C in prehybridization buffer containing 100 ng/ml digoxigenin-UTP-labeled cRNA probes. Sense and antisense probes were generated against the full-length coding sequence of Cx45 and Cx36 (500 bp) using a DIG RNA labeling kit (Roche, Nutley, NJ) was then hydrolyzed in 40 mM NaHCO3, 60 mM Na2CO3 for 25 minutes at 60°C to generate fragments of -300 nucleotides. Sections were then washed in 0.2X SSC at 65°C (1 hour) and blocked in 0.1 M Tris, pH 7.5, 0.15 M NaCl, and 10% heat inactivated sheep serum (Sigma) for 1 hour at room temperature (RT). Alkaline phosphatase conjugated anti-digoxigenin antibodies (1:5,000, Roche) containing 1% heat inactivated sheep serum were added to the sections and incubated overnight at 4°C. Color reactions were performed in 0.1 M Tris, pH 9.5, 0.1 M NaCl, 50 mM $MgCl_2$, 2 mM Levamisole (Sigma), 0.35 mg/ml nitro-blue tetrazolium (Roche), and 0.18 mg/ml 5-bromo-4-chloro-3-indolylphosphate (Roche). Reactions were terminated upon visual inspection (~18 hours) and mounted in Permount (Fisher Scientific, Houston, TX). Cells were identified and quantified with the use of Neurolucida software.

Labeled cells were counted and surface areas of these nuclei were measured. The outcomes of different slides per nucleus were averaged to a mean cell density (cells per mm^2) within the nuclei.

To confirm the *in situ* results obtained with the alkaline phosphatase method, we reexamined our findings using radioactive *in situ* hybridization. Brains from adult rats were removed, frozen on dry ice, and stored at –70˚C. Fourteen-pm sections were cut on a cryostat, mounted onto polylysine-coated glass slides, and stored at –70˚C. This form of *in situ* hybridization was performed essentially as described by French et al. (2001). Briefly, sections were thawed, fixed in 4% paraformaldehyde, acetylated in 1.4% triethanolamine and 0.25% acetic anhydride, dehydrated through graded ethanol solutions, and delipidated in chloroform. Sections were hybridized overnight at 42˚C in 100 pl buffer (pH 7.0) containing 50% formamide, 4X SSC, 10% dextran sulfate, 5X Denhardt's solution, 200 mg/ml acid alkali cleaved salmon testis DNA, 100 mg/ml long-chain polyadenylic acid, 25 mM sodium phosphate (pH 7.0), 1 mM sodium pyrophosphate, and 100,000 CPM radiolabeled probe (-1 ng/ml) under parafilm coverslips. Sections were washed in 1X SSC at 55˚C (30 minutes), 0.1X SSC at RT (5 minutes), and dehydrated in ethanol. Sections were then exposed to autoradiographic film. 35S-ATP end-labeled probes (NEN, Boston, MA) were generated using terminal deoxynucleotidyl transferase (Promega, Madison, WI) according to the manufacturer's instructions. Either a 50-fold excess of unlabeled anti-sense oligonucleotide or the complementary sense oligonucleotide were used as negative controls. Sequences were: Connexin45 antisense 5'-ccatcaccaaaacaacccc-3' and Connexin45 sense 5'-ggaagacacaacctgaaagttctgc-3'. Control sense oligos were complementary to the antisense oligo.

LacZ labeling

We used heterozygous Cx45-deficient mice with a mixed background of C57BL/6 and Sv129/Ola for LacZ-staining. These mice expressed the bacterial β-galactosidase protein under control of the endogenous Connexin45 promoter (Krüger et al., 2000). Connexin45 LacZ/+ mice were anesthetized with intraperitoneal Nembutal (75 mg/kg) and perfused transcardially with phosphate-buffered saline (PBS; pH 7.4) and 1% paraformaldehyde in 0.12 M PB. Whole brains were removed and postfixed in the same solution for 2 hours at room temperature. Brains were then transferred to 10% sucrose in 0.1 M PB at 4˚C overnight and embedded in 11% gelatin and 10% sucrose in 0.1 M PB. Tissues were incubated in 30% sucrose and 10% formaldehyde solution at room temperature for 2 hours.

Serial sections (40 μm) were cut on a cryo modified sliding microtome (Leica, SM2000R) and collected in multiwells containing 0.1 M PB. Sections were incubated overnight with X-gal staining solution (PB, pH 7.4, supplemented with 5 mM $K_3[Fe(CN)_6]$, 5 mM $K_4[Fe(CN)_6]$, and 0.8‰ X-gal [5-bromo-4-chloro-3-indolyl-[3-galactosidase]) at 37°C overnight. Subsequently, the 40-μm sections were mounted and counterstained with neutral red to highlight the cel-lular localization of the blue X-gal staining, dehydrated, and embedded in Permount (Fisher Scientific). To confirm the labeling pattern obtained with X-gal staining, we investigated the same regions using immunofluorescence. Cx45 LacZ/+ and wildtype mice were anesthetized by asphyxiation and sacrificed. Brains were then carefully re-moved, frozen on dry ice, and stored at –80°C. Sections (14 pm) were cut on a cryostat, mounted on polylysine-coated glass slides, and stored at –80°C. Cryosections were fixed in 4% paraformaldehyde (30 min-utes), rinsed in PBS, and incubated in 20 mM sodium citrate buffer (pH 8.7) at, respectively, 5 minutes 37°C, 5 minutes 60°C, and 3 hours 80°C. Sections were then blocked against endogenous peroxidaseactivity in PBS containing 0.5% H_2O_2 and 2% sodium azide. Sections were then transferred to blocking buffer (0.15% glycine and 0.5% Protifar in PBS, pH 7.6) for 30 minutes and incubated with ß-galactosidase antibody (1:500, Abcam, Cambridge, UK) in blocking buffer overnight at 4°C. After incubation, samples were rinsed in blocking buffer and incubated for 90 minutes at RT in a concentration of 1:200 with secondary antibodies Alexa Fluor 594 goat antimouse (Molecular Probes, Leiden, The Netherlands) in blocking buffer. Sections were mounted in Vectashield kit containing DAPI (Vector Laboratories, Bur-lingame, CA) for nuclear staining.

RT-PCR analysis

Young wildtype mice at P1 and adult wildtype mice were anesthetized by asphyxiation in CO2 and decapitated. Brains were carefully removed, frozen on dry ice, and stored at –80°C. The brainstem including the inferior olive, cerebellar nuclei, and cerebellar cortex was cut on a cryostat and stored at –80°C. The tissue was homogenized and RNA was extracted using the TRIzol procedure (Invitrogen, La Jolla, CA) according to the manufacturer's instructions. The integrity of the RNA samples was checked on an agarose gel. cDNA was synthesized at 50°C (1 hour) using Superscript III reverse transcriptase (Invitrogen Life Technologies) and T18-oligo as the starting antisense primer. As control, reactions were performed without the addition of Superscript III reverse transcriptase. Using OD 260/280 nm measurements 0.1 μg DNA out of each reverse transcriptase reaction was then used as tem-plate to am-plify specific sequences in a PCR reaction containing 10X buffer (pH 9.0) with $MgCl_2$, 0.4

μl dNTP, 0.4 μl primers, and 0.5 Taq DNA polymerase (Promega). Primers were: 5'-3': acttggaacacaccctctgc (Connexin45-sense primer), ttgctaggtccaatcgttcc (Connexin45-antisense primer), tctggagattgggtttctgg (Connexin36-sense primer), ggctacttgccacctagcag (Connexin36-antisense primer), ctttggacccatctggaatcg (Glucose-6-Phosphate Dehydrogenase sense primer), cactttgaccttctcatcacggac (Glucose-6-Phosphate Dehydrogenase antisense primer). PCR was performed for 30, 33, and 36 cycles under the following conditions: denaturation for 2 minutes at 95°C, (annealing for 45 seconds at 95°C), annealing for 45 seconds at 56°C, and polymerization for 1 minute at 72°C. After amplification, the PCR products were analyzed by agarose gel electrophoresis and quantified with the use of Typhoon scanner 9410 (Amersham, UK) and analyzed using Scion Image 4.0.2 (NIH Image, Bethesda, MD).

Electron microscopy

Adult Cx45flox/flox:Nestin-Cre mice of 87.5% C57BL/6 and 12.5% 129SV/Ola background, which are referred to as Cx45-/- mice, were generated as reported by Maxeiner et al. (2003). Cx45-/- mice and wildtype littermates were anesthetized with an overdose of Nembutal and transcardially perfused with 4% paraformaldehyde and 1% glutaraldehyde in 0.12 M cacodylate buffer (pH 7.4); the brainstem containing the inferior olive, cerebellar nuclei, and cerebellar cortex were then processed for electron micros-copy as described previously (De Zeeuw et al., 1989). In short, 100-μm-thick sections were cut on a vibratome, osmicated in OsO4, stained for 24 hours in tannic acid and uranyl acetate, dehydrated in dimethoxypropane, and embedded in Araldite. Subsequently, the various olivary subnuclei were identified on semithin sections, pyramids were made, and ultrathin sections were cut accordingly on a Reichert ultratome, counterstained with uranyl acetate and lead citrate, and examined with a Philips CM-100 electron microscope. The sections of the various tissue blocks were systematically screened per surface area and the gap junctions were identified and quantified. For our investigations of the cerebellar cortex we labeled the Purkinje cells using standard immunocytochemistry with calbindin antibodies (Sigma, Zwijndrecht, The Netherlands) to make sure that the identification of the sources of the dendrites was correct (Bastianelli, 2003). Electron micrographs and other photographs were stored with the use of Adobe PhotoShop 7.0 (San Jose, CA). If necessary, photographs were modified or adjusted by changing the brightness or contrast ratio in this program.

RESULTS

Expression of Cx45 as revealed by in situ hybridization

At P1, P8, and P14, Cx45 was found to be expressed by neurons in the inferior olive, cerebellar nuclei, and cerebellar cortex (Figure 1A). During these periods of postnatal development the labeling in the inferior olive was mostly confined to the dorsal accessory olive (DAO) and medial accessory olive (MAO). In the cerebellar nuclei scattered labeled neurons were present in anterior interposed nucleus and posterior interposed nucleus (Figure 1B,C), while in the cerebellar cortex the labeling was restricted to interneurons in the molecular layer. At ages of P21 and older only a few labeled neurons were observed in the inferior olive and cerebellar nuclei, and at a somewhat higher level in the cerebellar cortex (Figure 2). Even though the numbers of labeled cells in these regions were relatively small, their presence persisted throughout adulthood. For comparison we also quantified the number of labeled cells following *in situ* hybridization with the use of Cx36 probes (Figure 2) (for raw material, see Degen et al., 2004). In the inferior olive the density of neurons expressing Cx36 showed, in contrast to those expressing Cx45, a large and steady increase starting at P1, while a relatively high saturated level persisted into adulthood. However, the density of Cx36-positive cells in the cerebellar nuclei and cerebellar cortex gradually diminished over time (Figure 2). Ultimately, the densities of positively labeled neurons in both the nuclei and cortex reached a low but present level in the adult.

Expression of Cx45 as revealed by LacZ labeling

During early postnatal development (P1, P8, and P14) the spatial pattern of ß-galactosidase-activity in the olivocerebellar system of Cx45LacZ/+ mice largely mimicked that obtained with *in situ* hybridization described above (data not shown). Yet during adulthood the sensitivity of LacZ labeling was generally higher than that of *in situ* hybridization, in that the densities of labeled neurons were higher (Figures 3-5). In the inferior olive we found labeling at all rostrocaudal levels including the caudal MAO (b and c subnucleus), dorsal cap, dorsal and ventral leaf of the DAO, dorsal leaf of the principal olive (PO), ventrolateral outgrowth (VLO), and dorsomedial cell column (DMCC) (Figure 3). Other parts such as the ventral leaf of the PO, beta-nucleus and rostral MAO hardly showed any labeled cell. The distribution of labeling that we ob-served in the inferior olive using immunofluorescence against ß-galactosidase corresponded to that obtained with X-gal staining (compare Figure 3B,C).
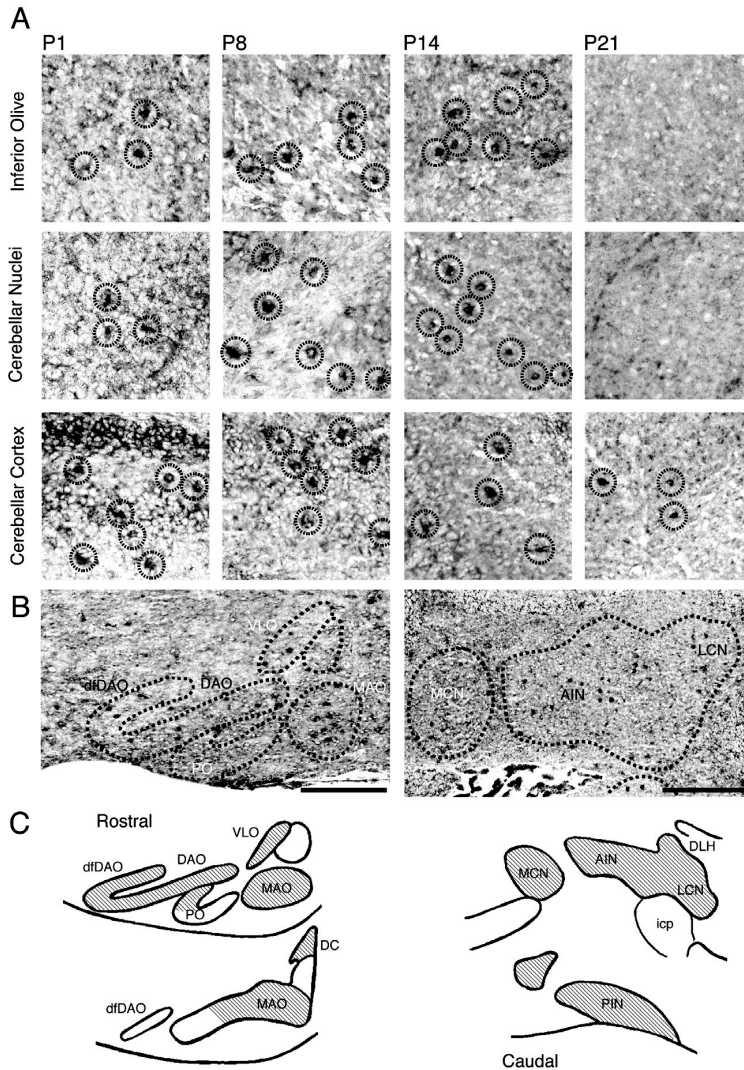
Figure 1. *In situ* **hybridization of Connexin45. A.** Labeled neurons are shown in the inferior olive, cerebellar nuclei, and cerebellar cortex at P1, P8, P14, and P21. At P14, labeling of neurons is largely absent in the inferior olive and cerebellar nuclei, while in the cerebellar cortex labeling persists, although fewer cells are labeled. Dashed circles indicate labeled neurons. **B.** Inferior olive and cerebellar nuclei show labeling of Cx45-expressing cells at P14. **C.** Schematic drawing showing the Cx45 distribution at P14. Striped areas represent subnuclei where labeled neurons were found after *in situ* hybridization. Subnuclei are marked as positive when one or more labeled neurons were found. DAO, dorsal accessory olive; MAO, medial accessory olive; PO, principal olive; DM, dorsomedial group of PO; DMCC, dorsomedial cell column; dfDAO, dorsal fold of DAO; VLO, ventrolateral outgrowth; DC, dorsal cap; PIN, posterior interposed nucleus; MCN, medial cerebellar nucleus; LCN, lateral cerebellar nucleus; AIN, anterior interposed nucleus; DLH, dorsolateral hump; icp, inferior cerebellar peduncle. Scale bars = 100 μm in B (applies A,B).

In the cerebellar nuclei we also observed X-gal staining in all their major subnuclei, including the lateral cerebellar nucleus, medial cerebellar nucleus, and anterior and posterior interposed nuclei (Figure 4). Moreover, we found labeling in both the dorsal lateral protuberance and dorsal lateral hump. Yet parts of the medial cerebellar nucleus and posterior interposed nucleus as well as the entire lateral vestibular nucleus were devoid of labeling. Here, too, the labeling that we observed using immunofluorescence against ß-galactosidase corresponded to that obtained with X-gal staining (compare Figure 4C,D). This correspondence did not only hold for the precise distribution of the subnuclei involved, but also for the differences in densities observed among the various subnuclei (for differences in high and low densities, see distributions indicated by dark and light blue in Figures 3 and 4, respectively). In addition, we observed many labeled interneurons in the molecular layer of the cerebellar cortex both during early postnatal development and adulthood (Figure 5A). In fact, after P21 it was hard to find a single stellate cell in the molecular layer that was not positively labeled (Figure 5B). In contrast, in the granular layer only few positively labeled cells were observed, while in the Purkinje cell layer no labeling was found at all.
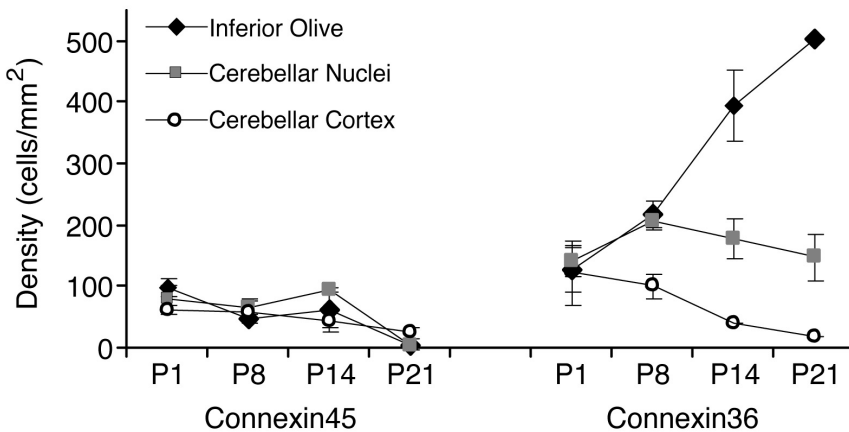
Figure 2. Developmental expression of Connexin45 and Connexin36. Graphs show cell densities of brain areas expressing Cx45 or Cx36 during development based on cell counts after *in situ* hybridization. Labeled cells were counted and the surface areas of the nuclei were measured. Outcomes of different sections were averaged to a mean cell density within the brain region. Cx45 expression shows a decrease over time in all areas. Cx45-expressing cells mostly disappear at P21 except for the cerebellar cortex, which still shows labeled cells. *In situ* hybridization for Cx36 shows a massive increase in Cx36-expressing cells in the inferior olive, while in the cerebellar cortex cell numbers decrease during development. Results are shown as mean ± SD.
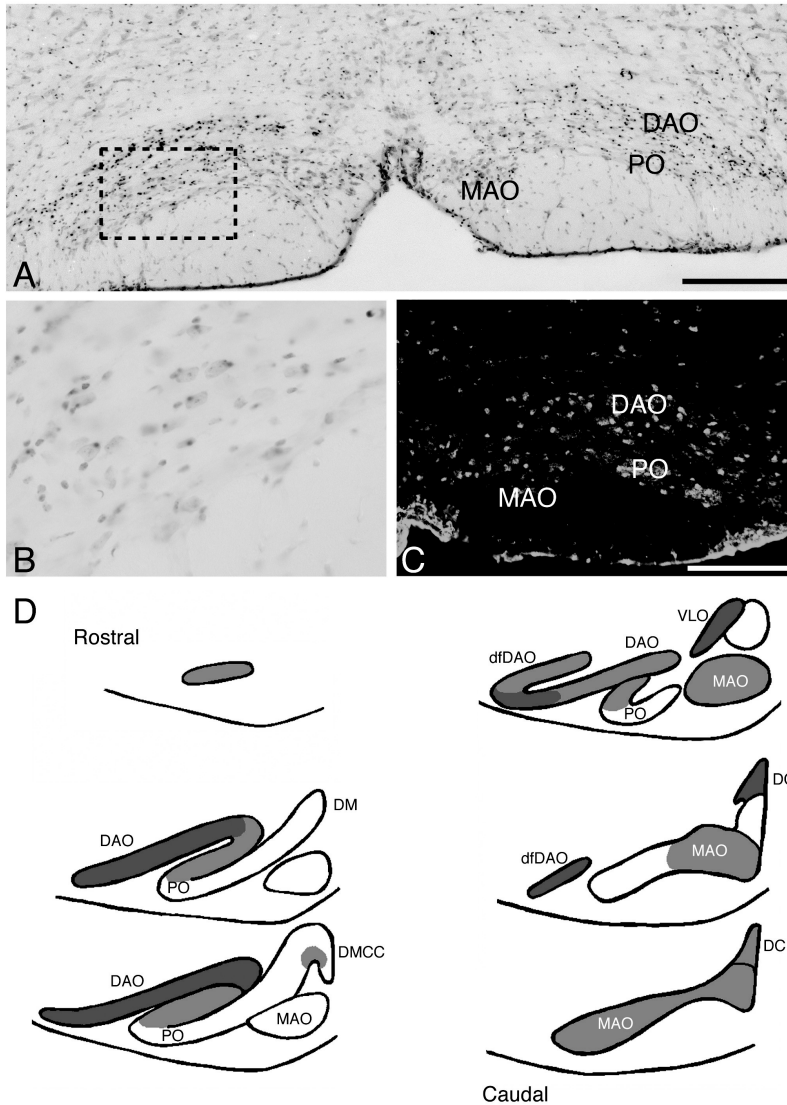
Figure 3. Connexin45 LacZ-staining in the inferior olive. A. LacZ staining in the inferior olive reveals prominent labeling in the dorsal accessory olive and principal olive. **B.** Higher magnification showing LacZ-staining present in olivary neurons. **C.** Distribution of LacZ-expression in the inferior olive of Cx45-LacZ mice with the use of immunofluorescence. Immunolabeling of olivary neurons with anti-ß-galactosidase antibodies depicts a pattern that resembles the LacZ-staining. **D.** Schematic drawing of LacZ-distribution in the inferior olive. The deep blue-light blue color gradients reflect high and low densities of LacZ-stained neurons, respectively. LacZ labeling is not present in the ventral leaf of principal olive and rostral part of the medial accessory olive. DAO, dorsal accessory olive; MAO, medial accessory olive; PO, principal olive; DM, dorsomedial group of PO; DMCC, dorsomedial cell column; dfDAO, dorsal fold of DAO; VLO, ventrolateral outgrowth; DC, dorsal cap. Scale bar = 100 μm in A, C (applies to B,C).
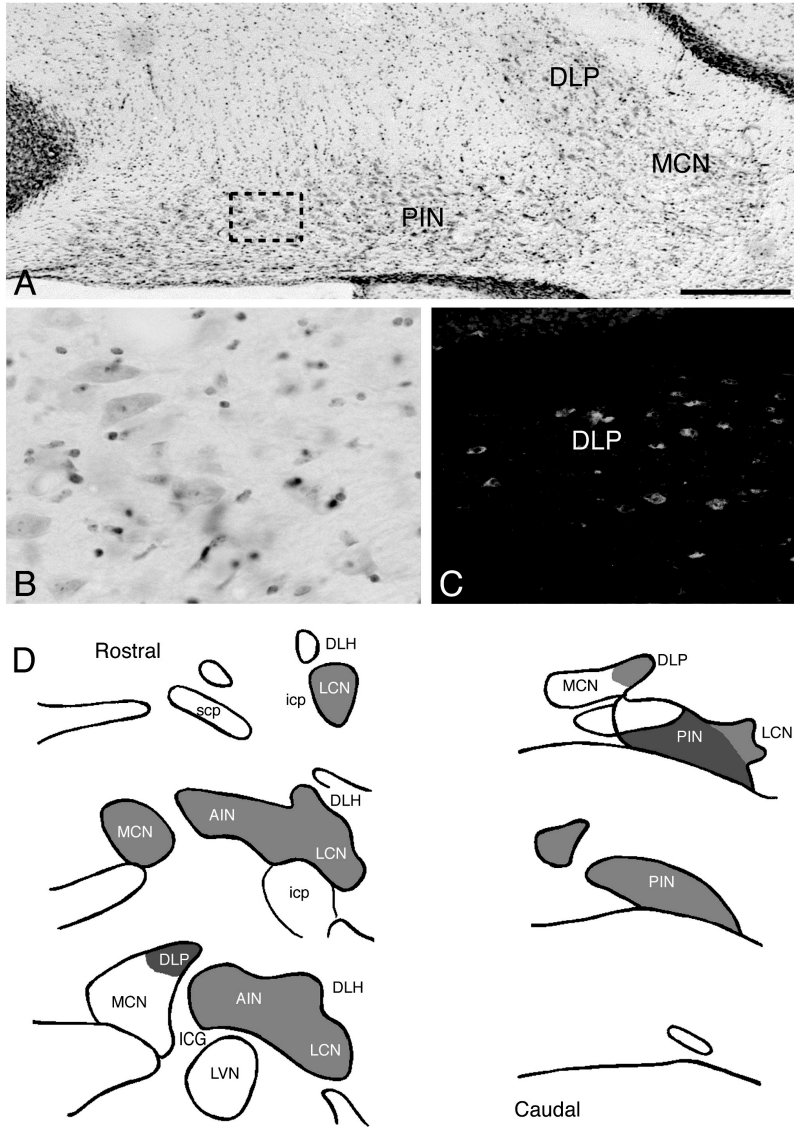
Figure 4. Connexin45 LacZ-staining in the cerebellar nuclei. A. LacZ staining shows strong labeling in the posterior interposed nucleus and dorsal lateral hump. **B.** Higher magnification from A showing labeling of the cerebellar nuclei neurons. **C.** The dorsolateral protuberance demonstrates immunolabeling of larger cerebellar nuclei neurons with the use of anti-ß-galactosidase antibodies. **D.** Schematic drawing of the LacZ-distribution the cerebellar nuclei. The deep blue-light blue color gradients reflect high and low densities of LacZ stained neurons, respectively. PIN, posterior interposed nucleus; DLP, dorsolateral protuberance; MCN, medial cerebellar nucleus; LCN, lateral cerebellar nucleus; LVN, lateral vestibular nucleus; AIN, anterior interposed nucleus; ICG, interstitial cell groups; DLH, dorsolateral hump; icp, inferior cerebellar peduncle; scp, superior cerebellar peduncle. Scale bar = 20 µm in A (applies to A-D).

One might argue that the LacZ labeling described above can be partly false-positive due to a long half-life of the ß-galactosidase-protein, which is not endogenous. However, we found several areas in the brainstem such as the cuneate nucleus and the lateral reticular nucleus that showed abundant labeling during development, but hardly any labeling during adult stages (data not shown). Thus, false-positive labeling patterns are unlikely to persist for long periods as a general pattern, and we conclude that the LacZ labeling can result in not more than a modest overestimation in time.
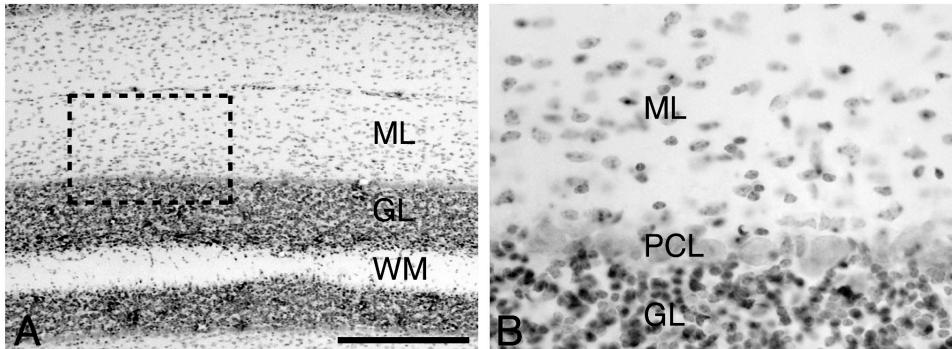
Figure 5. Connexin45 LacZ-staining in the cerebellar cortex. A. LacZ-labeling the cerebellar cortex was mostly restricted to the molecular layer. **B.** A higher magnification of A shows labeling of interneurons in the cerebellar cortex. Notice abundant labeling present in almost every interneuron. ML, molecular layer; GL, granular layer; WM, white mat-layer.; PCL, Purkinje cell layer. Scale bar = 100 um in A (applies to A,B).

Expression of Cx45 as revealed by RT-PCR analysis

Still, because the ß-galactosidase staining and *in situ* hybridization cannot be used as quantitative methods and because the LacZ labeling in the adult appeared somewhat more dense than the labeling obtained with *in situ* hybridization, we used RT-PCR analysis as an additional semiquantitative method to compare the expression level of Cx45 in the olivocerebellar system of P1 with that of the adult. The RT-PCR data followed the outcomes of the LacZ labeling in that Cx45 was indeed still expressed in all parts of the olivocerebellar system during adulthood, but it followed the *in situ* results in that its expression in the inferior olive was significantly decreased from 60 ± 1% to 15 ± 3% during transition into adulthood (P < 0.01, t-test), while in the cortex it did not (96 ± 4% vs. 83 ± 15%) (Figure 6). Expression in the cerebellar nuclei was also significantly reduced (from 65 ± 5% to 45 ± 3%; P < 0.01, t-test). The RT-PCR data obtained with Cx36 probes that were studied for control also correlated reasonably well with the histochemical data; the expression of Cx36 in the inferior olive increased from 73 ± 5% at P1 to 124 ± 6% in the adult (P < 0.01; t-test), while that in the

cerebellar nuclei and cerebellar cortex decreased significantly (from 93 ± 7% to 47 ± 2% and from 105 ± 7% to 86 ± 2%, respectively; P < 0.01 in both cases, t-test). Thus, taken together the RT-PCR data suggest that the higher sensitivity of the LacZ staining combined with the transient trends visible in the *in situ* studies provide a reliable view for the spatiotemporal distribution of the expression of Cx45.

Electron microscopic analysis of neuronal gap junctions

It is clear from the data described above that even though Cx45 is most prominently present in the olivocerebellar system during early postnatal stages, it is still expressed at low levels in the inferior olive, cerebellar nuclei, and cerebellar cortex of the adult. These findings raise the question as to whether neuronal gap junctions do not only occur within the inferior olive (Sotelo et al., 1974; De Zeeuw et al., 2003), but also between neurons in the cortex or nuclei. Thus, we set out experiments in wildtypes to find out whether neuronal gap junctions do occur between neurons in the cerebellum. In the cerebellar cortex of wildtypes we indeed found a substantial amount of dendrodendritic gap junctions (Figure 7). In several cases one could reasonably distinguish the characteristic morphology of dendrites of stellate cells from that of Purkinje cells, but frequently we were unable to do so with sufficient certainty. We therefore labeled the Purkinje cell dendrites with immunocytochemistry for calbindin and reexplored the cerebellar cortex. In this material, it was evident that all neuronal gap junctions in the cerebellar cortex occurred between stellate cells. The density of these gap junctions equaled 1 gap junction per 230,000 μm^2 of cerebellar cortex area. In contrast, in the cerebellar nuclei we did not find neuronal gap junctions with clear heptalaminar structures. We scanned more than a total area of 2,100,000 μm^2, but were unable to detect a single gap junction embedded in the membranes of neuronal somata, dendrites, or axons in these regions. This lack does not appear to be an artifact in the technical preparation of the material, because we found a high number of glial gap junctions within the cerebellar nuclei, which were easily recognized. Subsequently, we investigated the morphology and density of gap junctions in the neuropil of null-mutants of Cx45. In both the inferior olive and cerebellar cortex the gap junctions appeared totally normal with respect to their location in the neuropil as well as their morphology (Figure 8A, top micrographs). We did not observe any significant difference in the average interneuronal distance (3.05 ± 0.3 nm in wildtype and 3.02 ± 0.7 nm in Cx45–/– mice), plaque length (221 ± 47 vs. 220 ± 27 nm), interattachment distance (428 ± 53 vs. 436 ± 77 nm), or amount of electron-dense material on both cytoplasmic sides of the plaque among wildtypes

and Cx45 knockouts. Moreover, the densities of gap junctions in the Cx45 knockout mice did not differ from those in wildtypes, neither in the inferior olive (P > 0.25: t-test) nor in the cerebellar cortex (P > 0.5: t-test). In this respect the Cx45 knockouts differed completely from the Cx36 null mutants, in which all normal gap junctions in the inferior olive have been found to turn into "gap junction-like" structures with abnormally spatially separated membranes (Figure 8A, bottom micrographs) (for further details, see also De Zeeuw et al., 2003).
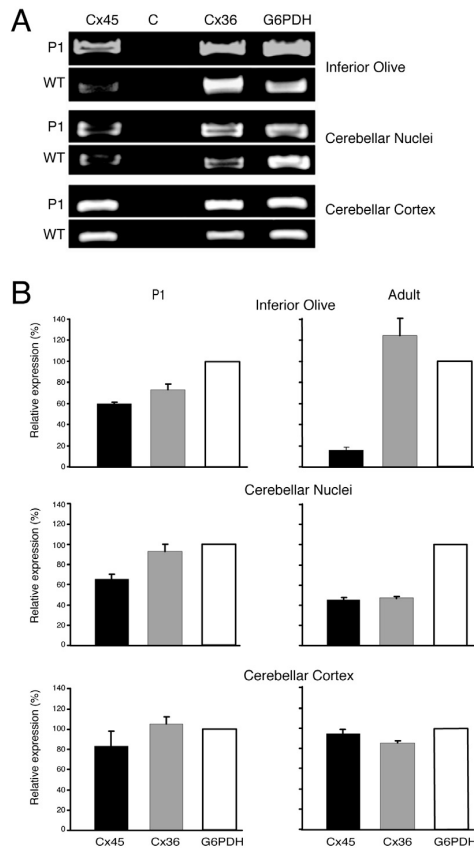
Figure 6. Expression analysis of Connexin45 and Connexin36 using RT-PCR. RT-PCR analysis of P1 wildtype and adult wildtype mice, respectively. Negative control (C) is RT-PCR performed without Superscript III. **A.** Expression analysis of Cx45, Cx36, and G6DPH in inferior olive, cerebellar nuclei, and cerebellar cortex. **B.** Graphs of relative expression compared to G6DPH-expression. The inferior olive expression pattern shows a relative upregulation of Cx36 and a down-regulation of Cx45. In the cerebellar nuclei both Connexins show a decrease in expression, while in the cerebellar cortex the expression stays almost consistent throughout development. All results are shown as mean ± SEM.
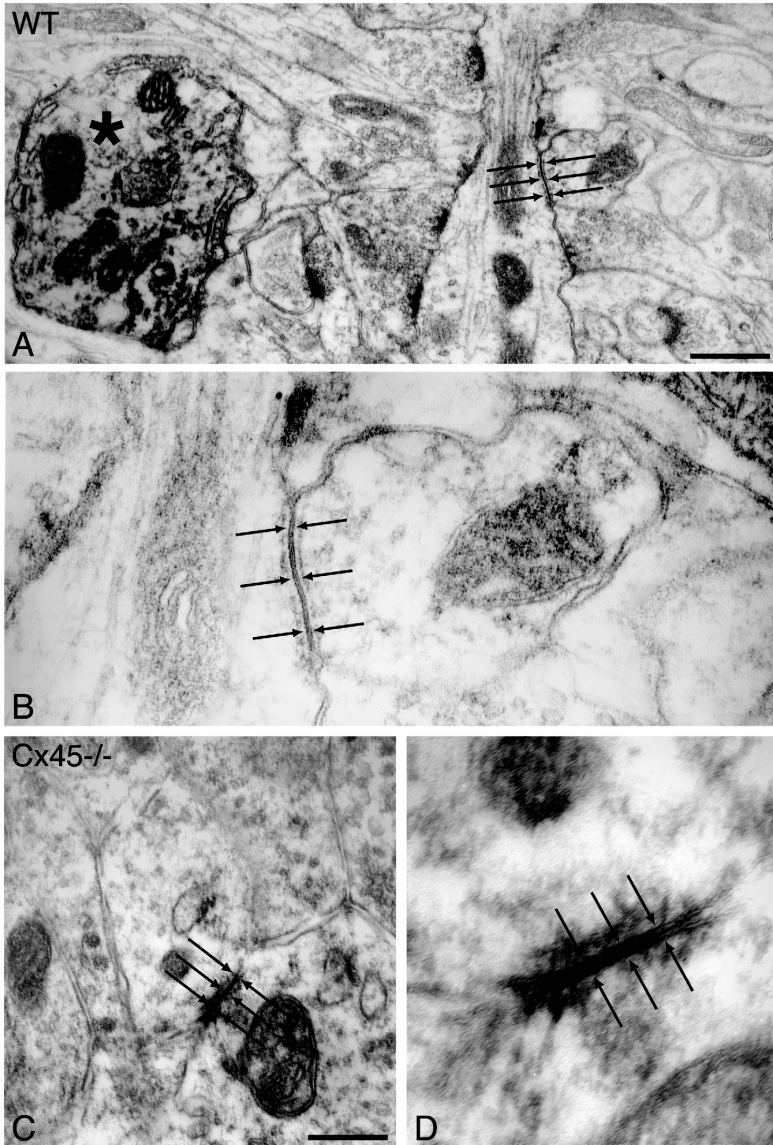
Figure 7. Gap junctions between stellate cells in the cerebellar cortex. A. Ultrastructural micrograph shows a dendrodendritic gap junction between stellate cell dendrites in a wildtype mouse (see arrows). To distinguish the dendrites from Purkinje cells (marked by asterisk), immunocytochemistry for calbindin was used to label the Purkinje cell dendrites. **B.** Higher magnification of the dendrodendritic gap junction, which shows a clear plaque with some dense material around the gap junction (plaque is indicated by arrows). **C.** A dendrodendritic gap junction (see arrows) between stellate cell dendrites in a Connexin45-deficient mouse. **D.** A higher magnification of a gap junction plaque (indicated by arrows) between stellate cells surrounded by dense material. Scale bars = 200 nm in A (applies to A,B), C (applies to C,D).
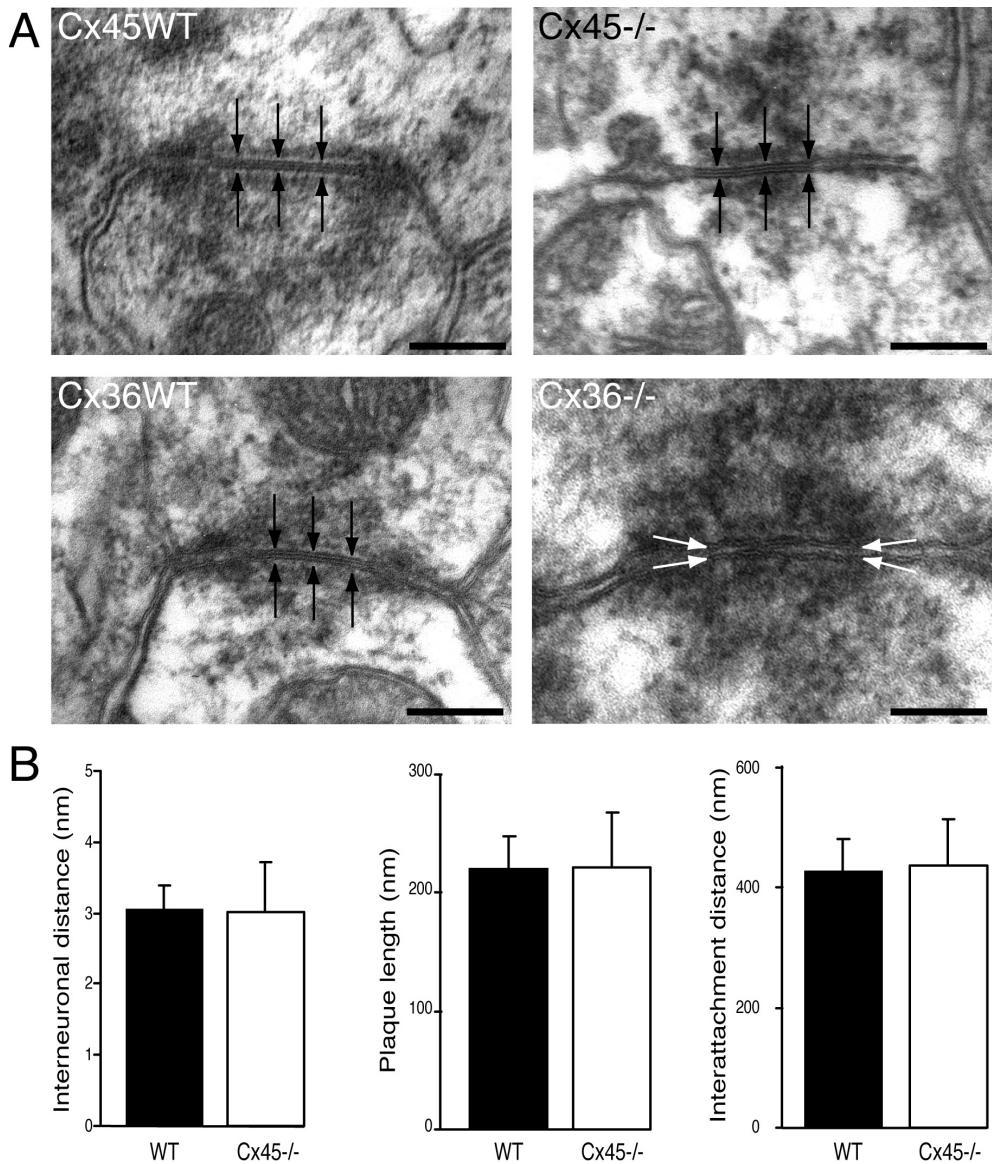
Figure 8. Olivary gap junctions in inferior olive. A. Ultrastructural micrographs showing dendrodendritic gap junctions in the inferior olive of wild type mice , Connexin45-deficient mice and Connexin36-deficient mice. In both the wildtype animals and Cx45-deficient mice normal gap junctions are found with a normal plaque (indicated by black arrows; see also histograms in B. In contrast gap junctions in the Cx36-deficient mutants show an in-creased interneuronal distance (indicated by white arrows). B. Histograms reveal the morphometric characteristics of gap junctions in wildtype and Cx45-deficient mice. The average interneuronal distance, plaque length, and interattachment distance were almost equal compared to the wildtype mice. All results are shown as mean ± SD. Scale bars = 100 nm.

Similarly, when we scanned more than 1,600,000 μm^2 in multiple slices of the cerebellar cortex of Cx36–/– mice for gap junctions between stellate cells in the present study, we got the same result: No normal gap junctions were detected between stellate cells in these mice. Thus, since Cx45–/– mice show, in contrast to Cx36–/– mice, normal gap junctions both between inferior olivary neurons and between stellate cells, Cx45 does not seem to be essential for the formation of neuronal gap junctions in the olivocerebellar system.

DISCUSSION

The major findings of the present study on the spatiotemporal distribution of Cx45 in the olivocerebellar system are that 1) Cx45 is expressed most prominently during early development; 2) Cx45 is expressed during adulthood but at relatively low levels; 3) Cx45 occurs in specific subnuclei of the inferior olive and cerebellar nuclei as well as interneurons of the molecular layer of the cerebellar cortex; and 4) Cx45 is not necessary for the structural formation of neuronal gap junctions in these regions. Below we discuss the spatiotemporal distribution of Cx45 for each of the three brain regions investigated, i.e., the inferior olive, cerebellar nuclei, and cerebellar cortex.

Inferior olive

Both the *in situ* hybridization and LacZ labeling methods showed that Cx45 is particularly prominently expressed in the inferior olive during early postnatal development. In fact, its expression even occurs slightly before the predecessors of normal gap junctions, i.e., the so-called "kissing junctions", as well as the concomitant expression of Cx36 occur in the inferior olive (between P10 and P15, see Bourrat and Sotelo, 1983; Degen et al., 2004). This temporal order raises the possibility that Cx45 facilitates the initial creation of the neuronal gap junctions in the olivocerebellar system. This possibility is further supported by the finding that the spatial distribution of the expression of Cx45 during adulthood follows that of early postnatal development (compare Figures 1C, 3D). However, at the same time it should be noted that not all olivary subnuclei expressed Cx45, while all neurons in all subnuclei do express Cx36 both during development and adulthood (De Zeeuw et al., 2003). Moreover, the morphological characteristics of the neuronal gap junctions in the Cx45 null-mutants appeared totally unaffected in contrast to those in Cx36 null-mutants.

Thus, if Cx45 plays a role in the formation of neuronal gap junctions, it has to be limited to particular subsets of neurons and it has to be reflected by physiological parameters rather than structural characteristics. Since all olivary cells express Cx36 (De Zeeuw et al., 2003), while only part express Cx45 during adulthood (present study), it is clear that the inferior olive does not have any neuron that solely expresses Cx45. This finding raises the possibility that Cx45 may serve to modify the electrical properties of the neuronal gap junctions that are predominantly formed by Cx36. Such a possibility is supported by the fact that Cx45 contains phosphorylation sites, which can affect the conductance properties, and that Cx45 can form, apart from homomeric, also heteromeric or heterotypic gap junctions (Hertlein et al., 1998; van Veen et al., 2000; Valiunas, 2002; Maxeiner et al., 2005). Moreover, a subtle functional role of Cx45 is also in line with the observation that Cx45 itself cannot fully compensate for a lack of Cx36 (De Zeeuw et al., 2003). Thus, the expression of Cx45 in the adult mice might play a role in altering various functional properties of the gap junctions by forming protein complexes with other connexins in the inferior olive.

Cerebellar nuclei

The *in situ* hybridization experiments, the LacZ labeling experiments, as well as the RT-PCR analyses showed that Cx45 and Cx36 are both prominently expressed in various parts of all cerebellar nuclei both during development and adulthood. Even so, we have not been able to detect any neuronal gap junction in our electron microscopic examination. In some cases there was a hint of an axosomatic junction similar to structures described for the vestibular nuclei (Korn et al., 1973; De Zeeuw and Berrebi, 1995), but we have not been able to identify a clear heptalaminar structure in any of these membranous processes. Possibly, we and other electron microscopists of the cerebellar nuclei have failed to detect neuronal gap junctions because they may be extremely difficult to find (Van der Want et al., 1989). Perhaps the plaques in these nuclei are much smaller than in other regions and may be even harder to detect than those of glial gap junctions, which can also be readily observed in the cerebellar nuclei (present study). Alternatively, one might wonder whether the connexins expressed in the nuclei are being used at another place, for example, the inferior olive. One could speculate that the connexins are transported via the axons of the cerebellar GABAergic neurons to their terminals, which are indeed known to be located directly at the spines that are coupled by dendrodendritic gap junctions in the olivary glomeruli (De Zeeuw et al., 1989; De Zeeuw et al., 1998).

Such a process could in fact be used as a mechanism to make sure that the vast majority of the olivary gap junctions are located at the peripheral spines that are strategically innervated by the GABAergic input from the nuclei. Interestingly, the subnuclei of the inferior olive that do not express Cx45, i.e., the ventral leaf of the PO and rostral MAO, do receive this GABAergic input from the cerebellar nuclei that prominently express Cx45, i.e., the lateral cerebellar nucleus and posterior interposed nucleus, respectively (present study; Ruigrok and Voogd, 2000). Thus, although this wild speculation reaches beyond the natural cell biological rule that proteins are used by the cells by which they are made, there are arguments and observations that are compatible with it.

Cerebellar cortex

Both the *in situ* hybridization experiments and the LacZ labeling experiments demonstrated that all interneurons in the molecular layer of the cerebellar cortex express Cx45 during both early postnatal development and adult-hood. Guided by the labeling, we indeed showed for the first time the existence of neuronal gap junctions between stellate cells. These data agree well with the cell physiological findings of Mann-Metzer and Yarom (1999, 2000), who demonstrated electrotonic coupling between inhibitory interneurons in the molecular layer within the cerebellar cortex. Yet in this region, too, the presence of Cx45 was not essential for the structural formation of neuronal gap junctions, as their morphology was not abnormal. Thus, similar to the inferior olive, Cx45 in the cerebellar cortex may serve a role so as to subtly modify the function of neuronal gap junctions, but it appears unlikely that it is necessary for the occurrence of electrotonic coupling itself.

REFERENCES

Bastianelli E. 2003. Distribution of calcium-binding proteins in the cerebellum. Cerebellum 2:242–262.

Belluardo N, Mudo G, Trovato-Salinaro A, Le Gurun S, Charollais A, Serre-Beinier V, Amato G, Haefliger JA, Meda P, Condorelli DF. 2000.
Expression of Connexin36 in the adult and developing rat brain. Brain Res 865:121–138.

Bevans CG, Kordel M, Rhee SK, Harris AL. 1998. Isoform composition of connexin channels determines selectivity among second messengers and uncharged molecules. J Biol Chem 273:2808–2816.

Bourrat F, Sotelo C. 1983. Postnatal development of the inferior olivary complex in the rat. I. An electron microscopic study of the medial accessory olive. Brain Res 284:291–310.

Bukauskas FF, Angele AB, Verselis VK, Bennett MV. 2002. Coupling asymmetry of heterotypic connexin 45/connexin 43-EGFP gap junctions: properties of fast and slow gating mechanisms. Proc Natl Acad Sci U S A 99:7113–7118.

Condorelli DF, Parenti R, Spinella F, Trovato Salinaro A, Belluardo N, Cardile V, Cicirata F. 1998. Cloning of a new gap junction gene (Cx36) highly expressed in mammalian brain neurons. Eur J Neurosci 10: 1202–1208.

Condorelli DF, Trovato-Salinaro A, Mudo G, Mirone MB, Belluardo N. 2003. Cellular expression of connexins in the rat brain: neuronal localization, effects of kainate-induced seizures and expression in apoptotic neuronal cells. Eur J Neurosci 18:1807–1827.

De Zeeuw CI, Berrebi AS. 1995. Postsynaptic targets of Purkinje cell terminals in the cerebellar and vestibular nuclei of the rat. Eur J Neurosci 7:2322–2333.

De Zeeuw CI, Holstege JC, Ruigrok TJ, Voogd J. 1989. Ultrastructural study of the GABAergic, cerebellar, and mesodiencephalic innervation of the cat medial accessory olive: anterograde tracing combined with immunocytochemistry. J Comp Neurol 284:12–35.

De Zeeuw CI, Hertzberg EL, Mugnaini E. 1995. The dendritic lamellar body: a new neuronal organelle putatively associated with dendrodendritic gap junctions. J Neurosci 15:1587–1604.

De Zeeuw CI, Simpson JI, Hoogenraad CC, Galjart N, Koekkoek SK, Ruigrok TJ. 1998. Micro-circuitry and function of the inferior olive. Trends Neurosci 21:391–400.

De Zeeuw CI, Chorev E, Devor A, Manor Y, Van Der Giessen RS, De Jeu MT, Hoogenraad CC, Bijman J, Ruigrok TJ, French P, Jaarsma D, Kistler WM, Meier C, Petrasch-Parwez E, Dermietzel R, Söhl G, Güldenagel M, Willecke K, Yarom Y. 2003. Deformation of network connectivity in the inferior olive of connexin 36-deficient mice is compensated by morphological and electrophysiological changes at the single neuron level. J Neurosci 23:4700–4711.

Degen J, Meier C, Van Der Giessen RS, Söhl G, Petrasch-Parwez E, Urschel S, Dermietzel R, Schilling K, De Zeeuw CI, Willecke K. 2004. Expression pattern of lacZ reporter gene representing Connexin36 in transgenic mice. J Comp Neurol 473:511–525.

Duan L, Yuan H, Su CJ, Liu YY, Rao ZR. 2004. Ultrastructure of junction areas between neurons and astrocytes in rat supraoptic nuclei. World J Gastroenterol 10:117–121.

French PJ, O'Connor V, Voss K, Stean T, Hunt SP, Bliss TV. 2001. Seizure-induced gene expression in area CA1 of the mouse hippocampus. Eur J Neurosci 14:2037–2041.

Hertlein B, Butterweck A, Haubrich S, Willecke K, Traub O. 1998. Phosphorylated carboxy terminal serine residues stabilize the mouse gap junction protein Connexin45 against degradation. J Membr Biol 162: 247–257.

Hombach S, Janssen-Bienhold U, Söhl G, Schubert T, Bussow H, Ott T, Weiler R, Willecke K. 2004. Functional expression of connexin57 in horizontal cells of the mouse retina. Eur J Neurosci 19:2633–2640.

Korn H, Sotelo C, Crepel F. 1973. Electronic coupling between neurons in the rat lateral vestibular nucleus. Exp Brain Res 16:255–275.

Krüger O, Plum A, Kim JS, Winterhager E, Maxeiner S, Hallas G, Kirchhoff S, Traub O, Lam-

ers WH, Willecke K. 2000. Defective vascular development in connexin 45-deficient mice. Development 127:4179– 4193.

Kumar NM, Gilula NB. 1996. The gap junction communication channel. Cell 84:381–388.

Mann-Metzer P, Yarom Y. 1999. Electrotonic coupling interacts with intrinsic properties to generate synchronized activity in cerebellar net-works of inhibitory interneurons. J Neurosci 19:3298–3306.

Mann-Metzer P, Yarom Y. 2000. Electrotonic coupling synchronizes inter-neuron activity in the cerebellar cortex. Prog Brain Res 124:115–122.
Maxeiner S, Krüger O, Schilling K, Traub O, Urschel S, Willecke K. 2003.

Spatiotemporal transcription of Connexin45 during brain development results in neuronal expression in adult mice. Neuroscience 119:689– 700.

Maxeiner S, Dedek K, Janssen-Bienhold U, Ammermuller J, Brune H, Kirsch T, Pieper M, Degen J, Krüger O, Willecke K, Weiler R. 2005. Deletion of Connexin45 in mouse retinal neurons disrupts the rod/cone signaling pathway between AII amacrine and ON cone bipolar cells and leads to impaired visual transmission. J Neurosci 25:566–576.

Nelles E, Butzler C, Jung D, Temme A, Gabriel HD, Dahl U, Traub O, Stumpel F, Jungermann K, Zielasek J, Toyka KV, Dermietzel R, Willecke K. 1996. Defective propagation of signals generated by sympathetic nerve stimulation in the liver of connexin32-deficient mice. Proc Natl Acad Sci U S A 93:9565–9570.

Ruigrok TJ, Voogd J. 2000. Organization of projections from the inferior olive to the cerebellar nuclei in the rat. J Comp Neurol 426:209–228.

Söhl G, Degen J, Teubner B, Willecke K. 1998. The murine gap junction gene Connexin36 is highly expressed in mouse retina and regulated during brain development. FEBS Lett 428:27–31.

Söhl G, Odermatt B, Maxeiner S, Degen J, Willecke K. 2004. New insights into the expression and function of neural connexins with transgenic mouse mutants. Brain Res Brain Res Rev 47:245–259.

Sotelo C, Llinás R, Baker R. 1974. Structural study of inferior olivary nucleus of the cat: morphological correlates of electrotonic coupling. J Neurophysiol 37:541–559.

Theis M, Söhl G, Speidel D, Kuhn R, Willecke K. 2003. Connexin43 is not expressed in principal cells of mouse cortex and hippocampus. Eur J Neurosci 18:267–274.

Theis M, Söhl G, Eiberger J, Willecke K. 2005. Emerging complexities in identity and function of glial connexins. Trends Neurosci 28:188–195.

Valiunas V. 2002. Biophysical properties of connexin-45 gap junction hemichannels studied in vertebrate cells. J Gen Physiol 119:147–164.

Van der Want JJ, Wiklund L, Guegan M, Ruigrok T, Voogd J. 1989. Anterograde tracing of the rat olivocerebellar system with Phaseolus vulgaris leucoagglutinin (PHA-L). Demonstration of climbing fiber collateral innervation of the cerebellar nuclei. J Comp Neurol 288:1–18.

van Veen TA, van Rijen HV, Jongsma HJ. 2000. Electrical conductance of mouse Connexin45 gap junction channels is modulated by phosphorylation. Cardiovasc Res 46:496–510.

Weber PA, Chang HC, Spaeth KE, Nitsche JM, Nicholson BJ. 2004. The permeability of gap junction channels to probes of different size is dependent on connexin composition and permeant-pore affinities. Biophys J 87:958–973.

Willecke K, Eiberger J, Degen J, Eckardt D, Romualdi A, Güldenagel M, Deutsch U, Söhl G. 2002. Structural and functional diversity of connexin genes in the mouse and human genome. Biol Chem 383:725–737.

Chapter 3

Consequences of a lack of Connexin36 on olivary neurons at the cellular electrophysiological level

CHAPTER 3.1

Deformation of Network Connectivity in the Inferior Olive of Connexin 36-Deficient Mice Is Compensated by Morphological and Electrophysiological Changes at the Single Neuron Level

CHRIS I. DE ZEEUW[1], EDITH CHOREV[2], ANNA DEVOR[2], YAIR MANOR[3], RUBEN S. VAN DER GIESSEN[1], MARCEL T. DE JEU[1], CASPER C. HOOGENRAAD[1], JAN BIJMAN[1], TOM J. H. RUIGROK[1], PIM J.FRENCH[1], DICK JAARSMA[1], WERNER M. KISTLER[1], CAROLA MEIER[4], ELISABETH PETRASCH-PARWEZ[4], ROLF DERMIETZEL[4], GORAN SÖHL[5], MARTIN GÜLDENAGEL[4], KLAUS WILLECKE[5], AND YOSI YAROM[2]

[1]*Department of Neuroscience, Medical Faculty, Erasmus MC, 3000DR Rotterdam, The Netherlands*
[2]*Department of Neurobiology, Institute of Life Sciences, Hebrew University, Jerusalem 91904, Israël*
[3]*Department of Life Sciences and Zlotowski Center for Neuroscience, Ben-Gurion University, Beer-Sheva 84105, Israël*
[4]*Department of Neuroanatomy and Molecular Brain Research, Institute of Anatomy, Ruhr-University Bochum, D-44801 Bochum, Germany,*
[5]*Institute of Genetics, Division of Molecular Genetics, University of Bonn, 53117 Bonn, Germany*

ABSTRACT

Compensatory mechanisms after genetic manipulations have been documented extensively for the nervous system. In many cases, these mechanisms involve genetic regulation at the transcription or expression level of existing isoforms. We report a novel mechanism by which single neurons compensate for changes in network connectivity by retuning their intrinsic electrical properties. We demonstrate this mechanism in the inferior olive, in which widespread electrical coupling is mediated by abundant gap junctions formed by Connexin36 (Cx36). It has been shown in various mammals that this electrical coupling supports the generation of subthreshold oscillations, but recent work revealed that rhythmic activity is sustained in knock-outs of Cx36. Thus, these results raise the question of whether the olivary oscillations in Cx36 knock-outs simply reflect the status of wild-type neurons without gap junctions or the outcome of compensatory mechanisms. Here, we demonstrate that the absence of Cx36 results in thicker dendrites with gap-junction-like structures with an abnormally wide interneuronal gap that prevents electrotonic coupling. The mutant olivary neurons show unusual voltage-dependent oscillations and an increased excitability that is attributable to a combined decrease in leak conductance and an increase in voltage-dependent calcium conductance. Using dynamic-clamp techniques, we demonstrated that these changes are sufficient to transform a wild-type neuron into a knock-out-like neuron. We conclude that the absence of Cx36 in the inferior olive is not compensated by the formation of other gap junction channels but instead by changes in the cytological and electro-responsive properties of its neurons, such that the capability to produce rhythmic activity is maintained.

INTRODUCTION

Gap junctions, the morphological correlate of electrical transmission (Bennett, 2002), have been described in a substantial number of brain areas, including the cerebral cortex (Peters, 1980), hippocampus (MacVicar and Dudek, 1981), olfactory bulb (Lan-dis et al., 1974), cerebellar cortex (Sotelo and Llinás, 1972), spinal cord (Matsumoto et al., 1988), trigeminal nucleus (Hinrichsen and Larramendi, 1968), and inferior olive (Sotelo et al., 1974; De Zeeuw et al., 1989). Most, if not all, of the neuronal gap junctions in these brain regions are formed by Connexin36 (Cx36), a gap junction protein specific for neurons (Condorelli et al., 1998; Rash et al., 2000). The functions of Cx36 in the hippocampus and cerebral cortex were ad-

dressed recently in a series of knockout studies. It was suggested that axo-axonal gap junctions are crucial for high-frequency ripple oscillations in CA1 pyramidal cells (Schmitz et al., 2001; Spruston, 2001; Maier et al., 2002), whereas gap junctions between interneurons in the cerebral cortex may be necessary for the generation of synchronous inhibitory activities underlying gamma oscillations (Deans et al., 2001; Hormuzdi et al., 2001). In addition, it has been shown that visual transmission is probably delayed in Cx36-deficient mice because of impaired coupling between amacrine and bipolar cells in the retina (Güldenagel et al., 2001). Despite these evidences, the correlation between the absence of Cx36 and neuronal gap junctions remains to be demonstrated at the ultrastructural level. This issue is particularly relevant because compensatory mechanisms such as an upregulation of other connexins or secondary morphological or cell physiological reactions could occur.

The high levels of Cx36 found in the rat inferior olive suggest that electrotonic coupling is most prominent in this brain region (Condorelli et al., 1998; Belluardo et al., 2000). This notion is also supported by the high density and distribution of dendritic lamellar bodies, which are associated with dendrodendritic gap junctions (De Zeeuw et al., 1995, 1997). Several roles have been proposed for electrotonic coupling in the inferior olive. For example, clustering of coupled olivary cells could play a role during development in the formation of sagittally organized zones in the cerebellar cortex, each of which receives its climbing fiber input from a particular olivary subnucleus (Voogd and Bigaré, 1980; De Zeeuw et al., 1994). Other reports propose that electrotonic coupling in the olivary neurons may underly their ability to fire synchronously and thereby to trigger the onset of movements (Welsh et al., 1995; Ivry, 1996; Lang, 2001), or they raise the possibility that this process may, in fact, contribute to cerebellar motor learning (De Zeeuw et al., 1998; Kistler et al., 2000). Furthermore, several studies have provided evidence that electrical coupling is essential for the generation of subthreshold oscillations in the inferior olive (Llinás and Yarom, 1981a,b, 1986; Lampl and Yarom, 1993, 1997; Manor et al., 1997, 2000; Loewenstein et al., 2001), which in turn could serve as a generator of temporal patterns (Yarom and Cohen, 2002).

However, a recent study of Cx36-deficient mice showed that their olivary neurons display subthreshold rhythmic activities, despite the fact that they lack functional coupling (Long et al., 2002). Moreover, these mutants show a normal motor behavior, in that their locomotion and compensatory eye movements are relatively unaffected and they show a synchronized tremor after harmaline injections, which is comparable with that in wild-type mutants (Kistler et al., 2002). These findings raise the question of how the rhythmic subthreshold activities in olivary neurons can be sustained in the Cx36 knock-out mutants and whether

gap junctions are, in fact, essential for the generation of subthreshold rhythmic activities in wild-type mutants. After all, if there are no secondary compensations in the mutants, one could argue indeed that gap junctions between olivary neurons are not essential for the oscillations in wild types (Long et al., 2002).

Here, we demonstrate that a lack of Cx36 in the inferior olive leads to abnormally thick dendrites with nonfunctional gap junction-like structures, which in turn results in altered membrane properties that can account for the ability of olivary neurons to produce oscillatory behavior in the absence of normal gap junctions. We propose that the adaptive changes in intrinsic properties in the noncoupled network, such as to enable rhythmic activity, emphasize the importance of these oscillations for the normal function of the olivocerebellar system.

MATERIAL AND METHODS

In situ hybridization.

Cx36-deficient and wild-type mice were generated and characterized as described by Güldenagel et al. (2001). Subsequently, they were anesthetized by asphyxiation in CO_2 and decapitated, and their brains were carefully removed, frozen on dry ice, and stored at -80°C. The brainstems containing the inferior olive were cut into 14 μm sections on a cryostat, mounted on polylysine-coated glass slides, and stored at -80°C. Slides were fixed in 4% paraformaldehyde (5 min) and acetylated in 1.4% triethanolamine and 0.25% acetic anhydride. Sections were then prehybridized (1 hr) in buffer containing 50% formamide, 5X SSC, 5X Denhardt's solution, 250 μg/ml yeast tRNA (Sigma, St. Louis, MO) and 500 μg/ml acid-alkali cleaved salmon testis DNA (Sigma). Hybridization was performed overnight at 65°C in prehybridization buffer containing 100 ng/ml digoxigenin–UTP-labeled cRNA probes. Probes were generated using a digoxigenin RNA labeling kit (Roche) according to the manufacturer's instructions.Sense and antisense probes generated against the full-length coding sequence of Cx36 were then hydrolyzed in 40 mM $NaHCO_3$ and 60 mM Na_2CO_3 for 25 min at 60°C to generate fragments of ~300 bases. After hybridization, sections were washed in 0.2X SSC at 65°C and blocked in 0.1 M Tris, pH 7.5, 0.15 M NaCl, and 10% heat-inactivated sheep serum (Sigma) for 1 hr at room temperature. Alkaline phosphatase-conjugated anti digoxigenin antibodies (Roche) were added to the sections in a dilution of 1:5000 in 0.1 M Tris, pH 7.5, 0.15 M NaCl, and 1% heat-inactivated sheep serum and incubated overnight at 4°C. After

washing of the sections, color reactions were performed in 0.1 M Tris, pH 9.5, 0.1 M NaCl, 50 mM $MgCl_2$, 2 mM levamisole (Sigma), 0.35mg/ml nitroblue tetrazolium (Roche),and 0.18 mg/ml 5-bromo-4-chloro-3-indolylphosphate (Roche). Reactions were terminated on visual inspection (~18 hr), counterstained in 0.1% Fast Red, dehydrated, and mounted in Permount (Fisher Scientific, Houston, TX).

Immunocytochemistry.

Cx36-deficient and wild-type mice were anesthetized by asphyxiation in CO_2 and decapitated. Brains were dissected, cut into frontal brain blocks, and frozen in 8% methylcyclohexan in 2-methylbutan (v/v, -80°C). Immunohistochemistry was performed on cryosections of 14 μm thickness fixed in cold ethanol for 10 min at -20°C, rinsed in PBS, and preincubated in blocking buffer (10% normal goat serum and 0.1% Triton X-100 in PBS) for 30 min. The Cx36 anti-body was diluted in blocking buffer (dilution 1:500), and sections were incubated overnight at room temperature. This affinity-purified polyclonal antibody was directed to the cytoplasmic loop of mouse Cx36 and has been described by Teubner et al. (2000). Preimmune serum to this antibody served as an additional control for the specificity of the immunoreaction. After incubation, samples were rinsed in PBS, followed by a 30 min incubation in 0.2% BSA in PBS. Incubation with the secondary antibody (Alexa Fluor 488 goat anti-rabbit; Molecular Probes, Leiden, The Netherlands) was performed at a 1:4000 dilution in blocking buffer for 2 hr at room temperature. After rinsing in PBS, the sections were mounted using the ProLong Antifade kit (Molecular Probes). Fluorescence was documented using confocal imaging microscopy (LSM 510 inverted confocal microscope, argon/krypton laser; Zeiss Oberkochen, Germany). Data were collected as single planes using the single track scanning module. All data were exported as TIFF files into Adobe Photoshop 5.5 (Adobe Imaging Systems Inc., San Jose, CA) for documentation.

Rapid Golgi staining.

Cx36-deficient and wild-type mice were anesthetized by asphyxiation in CO_2, perfused with 0.01 M sodium cacodylate in 9% NaCl and 4% paraformaldehyde in 0.1 sodium cacodylate, and decapitated. Brainstems including the inferior olive were dissected, cut into 80 μm slices, and incubated for 2 d in 3.5% $K_2Cr_2O_7$/0.12% OsO_4. Subsequently, the sections were rinsed in 3.5% $K_2Cr_2O_7$, embedded in 4% agar, and rinsed in 0.75% $AgNO_3$ and Aquadest at 4°C. After 60 min in kodalith, the sections were rinsed in Aquadest at 4°C, 1% $Na_2S_2O_3$, and 5% H_2O, and mounted.

Quantitative analyses of the Golgi material were performed with the use of automized camera lucida equipment. Quantitative analyses were done with the use of camera lucida equipment.

Electron microscopy.

Adult Cx36-/- mice, Cx36+/- mice, and wild-type littermates were anesthetized with an overdose of Nembutal and transcardially perfused with 4% paraformaldehyde and 1% glutaraldehyde in 0.12 M cacodylate buffer; the brainstem containing the inferior olive was then processed for electron microscopy as described by De Zeeuw et al. (1989). In short, 100-μm-thick sections were cut on a vibratome, osmicated in OsO_4, stained en bloc in tannic acid and uranyl acetate, dehydrated in dimethoxypropane, and embedded in Araldite. Subsequently, the various olivary subnuclei were identified on semithin sections, pyramids were made, and ultrathin sections were cut accordingly on a Reichert ultratome, counterstained with uranyl acetate and lead citrate, and examined with the use of a Philips CM-100 electron microscope. The sections of the various tissue blocks were systematically screened per surface area, and the gap junctions and gap-junction-like structures were identified and quantified.

Dye coupling.

The experiments were performed on 300 μm coronal slices of the inferior olive obtained from the brainstem of adult wild-type and homozygous Cx36 null-mutant mice. After identification of an olivary neuron, glass micropipettes containing either Lucifer yellow (2– 4%) or Neurobiotin (5%) were inserted into the cell according to Bacskai and Matesz (2002). In the Lucifer yellow experiments, frozen sections were examined under a fluorescent microscope, whereas Neurobiotin was visualized with the use of ABC reagent and a DAB solution according to standard procedures.

Electrophysiology.

Whole-cell patch technique was used for intracellular recordings of either voltage or current activity of olivary neurons in brainstem slices. Parasagittal slices (300 μm) were prepared from the brainstem of wild-type and homozygous Cx36 null-mutant mice that were at least 1 month of age. Slice preparation and recording techniques have been described in detail previously by Devor and Yarom (2002a,b).

Recordings were performed at room temperature (22–25°C) in a physiological solution containing (in mM): 127.2 NaCl, 1.8 KCl, 1.3 $MgSO_4$, 1.2 KH_2PO_4, 26 $NaHCO_3$, 10 glucose, and 2.4 $CaCl_2$. The pipette solution contained (in mM): 4 NaCl, 10^{-3} $CaCl_2$, 140 K-gluconate, 10^{-2} EGTA, 4 Mg-ATP, and 10 HEPES, pH 7.2. In the voltage-clamp experiments, 1 µM TTX was added to the physiological solution. To characterize the densities of ionic currents, we measured the current responses to a series of negative voltage steps from a holding potential of -50 mV. The current traces (Figure 1A) were averaged and saved for off-line analysis. The capacitive current (used for estimating the surface area; inset A) and the input resistance were measured from the response to -4 mV voltage step (top trace). The h current and the Ca^{2+} current (inset B) as well as the late outward current (I_{AHP}) were measured as indicated in the figure. Because the capacitive current is correlated with surface area, we used this current to compute current densities. It is therefore of utmost importance to measure the capacitive current with maximal reliability.
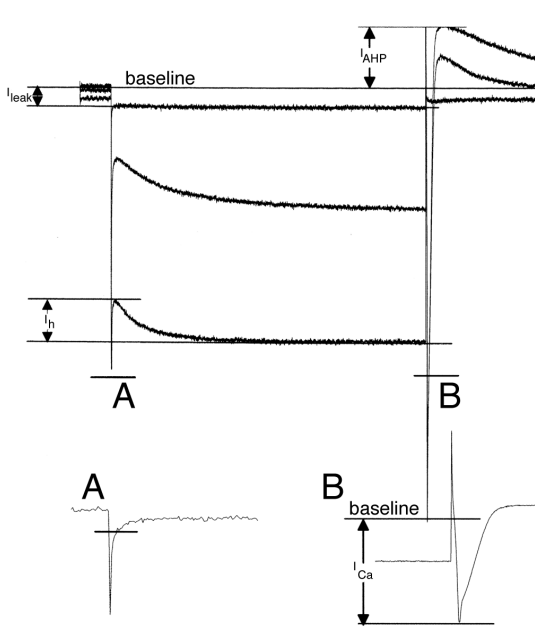
Figure 1. Characterizing ionic currents. Negative voltage steps from a holding potential of -50 mV were used to characterize the ionic currents. Three examples of current responses to voltage steps of -4, -28, and -56 mV are shown. The input resistance (R_{in}) was measured from the amplitude of the current response to a -4 mV voltage step as shown on the trace (I_{leak}). The afterhyperpolarizing current (I_{AHP}) was measured from the baseline to the peak of the outward current at the end of the voltage step. The I_{AHP} current is a mixture of hcurrent and possibly Ca^{2+}-dependent K^+ current. The Ih was measured as the difference between the initial current and the steady-state current developed at the end of the hyperpolarizing voltage step. The capacitance was calculated from the integral of the capacitive current induced by a -4 mV voltage step (inset A). The area to integrate was limited to the fast transient only (horizontal bar). As expected, this definition resulted in a linear relationship between the input conductance and the cell capacitance, as demonstrated in Figure 2. The calcium current is enlarged in inset B, and the amplitude is measured as shown.
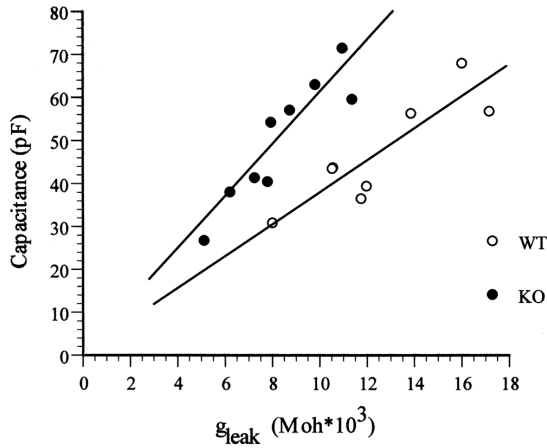
Figure 2. The measured input resistance (R_{in}) is correlated with the calculated capacitance. $1/R_{in}$ is linearly related to the capacitance (R^2 = 0.76 for wild type and R^2 = 0.85 for knockout). The slope of the linear feet gives us the average time constant of these cells (T = 3.7 msec for wild type and T = 6.03 msec for knockout). WT, Wild type; KO, knock-out.

To demonstrate the validity of our measurement method, we plotted the cell capacitance (calculated from the integral of the capacitive current) as a function of the input conductance (Figure 2). The linear relationships for both wild type and knock-out assessed the validity of our measurement protocol. The slopes of these linear curves closely represent the membrane time constants (3.7 and 6.0 msec for wild type and knock-out, respectively).

Dynamic clamp.

We used the dynamic-clamp technique (Sharp et al., 1993) to artificially decrease a leak conductance, or add a low-threshold calcium (LTC)-like conductance, into olivary neurons. Briefly, we continuously acquired the voltage of the cell (V), computed a conductance, calculated the driving force, and injected the product back into the cell, using an update rate of 2 kHz. To decrease a leak conductance g_L, before the dynamic-clamp injection, we measured the resting potential of the cell (V_r) and used this value as the equilibrium potential for this conductance. To add an LTC-like conductance, g_T, we solved on-line a set of differential equations that described the voltage dependence and time dependence of this conductance. We used the following equation: $g_T = G_T \, m \, h$, where G_T is the maximal conductance and x= m, h are state variables that obey the following kinetics: $dx/dt = (x\infty(V) - x)/\tau_x$, where $x\infty(V)$ is a steady-state curve of the form $(1 + exp^{(V - V1/2)/ k)-1}$; $V_{1/2}$ in mV: m =-61, h =-85.5; k in mV: m =4.3, h =8.6; τ_m =5 msec; and τ_h is voltage dependent equal to 220 msec at -90 mV (for details, see Manor et al., 1997).

RESULTS

In situ hybridization and immunocytochemistry.

To find out whether Cx36 is ubiquitously expressed among neurons of the olivary subnuclei in mice, we investigated the murine inferior olive using *in situ* hybridization and immu-

nocytochemistry. After application of antisense Cx36 probes, all neurons of all olivary subnuclei of wild-type mice were positively labeled at all rostrocaudal levels (Figure 3). In contrast, none of the olivary neurons in wild-type mice were labeled with the use of sense probes, and none of the olivary neurons in Cx36 knock-out mice were labeled with the use of antisense probes. After immunocytochemical application of antibodies against Cx36, all olivary subnuclei of wild-type mice showed a clear punctate labeling throughout their neuropil, whereas no labeling was observed in Cx36 null-mutant mice (Figure 4). Together, these data indicate that all olivary neurons in wild-type mice express Cx36 and form gap junctions.

Figure 3. Ubiquitous distribution of Cx36 mRNA in the inferior olive of the mouse. A. Low magnification of labeled olivary neurons in medial accessory olive, dorsal accessory olive, and principal olive after *in situ* hybridization; with the use of Cx36 antisense probes,all neurons of all olivary subnuclei of wild-type (WT) mice were positively labeled. **B.** High magnification of labeled neurons in the medial accessory olive. **C.** In contrast, none of the olivary neurons in Cx36 knock-out mice were labeled with the use of antisense probes. Scalebars:A, 100µm; B ,20µm; C, 120 µm.

Cytoarchitecture.

Analyses of Golgi-stained sections of the inferior olive of wild-type mice (n = 4) and Cx36 knock-out mice (n = 4) did not reveal a significant difference in average diameter of the cell bodies (12.8 ± 1.4 µm for wild-type mice vs 13.7 ± 0.9 µm for Cx36 knock-out mice), average length of the stained dendrites (59 ± 23 vs 60 ± 25µm), or average density of stained spines per micrometer of dendrite (0.13 ± 0.05 vs 0.12 ± 0.04).
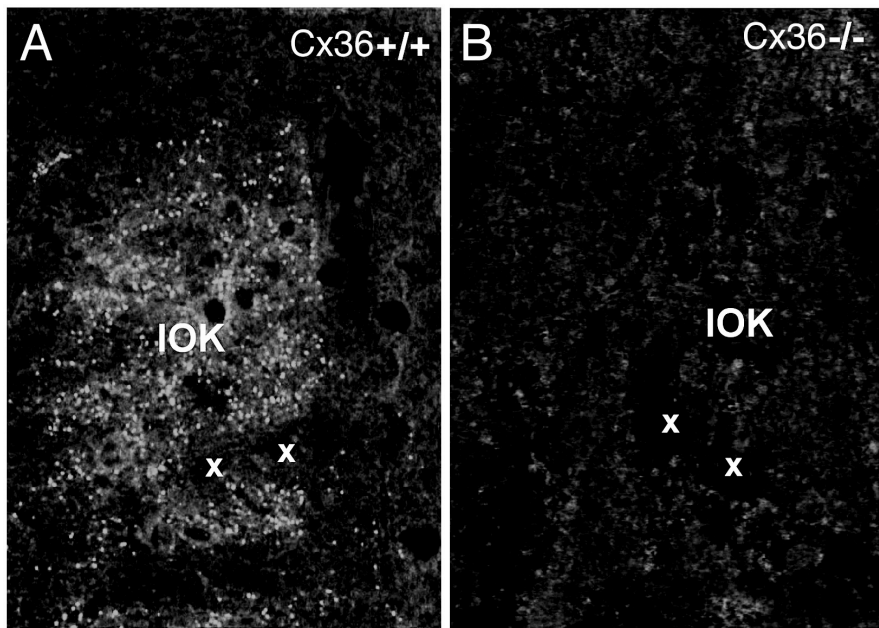
Figure 4. Punctate labeling in olivary neuropil after immunocytochemistry with the use of anti-Cx36. A. In wild-type mice, the entire neuropil was filled with labeled puncta; this micrograph shows an example of labeling in the smallest olivary subnucleus, the dorsal cap of Kooij (IOK). **B.** In the Cx36-deficient mouse, no puncta were visible. x, Examples of cell bodies.

However, we did observe a significant difference in the average thickness of the proximal dendrites (Figure 5). When measured 5 µm distally to the soma, the average diameter of the dendrites was 1.9 ± 0.3 µm in wild types and 2.6 ± 0.3 µm in Cx36 knock-outs ($p < 0.05$; t test). The ramifications of the dendrites, in contrast, were not different when analyzed with topological analyses that provided values for the symmetry of arborizations (Van Pelt et al., 1992).

Electron microscopy.

Ultrastructural analyses of gap junctions (n = 178) of neurons in the inferior olive of wild-type mice (n = 6) showed that they have the same general morphological characteristics as described for other mammals (for review, see De Zeeuw et al., 1998). Characteristics consist of a plaque with an average diameter of 272 ± 26 nm and an interneuronal space of 3.2 ± 0.4 nm thickness; they show electron-dense deposits at both sides of the membrane and have attachment plaques surrounding the plaque with gap junction channels (Figure 6). Moreover, the vast majority of olivary gap junctions in mice connect two dendritic spines

that are located in the core of a glomerulus, which is surrounded by both inhibitory and excitatory terminals. In all olivary subnuclei of homozygous Cx36-deficient mice (n = 5), we observed gap-junction-like structures (n = 144) that met all criteria mentioned previously, except that they lacked a plaque with a narrow interneuronal space; their average inter-neuronal space was approximately three times wider (9.2 ± 1.4 nm; $p < 0.004$; Student's t test) (Figures 7, 8). The average distance between the attachment plaques (423 ± 92 nm) of the gap junction-like structures was not significantly different ($p = 0.64$; F test) from that of gap junctions in wild-type littermates (416 ± 46 nm). All gap-junction-like structures were also positioned between two dendritic profiles in the core of glomeruli. Moreover, the morphological characteristics of the glomeruli themselves, just as those of the extraglo-merular neuropil, including the presence and shape of dendritic lamellar bodies, appeared normal. However, the average density of gap-junction-like structures in the olive of Cx36-deficient mice (56 per mm^2) was significantly lower ($p < 0.01$; Student's t test) than that of gap junctions in wild-type littermates (85 per mm^2). Smaller-sized gap-junction plaques, as described by Raviola and Gilula (1975) for example, were not observed in the mutants.
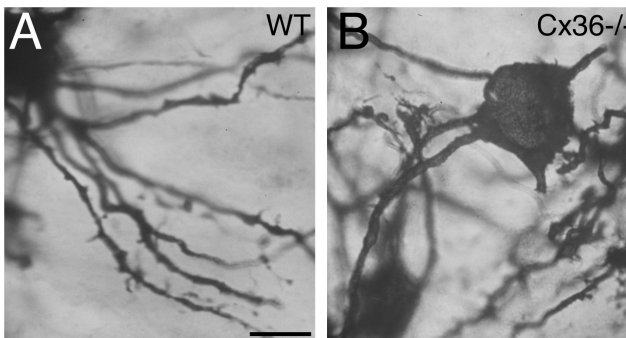
Figure 5. Rapid Golgi staining of olivary neurons in wild-type (WT) mice (A) and Cx36-/- mice (B). Note that the proximal dendrites of Cx36-/- mice are thicker than those of the wild-type mice.The magnifications of A and B are the same. Scalebar, 9.7 µm.

With regard to the size of the dendrites, we observed that the average diameter of proximal dendrites (2.7 ± 0.4 µm), as identified by the presence of ribosomes (De Zeeuw et al., 1989), was significantly larger ($p < 0.03$; t test) in mutants than in wild types (1.8 ± 0.4 µm). No significant differences were observed for the diameters of distal dendrites. The morphology and density of glial gap junctions were not affected in Cx36-deficient mice. Finally, the density of neurons as counted in both the ultrathin and semithin sections was not significantly different in Cx36-deficient mice. In the inferior olive of heterozygous Cx36-deficient mice (n = 4), we observed gap junctions (n = 73) that showed all essential criteria for true gap junctions, including a normal interneuronal space of -2.9 ± 0.3 nm.
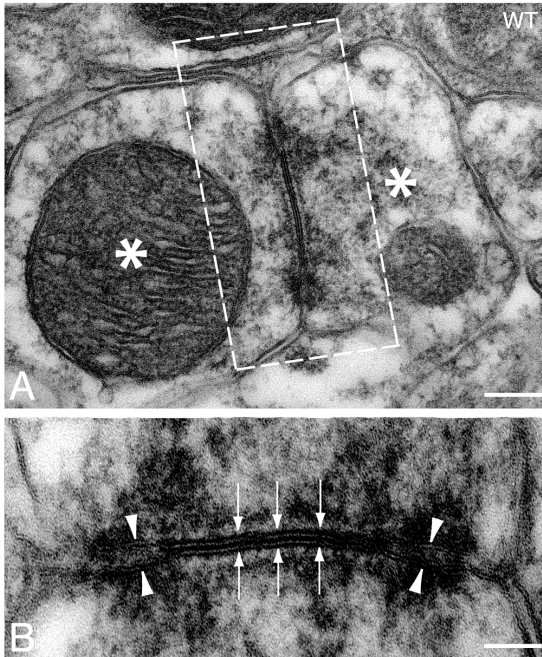
Figure 6. Ultrastructural characteristics of a dendrodendritic gap junction in the inferior olive of a wild-type (WT) mouse. In wild-type mice, the gap junctions between olivary dendritic spines (asterisks) showed electron-dense deposits in the cytoplasm at both sides of the membrane; in addition, they had attachment plaques (arrowheads) surrounding the plaque with gap-junction channels (arrows), and the interneuronal gap of this plaque was -3 nm thick. B shows a higher magnification of the inset depicted in A. Scale bars: A, 167 nm; B, 82 nm.

Yet, the average diameter of the plaque was significantly reduced to 209 ± 27 nm compared with wild-type mice ($p < 0.05$; Student's t test) (Figures. 7, 8). Even so, the average distance between the attachment plaques bordering the gap junction plaque as analyzed in the two-dimensional electron microscopic plane (454 ± 77 nm) was similar to those in wild types (416 ± 46 nm) and homozygous (423 ± 92 nm) animals, and the density of gap junctions (78 per mm2) was not significantly lower than that of wild-type animals. We conclude from these data that (1) the absence of Connexin36 leads to plaque-lacking gap-junction-like structures with an abnormally wide interneuronal space, (2) reduced expression of this connexin results in gap junctions with smaller plaques, and (3) Cx36 is therefore probably necessary for the formation and assembly of connexin-hemichannels in plaques of neuronal gap junctions in the inferior olive. Thus, if there is any morphological compensation in the homozygous knock-out mice, it appears to occur at the level of proximal dendrites rather than at the abnormally noncoupled dendritic spines.

Dye coupling.

The ultrastructural data described above suggest that there is no functional coupling in the inferior olive of Cx36-deficient mice. To confirm this observation, we injected Lucifer yellow into olivary neurons in 250-µm-thick slices of both wild-type and Cx36-deficient mice (Figure 9). In slices of wild-type animals (n = 21), the intracellular injections provided labeled clusters of 4–14 neurons (with an average of 9 ± 3.2). In contrast, virtually all injections in mutant slices yielded single labeled neurons (n = 16), with the exception of two cases in which we obtained a cluster of two and three cells. Apart from the differences in the size of the proximal dendrites, we did not observe any sign of abnormal morphology or collateralization of the olivary axons or dendrites. In addition, we investigated the coupling with the use of intracellular injections of Neurobiotin in Cx36-deficient mice (n = 8) and wild-type littermates (n = 6); in all Cx36-deficient mice, the injections resulted in labeling of single neurons only (n = 16), whereas those in the wild types always provided clusters of multiple neurons (n = 18, with an average of 8 ± 3.8).
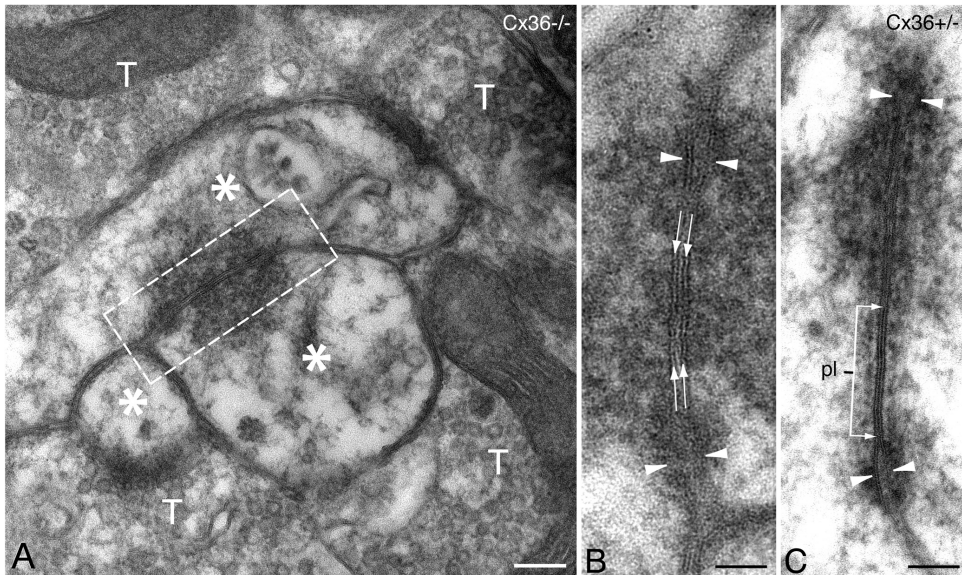
Figure 7. Ultrastructural characteristics of a dendrodendritic gap-junction-like structure in the inferior olive of a Cx36-deficient mouse (A, B) and a Cx36+/- mouse (C). In homozygous Cx36-deficient mice, no normal gap junctions were observed, but instead the dendrites showed numerous gap-junction-like structures with a widened interneuronal gap of ~9 nm (arrows in B). Note that the micrograph in A shows a typical olivary glomerulus with a core of dendritic spines (asterisks) surrounded by terminals (T) and glia.In heterozygous Cx36-deficient mice, the olivary gap junctions showed a normal interneuronal gap of ~3 nm, but the average diameter of the plaque (pl in C) was significantly reduced, whereas the distance between the attachment plaques (arrowheads) remained normal. B shows a higher magnification of the inset depicted in A. Scale bars: A, 150 nm; B, 75 nm; C, 105 nm.

These results indicate that electrotonic coupling in the inferior olive is severely affected in Cx36-deficient mice.

Electroresponsive properties.

To investigate the impact of a lack of Cx36 on electroresponsive properties of olivary neurons, whole-cell patch recordings were performed in wild-type mice (n = 43) and homozygous Cx36-deficient mice (n = 22). In dual recordings from wild-type olivary neurons, 62% (n = 8) of the pairs showed bidirectional direct current flow (Figure 10A). None of the 10 pairs of knock-out neurons showed direct coupling (Figure 10B). These findings support our anatomical findings, which suggest that no functional gap junctions exist in the homozygous mutants. In addition, they illustrate that our Cx36-deficient mutants, which were created in a different laboratory with a different cloning strategy (Güldenagel et al., 2001), show the same basic cellular deficits as the line of Cx36 knock-out mice used by Long et al. (2002).
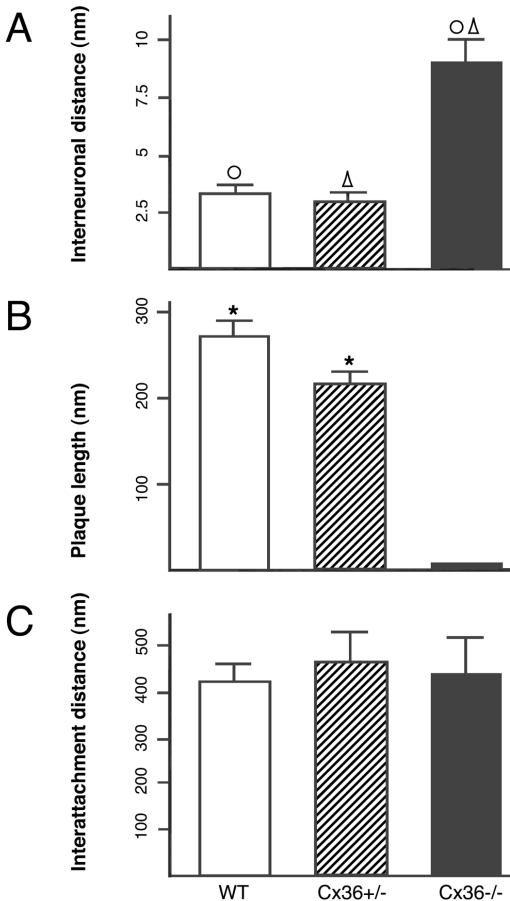
Figure 8. Histograms showing morphometrics of gap junctions and gap-junction-like structures in wild-type (WT), Cx36+/-, and Cx36-/- mutants. A. The average interneuronal space of gap-junction-like structures in Cx36-/- mutants was significantly smaller than that of gap junctions in wild-type and Cx36+/- mutants. **B.** The length of the gap-junction plaque in wild-type mutants was significantly longer than that of Cx36+/- mutants, whereas it was absent in homozygous Cx36-deficient mice. **C.** In contrast, the distance between the attachment plaques did not differ among the three groups of animals. For visualization of parameters, see Figure 7. Open circles and triangles indicate p < 0.0001; asterisks indicate p < 0.001.
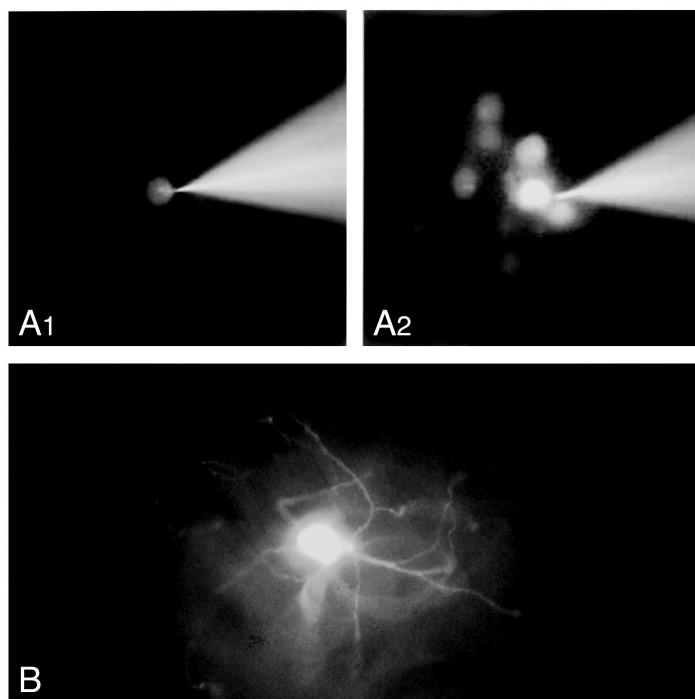
Figure 9. Dye coupling in wild-type mice and homozygous Cx36-deficient mice. A. In slices of the inferior olive of wild-type animals, intracellular injections with Lucifer yellow provided clusters of approximately nine neurons within a few minutes; the time difference between micrograph of A1 and A2 is 136 sec. **B.** In contrast, injections in slices of Cx36-deficient mice yielded single labeled neurons; note the absence of labeling in neighboring cells despite the visualization of olivary dendrites.

Both wild-type and Cx36-deficient olivary neurons displayed characteristic high- and low-threshold Ca spikes on stimulation with a depolarizing current pulse (Figure 11, top). As shown previously in rats and guinea pigs (Llinás and Yarom, 1981a,b, 1987; Devor and Yarom, 2002a,b), the low-threshold Ca spike, which triggered a Na-dependent action potential, was readily elicited by a positive current pulse when the membrane voltage was held at hyperpolarized levels (less than -70 mV). When the membrane potential was held at depolarized levels (more than -45 mV), a positive current pulse elicited a Na-dependent action potential that triggered a high-threshold Ca spike. The latter was manifested as a prolongation of the action potential, followed by a long-lasting hyperpolarization. Although both wild-type and Cx36-deficient neurons showed similarity in their responses to depolarizing current pulses, they differed considerably in their responses to hyperpolarizing cur-rent pulses. The responses of wild-type neurons resembled those previously reported in guinea pig and rat olivary neurons (Llinás and Yarom, 1987; Bal and McCormick, 1997; Devor and Yarom, 2000). Specifically, during a prolonged hyperpolarization, the voltage response partially decreased (sag) and a rebound low-threshold response was elicited on termination of the hyperpolarization (Figure 11, bottom left). The responses of mutant olivary neurons were dramatically different.

With a sufficiently large hyperpolarizing pulse, the sag response developed into a low-threshold Ca spike (Figure 11, bottom right). An additional increase in the level of hyperpolarization increased the amplitude of the low-threshold Ca spike, eventually triggering a Na-dependent action potential.

A

B
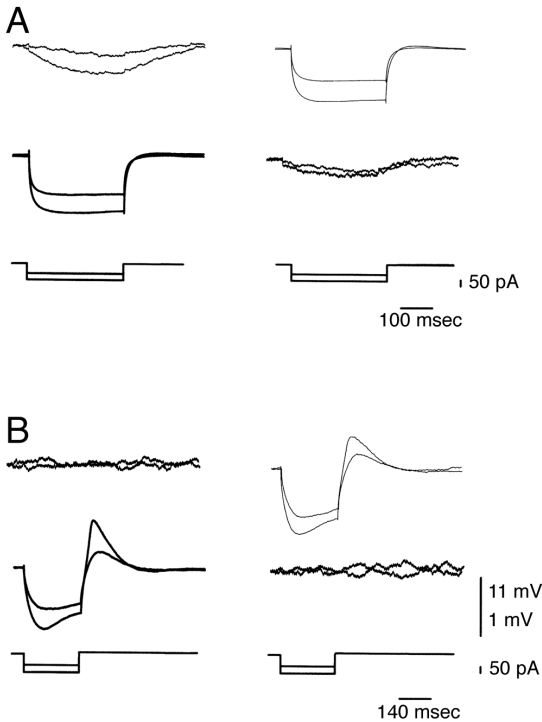
Figure 10. The absence of direct current flow between adjacent olivary neurons from knock-out mice. Dual recordings from olivary slices were performed in wild-type mice (A) and knock-out mice (B). In wild-type mice, current injections into cell 1 (middle) induced direct voltage responses in cell 1 and an indirect response in cell 2 (top). This current flow was bidirectional (right), indicating that these neurons are electrotonically coupled. In knock-out mice (B), indirect voltage responses were absent.

50 pA

100 msec

11 mV
1 mV

50 pA

140 msec

Rhythmic activity.

The extraordinary response of all mutant neurons (n = 22) to injection of negative current pulses indicates that the lack of Cx36 leads to abnormal electrical properties of olivary neurons. These properties were manifested as an increase in the neuronal excitability when the membrane potential was more negative than -60 mV. Indeed, when neurons were hyperpolarized by DC injections, rhythmic activity was elicited. Figure 12 (right) shows voltage traces recorded from a mutant neuron at different levels of membrane potential. With no current injected, the neuron was quiescent (top trace). Shifting the membrane potential by -8 mV evoked rhythmic activity that increased in amplitude and frequency with additional hyperpolarization. Occasionally, the amplitude reached the firing threshold and Na-dependent action potentials were elicited (fourth trace). An average frequency of 2.2 ± 0.7 Hz was calculated in seven cells.

Additional hyperpolarization blocked this spontaneous rhythmic activity (bottom trace). This behavior considerably differed from the subthreshold oscillatory activity recorded in wild-type neurons, where rhythmic activity was voltage independent and could not be elicited or abolished by current injection. An example of subthreshold oscillatory activities in a wild-type neuron, which were observed in 14 of 29 cells, is shown in the left panel of Figure 12. Across the different neurons, the average frequency of these oscillations was 1.28 ± 0.4 Hz. These results show that the subthreshold oscillations in the mutant olivary neurons are generated by the intrinsic properties of the cells, as opposed to the wild-type oscillations that emerge from a network of electrically coupled neurons (Manor et al., 1997; Loewenstein et al., 2001). Hence, the knock-out mutation triggers a cascade of events that transforms olivary neurons from quiescent cells to conditional oscillators.
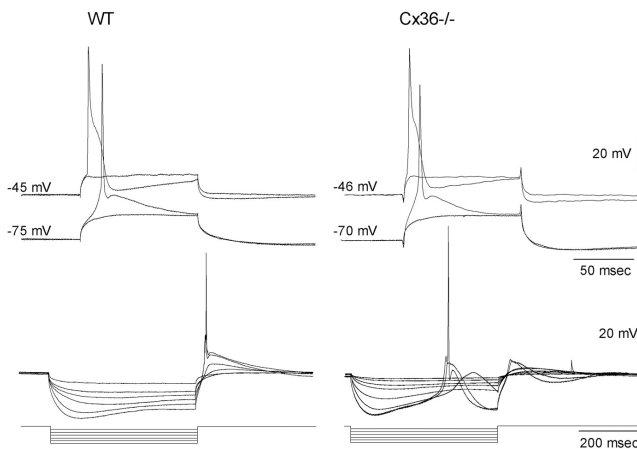
Figure 11. Olivary neurons from Cx36-deficient mice are more excitable at hyperpolarized states. Whole-cell patch recordings show the responses of olivary neurons from wild-type (WT) mice (left column) and mutant mice (right column) to depolarizing (top) and hyperpolarizing (bottom) current injections. The depolarizing pulses (top) elicited high- and low-threshold calcium responses (top and bottom traces, respectively) in both wild-type and Cx36-/- mice. The response to hyperpolarizing current steps of mutant mice is characterized by an activation of a low-threshold calcium spike that triggered a sodium-dependent action potential.

Current measurements.

The finding that olivary neurons seem to transform into conditional oscillators raises the question of what type of changes induce such a functional transformation. In previous modeling studies, we have shown that a model cell consisting of only leak and calcium conductances could be transformed from a quiescent cell into a conditional oscillator, by either reducing its leak conductance or increasing its Ca^{2+} conductance (Manor et al., 1997, 2000). This finding provides a possible explanation for the changes observed in the mutant mice, which can be directly measured by voltage-clamp experiments and tested with the use of the dynamic-clamp technique.

WT   Cx36-/-

Chapter 3.1
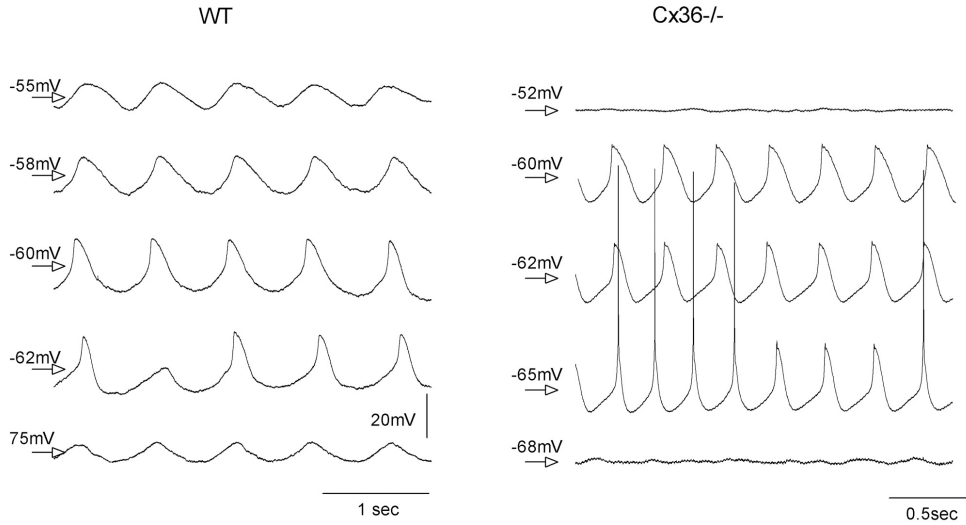
Figure 12. Oscillations are voltage dependent in the Cx36 knock-out mice (right) and independent in wild-type (WT) mice (left). Each panel shows five traces recorded at a different membrane potential, which was set by DC injection. The average voltage of each trace is marked (arrow). In mutant olivary neurons, the oscillations occurred at a limited range of voltages (traces 2–4), which does not include the resting potential (trace 1). In wild-type mice, the oscillations occurred at all levels of membrane potentials.

The analysis of these currents is summarized in Table 1 (see Materials and Methods). The average input resistances of wild-type and mutant neurons were 86.3 ± 20 MΩ (n = 9) and 127.1 ± 34.5 MΩ (n = 9), respectively. A higher input resistance in the mutant neurons is expected, because the loading effect of neighboring cells is removed.
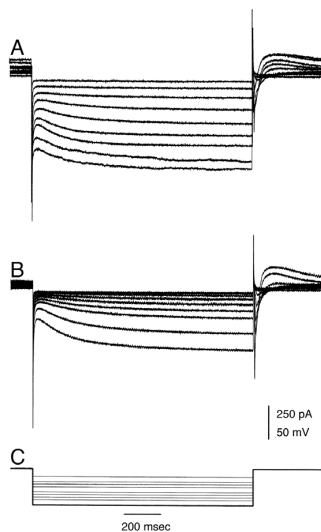
Figure 13. Current responses of wild-type and knock-out neurons to negative voltage steps. An example of the current responses of wild-type neurons (A) and knock-out neurons (B) to negative voltage steps is shown. Note that knock-out neurons have larger input resistance and larger calcium currents than wild-type neurons.
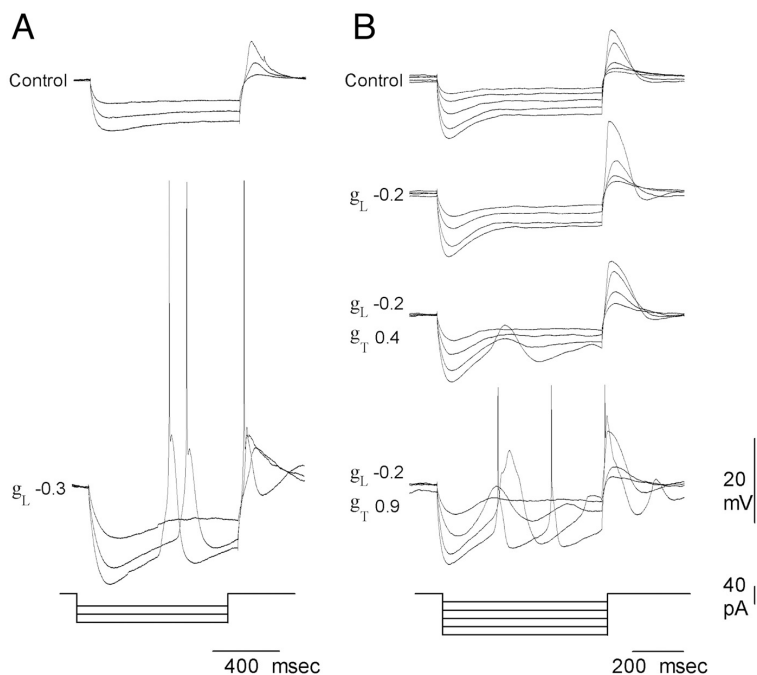
Figure 14. Changing leak and/or low-threshold calcium conductances can mimic mutant properties in wild-type mice. The dynamic-clamp technique was used to alter the leak and calcium conductances. Each panel shows the voltage response to series of negative current injections (bottom panel). The control responses are shown at the top of each panel. The responses of the dynamically clamped cell are shown below. **A.** Only a 200% increase in resistance of the cell could reproduce a knock-out-like phenotype. **B.** Reducing the leak conductance by 20% is not sufficient for reproducing the mutant phenotype (i.e., increased excitability manifested as a calcium spike and action potential from a hyperpolarized state;compare top panel with the second panel). An increase inlow-threshold calcium conductance enhances the sag (third panel), and an additional increment of low-threshold calcium conductance results in a low-threshold calcium spike and action potential similar to the phenotype of the mutant.

Table 1. Electrophysiological characteristics in wild-type and knock-out mice

	R (MΩ)		$R_{in}(\Omega{*}10{*}cm^2)$		Cell suface (cm^2)	
	Average	Sd	Average	Sd	Average	Sd
WT (n=9)	86.3	20.6	3.973	8.664	4.39E-05	9.698E-06
KO (n=9)	127.1	34.5	5.983	6.474	5.585E-05	1.826E-05
% Change	47.4		50.6		27.2	

	$I_h(\mu A/cm^2)$		$I_{Ca}(\mu A/cm^2)$		$I_{AHP}(\mu A/cm^2)$	
	Average	Sd	Average	Sd	Average	Sd
WT (n=9)	3.956	1.068	-17.029	4.837	3.379	2.522
KO (n=9)	4.294	1.584	-22.775	9.288	3.930	8.730
% Change	8.5		33.7		16.3	

Normalizing the input resistance by the surface area revealed a significantly higher specific membrane resistance (Rm) of knock-out neurons compared with wild-type neurons (50.6%). In addition, the knock-out neurons exhibited a significantly larger peak Ca^{2+} current (133.7%). The latter corresponds to an increase in current density of 0.03 mS/ cm^2. In contrast, neither the I_h nor the I_{AHP} showed any significant changes. Thus, we conclude that knock-out neurons are characterized by an increase in Ca^{2+} conductances and a decrease in leak conductances. Can these differences account for the observed changes in the electrical behavior of the neurons?

Dynamic clamp.

To examine this possibility, we used the dynamic-clamp technique to artificially decrease the leak conductance and increase the calcium conductance of wild-type neurons. Figure 14A shows the responses of a wild-type neuron to negative current pulses. When we decreased the leak conductance by 0.2 mS/cm^2 (a 50% increase in the input resistance), the amplitudeof the partial repolarization was enhanced, but it was not sufficient to generate an action potential (Figure 14A, second panel). The addition of 0.4 mS/cm^2 calcium conductance further increased the partial repolarization and triggered a regenerative calcium response (third panel). An additional increase in calcium conductance to 0.9 mS/cm^2 increased the calcium response, which at this level was sufficient to trigger a sodium-dependent action potential. Similar results were obtained when the kinetics of the low-threshold calcium conductance was modified, for example by shifting the activation curve in the hyperpolarized direction. Under these conditions, however, a much smaller increase in the low-threshold conductance was needed to mimic the knock-out phenotype.

We also examined the possibility that a wild-type cell could be transformed into a conditional oscillator by solely increasing the input resistance. Figure 14B shows that this was indeed possible. However, in this case, the average increase in input resistance required for eliciting an action potential by a hyperpolarizing current pulse was 240% (n = 9), five times larger than the measured difference between wild-type and mutant neurons (50%). We conclude that a wild-type neuron in which leak conductance was decreased and calcium conductance was increased best fit the electroresponsiveness of mutant cells.

DISCUSSION

Gap-junctional coupling and subthreshold oscillations are integral and related components of the olivary network. Yet, olivary oscillations are sustained in knock-outs of Cx36 (Long et al., 2002). Here, we show that these voltage-dependent oscillations in Cx36-deficient mice differ from those in wild-type mice, and that they are attributable to both structural and electrophysiological compensations. The structural compensations do not include a functional restoration of the gap-junction plaques but instead an increase in diameter of the proximal dendrites and a concomitant increase in surface area of the olivary neurons; the electrophysiological compensations include a decrease in leak conductance and an increase in voltage-dependent calcium conductance, leading to an increase in excitability. Thus the absence of Cx36 triggered such compensatory mechanisms that the capacity of the uncoupled olivary neurons to produce rhythmic activity was preserved.

Cytological and ultrastructural changes.

Several studies of higher brain regions, such as in the hippocampus and cerebral cortex, have demonstrated the impact of a lack of Cx36 at the cellular and systems physiological level (Deans et al., 2001; Hormuzdi et al., 2001; Schmitz et al., 2001; Spruston, 2001). To the best of our knowledge, our work is the first to demonstrate the consequences of the absence of electrical coupling at the ultrastructural level. Gap junctions of olivary neurons in wild-type mice showed the same morphological characteristics as described previously for other mammals (Sotelo et al., 1974, 1986; Rutherford and Gwyn, 1977; King et al., 1980; De Zeeuw et al., 1989, 1994). These gap junctions are predominantly located between dendritic spines within the olivary glomeruli. Each gap junction consists of a central plaque crossed by a narrow inter-neuronal space of ~3 nm thickness and surrounded by attachment plaques. The cytoplasm on both sides of the plaque contains electron-dense deposits. In contrast, in Cx36 null mutants, we observed a gap-junction-like structure that resembled the normal gap junction, except for an abnormally wide interneuronal space of ~9 nm, resulting in the absence of the central plaque. Indeed, other morphological characteristics associated with gap junctions, such as the electron-dense deposits, the dendritic lamellar bodies, the distance between the attachment plaques, or the glomeruli themselves, were not affected. In heterozygous animals, normal gap-junction structures were observed; although the central plaques had a reduced diameter, uniform gap junction-like structures were distributed throughout all olivary subnuclei. This observation is consistent with the experiments showing that all wild-type olivary neurons express Cx36 mRNA and that the en-tire neuropil of all

olivary subnuclei shows labeled puncta after immunocytochemistry with anti-Cx36. These data diverge somewhat from those presented by Long et al. (2002), who noted that not all olivary neurons in lacZ-Cx36 mice were positively labeled. The fact that not only all cells in the wild-type mice were positively labeled in our light-microscopic labeling studies, but also that all gap junctions of the knock-out mice were affected in both our electron microscopic and electrophysiological experiments suggest to us that all olivary neurons do express Cx36. Possibly, the lacZ Cx36 mutant provides partly false negative results because of some interference with gene regulation sites (Koponen et al., 2002).

In view of the ultrastructural observations, we suggest that the gap junction-like structures represent the sites at which gap junctions should have been formed. This leads to three conclusions: first, the site of gap junction formation is Cx36 independent and is probably determined by the other components that form the gap-junction-like structures. Second, there is no sufficient up-regulation or induction of expression of other connexin isoforms that may compensate for a lack of Cx36. Third Cx36 is necessary for attaching the membranes of two neurons, probably via direct binding between the opposing extracellular loops of the Cx36 hemichannels. Thus, the assembly of fully operational gap junctions in the olive cannot occur without Cx36. This possibility was confirmed by dye-coupling experiments and paired recordings, which failed to demonstrate direct electrical coupling between olivary neurons of homozygous Cx36-/- mice.

Physiological changes.

As shown by Long et al. (2002), olivary neurons of Cx36-deficient mice reveal oscillations de-spite the fact that they are not functionally electrotonically coupled. Yet, here we show that these oscillations are qualitatively different compared with those of the wild-type mice in that (1) they do not occur spontaneously, but are triggered by intracellular hyperpolarization; (2) they occur in a limited range of membrane potentials; and (3) their frequency depends on the membrane potential. These differences indicate that in contrast to the wild-type mutant, oscillations in the Cx36 mutant are a single-cell phenomenon. Thus, we propose that the lack of functional gap junctions induces compensatory processes that restore, at least partially, the propensity of olivary neurons to oscillate. Recently, analogous compensations have been observed in mutated neurons of the lobster stomatogastric ganglion in which a potassium conductance Shal was overexpressed (MacLean et al., 2003). This overexpression by RNA injection produced a large increase in IA but surprisingly little change in the firing properties of the neuron. The increase in IA was accompanied by a dramatic and

linearly correlated increase in a hyperpolarization activated inward current I_h. Thus, these results also suggest a selective coregulation of channels as a mechanism for constraining cell activity within appropriate physiological parameters.

What mechanisms could underlie the compensatory processes in the uncoupled olivary neurons? The observation that oscillations in Cx36 mutants are voltage dependent suggests that a change in the composition or type of ionic channels has occurred. Indeed, voltage-clamp experiments show that the membrane of knock-out neurons has a significantly higher specific membrane resistance and higher Ca^{2+} conductance. The higher membrane resistance of knock-out neurons is also inferred from the linear correlation between cell capacitance and input conductance. In addition, we found that knock-out neurons have a significantly larger membrane area. This is in contrast to the expected smaller area because of the lack of coupled neurons. However, this result is in line with our observations at both the light-microscopic and ultrastructural level, which showed that proximal dendrites are significantly thicker in mutants than in wild types. Although we did not observe any difference with respect to the length of the dendrites, we cannot exclude such an additional difference, because neither the rapid Golgi staining nor the dye coupling always completely extended into all peripheral dendrites.

The observations that knock-out neurons have both a higher input resistance and larger surface membrane point toward differences in the specific membrane properties. Using the dynamic-clamp technique, and on the basis of previous modeling studies (Manor et al., 1997, 2000), we have demonstrated that such differences are sufficient to replicate the electroresponsive properties of Cx36 mutants. It should be noted that the changes in specific membrane properties used in the dynamic-clamp experiments are larger than the measured changes between wild-type and knock-out olivary neurons. This overestimation of the dynamic-clamp approach is probably attributable to a technical limitation of the technique. Indeed, in the dynamic clamp we mimicked conductance changes distributed across the entire neuronal structure by injecting current in the soma. As a result of cable attenuation effects, we needed to inject large amounts of current to introduce changes to conductances that were far away from the soma. Nevertheless, this inconsistency does not detract us from our main conclusion, that such changes can transform a wild-type neuron into its knock-out variant. An interesting question is how these changes are produced. One possibility is that the expression of a specific gene, or a group of genes, is directly regulated, for example, by changes in calcium flow. Another possibility is that in early developmental stages the olivary nucleus consists of a heterogeneous population of neurons.

During maturation, a developmental process could select for a specific type of neuron that is endowed with the capability to produce oscillations at hyperpolarized membrane potentials. The advantage for selection of this type of conditional oscillators is clear, because sustained and unsynchronized oscillations are not useful for information processing. In the wild type, the occurrence and synchronization of oscillations are controlled via the extent and distribution of electrotonic coupling (Devor and Yarom, 2000). With this mechanism unavailable in mutants, regulation of rhythmic activity could be achieved by hyperpolarizing a specific subset of olivary neurons, for example by activating a common synaptic inhibitory input. Such input, if given in synchrony and with similar strength, would trigger an in-phase oscillation of identical frequency across the neurons of this subset. Regardless of the specific mechanism, the fact that compensatory processes are engaged points out the importance of these oscillations for the proper function of the olivocerebellar system.

The plasticity of the nervous system enables it to use different strategies to preserve patterns of activity under changing conditions. Here, we have demonstrated this general principle by preventing the use of electrical coupling. The system responded by choosing an alternative and novel strategy: modification of intrinsic properties of neurons.

REFERENCES

Bacskai T, Matesz C (2002) Primary afferent fibers establish dye-coupled connections in the frog central nervous system. Brain Res Bull 57:317–319.

Bal T, McCormick DA (1997) Synchronized oscillations in the inferior olive are controlled by the hyperpolarization-activated cation current I(h). J Neurophysiol 77:3145–3156.

Belluardo N, Mud G, Trovato-Salinaro A, Le Gurun S, Charollais A, Serre-Beinier V, Amato G, Haefliger JA, Meda P, Condorelli DF (2000) Expression of Connexin36 in the adult and developing rat brain. Brain Res 865:121–138.

Bennett MV (2002) Neoreticularism and neuronal polarization. Prog Brain Res 136:189–201.

Condorelli DF, Parenti R, Spinella F, Trovato Salinaro A, Belluardo N, Cardile V, Cicirata F (1998) Cloning of a new gap junction gene (Cx36) highly expressed in mammalian brain neurons. Eur J Neurosci 10:1202–1208.

Deans MR, Gibson JR, Sellitto C, Connors BW, Paul DL (2001) Synchronous activity of inhibitory networks in neocortex requires electrical synapses containing connexin 36. Neuron 31:477–485.

Devor A, Yarom Y (2000) GABAergic modulation of olivary oscillations. Prog Brain Res 124:213–220.

Devor A, Yarom Y (2002a) Electrotonic coupling in the inferior olivary nucleus revealed by simultaneous double patch recordings. J Neurophysiol 87:3048–3058.

Devor A, Yarom Y (2002b) Generation and propagation of subthreshold waves in a network of inferior olivary neurons. J Neurophysiol 87:3059–3069.

De Zeeuw CI, Holstege JC, Ruigrok TJ, Voogd J (1989) Ultrastructural study of the GABAergic, cerebellar, and mesodiencephalic innervation of the cat medial accessory olive: anterograde tracing combined with immunocytochemistry. J Comp Neurol 284:12–35.

De Zeeuw CI, Wylie DR, DiGiorgi PL, Simpson JI (1994) Projections of individual Purkinje cells of identified zones in the flocculus to the vestibular and cerebellar nuclei in the rabbit. J Comp Neurol 349:428–447.

De Zeeuw CI, Hertzberg EL, Mugnaini E (1995) The dendritic lamellar body: a new neuronal organelle putatively associated with dendrodendritic gap junctions. J Neurosci 15:1587–1604.

De Zeeuw CI, Hoogenraad CC, Goedknegt E, Hertzberg E, Neubauer A, Grosveld F, Galjart N (1997) CLIP-115, a novel brain specific cytoplasmic linker protein, mediates the localisation of dendritic lamellar bodies. Neuron 19:1187-1199.

De Zeeuw CI, Simpson JI, Hoogenraad CC, Galjart N, Koekkoek SKE, Ruigrok TJH (1998) Microcircuitry and function of the inferior olive. Trends Neurosci 21:391–400.

Güldenagel M, Ammermuller J, Feigenspan A, Teubner B, Degen J, Söhl G, Willecke K, Weiler R (2001) Visual transmission deficits in mice with targeted disruption of the gap junction gene connexin 36. J Neurosci 21:6036–6044.

Hinrichsen CF, Larramendi LM (1968) Synapses and cluster formation of the mouse mesencephalic fifth nucleus. Brain Res 7:296–299.

Hormuzdi SG, Pais I, LeBeau FE, Towers SK, Rozov A, Buhl EH, Whittington MA., Monyer H (2001) Impaired electrical signaling disrupts gamma frequency oscillations in connexin 36 deficient mice. Neuron 31:487–495.

Ivry RB (1996) The representation of temporal information in perception and motor control. Curr Opin Neurobiol 6:851–857.

King JS (1980) The synaptic organization of the inferior olivary nucleus. In: The inferior olivary nucleus (Courville J, De Montigny C, Lammare Y, eds), pp 1-35. New York: Raven.

Kistler WM, van Hemmen JL, De Zeeuw CI (2000) Time window control: a model for cerebellar function based on synchronization, reverberation, and time slicing. In: Cerebellar

modules: molecules, morphology, and function (De Zeeuw CI, Ruigrok TJH, Gerrits NGM, eds), pp 275–299. Amsterdam: Elsevier.

Kistler WM, De Jeu MTG, Elgersma Y, van der Giessen RS, Hensbroek R, Luo C, Koekkoek SKE, Hoogenraad CC, Hamers FPT, Güldenagel M, Söhl G, Willecke K, De Zeeuw CI (2002) Analysis of Cx36 knock out does not support tenet that olivary gap junctions are required for complex spike synchronization and normal motor performance. Ann NY Acad Sci 978:391–405.

Koponen JK, Turunen AM, Yla-Herttuala S (2002) Escherichia coli DNA contamination in AmpliTaq gold polymerase interferes with TaqMan analysis of lacZ. Mol Ther 5:220–222.

Lampl I, Yarom Y (1993) Sub-threshold oscillations of the membrane potential: a functional synchronizing and timing device. J Neurophysiol 70:2181–2186.

Lampl I, Yarom Y (1997) Sub-threshold oscillations and resonant behavior: two manifestations of the same mechanism. Neuroscience 78:325–341.

Landis DMD, Reese TS, Raviola E (1974) Differences in membrane structure between excitatory and inhibitory components of the reciprocal synapse in the olfactory bulb. J Comp Neurol 155:67–92.

Lang EJ (2001) Organization of olivocerebellar activity in the absence of excitatory glutamatergic input. J Neurosci 21:1663–1675.

Llinás R, Yarom Y (1981a) Electrophysiology of mammalian inferior olivary neurones *in vitro*. Different types of voltage-dependent ionic conductances. J Physiol (Lond) 315:549–567.

Llinás R, Yarom Y (1981b) Properties and distribution of ionic conductances generating electroresponsiveness of mammalian inferior olivary neurons *in vitro*. J Physiol (Lond) 315:569–584.

Llinás R, Yarom Y (1986) Oscillatory properties of guinea-pig inferior olivary neurones and

their pharmacological modulation: an *in vitro* study. J Physiol (Lond) 376:163–182.

Llinás R, Yarom Y (1987) Long-term modifiability of anomalous and delayed rectification in guinea pig inferior olivary neurons. J Neurosci 7:1166–1177.

Loewenstein Y, Yarom Y, Sompolinsky H (2001) The generation of oscillations in networks of electrically coupled cells. Proc Natl Acad Sci USA 98:8095–8100.

Long MA, Deans MR, Paul DL, Connors BW (2002) Rhythmicity without synchrony in the electrically uncoupled inferior olive. J Neurosci 22:10898–10905.

MacLean JN, Zhang Y, Johnson BR, Harris-Warrick RM (2003) Activity-independent homeostasis in rhythmically active neurons. Neuron 37:109–120.

MacVicar BA, Dudek FE (1981) Electrotonic coupling between pyramidal cells: a direct demonstration in rat hippocampal slices. Science 213:782–785.

Maier N, Guldenagel M, Söhl G, Siegmund H, Willecke K, Draguhn A (2002) Reduction of high-frequency network oscillations (ripples) and pathological network discharges in hippocampal slices from connexin 36-deficient mice. J Physiol (Lond) 541:521–528.

Manor Y, Rinzel J, Segev I, Yarom Y (1997) Low-amplitude oscillations in the inferior olive: a model based on electrical coupling of neurons with heterogeneous channel densities. J Neurophysiol 77:2736–2752.

Manor Y, Yarom Y, Chorev E, Devor A (2000) To beat or not to beat: a decision taken at the network level. J Physiol (Lond) 94:375–390.

Matsumoto A, Arnold AP, Zampighi GA, Micevych PE (1988) Androgenic regulation of gap junctions between motoneurons in rat spinal cord. J Neurosci 8:4177–4183.

Peters A (1980) Morphological correlates of epilepsy: cells in the cerebral cortex. Adv Neurol 27:21–48.

Rash JE, Staines WA, Yasumura T, Patel D, Furman CS, Stelmack GL, Nagy JI (2000) Immunogold evidence that neuronal gap junctions in adult rat brain and spinal cord contain connexin-36 but not connexin-32 or connexin-43. Proc Natl Acad Sci USA 97:7573–7578.

Raviola E, Gilula NB (1975) Intramembrane organization of specialized contacts in the outer plexiform layer of the retina. A freeze-fracture study in monkeys and rabbits. J Cell Biol 65:192–222.

Rutherford JG, Gwyn DG (1977) Gap junctions in the inferior olivary nucleus of the squirrel monkey, Saimiri sciureus. Brain Res 128:374–378.

Schmitz D, Schuchmann S, Fisahn A, Draguhn A, Buhl EH, Petrasch-Parwez E, Dermietzel R, Heinemann U, Traub RD (2001) Axo-axonal coupling: a novel mechanism for ultrafast neuronal communication. Neuron 31:831–840.

Sharp AA, O'Neil MB, Abbott LF, Marder E (1993) Dynamic clamp: computer-generated conductances in real neurons. J Neurophysiol 69:992–995.

Sotelo C, Llinás RR (1972) Specialized membrane junctions between neurons in the vertebrate cerebellar cortex. J Cell Biol 53:271–289.

Sotelo C, Llinás R, Baker R (1974) Structural study of inferior olivary nucleus of the cat: morphological correlates of electrotonic coupling. J Neurophysiol 37:541–559.

Sotelo C, Gotow T, Wassef M (1986) Localization of glutamic-aciddecarboxylase-immunoreactive axon terminals in the inferior olive of the rat, with special emphasis on anatomical relations between GABAergic synapses and dendrodendritic gap junctions. J Comp Neurol 252:32–50.

Spruston N (2001) Axonal gap junctions send ripples through the hippocampus. Neuron 31:669–671.

Teubner B, Degen J, Söhl G, Guldenagel M, Bukauskas FF, Trexler EB, Verse-lis VK, De Zeeuw CI, Lee CG, Kozak CA, Petrasch-Parwez E, Dermietzel R, Willecke K (2000) Func-

tional expression of the murine connexin 36 gene coding for a neuron-specific gap junctional protein. J Membr Biol 176:249-262.

Van Pelt J, Uylings HB, Verwer RW, Pentney RJ, Woldenberg MJ (1992) Tree asymmetry-a sensitive and practical measure for binary topological trees. Bull Math Biol 54:759-784.

Voogd J, Bigare F (1980) Topographical distribution of olivary and corticonuclear fibers in the cerebellum. A review. In: The inferior olivary nucleus (Courville J, De Montigny C, Lamarre Y, eds), pp 207-235. New York: Raven.

Welsh JP, Lang EJ, Sugihara I, Llinás R (1995) Dynamic organization of motor control within the olivocerebellar system. Nature 374:453-457.

Yarom Y (1991) Rhythmogenesis in a hybrid system—interconnecting an olivary neuron to an analog network of coupled oscillators. Neuroscience 44:263-275.

Yarom Y, Cohen D (2002) The olivocerebellar system as a generator of temporal patterns. Ann NY Acad Sci 978:122-134.

CHAPTER 3.2

Whole cell recordings of mouse inferior olivary neurons *in vivo*: heterogeneity in subthreshold oscillations and spiking patterns

R.S. Van Der Giessen*, S. Khosrovani*, C.I. De Zeeuw and M.T.G. De Jeu

Department of Neuroscience, Erasmus MC, 3000 DR Rotterdam, The Netherlands

*Authors contributed equally

ABSTRACT

In vitro whole-cell recordings of the inferior olive have demonstrated that its neurons are electrotonically coupled and have a tendency to oscillate. However, it remains to be shown to what extent subthreshold oscillations indeed occur in the inferior olive *in vivo* and whether its spatiotemporal firing pattern may be dynamically generated by including or excluding different types of oscillatory neurons. Here, we did whole-cell recordings of olivary neurons *in vivo* to investigate the relation between their subthreshold activities and their spiking behavior in an intact brain. The vast majority of neurons (85%) showed subthreshold oscillatory activities. The frequencies of these subthreshold oscillations were used to distinguish four main olivary subtypes by statistical means. Type I showed both sinusoidal subthreshold oscillations (SSTO's) and low threshold Ca^{2+} oscillations (LTO's) (16%); type II showed only SSTO's (13%); type III showed only LTO's (56%); and type IV did not reveal any subthreshold oscillations (15%). These subthreshold oscillation frequencies were strongly correlated with the frequencies of preferred spiking. The frequency characteristics of the subthreshold oscillations and spiking behavior of virtually all olivary neurons were stable throughout the recordings. However, the occurrence of spontaneous or evoked action potentials modified the subthreshold oscillation by resetting the phase of its peak towards 90^0. Together, these findings indicate that the inferior olive in intact mammals offers a rich repertoire of different neurons with relatively stable frequency settings, which can be used to generate and reset temporal firing patterns in a dynamically coupled ensemble.

INTRODUCTION

The Inferior olive (IO) forms the sole source of the climbing fiber input to Purkinje cells in the cerebellar cortex (De Zeeuw et al., 1998). Single climbing fibers excite Purkinje cells in the cerebellar cortex resulting in a powerful, all or none, depolarization called the complex spike. *In vitro* studies have shown that olivary neurons have a unique combination of cellular properties including electrotonic coupling and a propensity to oscillate (Llinás and Yarom, 1981a; Llinás and Yarom 1986; Llinás et al., 1974; Benardo and Foster, 1986). Their tendency to oscillate is mainly due to specific Ca^{2+} conductances, which are distributed differentially over their membrane compartments (Llinás and Yarom, 1981a; Llinás and Yarom, 1981b). Dendritic high-threshold and somatic low-threshold Ca^{2+} conductances can activate each other rhythmically and they can interact with a Ca^{2+}-dependent K^+ conductance resulting in the production of subthreshold oscillations with amplitudes of 3-10 mV (Llinás and Yarom,

1981a). To date, it is unknown to what extent these oscillations also occur *in vivo* and how they influence the generation of patterns of complex spike activities in the intact olivocerebellar system (see also Chorev et al., 2007).

In the intact system, olivary neurons are integrated in specific cerebellar modules (De Zeeuw et al., 1998; De Zeeuw et al., 1994; Voogd and Glickenstein, 1998). The climbing fibers of each olivary subnucleus innervate the Purkinje cells of a particular zone, which in turn project back to the same olivary subnucleus via one of the cerebellar nuclei. In this way the olivocerebellar system comprises many modules, which are each dedicated to specific motor domains and which can run in parallel if needed. The GABAergic feedback from the cerebellar nuclei to the inferior olive is peculiar in that its fibers terminate in a strategic position inside glomeruli directly apposed to the olivary dendrites that are coupled by gap junctions (De Zeeuw et al., 1989). By inducing a large shunting current these terminals may be able to dynamically uncouple olivary neurons and thereby influence the synchrony of complex spike activities that occur in the cerebellar cortex (Sasaki et al., 1989; De Zeeuw et al., 1996; Lang, 2002). Such a mechanism may for example be involved during the training and execution of rhythmic, tongue or whisker movements (Welsh et al., 1995; Lang et al., 2006).

If the inferior olive is indeed involved in setting the pace and composition of motor domains by controlling the activities of ensembles of coupled neurons then the question remains how the preferred frequency of an oscillating ensemble is determined. In principle, there are two main options for controlling such a frequency (De Zeeuw et al., 1998). Either olivary neurons are uniformly flexible and the preferred frequency of their oscillation can be controlled by activation of their excitatory afferents (in this constellation inhibitory input from the cerebellar nuclei could serve to merely control the size of the coupled ensemble) or, alternatively, individual olivary neurons have a more unique, but fixed, preferred frequency of oscillation, and the preferred frequency of the ensemble is determined by including or excluding particular cells via their cerebellar GABAergic input. In the latter case, one should find different categories of olivary neurons with different, but fixed, preferred frequencies and one should not be able to change this frequency by peripheral activation.

Thus, to investigate the occurrence and stability of subthreshold oscillations of olivary neurons *in vivo*, to find out how they may influence the temporal pattern of their climbing fiber activities, and to study the impact of peripheral stimulation on these oscillations and spiking patterns, we performed whole-cell recordings of olivary neurons in the intact olivocerebellar system during peripheral sensory stimulation.

MATERIAL AND METHODS

In vivo whole-cell recordings

C57Bl6 mice were anesthetized with a mixture of Ketamine and Xylazine (65 and 10 mg/kg i.p.), or a mixture of Medetomidine, Midazolam and Fentanyl (0.5 mg/kg, 5 mg/kg and 0.05 mg/kg i.p., respectively). The body temperature was maintained at 37ºC with the use of an anal thermosensor and a heating pad (FHC, Bowdoinham, Me., USA). To perform stable *in vivo* recordings the mouse was placed in supine position and the head was fixed (Margrie et al., 2002). Neck surgery was performed to expose the ventral surface of the medulla oblongata and the dura was removed. Whole-cell recordings were performed with borosilicate pipettes (with filament; outer diameter 1.5 mm, inner diameter 1.2 mm, Hilgenberg, Malsfeld, Germany) filled with (in mM) 4 NaCl, 3.48 $MgCl_2$, 9 KCl, 10 KOH, 120 K-gluconate, 10 HEPES, 17.5 Sucrose, 4 Na_2ATP and 0.4 Na_3GTP with pH 7.2 and osmolality at 290-310 mOsm kg^{-1}. To label the recorded neurons 0.5% Neurobiotin was added to the internal solution. Current clamp recordings were amplified with a Multiclamp 700A (Axon instruments, Foster city, CA, USA), filtered at 10 kHz and digitized at 20 kHz with a Digidata 1322A (Axon instruments, CA). Membrane potentials were corrected for an 8 mV junction potential. Peripheral stimulation was provided by electrical stimulation to the tongue or skin. The stimulation protocol consisted of short bipolar stimulations (2 ms, 1.25mA). Analysis was performed using Clampfit 9.0 software (Axon instruments, CA). All animal procedures were in accordance with the guidelines of the ethical committee of Erasmus MC.

Morphology

After labeling the cells with Neurobiotin, mice were transcardially perfused with 4% paraformaldehyde in 0.1 M phosphate buffer (PB). The brainstem was removed and post-fixed in perfusate and subsequently rinsed overnight at 4°C in 0.1 M PB, pH 7.4, containing 10% sucrose. The brainstem was embedded in 10% gelatine and 10% sucrose. Tissues were fixed in 10% formaldehyde and 30% sucrose solution at room temperature for 2 hours. Serial sections of 40 mm were cut on a cryo-modified sliding microtome (Leica SM2000R, Nussloch, Germany). Sections were incubated overnight at 4°C in avidin-biotin-peroxidase complex (Vector Laboratories, Burlingame, CA, USA), rinsed and incubated in DAB (75 mg/100 ml). The reaction was stopped after visual inspection by rinsing in PB. Neurobiotin labeled cells were reconstructed using Neurolucida software (Microbrightfield Europe, Magdeburg).

Membrane properties and responses

Data analysis was performed on neurons with resting membrane potentials negative to -45 mV, typical olivary spike waveforms and spike amplitudes larger than 60 mV. In each neuron the following membrane properties were determined: resting membrane potential, input resistance, membrane capacitance, time-dependent inward rectification (I_h), rebound depolarizations and after hyperpolarizations. Patterns of spontaneous firing were studied in recordings from membrane potentials of at least 2 minutes. The spontaneous firing rate was determined as the inverse of the mean of all spike intervals. The coefficient of variation (CV) of spike intervals was computed by dividing the standard deviation of the spike intervals by the mean of the spike intervals. Preferred spiking patterns were studied by autocorrelograms of spontaneous spiking patterns and burst patterns were evaluated using a burst analysis method (clampfit 9.0 software, Axon Instrument, CA). Burst patterns with a significant Poisson surprise value (>5) were selected, spike times of the spikes in this burst were averaged, and this value was taken as the center point of the preferred spiking period. Subthreshold oscillations were quantified by measuring the frequency and amplitude of the oscillations. Spontaneous membrane potential recordings of at least 2 minutes were analyzed by using a Hann windowed fast Fourier transformation to generate a power spectrum. The stability of subthreshold oscillations within a single recording was monitored by using a running Hann windowed fast Fourier transformation. Every 250 ms a power spectrum was generated by analyzing the last 819.2 ms. Membrane responses evoked by 150 peripheral sensory stimulations were analyzed. The response efficiency was determined by dividing the amount of evoked action potentials (i.e. action potentials in the 25 to 100 ms time window after the stimuli) by the amount of sensory stimuli. The response latency was calculated as the average time latency of these evoked action potentials after the peripheral stimuli. The occurrence of a preferred spiking period after the stimuli-induced action potential was determined by using again the burst analysis method. The average response latency of the spikes within this preferred spiking period was calculated.

To quantify the effect of action potentials on the subthreshold oscillation, the phase difference in subthreshold oscillation before and after action potential was determined. In spontaneous membrane potential and in stimuli induced activity recordings a sine-wave was fitted in the subthreshold oscillation before a spontaneous or evoked action potential. The fitted curve was extrapolated to the oscillations succeeding the action potential. Based on this curve-fit the position of the spike and the phase shift were calculated.

Statistics/Cluster analysis

Neurons were initially grouped by visual inspection of their subthreshold activity. Hierarchical cluster analysis was used to confirm the grouping produced by this visual inspection and to generate a more reliable classification of the different groups. Hierarchical cluster analysis was performed using the frequencies of subthreshold oscillations as distinguishing variable. In this hierarchical clustering, we used standardized parameter values to compute the euclidean distance between objects. The calculated linkage distance was used to define the cell clusters. In order to reveal cluster differences in basic membrane or stimulus response properties statistic analyses were performed using ANOVA or the X^2-test's and post-hoc analysis was performed using Least Significant Difference test. All numerical values in the text refer to mean ± S.E.M.

RESULTS

Basic membrane properties

Results described in this study were obtained from 61 neurons of the inferior olive (i.e. principal olive, accessory olives and dorsal cap of Kooy) measured by *in vivo* whole-cell recording technique. The basic membrane properties measured *in vivo* were comparable to those measured *in vitro* (Llinás and Yarom, 1981a; De Zeeuw et al., 2003; Leznik and Llinás, 2005; Long et al., 2002) (Table 1). The *in vivo* recorded IO neurons fired action potentials with

Table 1. Overview of membrane properties of IO neurons measured in vivo with the whole cell patch clamp technique.

Parameter	Mean±s.e.m.	Range	n
Resting membrane potential (mV)	-55.6±0.7	-45.0 to -65.0	61
Input resistance (MΩ)	45.9±4.2	14.8 to 74.7	60
Membrane capacitance (pF)	184.0±11.3	50.5 to 577.0	60
Firing rate (Hz)	0.87±0.22	0 to 13.2	61
Coefficient of variation for spike intervals	0.74±0.02	0.27 to 1.20	60
% Cells expressing depolarizing sag	18	10 out of 57	57
% Cells expressing rebound depolarization	61	34 out of 56	56
% Cells expressing rebound hyperpolarization	23	11 out of 48	48
% Cells expressing spontaneous SSTO's	30	18 out of 61	61
SSTO frequency (Hz)	5.7±0.3*	3.6 to 7.5	18
SSTO amplitude (mV)	5.6±0.6*	1.5 to 8.9	18
% Cells expressing spont. LT Ca2+ spikes.	72	44 out of 61	61
LT Ca2+ spike frequency (Hz)	1.8±0.1*	1.0 to 3.1	44
LT Ca2+ spike amplitude (mV)	4.2±0.3*	1.5 to 8.5	44
% Cells expressing no spont. SSTO's or LT spikes	15	9 out of 61	61

Values represent means ± S.E.M. * A single cell can have multiple subthreshold oscillation frequencies. SSTO: sinusoidal subthreshold oscillation, LT: low threshold.

an average frequency of 0.87 ± 0.22 Hz and a mean regularity of 0.74 ± 0.02 (coefficient of variation (CV) of spike intervals). They had a resting membrane potential of -55.6 ± 0.7 mV, a membrane capacitance of 184.0 ± 11.3 pF, and an input resistance of 45.9 ± 4.2 MΩ. Electrophysiological behavior of IO neurons was further studied by injection of positive and negative current pulses (Figures 1A and B). In contrast to previous *in vitro* studies, which often revealed a strong "depolarizing sag" as a result of activating H-currents (19, 20), our *in vivo* study only showed a depolarizing sag in a minority of the cases (18%; Figure 1A). Moreover, the same negative current injection evoked a strong rebound depolarization in
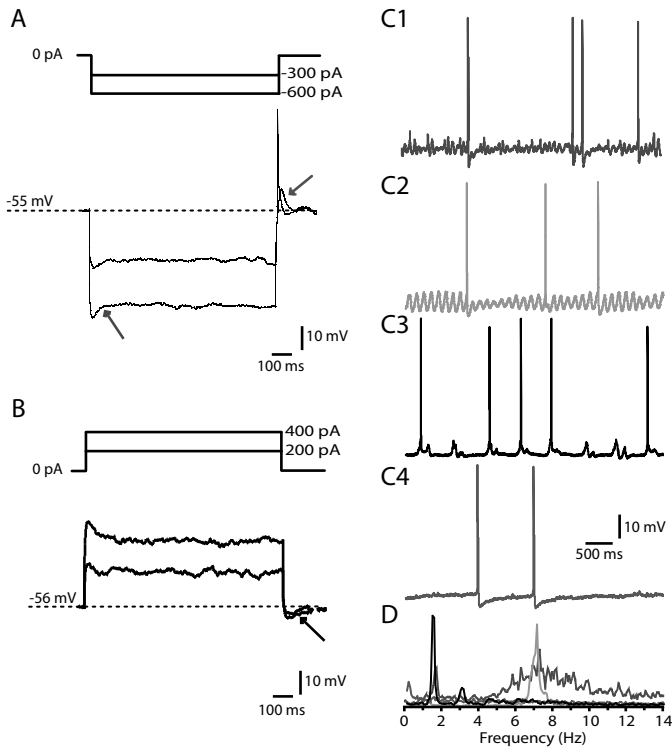
Figure 1. Membrane properties of olivary neurons recorded in current clamp mode. A. Hyperpolarizing current injections of 1s were applied to evoke the time-dependent inward rectification (I_h; blue arrow) and rebound depolarizations (red arrow) as well as rebound spikes. It should be noted that type I and II neurons, which express a rebound depolarization, can initiate sinusoidal oscillations in response to this rebound depolarization. **B.** Depolarizing current injections of 1s were applied to induce an after hyperpolarization (AHP; black arrow). **C.** Different types of subthreshold activity in the membrane potential were observed in olivary neurons. (C1) Neuron showing a subthreshold activity composed of two different frequencies, namely 1.9 Hz and 7.2 Hz. (C2) Neuron showing sine-wave shaped oscillations of 7 Hz. (C3) Cell with low-threshold Ca2+ spikes, which exhibited a rhythmic behavior of 1.8 Hz. (C4) Cells without any substantial subthreshold activity. **D.** Power spectra of the recordings shown in C1, C2, C3 and C4.

a majority of the cases (61%). Increasing the amplitude of negative current resulted in an increase of rebound depolarization and eventually a somatic low-threshold Ca^{2+} spike was induced (Figure 1A), which in turn triggered a fast sodium spike. Intracellular depolarizing current pulses hardly initiated action potentials or spike-adaptation and depolarizing steps were followed by a hyperpolarizing sag in only 23% of the cells (Figure 1B).

Whole-cell recordings of IO neurons *in vivo* exhibited various patterns of resting membrane potential activity (Figure 1C). In contrast to *in vitro* studies in which subthreshold sine-wave-shaped oscillations and rhythmic low-threshold Ca^{2+} spikes virtually only occur in hyperpolarized neurons and in which they rarely occur together in the same neuron (Llinás and Yarom, 1981a; Llinás and Yarom, 1981b), our *in vivo* recordings revealed that IO neurons can also exhibit these two types of oscillations spontaneously and relatively frequently together. We observed four different types of patterns of subthreshold activities: a) Typical rhythmic 4 to 8 Hz sinusoidal subthreshold oscillations (SSTO's) with a mean amplitude of 5.6 ± 0.6 mV (Figure 1C2); b) rhythmic 1 to 3 Hz low-threshold Ca^{2+} oscillations (LTO's) with a mean amplitude of 4.2 ± 0.3 mV (Figure 1C3); c) a pattern in which both oscillatory activities described above were combined (Figure 1C1); and d) a pattern in which no subthreshold oscillations were present in the resting membrane potential (Figure 1C4). In the first three patterns the amplitude of the oscillations could either be constant or vary in a cyclic manner. In the fourth pattern there was a subpopulation (only 3 neurons) in which no low-threshold Ca^{2+} currents were observed and in which the high firing frequencies (up to 30 Hz) could be evoked by depolarizations.

Categorization of neurons

Since the patterns of subthreshold membrane activities appeared to vary considerably among IO neurons, we investigated whether the differences described above could be established by statistical means. Using the frequency of the subthreshold membrane oscillations as a distinguishing property in a hierarchical cluster analysis, we were indeed able to readily divide the population of 61 olivary neurons into four clusters (Figure 2A): 16% of the neurons exhibited both SSTO's and LTO's (type I); 13% exhibited only SSTO's (type II); 56% contained neurons that exhibited only LTO's (type III); and 15% did not show any subthreshold oscillation (type IV). Moreover, the identity of these clusters could be readily confirmed in a matrix in which the LTO and SSTO activities were plotted against each other in the order of their frequencies (Figure 2B). Despite their clear characteristics at the cell physiological level, type I, II, and III neurons that were intracellularly injected with neurobiotin were indistin-

guishable from each other at the morphological level (for all n = 4; Supporting information Panel 1: Figure A); they all showed the characteristic olivary dendrites that tend to curl back towards the soma (De Zeeuw et al., 1998) and they were not restricted to any particular olivary subnucleus (Figure 2C). Due to their low occurrence type IV neurons were not labeled, but three of these neurons were recorded in the medial part of the inferior olive at a depth ranging from 500-750 μm and their activity closely resembles that of the neurons that were described by Urbano et al. (Urbano et al., 2006), therefore these neurons are probably olivary neurons from the dorsal cap of Kooy.
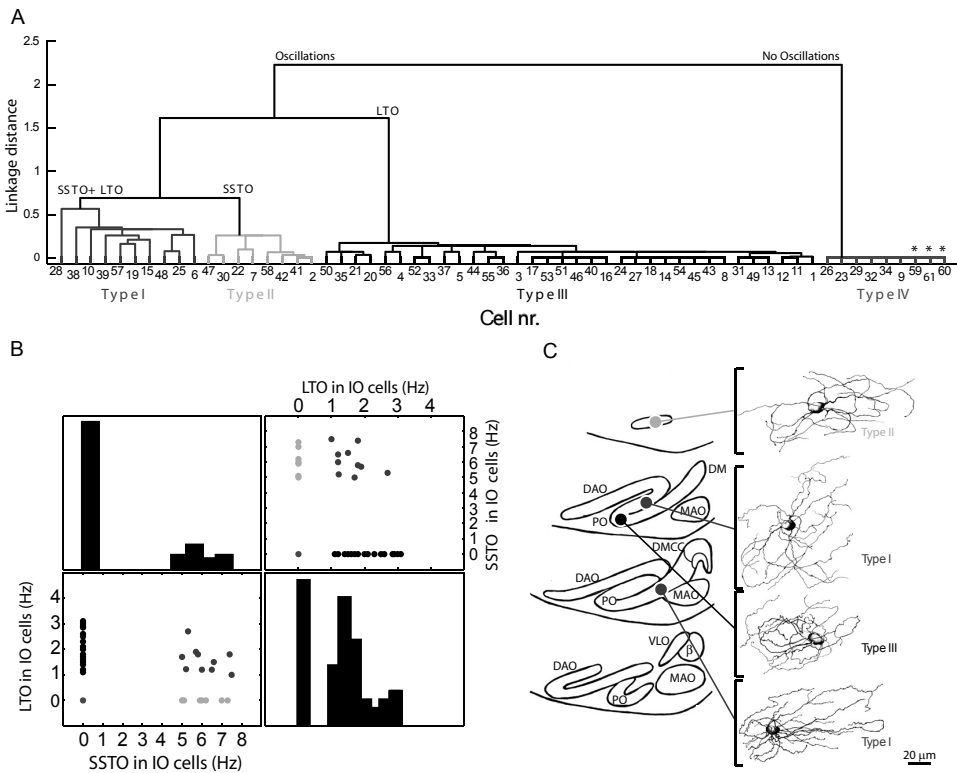
Figure 2. Cluster analysis based on subthreshold oscillations in membrane potential. A. Hierarchical cluster analysis shows clustering into four distinctive groups: Type I neurons (blue) exhibit SSTO's and LTO's; type II neurons (green) express only pure SSTO; type III (black) neurons express only LTO; and type IV neurons (red) exhibit no subthreshold activity. **B.** Matrix plot representation of the subthreshold oscillation frequencies of olivary neurons and their classification by hierarchical cluster analysis. * Olivary neurons presumably from the dorsal cap of Kooy (21). C. Reconstruction of Neurobiotin labeled neurons. All labeled cells (three cell types) were located in the inferior olive and revealed similar morphology. DAO, dorsal accessory olive; PO, Principal olive; DM, dorsomedial group of PO; MAO, Medial Accessory olive; DMCC, Dorsomedial cell column; VLO, Ventrolateral outgrowth; ß Beta cell group.

A

Type I

Type II

Type III

B
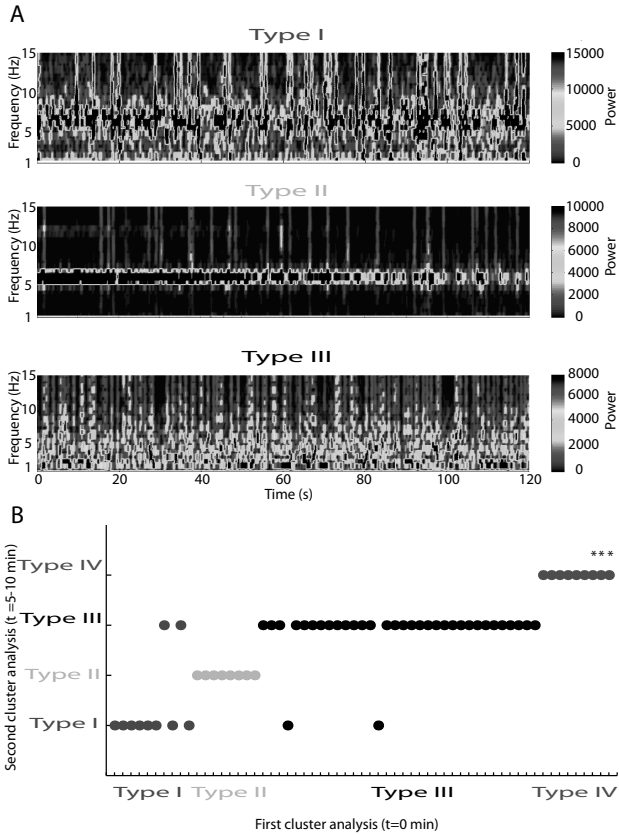
Figure 3. Stability of sub-threshold oscillation frequencies in olivary neurons. A. Time - subthreshold oscillation frequency representation of 120 s of spontaneous recordings from a type I, type II and type III neuron. The amplitude of the power spectra is coded in color. B. Olivary neurons were subjected to two cluster analyses that were performed on oscillatory behavior that was obtained at 2 different time frames that were separated by 5-10 minutes. * Olivary neurons presumably from the dorsal cap of Kooy (Urbano et al., 2006).

To determine whether the identity of an individual olivary neuron is fixed, we investigated the stability of their subthreshold oscillations over time (on average 23 minutes). Two minutes of spontaneous recordings were compared to the same episodes of recordings at least 5 to 10 minutes later. Within the two minutes timeframes themselves no transitions in subthreshold activities were observed (Figure 3A). However, 4 out of the 61 neurons (7%) showed a change in one of the subsequent episodes with respect to the first one (Figure 3B). Two type I cells became type III cells and two type III cells became type I cells. All these four alterations were single event transitions in SSTO activities indicating that the presence or absence of LTO's is a definitive characteristic of a given cell, while those of the SSTO's can appear and disappear in rare cases. In addition, when we made whole cell recordings in animals anesthetized with a mixture of Midazolam, Medetomidine and Fentanyl (n = 21; on top of the 61 reported above) instead of Ketamine and Xylazine we observed the same consistent types of oscillations.

Table 2. Olivary neurons recorded during different stages of anesthesia

Cell no.	Guedel stage of anesthesia	Cell type
1	III-3	III
2	III-3	III
3	III-2 & III-3	Only I
4	III-2 & III-3	Only I
5	III-3	I
6	III-2	II
7	III-3	I
8	III-2	I

Moreover, we did not find any evidence that the depth of Ketamine-Xylazine anaesthesia affected the characteristics of the oscillations (n = 8; on top of the cells reported above) (Supporting information Panel 1: Figure B).

Table 3: Overview of membrane and response properties per olivary neuron type

	Type I	Type II	Type III	Type IV	Statistical significance ANOVA/X²-test
Distinguishing set of properties	SSTO LTO	SSTO No LTO	No SSTO LTO	No SSTO No LTO	
Number of cells	10	8	34	9	
Resting membrane potential (mV)	-56.5±1.7	-54.6±1.4	-56.4±0.8	-52.3±1.9	ns
Input resistance (MΩ)	33.8±3.6	39.7±2.4	42.8±4.4	76.5±19.9	<0.02
Membrane capacitance (pF)	215±30	182±20	186±16	139±17	ns
Firing rate (Hz)	0.71±0.09	0.39±0.13	0.68±0.05	2.07±1.41	ns
Coefficient of variation for spike intervals	0.75±0.03	0.79±0.06	0.73±0.02	0.71±0.12	ns
Cells expressing depolarizing sag (%)	29	33	9	25	<0.03
Cells expressing rebound depolarizations (%)	71	67	63	38	ns
Cells expressing hyperpolarizing sag (%)	0	50	13	50	ns
Cells expressing SSTO (%)	100	100	0	0	DP
SSTO frequency (Hz)	6.2±0.3	5.9±0.3	-	-	DP
SSTO amplitude (mV)	4.9±0.7	6.8±0.5	-	-	DP
Cells expressing spontaneous LT Ca²+spikes (%)	100	0	100	0	DP
LT Ca2+ oscillation frequency (Hz)	1.5±0.2	-	1.8±0.1	-	DP
LT Ca2+ oscillation amplitude (mV)	4.1±0.5	-	4.1±0.3	-	DP
Shortest preferred ISI (ms)	139.3±7.7	144.3±15.5	550.3±43.8	-	<0.01
Cells responding to peripheral stimuli (%)	67	100	88	0	<0.05
Response efficiency (%)	26.3±6.1	18.7±3.8	22.7±4.3	-	<0.02
Response latency 1st spike (ms)	37.1±7.1	36.7±3.2	51.2±5.0	-	ns
Response latency 2nd spike (ms)	411±113	172±23	516±38	-	<0.02

Values represent means ± S.E.M and indicate the levels of statistical significance according to either ANOVA or X²-test.
SSTO: sinusoidal subthreshold oscillation, LT: low threshold, DP: distinguishing property.

In the latter recordings the states and depths of anaesthesia were determined with the use of EEG recordings and qualified according to the frequency bands as described by Guedel (Guedel, 1920, also see Friedberg et al., 1999), and we compared Guedels' stages III-2 and III-3 during recordings that lasted at least 40 minutes (Table 2). Post hoc analysis revealed that properties such as resting membrane potential, membrane capacitance, firing rate, coefficient of variation for spike intervals, and the occurrence of rebound depolarizations and/or hyperpolarizing sags were all not significantly different among the four cell types (Table 3). In contrast, the occurrence of H-current induced-depolarizing sags was significantly lower in type III neurons, while their shortest preferred ISI was significantly longer (all p's < 0.02), and the mean input resistance was significantly higher in type IV neurons (for comparisons

with type I, II and III neurons all p's < 0.03) (Table 3). Thus, we conclude that olivary neurons can be divided into four types with specific frequency characteristics of their subthreshold oscillations and specific membrane and response properties that are all relatively stable over time.

Preferred spiking patterns

To find out whether subthreshold oscillations contribute to the firing behavior of olivary neurons, their spiking patterns were analyzed in relation to their subthreshold activities. Even though the firing frequencies among the four types were not significantly different, their patterns of preferred spiking varied (Figure 4). Type I neurons had a dominant preferred spiking pattern with an interspike interval (ISI) of 139 ± 8 ms ranging from 120 to 190 ms
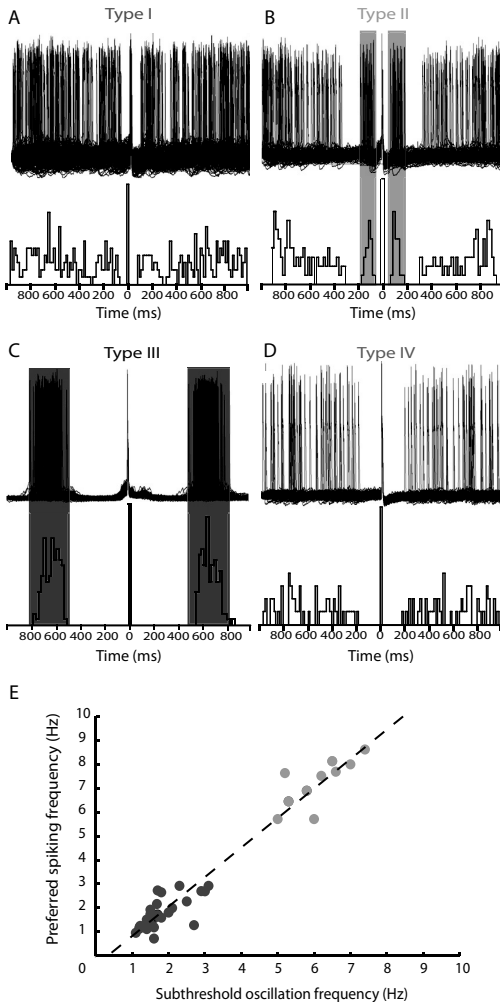
Figure 4. Autocorrelograms showing preferred spiking patterns. A. A type I neuron showing multiple preferred spiking patterns. **B.** A type II neuron showing a preferred spiking pattern with at 80-200 ms (indicated by green box). **C.** Example of a type III neuron, which shows a preferred spiking pattern at 600-800 ms (indicated by grey box). **D.** A type IV neuron showing no preferred spiking pattern. **E.** Correlation between olivary oscillation frequency and preferred spiking pattern frequency (linear fit: y= 1.2x-0.4, r^2=0.95).

in agreement with the rhythm of SSTO's (Figure 4A). In addition, type I cells had a second preferred spiking pattern with an average ISI of 629 ± 74 ms ranging from 454 to 802 ms corresponding with the presence of LTO's. Type II neurons showed preferred spiking patterns with an interspike interval ranging from 78 to 211 ms, which was again in accordance with the wavelength of their SSTO's (Figure 4B). In type III neurons only spiking patterns with long ISI's were found ranging from 460 to 641 ms (Figure 4C), which was also in line with the presence of LTO's; this preferred spiking pattern was significantly different from those of neurons in the other types (Table 3; ANOVA: $p < 0.01$; Post hoc Least Significant Difference test: $p < 0.01$). Finally, as expected from the subthreshold activities, type IV neurons showed no preferred spiking patterns (Figure 4D). If one directly correlates the frequencies of preferred spiking with those of the subthreshold oscillations on a cell by cell basis, the correlation becomes evident ($r^2 = 0.95$) (Figure 4E).
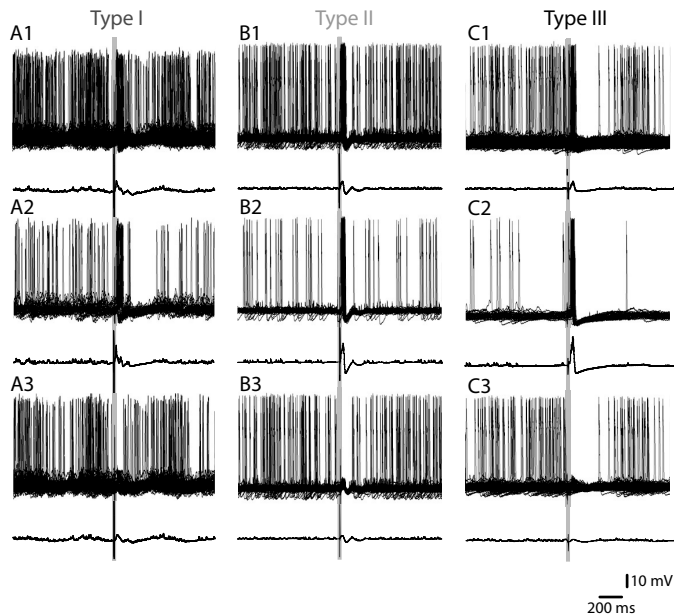
Figure 5. Response properties after peripheral sensory stimulation. A1. 150 traces of a type I neuron responding to peripheral stimulation and the resultant averaged trace indicated in the lower trace. **A2.** Subpopulation of A1: The traces of the same neuron that responded with an action potential and their averaged trace indicated below. **A3.** The complementary subpopulation of A1: The traces that did not respond with a spike and their averaged trace indicated below. **B.** and **C.** show the same panels as in A, but for type II and type III cells. Note that the stimulus can induce a period of inhibition not only when it does induce an action potential (see A2, B2 and C2), but also when it does not (A3, B3, and C3). In B3 it can be seen that peripheral stimulation can even reset the phase of the oscillating subthreshold responses without action potentials. Red bars indicate the time of peripheral stimuli administration.

Response properties

Somatosensory stimulation evoked action potentials and EPSP's in vast majority (85 %) of the type I, II, and III neurons, but in none of the type IV neurons (X^2-test, p < 0.05; Table 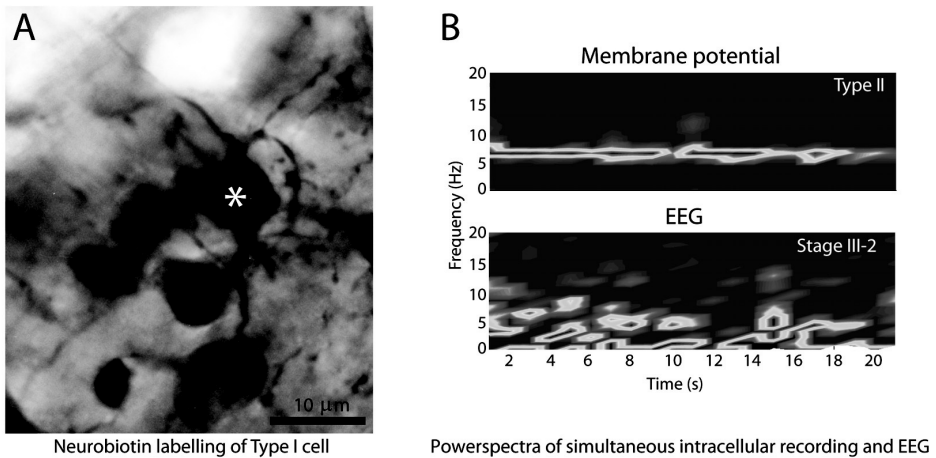2). The average response/stimulus efficiency was 23.6 ± 3.2 % (n = 20) with an average response latency of 47.2 ± 3.9 ms (n = 20). Each cell type had a characteristic pattern of responding. In type I neurons stimuli evoked action potentials as well as EPSP's at short latencies of 37.1 ± 7.1 ms or long latency responses of 411 ± 113 ms (for mixture of short and long second latency responses, see Figure 5A). In type II neurons the short latency responses were comparable to those in type I neurons, but the long latency responses (172 ± 23 ms) were significantly shorter (p < 0.02) (Figure 5B). Moreover, in these neurons the stimuli did not only elicit action potentials or subthreshold potentials but they also reset the phase of the sinusoidal subthreshold oscillations; these resettings did occur both after the stimuli that evoked action potentials ánd after those that only evoked subthreshold potentials (Figure 5B2 and Figure 5B3). In type III neurons both the short latency responses (51.2 ± 5 ms) and long latency responses (516 ± 38 ms) were longer than those of type I and type II neurons (p < 0.02) (Figure 5C). Moreover, the average inhibition period (465 ± 43 ms) that followed the stimulus evoked responses was significantly longer in these cells (p < 0.02). In general, the length of these inhibition periods was longer when the stimulus evoked an action potential than when it only evoked an excitatory subthreshold response (compare Figure 5B and Figure 5C). These results indicate a strong modulatory influence of peripheral inputs on olivary subthreshold oscillations and spiking patterns (i.e. olivary output).
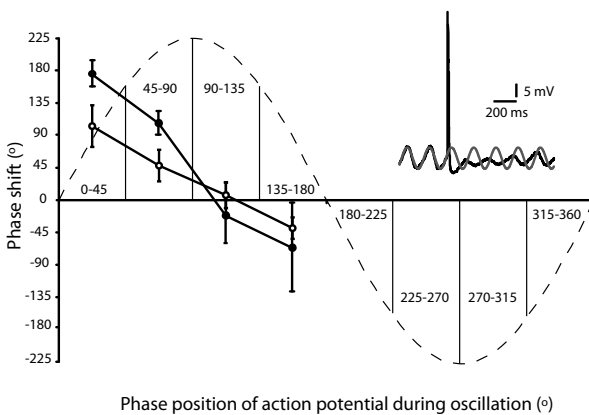
Figure 6. Phase-response curves. The phase of the subthreshold oscillations of type II neurons was reset after the occurrence of spontaneous (open circles) or stimulus evoked (filled circles) action potentials when these action potentials did not occur exactly at the peak of the oscillation. Inset: Example of a comparison of the phase values of the subthreshold oscillations before and after the occurrence of an action potential. Red trace is a sinusoidal fit of the trace before the occurrence of the action potential followed by an extrapolation after the occurrence of the action potential.

Supporting Information

Neurobiotin labelling of Type I cell   Powerspectra of simultaneous intracellular recording and EEG

Figure 7. Supporting information. A. Neurobiotin labeling of an in vivo whole-cell recorded olivary neuron (*, type I) and neighboring dye-coupled neurons. **B.** Time-frequency representation of simultaneously recorded electroencephalogram and the membrane potential of an olivary type II neuron. The depth of anesthesia was Guedel's stage III-2.

Interactions oscillations and spiking behavior

The data provided above suggest that action potentials can reset the phase of the subsequent subthreshold oscillations in an accurate manner, which has also been observed *in vitro* (Leznik et al., 2002). To further quantify this relationship we compared the phase of the oscillations before and after the action potentials in type II neurons (Figure 6). The phase of the subthreshold oscillations of type II neurons was only reset after the occurrence of spontaneous or stimulus evoked action potentials when these action potentials did not occur exactly at the peak of the oscillation. The phase of their oscillations áfter the action potential was consistently reset such that the new sinusoidal peaks occurred in cycles of approximately 360 degrees after the preceding action potential (Figure 6). This relation held true for both spontaneous action potentials and stimulus evoked action potentials, but the phase shift appeared to be somewhat greater after the stimulus evoked potentials (Figure 6).

The interaction between spiking behavior and subthreshold oscillations was not a one way interaction: The spiking behavior did not only influence the phase of the following oscillations, but the phase of the oscillation also strongly influenced the probability for an action potential to occur. Figure 6 illustrates that there were virtually no cells spiking in the trough of the oscillation (between 180 and 360 degrees). Thus, we can conclude that spiking behavior and subthreshold oscillatory behavior of olivary neurons strongly interact *in vivo*.

DISCUSSION

The present whole-cell recordings *in vivo* demonstrated that the vast majority of olivary neurons show subthreshold oscillations, that olivary neurons can be divided into four different categories dependent on the presence, shape and frequency of oscillation and that peripheral stimulation does not alter the characteristic stable oscillatory activities of an olivary cell other than resetting their phase. These findings have implications for the firing patterns of individual olivary neurons and they suggest that a wide variety of temporal patterns of olivary ensembles are composed by dynamically coupling or uncoupling specific types of olivary cells.

Electrophysiological composition of the inferior olive

The current *in vivo* study indicates that about 85% of the inferior olivary neurons have spontaneous subthreshold oscillations. This finding suggests that the actual level of oscillations in intact mammals is higher than observed in *in vitro* studies, in which relatively few spontaneous oscillations occur and in which hyperpolarizing current injections or electrical stimulations are usually required to induce oscillatory activity (Llinás and Yarom, 1981a; Llinás and Yarom 1981b; Bal and McCromick, 1997). Possibly, the reverberating loops in which the inferior olive is embedded enhance the intrinsic oscillatory properties of its neurons (Kistler and De Zeeuw, 2002). These loops include the excitatory trajectories from the cerebellar nuclei and mesodiencephalic junction (De Zeeuw et al., 1990; Ruigrok and Voogd, 1995) as well as the olivocerebellar modules comprising the olivary subnuclei, Purkinje cell zones and deep cerebellar nuclei (Voogd and Bigare, 1980). Such an extrinsic enhancing mechanism is in line with findings which indicate that serotonergic afferents to the olivary neurons as well as their level of electrotonic coupling can also modulate their propensity to oscillate (Llinás and Yarom, 1986; Placantonakis et al., 20003).

Apart from the non-oscillating cells, which presumably represent the neurons of the dorsal cap and ventrolateral outgrowth (Urbano et al., 2006), we found 3 types of oscillating cells that could be identified based upon their spontaneous subthreshold activities and categorized accordingly using statistical cluster-analysis. They include type I cells, which show both SSTO's and LTO's and which have a wide range of preferred frequencies for both their oscillations and spiking activities varying from 1 to 8 Hz; type II cells, which show only SSTO's and which have preferred oscillatory and spiking frequencies of 5 to 8 Hz; and type III cells, which show only LTO's and which oscillate and fire at preferred frequencies of 1 to 3 Hz. *In vitro* studies, in which the SSTO's and LTO's can be studied in isolation, have

shown that these oscillations in the olive are generated by rhythmic activation of dendritic high-threshold and somatic low-threshold Ca^{2+} conductances and their interaction with a Ca^{2+}-dependent K^+ conductance (Llinás and Yarom, 1986; Bal and McCormick, 1997). In addition, the H-current can also contribute to the olivary oscillations (Bal and McCormick, 1997). H-current dependent depolarizing sags were frequently observed in all three main oscillating cell types, but our data show that this current does not necessarily need to be expressed in order for the oscillations to occur. Thus, while the basic membrane properties of all olivary neurons are rather similar (see Table 3), they can vary substantially in their type of subthreshold oscillations.

The different sorts of oscillations of the various cell types were reflected in the spiking patterns in that the preferred frequencies of the autocorrellograms of olivary spike activities corresponded to those obtained from the spectral analyses of the subthreshold oscillations. Likewise the temporal spiking patterns that occurred after peripheral stimulation also reflected the type of oscillatory cell they were recorded from and varied accordingly. Type II neurons (SSTO-only) responded with an action potential or an EPSP, type III neurons (LTO-only) responded with a low-threshold Ca^{2+} spike with or without an action potential followed by a long afterhyperpolarization, and type I neurons revealed a mixed response. The main response properties (rate and latency) described here for the mouse inferior olive were comparable to those found for the olive in the awake cat and rabbit (Gellman et al., 1985; Leonard et al., 1988), except for type III neurons that responded with slightly longer latencies. In addition, peripheral stimulation had a clear effect on the phase of the subthreshold oscillations; it consistently reset the phase of its peak towards 90 degrees. Thus, peripheral inputs to the olive can modify the temporal code of its neurons both in relative terms (firing frequency) and absolute terms (precise moment in time).

Functional implications

Importantly, the subthreshold activity and thereby the identity of the cells appeared remarkably stable throughout the recordings. Virtually none of the recorded cells switched during the recordings from one category to the other even though many of them lasted longer than ½ an hour. We hardly ever observed the short episodic oscillatory behaviour, which has been described by Chorev et al., 2007. This difference might be due to differences in species used or in methodology such as the use of sharp electrode recordings instead of whole cell recordings. We cannot exclude the possibility that the state of the animal affects the oscillations (Tso et al., 2004), but the stability was so profound that even unphysiologi-

cally strong, electrical stimulation of the tongue was not sufficient to convert the identity characteristics of the olivary neurons. These data suggest that individual olivary neurons have a rather unique, preferred frequency of oscillation, which is relatively fixed. Such an organization raises the possibility that the overall temporal structure of an ensemble of coupled olivary neurons can in principle be manipulated by including or excluding cells with particular preferred frequencies to the ensemble. Thus, since the olivary neurons can be dynamically uncoupled by the cerebellar GABAergic terminals that are apposed to the spines that are coupled by dendrodendritic gap junctions in the olivary glomeruli (De Zeeuw et al., 1998; Llinás et al., 1974; De Zeeuw et al., 1989; Devor, 2002, Onodera and Hicks, 1995), it may well be that this input also controls both the size of and the overall preferred frequency of the olivary ensembles. In this constellation the excitatory inputs could then deliver the firing frequency and the fine-tuning for the phase of the activity in absolute time.

ACKNOWLEGDMENTS

REFERENCES

De Zeeuw, C. I., Simpson, J. I., Hoogenraad, C. C., Galjart, N., Koekkoek, S. K. & Ruigrok, T. J. (1998) Microcircuitry and function of the inferior olive. Trends Neurosci 21, 391-400.

Llinás, R. & Yarom, Y. (1981a) Electrophysiology of mammalian inferior olivary neurones *in vitro*. Different types of voltage-dependent ionic conductances. J Physiol (London) 315, 549-67.

Llinás, R. & Yarom, Y. (1986) Oscillatory properties of guinea-pig inferior olivary neurones and their pharmacological modulation: an *in vitro* study. J Physiol (London) 376, 163-82.

Llinás, R., Baker, R. & Sotelo, C. Electrotonic coupling between neurons in cat inferior olive (1974) J Neurophysiol 37, 560-71.

Benardo, L. S. & Foster, R. E. (1986) Oscillatory behavior in inferior olive neurons: mechanism, modulation, cell aggregates. Brain Res Bull 17, 773-84.

Llinás, R. & Yarom, Y. (1981b) Properties and distribution of ionic conductances generating electroresponsiveness of mammalian inferior olivary neurones *in vitro*. J Physiol (London) 315, 569-84.

Chorev, E., Yarom, Y. & Lampl, I. (2007) Rhythmic episodes of subthreshold membrane potential oscillations in the rat inferior olive nuclei *in vivo*. J Neurosci 27, 5043-52.

De Zeeuw, C. I., Wylie, D. R., DiGiorgi, P. L. & Simpson, J. I. (1994) Projections of individual Purkinje cells of identified zones in the flocculus to the vestibular and cerebellar nuclei in the rabbit. J Comp Neurol 349, 428-47.

Voogd, J. & Glickstein, M. (1998) The anatomy of the cerebellum. Trends Neurosci 21, 370-5.

De Zeeuw, C. I., Holstege, J. C., Ruigrok, T. J. & Voogd, J. (1989) Ultrastructural study of the GABAergic, cerebellar, and mesodiencephalic innervation of the cat medial accessory olive: Anterograde tracing combined with immunocytochemistry. J Comp Neurol 284, 12-35.

Sasaki, K., Bower, J. M. & Llinás, R. (1989) Multiple Purkinje cell recording in rodent cerebellar cortex.Eur J Neurosci 1, 572-586.

De Zeeuw, C. I., Lang, E. J., Sugihara, I., Ruigrok, T. J., Eisenman, L. M., Mugnaini, E. & Llinás, R. (1996) Morphological correlates of bilateral synchrony in the rat cerebellar cortex.J Neurosci 16, 3412-26.

Lang, E. J. (2002) GABAergic and glutamatergic modulation of spontaneous and motor-cortex-evoked complex spike activity. J Neurophysiol 87, 1993-2008.

Welsh, J. P., Lang, E. J., Sugihara, I. & Llinás, R. (1995) Dynamic organization of motor control within the olivocerebellar system. Nature 374, 453-7.

Lang, E. J., Sugihara, I. & Llinás, R. (2006) Isochrony in the olivocerebellar system underlies complex spike synchrony. J Physiol (London) 571, 101-20.

De Zeeuw, C. I., Chorev, E., Devor, A., Manor, Y., Van Der Giessen, R. S., De Jeu, M. T., Hoogenraad, C. C., Bijman, J., Ruigrok, T. J., French, P., Jaarsma, D., Kistler, W. M., Meier, C., Petrasch-Parwez, E., Dermietzel, R., Söhl, G., Güldenagel, M., Willecke, K. & Yarom, Y. (2003) Deformation of Network Connectivity in the Inferior Olive of Connexin 36-Deficient Mice Is Compensated by Morphological and Electrophysiological Changes at the Single Neuron Level J Neurosci 23, 4700-11.

Leznik, E. & Llinás, R. (2005) Role of gap junctions in synchronized neuronal oscillations in the inferior olive. J Neurophysiol 94, 2447-56.

Long, M. A., Deans, M. R., Paul, D. L. & Connors, B. W. (2002) Rhythmicity without synchrony in the electrically uncoupled inferior olive. J Neurosci 22, 10898-905.

Yarom, Y. & Llinás, R. (1987) Long-term modifiability of anomalous and delayed rectification in guinea pig inferior olivary neurons. J Neurosci 7, 1166-77.

Bal, T. & McCormick, D. A. (1997) Synchronized oscillations in the inferior olive are controlled by the hyperpolarization-activated cation current I(h). J Neurophysiol 77, 3145-56.

Urbano, F. J., Simpson, J. I. & Llinás, R. R. (2006) Somatomotor and oculomotor inferior olivary neurons have distinct electrophysiological phenotypes. Proc Natl Acad Sci U S A 103, 16550-5.

Friedberg, M. H., Lee, S. M. & Ebner, F. F. (1999) Modulation of receptive field properties of thalamic somatosensory neurons by the depth of anesthesia. J Neurophysiol 81, 2243-52.

Guedel, A. E. (1920) Signs of inhalational anesthesia (Macmillan, New York).

Leznik, E., Makarenko, V. & Llinás, R. (2002) Electrotonically mediated oscillatory patterns in neuronal ensembles: an *in vitro* voltage-dependent dye-imaging study in the inferior olive. J Neurosci 22, 2804-15.

Kistler, W. M. & De Zeeuw, C. I. (2002) Dynamical working memory and timed responses: the role of reverberating loops in the olivo-cerebellar system. Neural Comput 14, 2597-626.

De Zeeuw, C. I., Holstege, J. C., Ruigrok, T. J. & Voogd, J. (1990) Mesodiencephalic and cerebellar terminals terminate upon the same dendritic spines in the glomeruli of the cat and rat inferior olive: an ultrastructural study using a combination of [3H]leucine and wheat germ agglutinin coupled horseradish peroxidase anterograde tracing. Neuroscience 34, 645-55.

Ruigrok, T. J. & Voogd, J. (1995) Cerebellar influence on olivary excitability in the cat. Eur J Neurosci 7, 679-93.

Voogd, J. & Bigaré, F. (1980) The inferior olivary nucleus. Raven Press New York., 207-305.

Placantonakis, D. G., Schwarz, C. & Welsh, J. P. (2000) Serotonin suppresses subthreshold and suprathreshold oscillatory activity of rat inferior olivary neurones *in vitro*. J Physiol (London) 524 Pt 3, 833-51.

Gellman, R., Gibson, A. R. & Houk, J. C. (1985) Inferior olivary neurons in the awake cat: detection of contact and passive body displacement. J Neurophysiol 54, 40-60.

Leonard, C. S., Simpson, J. I. & Graf, W. (1988) Spatial organization of visual messages of the rabbit's cerebellar flocculus. I. Typology of inferior olive neurons of the dorsal cap of Kooy. J Neurophysiol 60, 2073-90.

Tso, M. M., Blatchford, K. L., Callado, L. F., McLaughlin, D. P. & Stamford, J. A. (2004) Stereoselective effects of ketamine on dopamine, serotonin and noradrenaline release and uptake in rat brain slices. Neurochem Int 44, 1-7.

Devor, A. (2002) The great gate: control of sensory information flow to the cerebellum. Cerebellum 1, 27-34.

Onodera, S. & Hicks, T. P. (1995) Patterns of transmitter labelling and connectivity of the cat's nucleus of Darkschewitsch: a wheat germ agglutinin-horseradish peroxidase and immunocytochemical study at light and electron microscopical levels. J Comp Neurol 361, 553-73.

Margrie, T. W., Brecht, M. & Sakmann, B. (2002) *In vivo*, low-resistance, whole-cell recordings from neurons in the anaesthetized and awake mammalian brain. Pflugers Arch 444, 491-8.

Chapter 4

Consequences of a lack of Connexin36 on olivary neurons at the systems level

CHAPTER 4.1

Analysis of Cx36 Knockout Does Not Support Tenet That Olivary Gap Junctions Are Required for Complex Spike Synchronization and Normal Motor Performance

W.M. KISTLER[1]*, M.T.G. DE JEU[1]*, Y. ELGERSMA[1], R.S. VAN DER GIESSEN[1], R. HENSBROEK[1], C. LUO[1], S. K. E. KOEKKOEK[1], C.C. HOOGENRAAD[1], F.P.T. HAMERS[2], M. GÜLDENAGEL[3], G. SÖHL[3], K. WILLECKE[3], AND C.I. DE ZEEUW[1]

[1]*Department of Neuroscience, Erasmus MC, University Medical Center Rotterdam, 3000DR Rotterdam, The Netherlands*
[2]*Department of Medical Pharmacology and Anatomy, Rudolf Magnus Institute for Neurosciences, University Medical Center Utrecht, 3584CG Utrecht, The Netherlands*
[3]*Institute of Genetics, Division of Molecular Genetics, University of Bonn, 53117 Bonn, Germany*

*Both authors contributed equally to this paper

ABSTRACT

Electrotonic coupling by gap junctions between neurons in the inferior olive has been claimed to underly complex spike (CS) synchrony of Purkinje cells in the cerebellar cortex and thereby to play a role in the coordination of movements. Here, we investigated the motor performance of mice that lack Connexin36 (Cx36), which appears necessary for functional olivary gap junctions. Cx36 null-mutants are not ataxic, they show a normal performance on the accelerating rotarod, and they have a regular walking pattern. In addition, they show normal compensatory eye movements during sinusoidal visual and/or vestibular stimulation. To find out whether the normal motor performance in mutants reflects normal CS activity or some compensatory mechanism downstream of the cerebellar cortex, we determined the CS firing rate, climbing-fiber pause, and degree of CS synchrony. None of these parameters in the mutants differed from those in wildtype littermates. Finally, we investigated whether the role of coupling becomes apparent under challenging conditions, such as during application of the tremorgenic drug harmaline, which specifically turns olivary neurons into an oscillatory state at a high frequency. In both the mutants and wildtypes this application induced tremors of a similar duration with similar peak frequencies and amplitudes. Thus surprisingly, the present data does not support the notion that electrotonic coupling by gap junctions underlies synchronization of olivary spike activity and that these gap junctions are essential for normal motor performance.

INTRODUCTION

Despite the fact that the microcircuitry of the olivocerebellar system is known in considerable detail, its function is still a matter of fervent debate. The fnnction that is classically assigned to the cerebellum is the coordination of motor behavior-a conclusion that is widely supported by clinical observations (Luciani, 1891). A design principle that could explain convincingly how cerebellar function emerges from its morphological and electrophysiological peculiarities, however, is still elusive, despite the many attempts that have been made to link "form and function" (Albus, 1971; Braitenberg, 1967; Houk et al., 1996; Kistler et al., 2000; Marr, 1969). Recently, attention has been paid particularly to the inferior olivary nucleus, which is an extraordinary structure in several aspects. First, the inferior olive (IO) is the sole source of cerebellar climbing fibers that form highly efficient synaptic contacts with their respective Purkinje cell. A single climbing-fiber spike suffices to trigger a postsynaptic action potential followed by a burst of spikelets, the so-called complex spike response (Ec-

cles et al., 1966). Second, olivary neurons fire at a frequency of only 1 Hz, but they exhibit a high degree of temporal order. Slice recordings reveal synchronous subthreshold activities (Devor and Yarom, 2002; Lampl and Yarom, 1993; Llinás and Yarom, 1986), and Purkinje cells within a common rostro-caudal strip tend to fire complex spikes synchronously (Bell et al., 1972; Sasaki et al., 1989). This synchronization of complex spikes, which can occur in a millisecond time scale, has been suggested to result from dense coupling by fast electrical synapses between olivary dendrites (De Zeeuw et al., 1997; De Zeeuw et al., 1996; De Zeeuw et al., 1998; Lang, 2001; Lang et al., 1996; Llinás, 1991; Llinás and Sasaki, 1989; Llinás et al.1974). Moreover, since the dendrodendritic gap junctions are surrounded by strategically positioned chemical synaptic inputs (De Zeeuw et al., 1998) and GABA antagonists can influence the complex spike synchrony , (Lang et al. 1996; Llinás and Sasaki, 1989) it has been reasoned that regulation of dynamic coupling in the olive may play an important role in the timing and coordination of motor behavior (Lang et al., 1999;Llinás, 1991; Welsh et al. 1995). Recently, global knockout mice of gap junction protein Connexin36 (Cx36) have been created, and the inferior olive of these mutants turns out to be devoid of functional neuronal gap junctions (Long et al., 2001). Hence, Cx36–/– mice provide an exciting substrate to test the hypotheses on the role of gap junctions in complex spike synchrony and motor coordination. In the present report we address these hypotheses using both behavioral tests and *in vivo* electrophysiology. Our findings raise the possibility that the major current ideas on the role of olivary coupling gap junctional coupling may have to be reevaluated.

MATERIALS AND METHODS

Cx36-deficient and wildtype mice were generated and characterized as described by Güldenagel et al., 2001. Tests were performed on adult animals only. All animal procedures described were carried out onder animal care protocols approved by the Erasmus University Rotterdam.

Walking Pattern Analysis

Walking patterns were recorded and analyzed using the Catwalk system described previously (Hamer et al. 2001). In short, mice were directed over a clear, Plexiglas renway (60 cm long, 5 cm wide). Light was passed through the Plexiglas floor using a fluorescent light bulb, and wherever the floor was touched, light was deflected. This deflected light was recorded by a camera allowing a spatiotemporal analysis of walking pat-

terns. The following parameters were calculated: step regularity (percentage of regular step patterns), step length, base of support (the width between paws), and paw contact area (the paw area contacted at the moment of maximum paw-floor contact).

Rotarod Test

More complicated motor behaviors and motor learning were assessed with the accelerating rotarod test. The rotarod consists of a smooth plastic roller (8 cm diameter; 14 cm long) flanked by two large round plates (30 cm diameter) to prevent animals from escaping. On day 1, mice were placed on the stationary roller, and the time was measured until they fell off again (2 minutes max.). The next day, the test was repeated with the rod rotating at a constant velocity of 2 rpm. On days 3-6, the mice were initially put on the rod spinring at constant velocity (2 rpm). After 10 s the rotational velocity was gradually increased in 2 minutes to 12 rpm until the mice fell off. Each test was repeated three times per day per mouse.

Eye Movement Recording

Horizontal eye movements were recorded using the magnetic search coil technique described previously (De Zeeuw et al., 1998; Stahl et al., 2000). In short, the mouse head was restrained during recording by an acrylic pedestal fixed to the scull. After induction of halothane/nitrous oxide anesthesia, the scalp was incised, and four stainless steel screws (M 1 × 1.5 mm) were implanted in the calvarium and then encased in dental acrylic. Additional acrylic was used to fix two M2 nuts to this mass. Under general (halothane/nitrous oxide) and local (Novesine, 0.4%; Bournonville Pharma B.V., the Netherlands) anesthesia, a scleral search coil (1 mm outside diameter, 60 turn of copper wire, 1.0 mg) was implanted in the conjunctiva on the temporal side of the eyeball and flxed to the sclera with two sutures (10/0 nylon, Ethicon). The leads of the coil were carefully tunnelled subconjunctivally around the inferior margin of the eye and then out of the medial superior aspect of the orbit to a miniature coaxial MMCX connector that was attached to the acrylic head pedestal. After the mouse recovered from surgery (3 days), compensatory eye movements were recorded using a magnetic measurement system (Skalar Medical). Visual and vestibular stimuli were delivered with the use of a drum with a black-and-white strip pattern and a turntable. Stimulus parameters and data acquisition was controlled by a PC via a Power1401 interface (Cambridge Electronics Design, Cambridge, UK) and Spike2 for Windows. The performance of the optokinetic (OKR) and the vestibulo-ocular reflex (VOR) was assessed on four consecutive days by using sinusoidal stimuli at various frequencies and amplitudes. The response latency of the

OKR was measured by using velocity steps rom –4˚/s to +4˚/s in intervals with random durations of 1-2 seconds. Each recording session lasted or about one hoor. Eye-movement data was analyzed offline with custom-made C programs and Mathematica (Wolfram Research).

Electrophysiology

The mouse head was restrained during recording in a stereotaxic instrument by an acrylic pedestal that was built one day before the recording, as described above. To prepare the animal for recording it was anesthetized with ketamine (50 mg/kg, i.p.) and xylazine (8 mg/kg, i.p.). Additional doses were delivered every 60 min or as needed to maintain anesthesia. Neck muscles, occipital bone, and dura were removed to expose the dorsal surface of the cerebellum, which was then covered by a layer of agar (2% Agar Agar in 0.9% NaCI) to prevent dehydration of the tissue.

Extracellular recordings of complex spike (CS) and simple spike (SS) activity were obtained with glass microelectrodes with a tip diameter ofabout 2 μm (<2 MΩ) containing 2 M saline. Electrodes were positioned independently with two precision micromanipulators (TSE Systems, Germany). Particular care was taken to position the electrodes close to each other (rostrocaudal tip distance 0-200 μm). As soon as a stable recording was obtained with one of the electrodes, the other electrode was used to explore the neighborhood mediolaterally in steps of100 μm (mediolateral tip distance < 200 μm). Spike trains were recorded or about 20 min per cell pair. Single units of Purkinje cells could easily be identified by the presence of complex spikes followed by a brief pause in simple spike activity. Signals where preamplified (×50 ultralow noise differential amplifier AI 402, Axon Instruments, USA), band-pass filtered in the range of 300 Hz-4 kHz (CyberAmp 380, Axon Instruments, USA), digitalized with a sampling rate of 10 kHz and 16 bit resolution (Power1401, Cambridge Electronic Design, Cambridge UK), and stored on computer hard disk for off-line analysis.

Spike Sorting and Analysis

Complex spikes were identified by their characteristic wave form. In a first step, all spikes were extracted from the recording files using a simple threshold criterion. The form of the spikes (0.5 ms before and 5.0 ms after the first downstroke) was analyzed by principal component analysis (PCA) using custom-made C-programs and Mathematica (Wolfram Research, USA). Projecting the high-dimensional set of data points to the first few principal components usually produced two well-separated clouds for simple and complex spikes.

Trains of complex spikes were discretized using bin widths of Δt equal to 1, 2, 5, or 10 milliseconds. The degree of synchrony between two complex spike trains was quantified by the zero-time difference cross-correlation coefficient,

$$C_{1,2}(0) = (n^2 \bar{S}_1 \bar{S}_2)^{-1/2} \left[\sum_{i=1}^{n} S_1(i\Delta t) S_2(i\Delta t) - n\bar{S}_1\bar{S}_2 \right], \quad (1)$$

with $S_k(i\Delta t) = 1$; if time bin i contains the onset of a complex spike of neuron k, $k = 1, 2$, or else $S_k(i\Delta t) = 0$. Furthermore, n is the total number of time bins and

$$S_k = n^{-1} \sum_{n=1}^{n} S_k(i\Delta t) \,.$$

Tremor Measurements and Analysis

Harmaline-induced tremors were studied in 10 Cx36 wildtype (WT), 10 Cx36 knockout (KO), and 3 Lurcher mice (ages 71-152 days). Animals were shortly anesthetized with isoflurane (1.5-2%) and equipped with a harness (Instech Laboratories, Plymouth Meeting, PA) that contained three accelerometer chips (VTI Hamlin, Vantaa, Finland). After putting on the harness, harmaline (Sigma, St. Louis, USA) was injected intraperitoneally (50 mg/kg body weight). The accelerometer chips were oriented in the anterior-posterior (x axis), medial-lateral (y axis), and dorsal-ventral direction (z axis). Signals were acquired using a Cyber-Amp (Axon Instruments, USA) and relayed by a Power1401 interface (CED, Cambridge, UK) to a personal computer equipped with Spike2 (CED, Cambridge, UK). Signals were recorded at a sample rate of 200 Hz.

The acceleration traces of all three axes (1200 s) were analyzed by using a Hann windowed 1024-point Fast Fourier Transformation. Every second a power spectrum was generated by analysing the last 5.12 seconds. Episodes of tremor were detected by the peaks in the power spectra at the 5-15 Hz frequency band. These episodes of tremor were then used to generate a global power spectrum. The central peak of this spectrum was fitted to a Gaussian function.

RESULTS

We have addressed the role of electrotonic coupling of IO neurons in mice at both the behavioral and electrophysiological level. We compare results obtained in wildtype animals with those in mice that had a homozygous deletion of Connexin36 and have been reported to be devoid of functional neuronal gap junctions (Long et al., 2001).

Motor Behavior

To our great surprise Cx36−/− mice showed no obvious signs of motor impairment or ataxia. In order to obtain quantitative data, we carefully analyzed the walking pattern of Cx36−/− and wildtype mice using the "catwalk" technique, described in the METHODS section. Parameters such as step regularity, step length, base of support, and paw contact area did not exhibit a significant difference (Figure 1 A-D), while the base of support of the hind limbs, hut not of the forelimbs, was significantly smaller in the Cx36−/− mice (p value = 0.014, two-sided Student t test). This diference, however, turned out not to be significant in an ANOVA test that also accounted or variations in body weight. As a positive control, we also tested a weight-matched group of lurcher mice. These mice had, or example, a significantly (p < 0.004) reduced step regularity, signifying their general ataxia (data not shown). To see whether Cx36−/− mice are impaired in a motor task that is more challenging than walking on a smooth surface, we tested the Cx36−/− mice on the accelerating rotarod.
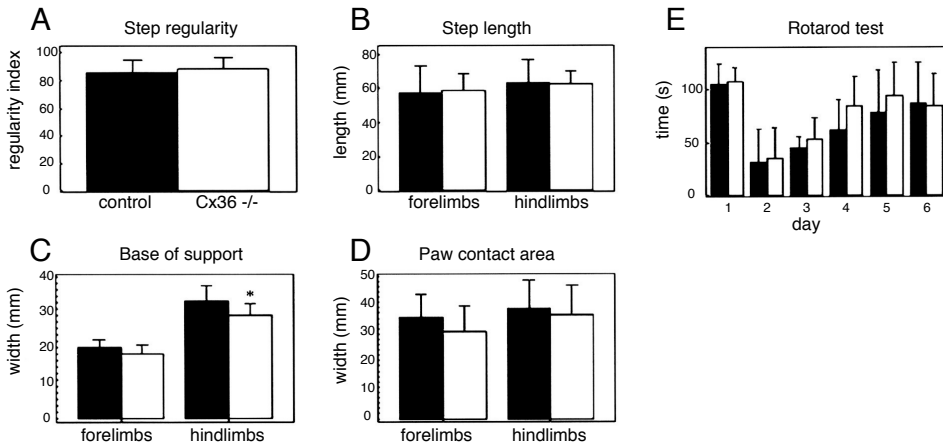
Figure 1. Motor behavior analysis. (A-D) Walking pattern analysis of Cx36−/− (n = 13, open bars) and wildtype (n = 12, filled bars) mice. None of the measured parameters revealed a significant difference between the two groups except the base of support of the bind limbs (see RESULTS). (E) Rotarod test. The bars give the time the mice managed to stay on the stationary (day 1), slowly rotating (day 2), or accelerating rod (days 3-6). No difference in the performance of Cx36−/− (n = 7, open bars) and wildtype mice (n = 7, filled bars) could be detected. Error bars correspond to 1 SD.

Again, no significant diference in the performance of Cx36−/− and the wildtype control group could be detected (Figure 1E).

The olivocerebellar system is known to be critically involved in the control of compensatory eye movements, such as OKR and VOR (Ito, 1984). To check whether the absence of olivary gap junctions had any effect on the performance of these reflexes, we measured amplitude and phase lag of the eye movements elicited by sinusoidal visual and vestibular stimuli. We used a broad range of different stimulation frequencies and amplitudes, hut none of these paradigms revealed a significant difference between Cx36−/− mice and the wildtype control group (Figure 2A-D).

The absence of the connexin protein not only affects olivary neurons hut also gap junctions in the retina (Güldenagel et al., 2000; Rash et al., 2000). The impaired coupling of AII amacrine cells and bipolar cells causes deficiencies in early vision (Güldenagel et al., 2001). To test whether these deficiencies show up at the behavioral level, we measured the latency of the OKR to velocity steps of the visual stimulation. In wildtype animals (n = 6) the latency amounts to 82.1 ms ± 4.0 ms (mean ± SEM), whereas in Cx36−/− (n = 7), we found slightly, but significantly, delayed responses with a latency of 93.8 ms ± 2.3 ms (p < 0.033, two-sided Student t test) (Figure 2E).
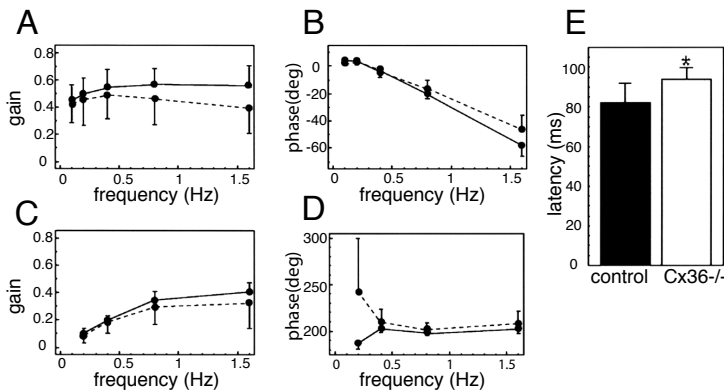
Figure 2. Compensatory eye movements. (A-D) Gain and phase lag for OKR (A and B) and VOR (C and D) performance of Cx36−/− (n = 5, solid line) and wildtype mice (n = 4, dashed line) at various stimulus frequencies. Error bars correspond to 1 SD. There is no significant difference in the performance of both groups. (E) Latency of the OKR response to velocity steps of the visual stimulus. The response of Cx36−/− mice (n = 7, empty bar) was significantly (p < 0.033, two-sided Student t test) delayed with respect to the wildtype control group (n = 6, solid bar). Error bars correspond to 1 SD.

Thus, even though the optokinetic signals are delayed, probably due to retinal dysfunction, the control of the vestibulocerebellum over the compensatory eye movements appears intact.

Complex Spike Activity

To find out whether a lack of coupling in the inferior olive affects the level of complex spike synchrony, we recorded activities of Purkinje cell pairs by means of extracellular recordings with two independently manipulable glass electrodes. We recorded a total of 94 pairs of nearby Purkinje cells that were located in the same parasagittal plane in either the Vermis or Crus IIa. About half of these recordings (n = 50 pairs) showed a sufficiently high signal-to-noise ratio so that not only the complex spikes but also the simple spikes could be reliably discerned as single units. Apart from two extreme cases (see below), the complex spikes of the cell pairs in both Cx36−/− and wildtype mice were only loosely synchronized; the corresponding peaks in their cross-correlograms had a width of tens of milliseconds (Figure 3).
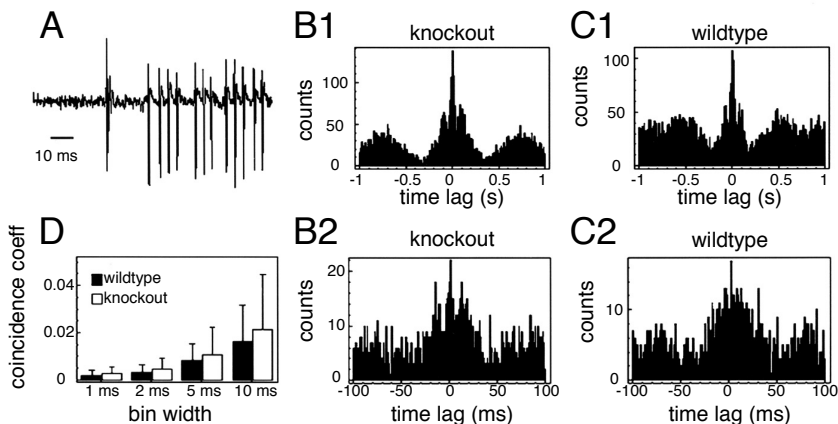
Figure 3. Complex spike synchrony in Cx36 knockout and wildtype mice. A. Extracellular recording of Purkinje cell activity. Complex and simple spikes can clearly be discerned by their wave form. **B.** Typical cross-correlograms of complex spike activity in Cx36 knockout compiled for 10-ms bins (B1) and 1-ms bins (B2). **C.** Cross-correlograms of complex spike activity for wildtype mice compiled for 10-ms bins (Cl) and 1-ms bins (C2). **D.** Mean coincidence coefficients or Cx36 knockout (n = 21 cell pairs, empty bars) and wildtype (n = 29 cell pairs, solid bars) mice compiled at different bin widths. Error bars correspond to 1 SD. The degree of synchrony in knockout and wildtype is not significantly different whatever the bin width.

To quantify the degree of synchrony we calculated the cross-correlation coefficient at time difference zero using bin widths of 1, 2, 5, and 10 ms for each cell pair. The mean cross-correlation coefficients in Cx36-/- mice were 0.0027 ± 0.0027, 0.0047 ± 0.0046, 0.0107 ± 0.0118, 0.0214 ± 0.0231 or bin widths of 1, 2, 5, and 10 ms, respectively (mean ± SD), while in the wildtype control group the corresponding coefficients equalled 0.0018 ± 0.0023, 0.0032 ± 0.0031, 0.0081 ± 0.0072, and 0.0162 ± 0.0154 (Figure 3).

The degree of synchrony was not significantly diferent between knockout and wildtype animals whatever bin width was used (two-sided Student t test, p > 0.20) (Figure 3D).

In only two cases both cells fired complex spikes in an almost perfectly synchronized ashion. In these cases (both Cx36-/-) all complex spikes were accompanied by a complex spike in the other cell, and the onsets of both complex spikes occurred within the same millisecond (Figure 4). The cross-correlation coefficients of these two pairs, C12(0), which equalled 0.85, differed by several orders of magnitude from those of the group of loosely synchronized cell pairs described above, and the data were therefore not pooled for analysis. Since
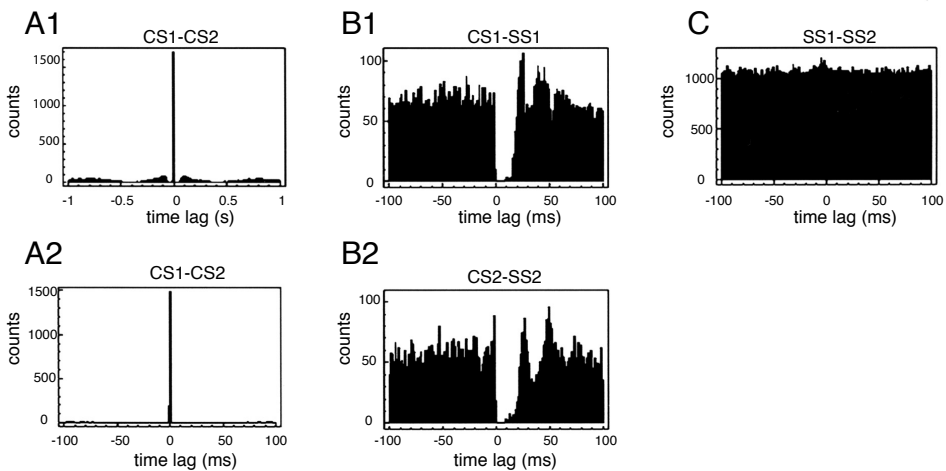
Figure 4. Ultraprecisely synchronized complex spikes. A. Complex spike crosscorrelograms with 10-ms (A1) and 1-ms (A2) bin width. The width of the central peak in A2 is less than 1 ms. **B.** Complex-spike triggered histogram of simple spikes for cell 1 (B1) and cell 2 (B2). Each complex spike is followed by a clear pause in the simple spike activity, indicating that we are recording from a single unit. **C.** The simple spike cross-correlogram is virtually flat, which implies that the recordings have been obtained from two different Purkinje cells.

the tips of the recording electrodes were relatively close, sometimes at a distance of about 160 μm in the rostro-caudal direction, we had to exclude the possibility that the highly synchronized activities were, in fact, derived from the same single cell. Therefore, we cross-correlated the simple spike activities of these cell pairs, and we examined the zero-bin peaks. Since these simple spike correlograms were virtually flat and both cells showed a clean climbing-fiber pause (Figures 4B and C), we concluded that the activities were indeed obtained from two distint Purkinje cells.

In addition to the complex spike correlations of two Purkinje cells, we also checked single cell parameters, such as the average complex spike firing rate (Cx36−/−: 0.95 ± 0.48 Hz; control: 1.03 ± 0.45 Hz), mean interspike interval (Cx36−/−: 1.19 ± 0.6 s; control: 1.10 ± 0.5 s), coefficient of variation (Cx36−/−: 0.74 ± 0.39; control: 0.66 ± 0.45), and the duration of the complex spike pause (Cx36−/−: 23.3 ± 7.6 ms; control: 27.0 ± 8.5 ms; all numbers mean ± SD). None of these parameters revealed a significant difference between Cx36−/− and controls.

Harmaline-Induced Tremor

Because we were unable to detect any effect due to the absence of functional olivary gap junctions, either on motor performance or on complex spike activity, we wanted to investigate whether the role of the coupling becomes apparent under more challenging conditions. We therefore applied the tremorgenic drug harmaline, which specifically turn olivary neurons into an oscillatory state at a high frequency (Llinás and Volkind, 1973). If the degree of spike synchrony in the IO was relatively reduced in the Cx36 knockout under this artificial condition, we would expect to see a reduced residual tremor.
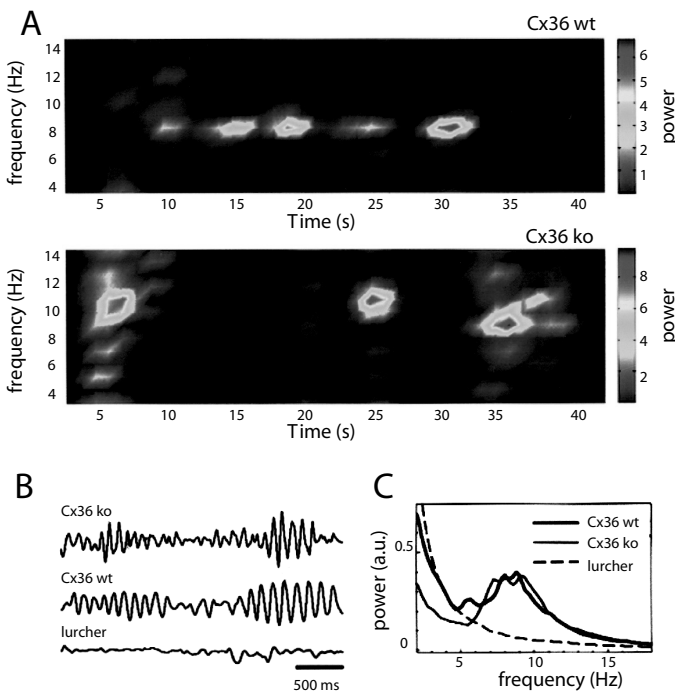
Figure 5. Harmaline-induced tremors in Cx36−/−, wildtype, and lurcher mice. A. Time-tremor frequency representation of a Cx36−/− and wildtype mouse injected with harmaline. The amplitude of the power spectra is coded in color so that (red) corresponds to the higher amplitude. B. Acceleration recordings of a Cx36−/−, wildtype, and lurcher mouse injected with harmaline. C. Averaged power spectra of harmaline-induced tremors of Cx36−/− (n = 10), wildtype (n = 10), and lurcher (n = 3) mice.

The tremorgenic efect of harmaline was studied in wildtype, Cx36−/−, and, as a control, in lurcher mice. Harmaline induced pronounced tremors in the Cx36−/− and wildtype mice, but not in the lurcher mice (Figure 5). Tremor frequency, amplitude, and spectral distribution were not significantly different between Cx36−/− and wildtype mice (two-sided Student t test, all p > 0.1; see Figure 5); the average tremor requency amounted to 8.1 ± 0.4 Hz or Cx36−/− mice and 8.5 ± 0.4 Hz or wildtype mice. The lack of harmaline-induced tremors in the lurcher mice has already been reported by Milner et al.,1995 and was used as a negative control.

DISCUSSION

Given the large amount of attention that gap junctions have attracted throughout the last decades and the importance that has been assigned to olivary electrotonic coupling or complex spike synchronization and motor coordination, it was surprising to see that Cx36−/− mice, which appear to lack functional neuronal gap junctions in their inferior olive (Long et al., 2001), exhibit no obvious motor impairments. The astounding absence of an overt behavioral phenotype in Cx36−/− mice raises some questions about the functional role of olivary gap junctions. The animals that we used were global knockouts, and it is thus possible that compensatory mechanisms occlude the effect of missing gap junctions. Possibly, other unknown gap junction proteins or particular conductances may be up- or downregulated to change the kinetics of the olivary neurons, but it is difficult to envision potential mechanisms other than gap junctions that can account for fast electrical coupling leading to synchronization of action potentials. Therefore, it remains possible that the primary function of olivary gap junctions is not the synchronization of olivary firing patterns. This option would be consistent with the observations that the level of synchrony between complex spikes is not significantly higher than that of the simple spikes of the same cell pairs in the alert behaving animal,(De Zeeuw et al., 1997) that the electrical conductivity of Cx36 gap junctions is exceptionally weak, (Srinivas et al., 1999) and that the coupling coefficient of olivary cells is usually well below 5 percent (Devor and Yarom, 2002).

We have directly addressed the role of electrotonic coupling of inferior olivary neurons by means of dual-electrode recordings of complex spike activities in coupling-deficient mice. We recorded extracellularly from nearby Purkinje cells located in the same parasagittal plane and found that the degree of complex spike synchrony in Cx36−/− mice is not diferent rom wildtype control animals. We have also shown that there are two different types of synchrony. Most of the cell pairs were only loosely synchronized; cross-correlograms had

broad central peaks, and not all spikes in one cell were accompanied by a spike in the other cell. Additionally, there were two pairs that exhibited perfect synchrony, in the sense that each spike was accompanied by a spike in the other cell with a temporal precision better than 1 millisecond.

Both forms of synchrony can easily be accounted for by mechanisms that do not rely on electrotonic coupling. A loose synchronization on a time scale of several tens of milliseconds is most likely due to common synaptic input or to locking phenomena within the reverberating loop formed by olivary neurons, Purkinje cells, and the deep cerebellar nuclei (Gerstner et al., 1996; Kistler and van Hemmen, 1999; Kistler et al., 2000). Perfectly synchronized complex spikes with a one-to-one relationship in the firing times, on the other hand, are a signature of two Purkinje cells receiving input from the very same olivary neuron via climbing-fiber collaterals (Bell and Kawasaki, 1972). This interpretation is also consistent with the results of Sugihara et al., 2001 who found that collaterals from a given olivary neuron are restricted to a narrow parasagittal strip of the cerebellar cortex and that climbing-fiber collaterals can contact Purkinje cells in the same folium.

Our results on the degree of complex spike synchrony in (wildtype) mice confirm results obtained previously with a similar recording technique in guinea pigs (Bell and Kawasaki, 1972). These results are, however, in conflict with multielectrode recordings of the rat (Lang, 2001; Lang et al., 1996; Lang et al., 1997; Lang et al., 1999) and dual-electrode recordings of the rabbit (De Zeeuw et al., 1997; Wylie et al.,1995), which showed higher cross-correlation coefficients at time zero. The reasons for this discrepancy elude us. They could be either technical, such as the induction of artifactual synchrony due to capacitive coupling of multiple electrode arrays (Zhu et al., 2002), or they could reflect species differ-ences. For example, recordings of CS activities in cat and monkey have also shown timing properties that diverge from those reported for rat and rabbit (Aggelopulos et al., 1995; Keating et al., 1995); or, the synchrony levels in the mouse may be, in contrast to those in the rabbit, too low to be detected with dual-electrode recording techniques.

The fact that the absence of functional neuronal gap junctions does not affect the degree of complex spike synchrony is further corroborated by experiments, where we compared the amplitude and frequency of harmaline-induced tremors in Cx36 knockouts and wildtypes. Harmaline specifically increases the resting activity of olivary neurons and thus leads to a pronounced tremor at about 7-12 Hz, that is, at the frequency of the intrinsic oscillatory properties of IO neurons (Llinás and Volkind, 1973) If the olivary neurons were no longer synchronized in Cx36 knockout, we would expect to see a reduced residual tremor. However,

the amplitude and distribution of frequencies were comparable in both groups.

Altogether, the conclusions that are to be drawn are twofold. First, the submillisecond synchronization of complex spikes is the result of collateral innervation of two Purkinje cells with the same IO neuron. In particular, this form of synchrony is not due to gap junctional coupling and thus not subject to a dynamical modulation by GABAergic terminals in the IO. Second, gap junctions may not be essential for the observed loose synchronization of complex spikes, because this form of synchrony is not affected in mice that lack functional gap junctions. Moreover, common synaptic input to IO neurons provides a more likely mechanism for the generation of synchrony on a 10-ms timescale than fast electrotonic coupling. Thus, the present data do not support the idea that olivary gap junctions synchronize complex spike activity on a millisecond timescale.

Even though we have been unable to correlate the level of complex spike synchrony in the vestibulocerebellum of the alert rabbit to a particular stimulus paradigm or eye movement behavior (De Zeeuw et al., 1997), the millisecond synchronization of complex spikes and a dynamic uncoupling of olivary neurons by activation of GABAergic synapses at the site of the gap junctions has been suggested to play an important role in the precise coordination and timing of movements (Lang et al., 1999; Llinás et al., 1991; Welsh et al., 1995). We have tested motor behavior on different levels, including compensatory eye movements, locomotion, and complex motor tasks. The only diference between Cx36−/− and wildtype mice we could detect was in the latency ofthe OKR to velocity steps in the visual stimulus. This difference, however, is most likely due to an impairment of signal transmission in the retina (Güldenagel et al., 2001) and not to the absence of gap junctions in the inferior olive, because the onset of climbing fiber activation following velocity step stimulation is not sufficiently early to explain the latency of the eye movements (Simpson et al., 1996). Other eye-movement parameters, such as gain and phase-lag of the vestibulo-ocular reflex and the OKR, were also normal in the Cx36−/− mutant. The results rom all the other behavioral tests we performed were very much in the same line. The walking pattern analysis demonstrated that Cx36−/− mice do not show any sign ofataxia. Even performance of complex motor tasks as tested in the accelerating rotorod test is not impaired in Cx36−/− mice. In short, the results of our experiments indicate that mice that have no functional olivary gap junctions hardly show any behavioral deficiencies.

At this point, the natural question is: What is the function of (olivary) gap junctions? In the inferior olive, gap junctions and synapses are located at dendritic spines with exceptionally long and thin spine necks (De Zeeuw et al., 1998). Spines from several neu-

rons and GABAergic as well as glutamatergic terminals are packed together in glomeruli shielded by several layers of glia. Assuming that the electrical resistance of spine neck and gap junctions are of the same order of magnitude (Srinivas et al., 1999, and Kistler and De Zeeuw, unpublished), the coupling between spine heads must be much more pronounced than the coupling between somata. Therefore, we propose that olivary gap junctions link spines within the glomerulus to a functional unit. Active ion channels in the spin heads can boost the synaptic input and create local "micro spikes" that readily propagate through gap junctions to neighboring spines. Synaptic input to only one or two spine(s) in a given glomerulus can thus trigger unitary responses in all the other spines within the glomerulus, and ultimately lead to synaptic potentials at the somata of all "postglomerular" neurons. In this sense, gap junctions synchronize synaptic input to olivary cells rather than spike output. The appealing aspect of this hypothesis is that it open new vistas on potential compensatory mechanisms for the absence of Cx36. Synchronization of synaptic input, for example, can also be achieved by an altered pattere of synaptic innervation in the glomeruli. Moreover, it raises the possibility that the dynamics in the olivary glomeruli ultimately regulate the firing patterns of olivary neurons over time in absolute terms, without necessarily affecting the synchrony.

ACKNOWLEDGMENTS

REFERENCES

Aggelopulos, N.C., C. Duke & S.A. Edgley. 1995. Non-uniform conduction time in the olivo-cerebellar pathway in the anaesthetized cat. J. Physiol. (Lood.) 486: 763-768.

Alabus, J.S. 1971. A theory of cerebellar function. Math. Biosci. 10: 25-61.

Bell, C.C. & T. Kawasaki. 1972. Relations among climbing fiber responses of nearby Purkinje cells. J. Neurophysiol. 35: 155-169.

Braitenberg, V. 1967. Is the cerebellar cortex a biological clock in the millisecond range? In Progress in Brain Research. C.A. Fox & R.S. Snider, Eds.: 25: 334-346. Elsevier Publishing Company. Amsterdam.

De Zeeuw, C.I., S.K.E. Koekkoek, D.R.W. Wylie & J.I. Simpson. 1997. Association between dendritic lamellar bodies and complex spike synchrony in the olivocerebellar system. J. Neurophysiol. 77: 1747-1758.

De Zeeuw, C.I., E.J. Lang, I. Sugihara, et al. 1996. Morphological correlates of bilateral synchrony in the rat cerebellar cortex. J. Neurosci. 16: 3412-3426.

De Zeeuw, C.I., J.I. Simpson, C.C. Hoogenraad, et al. 1998. Microcircuitry and function of the inferior olive. Trends Neurosci. 21: 391-400.

De Zeeuw, C.I., C. Hansel, F. Bian, et al. 1998. Expression of a protein kinase C inhibitor in Purkinje cells blocks cerebellar LTD and adaptation of the vestibulo-ocular reflex. Neuron 20: 495-508.

Devor, A. & Y. Yarom. 2002. Electrotonic coupling in the inferior olivary nucleus revealed by simultaneous double patch recordings. J. Neurophysiol. 87: 3048-3058.

Devor, A. & Y. Yarom. 2002. Generation and propagation of subthreshold waves in a network of inferior olivary neurons. J. Neurophysiol. 87: 3059-3069.

Eccles, J.C., R. Llinás & K. Sasaki. 1966. The excitatory synaptic action of climbing flbres

on the purinje cells of the cerebellum. J. Physiol. 182: 268-96.

Gerstner, W., J.L. Van Hemmen & J.D. Cowan. 1996. What matters in neuronal locking? Neural Comput. 8: 1653-1676.

Güldenagel, M., J. Ammermüller, A. Feugenspan, et al. 2001. Vlsual transmission deficits in mice with targeted disruption of the gap junction gene Connexin36. J. Neurosci. 21: 6036-6044.

Güldenagel, M., G. Söhl, A. Plum, et al. 2000. Expression patterns of connexin genes in mouse retina. J. Comp. Neurol. 425: 193-201.

Hamers, F.P., A.J. Lankhorst, T.J. Van Laar, et al. 2001. Automated quantitative gait analysis during overground locomotion in the rat: its application to spinal cord contusion and transection injuries. J. Neurotraurna. 18: 187-201.

Houk, J.C., J.T. Buckingham & A.G. Barto. 1996. Models of the cerebellum and motor learning. Behav. Brain Sci. 19: 368-383.

Ito, M. 1984. The Cerebellum and Neural Control. Raven Press. New York.

Keating, J.G. & W.T. Thach. 1995. Nonclock behaviour of inferior olive neurons: interspike interval of Purkinje cell complex spike discharge in the awake behaving monkey is random. J. Neurophysiol. 73: 1329-1340.

Kistler, W.M. & J.L. Van Hemmen. 1999. Delayed reverberation through time windows as a key to cerebellar function. Biol. Cybern. 81: 373-380.

Kistler, W.M., J.L. Van Hemmen & C.I. De Zeeuw. 2000. Time window control: A model for cerebellar function based on synchronization, reverberation, and time slicing. Progr. Brain Res. 124: 275-297.

Lampl, I. & Y. Yarom. 1993. Subthreshold oscillations of the membrane potential: A functional synchronizing and timing device. J. Neurophysiol. 70: 2181-2186.

Lang, E.J. 2001. Organization of olivocerebellar activity in the absence of excitatory gluta-matergic input. J. Neurosci. 21: 1663-1675.

Lang, E.J., I. SugiharaA & R. Llinás 1996. GABAergic modulation of complex spike activity by the cerebellar nucleoolivary pathway in rat. J. Neurophysiol. 76: 255-275.

Lang, E.J., I. Sugihara & R. Llinás. 1997. Differential roles of apamin- and charybdotoxin-sensitive K+ conductances in the generation of inferior olive rhythmicity *in vivo*. J. Neuro-sci. 17: 2825-2838.

Lang, E.J., I. Sugihara, J.P. Welsh & R. Llinás 1999. Patterns of spontaneous Purkinje cell complex spike activity in the awake rat. J. Neurosci. 19: 2728-2739.

Llinás, R. 1991. The noncontinuous nature of movement execution. In Motor Control: Con-cepts and Issues. D.R. Humphrey & H.J. Reund, Eds.: 223-242. Wiley. New York.

Llinás, R. & K. Sasaki. 1989. The functional organization of the olivo-cerebellar system as examined by multiple Purkinje cell recordings. Eur. J. Neurosci. 1: 587-602.

Llinás, R. & Y. Yarom. 1986. Oscillatory properties of guinea-pig inferior olivary neurones and their pharmacological modulation: An *in vitro* study. J. Physiol. (Lood.) 376: 163-182.

Llinás, R. & R.A. Volkind. 1973. The olivo-cerebellar system: functional properties as re-vealed by harmaline-induced tremor. Exp. Brain Res. 18: 69-87.

Llinás, R.R., R. Baker & C. Sotelo. 1974. Electrotonic coupling between neurons in cat inferior olive. J. Neurophysiol. 37: 560-571.

Long, M.A., M.R. Deans, S.L. Patrick, et al. 2001. Connexin36-dependent electrical cou-pling synchronizes subthreshold rhythmic activity of inferior olivary neurons. Soc. Neuro-sci. Abstr. 70.13.

Luciani, L. 1891. Il cervelletto: nuovi studi di fisiologia normale e patologica. Le Monnier. Florenz.

Mark, D. 1969. A theory of cerebellar cortex. J. Physiol. (Lood.) 202: 437-470.

Milner, T.E., G. Cadoret, L. Lessard & A.M. Smith. 1995. EMG analysis of harmaline-induced tremor in normal and three strains of mutant mice with Purkinje cell degeneration and the role of the inferior olive. J. Neurophysiol. 73: 2568-2577.

Rash, J.E., W.A. Staines, T. Yasumura, et al. 2000. Immunogold evidence that neuroval gap junctions in adult brain and spinal cord contain connexin-36 but not connexin-32 or con-nexin-43. Proc. Natl. Acad. Sci. USA 97: 7573-7578.

Sasaki, K., J.M. Bower & R. Llinás. 1989. Multiple Purkinje cell recording in rodent cer-ebellar cortex. Eur. J. Neurosci. 1: 572-586.

Simpson, J.I., D.R. Wylie & C.I. De Zeeuw. 1996. On climbing fiber signals and their consequence(s). Behav. Brain Sci. 19: 384-398.

Srinivas, M., R. Rozental, T. Kojima, et al. 1999. Functional prop erties of channels formed by the neuronal gap junction protein Connexin36. J. Neurosci. 19: 9848-9855.

Stahl, J.S., A.M. Van Alphen & C.I. De Zeeuw. 2000. A comparison of video and magnetic search coil recordings of mouse eye movements. J. Neurosci. Methods 99: 101-110.

Sugihara, I., H.S. Wu & Y. Shinoda. 2001. The entire trajectories of single olivocerebellar axons in the cerebellar cortex and their contribution to cerebellar compartmentalization. J. Neurosci. 21: 7715-7723.

Welsh, J.P., E.J. Lang, I. Sugihara & R. Llinás. 1995. Dynamic organization of motor control within the olivocerebellar system. Nature 374: 453-457.

Wylie, D.R., C.I. De Zeeuw & J.I. Simpson. 1995. Temporal relations of the complex spike activity of Purkinje cell pairs in the vestibulocerebellum of rabbits. J. Neurosci. 15:2875-2887.

Zhu, Z., K. Lin & T. Kasamatsu. 2002. Artifactual synchrony via capacitance coupling in multi-electrode recording from cat striate cortex. J. Neurosci. Methods 115: 45-53.

CHAPTER 4.2

Altered olivocerebellar activity patterns in the Connexin36 knockout mouse

SARAH P. MARSHALL[1], RUBEN S. VAN DER GIESSEN[2], CHRIS I. DE ZEEUW[2] & ERIC J. LANG[1]

[1]Department of Physiology & Neuroscience, New York University, School of Medicine, New York, USA
[2]Department of Neuroscience, Erasmus MC, Rotterdam, The Netherlands

ABSTRACT

The inferior olive (IO) has among the highest densities of neuronal gap junctions in the nervous system. These gap junctions are proposed to be the underlying mechanism for generating synchronous Purkinje cell complex spike (CS) activity. Gap junctions between neurons are formed mostly by Connexin36 proteins. Thus, the Connexin36 knockout (Cx36K0) mouse provides an opportunity to test whether gap junction coupling between IO neurons is the basis of CS synchrony. Multiple electrode recordings of crus 2 CSs were obtained from wildtype (Wt) and Cx36K0 mice. Wts showed statistically significant levels of CS synchrony, with the same spatial distribution as has been reported for other species: high CS synchrony levels occurred mostly among Purkinje cells within the same parasagittally-oriented cortical strip. In contrast, in Cx36KOs, synchrony was at chance levels and had no preferential spatial orientation, supporting the gap junction hypothesis. CS firing rates for Cx36KOs were significantly lower than for Wts, suggesting that electrical coupling is an important determinant of IO excitability. Rhythmic CS activity was present in both Wt and Cx36KOs, suggesting that individual IO cells can act as intrinsic oscillators. In addition, the climbing fiber reflex was absent in the Cx36KOs, validating its use as a tool for assessing electrical coupling of IO neurons. Zebrin II staining and anterograde tracing showed that cerebellar cortical organization and the topography of the olivocerebellar projection are normal in the Cx36K0. Thus, the differences in CS activity between Wts and Cx36KOs likely represent reflect the loss of electrical coupling of IO cells.

INTRODUCTION

Gap junctions are the physical substrate for electrical synaptic transmission (Bennett and Zukin, 2004). One of the first areas in the mammalian CNS where neuronal gap junctions and electrical coupling of neurons was demonstrated was the inferior olive (Sotelo et al., 1974; Llinás et al., 1974). These initial findings led to the hypotheses that gap junctions between IO neurons served to underlie synchronous activity in the olivocerebellar system, and that such activity was critical to the role of this system in motor coordination. Consistent with these hypotheses, synchronized olivocerebellar activity has been observed both in the IO itself (Llinás and Yarom, 1986; Long et al., 2002) and in the cerebellar cortex, as synchronous Purkinje cell complex spike (CS) activity (Bell and Kawasaki, 1972; Llinás and Sasaki, 1989; Lang et al., 1999), and patterns of synchronous CS activity have been associated with movements (Welsh et al., 1995; Lang et al., 2006).

Evidence consistent with the gap junction hypothesis of synchronous CS activity has also been obtained. IO neurons were demonstrated to be electrically coupled, both *in vivo* and *in vitro*, and to display synchronized subthreshold oscillations (Llinás et al., 1974; Llinás and Yarom 1986; Llinás and Yarom, 1981a); however, whether such synchronous oscillatory activity is the basis of CS synchrony remains to be established. In fact, there are arguments why it may not. For example, after cerebellar nuclear lesions, CS activity is highly synchronous but non-rhythmic (at least no evidence of any rhythmicity is present in autocorrelograms) (Lang et al., 1996). Pharmacological studies also provide indirect support for the gap junction hypothesis. Synchronous CS activity remains following block of both excitatory (glutamatergic) and inhibitory (GABAergic) synaptic transmission within the inferior olive (Lang et al., 1996; Lang et al., 2002; Lang, 2001), and disappears following the injection of carbenoxolone, a non-specific gap junction blocker, into the IO (Blenkinsop and Lang, 2006). While these results are strong evidence in favor of the gap junction hypothesis, they are not necessarily definitive. For example, carbenoxolone is not highly specific, as it blocks glial as well as neuronal gap junctions, and can affect other ionic membrane conductances.

Because of these questions, here we used a different approach to test this hypothesis: multiple electrode recording of CSs from normal and Connexin36 knockout (Cx36K0) mice. The Cx36K0 mouse is useful, because although there are now more than 20 identified members in the connexin family, Cx36 appears to form the overwhelming majority of neuronal gap junctions in the CNS, including the IO, and conversely, is not present in gap junctions formed between glial cells (Rash et al., 2000; Condorelli et al., 2000). Moreover, anatomical studies indicate normal gap junctions are absent in the IO of Cx36K0 mice (De Zeeuw et al., 2003), and recordings of IO neurons *in vitro* from Cx36K0 mice have shown that these cells lack electrical coupling (or at most are very weakly coupled relative to IO cells of Wt mice), and that the subthreshold oscillations of their membrane potentials are not synchronized, which contrasts with the case in Wts (Long et al., 2002).

We obtained recordings from these mice to test whether CS synchrony is lost in the absence of IO neuronal electrical coupling, and whether the climbing fiber reflex, which has been attributed to electrical coupling of IO neurons, is truly dependent on this coupling. Zebrin II staining of the cerebellar cortex and anterograde tracing were also carried out in order to characterize the topographic organization of the olivocerebellar pathway in the Cx36K0 mouse and to assess whether the physiological differences observed between the Cx36K0 and Wt mice reflected anatomic factors other than loss of gap junction coupling of IO neurons.

MATERIALS AND METHODS

Experiments were carried out in accordance with the National Institutes of Health guidelines for the care and use of laboratory animals. Experimental protocols were approved by the IACUC committee of New York University School of Medicine. Recordings were obtained from Wt and Cx36KO mice derived from the C57BL6 strain. Cx36 KOs were generated and genotyped as described previously (Güldenagel et al., 2001).

Surgical preparation and electrode implantation

Six to twelve month old mice were anesthetized with an initial intraperitoneal injection of ketamine (100 mg/kg) and xylazine (8 mg/kg); supplementary doses were administered as needed starting 1-2 hours after the initial dose. A tracheal tube was inserted to allow mechanical ventilation and delivery of supplemental oxygen. Body temperature was monitored with a rectal thermometer and maintained at ~37° C by means of a heating pad. The animal was placed in a stereotaxic apparatus and a ground screw was inserted into the skull over the cerebral cortex on the side contralateral to the recording area. Recordings were made of spontaneous and evoked CS activity from lobules crus 2a and 2b. To access these areas, the skin, muscle, bone and dura over the cerebellum were removed, and a platform was cemented in place over the cerebellum. The platform, an electron microscope grid encased in silicone rubber and fixed to tungsten rods, guided electrode placement and served to hold the electrodes in place after their release from the manipulator. Glass microelectrodes (~2 µm tip; 1:1 NaCl:glycerol) were individually attached to a joystick-controlled 3-axis micromanipulator (Marzhauzer, Germany) by a wax droplet and inserted through the grid. When CS activity was isolated in the molecular layer, approximately 50 µm below the cortical surface, the wax was melted in order to release the electrode, which was thereafter held in place by the silicon rubber. Electrodes were spaced 250 µm apart to form arrays of up to 9 rostrocaudal columns and 3 mediolateral rows.

Recording of spontaneous CS activity

CSs were recorded using a multichannel amplifier system (MultiChannel Systems, Germany), which consisted of 128 amplifier channels (total gain 1000x) with bandpass filters of 0.1 Hz - 8 kHz, and a per channel sampling rate of 25 kHz. The electrical signals were digitally high pass filtered using a cutoff frequency of 200 Hz using MultiChannel Systems MCRack data acquisition software. A voltage threshold (individually set for each channel) was used to detect CSs. Thresholds were set so as to detect the initial deflection of the CS, which was treated as a single event. On detection of a threshold crossing, the system recorded

the time and waveform of the voltage record, which were then used for subsequent off-line spike sorting and data analysis.

The MCRack software had oscilloscope and spike event displays for monitoring activity. The latter display comprised a grid onto which was mapped the electrode array such that each box in the grid corresponded to the relative location of an electrode in the brain. Each box flashed when the voltage threshold in its corresponding channel was crossed, and thus allowed for simultaneous monitoring of spike activity from the entire array. Recordings of spontaneous activity were typically made for 20 to 40 minute periods.

Data Analysis

All analyses were performed using procedures custom-written by one of the authors (EJL) for use with IGOR analysis software (WaveMetrics, OR). Statistical significance was assessed using 2-sided Student's paired t-tests, and mean values are presented with their corre-sponding SE, unless otherwise indicated.

To measure the relationship of activity in two different cells, a cross-correlation function was calculated as follows. The spike train of a cell was represented by X(i), where i repre-sents the time step (i=1, 2, ... , N). X(i)=1 if the CS onset occurs in the i time bin, otherwise X(i)=0. Y(i) was the same as X(i), but for the reference cell. The cross-correlation coeffi-cient, C(t), was then calculated as:

$$C(t) = \sum_{i=1}^{N} \{ V(i)W(i-t) \} \Big/ \sqrt{\sum_{i=1}^{N} V(i)^2 \sum_{i=1}^{N} W(i)^2}$$

$$V(i) = X(i) - \sum_{j=1}^{N} X(i)/N, \quad W(i) = Y(i) - \sum_{j=1}^{N} Y(i)/N$$

where V(i) and W(i) are the normalized forms of X(i) and Y(i), respectively.

A 1 ms time step was used, and thus for two spikes to be considered synchronous, their onsets must occur in the same 1 ms bin. The zero-time cross-correlation coefficient, C(0), was defined as the degree of synchrony between two cells. To assess CS rhythmicity, normal-ized autocorrelograms were computed for individual cells using the above formula for C(t), with X and Y both representing the same spike train. A 5 ms time step was used. Thus, the autocorrelogram values could range between 1 and -1, with the central peak always equal to 1. These individual cell autocorrelograms were averaged to obtain population autocorre-lograms. To assess the statistical significance of the experimentally observed synchrony, new 'data sets' were generated by randomly shuffling the interspike intervals of the real spike train of each cell in an experiment. For each experiment, ten such sets of shuffled spike trains were made for each cell, and C(t) was determined for all pairs in a set.

Climbing fiber reflex experiments

The cerebellum was exposed, as described above; however, instead of the recording plat-form, Gelfoam soaked in Ringer's solutions was used to cover the cerebellar surface. A bipo-lar stimulating electrode was inserted into the cerebellar white matter in the lobule rostral to the desired recording area. Single shocks (100 µs, 150-600 µA pulses) were delivered ev-ery 2 s and evoked responses were recorded with a single microelectrode. Electrical signals were fed into one channel of the multichannel amplifier described earlier.

Zebrin staining

Cx36K0 and Wt mice were anesthetized with Nembutal (75 mg/kg i.p.) and perfused trans-cardially with phosphate-buffered saline (PBS; pH 7.4) and 4% paraformaldehyde in 0.1 M PB. Whole brains were removed and post-fixed in perfusate for an additional 2 hours and subsequently rinsed and stored overnight at 4°C in 0.1 M PB, pH 7.4, containing 10% sucrose. The brainstem and cerebellum were embedded in 10% gelatin and 10% sucrose. Tissues were fixed in 10% formaldehyde and 30% sucrose solution at room temperature for 2 hours. Serial sections of 40 µm were cut on a cryo-modified sliding microtome (Leica SM2000R) and col-lected in vials containing 0.1 M PB. The vials were rinsed in PBS and incubated, free floating, for 48 hours in anti-Zebrin II (1:150, kindly provided by Dr. R. Hawkes, Calgary, Canada) con-taining 2% NHS and 0.5% Triton in PBS at 4°C. After rinsing in PBS, sections were incubated for 2 hours in rabbit anti mouse HRP (1:150, p260 Dako) in PBS, containing 2% NHS and 0.5% Triton. Subsequently, sections were thoroughly rinsed in 0.05 M PB and incubated in a DAB staining for 15-20 minutes and rinsed in 0.05 M PB. All sections were mounted on slides in a chromic alum solution, air-dried, and counterstained with thionin. Subsequently, slides were dehydrated in graded alcohol and xylene and coverslipped with Permount.

Intraolivary BDA-injections

Cx36K0 and Wt mice were anesthetized with a ketamine/xylazine mixture (65 mg/kg and 10 mg/kg, respectively) administered intraperitoneally. The body temperature was monitored and kept at ~37°C using a heating pad. After surgery, the ventral surface of the medulla ob-longata was exposed for exploration of the inferior olive. Subsequently a recording pipette was filled with 1070 BDA-10,000 MW (Molecular Probes, Leiden, The Netherlands), posi-tioned in the IO and multiple iontophoretic injections were made using a constant positive current (8 µA; 7 seconds on/off cycle for 10 minutes). After 5 to 7 days the mice were deeply anesthetized with Nembutal (75 mg/kg i.p.) and perfused transcardially with phosphate buffered saline (PBS; pH 7.4) and paraformaldehyde in 0.1 M PB. Brains were removed and

post-fixed in perfusate for an additional 1 hour and subsequently rinsed and stored over-night at 4°C in 0.1 M PB, pH 7.4, containing 1070 sucrose. The brainstem and cerebellum were embedded in 1070 gelatin and 1070 sucrose. Tissues were fixed in 1070 formaldehyde and 3070 sucrose solution at room temperature for 2 hours. Serial sections of 40 μm were cut on a cryomodified sliding microtome (Leica SM2000R) and collected in vials containing 0.1 M PB. Sections containing the BDA injection sites were incubated overnight at 4°C in avidin-biotinperoxidase complex (Vector Laboratories, Inc., Burlingame, CA), rinsed again, and finally incubated in DAB (75 mg/ 100 ml) and 0.02% Cobalt chloride. The reaction was stopped after 15 minutes by rinsing in PB. In order to identify the climbing fibers within their zonal projections, a Zebrin staining protocol was applied as above.

RESULTS

CS synchrony is reduced in Cx36KOs compared to Wts.

Extracellular CSs were recorded from groups of crus 2 Purkinje cells in Wts (n= 9 animals, 105 cells, 484 cell pairs) and in Cx36KOs (n= 6 animals, 37 cells, 112 cell pairs). CS activity was recorded from both Wt and Cx36K0 mice at depths of ~50 μm from the folial surface, and typically consisted of a high frequency burst with a large initial negative-going deflection followed by 2-3 smaller spikes riding on a slow positivity (Figure 1).
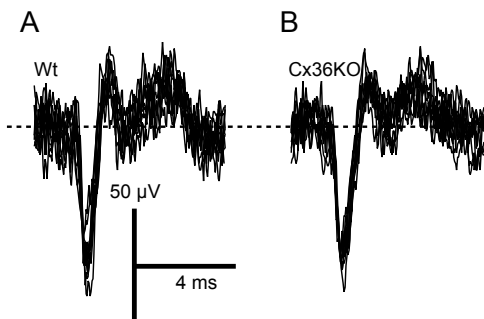
Figure 1. Complex spikes have similar waveforms in Wts and Cx36KOs. A,B. Extracellular recording of CSs from crus 2a in a Wt (A) and Cx36K0 (B) mouse. In each panel 10 overlapped traces are shown. Note the typical waveform in both cases: a large initial negativity followed by smaller wavelets riding on a slow positivity.

The role of Cx36 gap junctions in mediating CS synchrony patterns was assessed using multiple electrode arrays to record CSs from groups of Purkinje cells in Wts and Cx36KOs. Typical results for a Wt and Cx36K0 are shown in figure 2A1, in which the synchrony distribution relative to a master reference cell 'M' is presented in each bubble graph. Here, each circle shows the position of a recorded cell relative to cell M, and its area corresponds to the degree of synchrony between the cell at that location and cell M.

In the Wt, cell M's activity is more strongly synchronized with the activity of its neighbors (0-250 μm) than with the activity of cells at greater mediolateral distances from it, consistent with previous findings in other species (Sasaki et al., 1989). The rapid reduction in synchrony with mediolateral distance combined with a much lesser decrease with distance in the rostrocaudal direction leads to a rostrocaudal banding pattern, such as demonstrated by the Wt bubble graph of figure 2A1. Although the sharpness of the banding pattern varies with choice of reference cell, plots of average synchrony as a function mediolateral separation between cells show that these bands are the dominant pattern (Figure 2A2, filled circles). That is, ML synchrony curves in Wts were highest at small separation distances and dropped for larger separations. Note that the Wt curve in figure 2A2 was generated from all recorded cell pairs from all Wt experiments (n = 9 animals, 105 cells, 484 pairs).
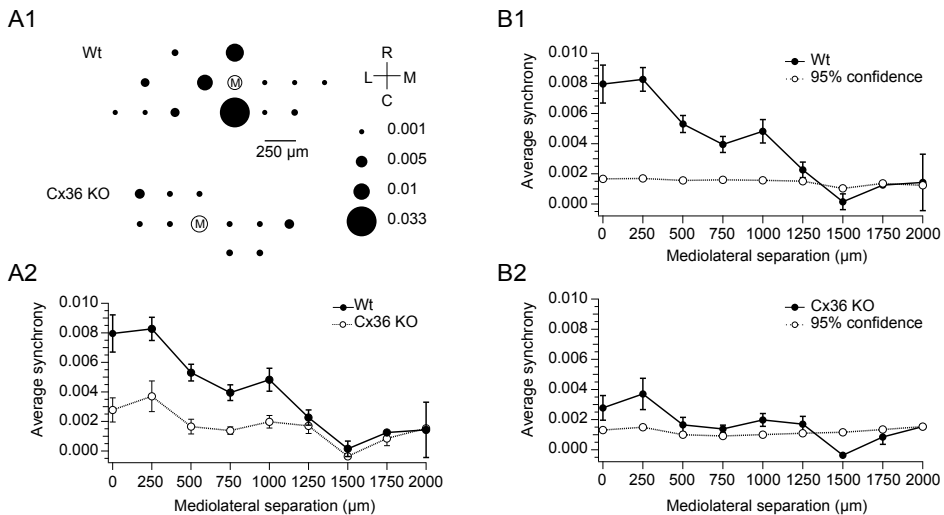
Figure 2. Comparison of CS synchrony distribution in the Wt and Cx36KO. A1. Bubble plots show the relative positions of electrodes in the recording array from one Wt and one Cx36KO experiment. The area of each bubble corresponds to the degree of synchrony between that cell and the reference cell (labeled 'M'). Note the high synchrony surrounding cell M in the Wt but not in the Cx36KO. **A2.** Graph of average CS synchrony values between all cell pairs plotted as a function of mediolateral separation between cells for Wts (filled circles) and Cx36KOs (open circles). All cell pairs from 9 animals (Wt) and 6 animals (Cx36KO) veere used to calculate averages. Error bars are SE. The number of cell pairs at each separation is as follows: for Wts, 0μm=59; 250 μm=154 pairs; 500 μm=120 pairs; 750 μm=83 pairs; 1000 μm=41 pairs; 1250 μm=20 pairs; 1500 μm=4 pairs; 1750 μm=1 pair; 2000 μm=2 pairs; for Cx36KOs, 0μm, n=12 pairs; 250 μm, n=42 pairs; 500 μm, n=26 pairs; 750 μm, n=16 pairs; 1000 μm, n=8 pairs; 1250 μm, n=4 pairs; 1500μm, n=1 pair; 1750 μm, n= 2 pair; 2000 μm, n=1 pair. **B.** Comparison of synchrony levels in Wts (B1) and Cx36KOs (B2) to synchrony levels calculated from pairs of randomized spike trains. synchrony curves for Wt and Cx36K0 spike trains are replotted from A2 using filled circles and solid lines in B1 and B2, respectively. synchrony values (95th percentile) from the randomized data values are plotted witti open circles and dotted lines.

In contrast to the Wt, a rostrocaudal banding pattern was not found in Cx36K0 mice. Indeed, as shown by the example in figure 2A1, Cx36K0 mice had much lower levels of CS synchrony compared to Wt animals. This reduced level of CS synchrony was confirmed by generating a mediolateral synchrony curve using all of the Cx36K0 cell pairs from 6 experiments (37 cells, 112 pairs). Comparison of their mediolateral synchrony curves shows that there was significantly less CS synchrony in Cx36KOs than in Wts (Figure 2A2, open circles versus closed circles). This difference, however, does not necessarily imply that the Cx36KOs have no statistically significant synchronization of CS activity. Indeed, while the absolute levels are low, they are above zero. On the other hand, because our data sets are finite, some degree of correlation arises because of the periodicity of CS activity. To determine the statistical significance of the CS synchrony levels in the Cx36KOs, each cell's spike train was converted to a series of interspike intervals (ISIs) that were randomly shuffled and reassembled to form a randomized spike train with the same set of primary ISIs. Ten such randomized datasets were generated from each experiment. These datasets were used to calculate synchrony values between cells. The synchrony values from all datasets of the same experimental type (i.e., Wt or Cx36K0) were combined and grouped according to mediolateral separation between cells. Both distributions had means that were not statistically different from zero (Wt, $1.8 \times 10^{-6} \pm 1.1 \times 10^{-5}$, n = 5750 pairs; Cx36KO, $6.7 \times 10^{-5} \pm 2.0 \times 10^{-5}$, n = 1120 pairs). The 95th percentile value for each separation distance is plotted for the randomized Wt and Cx36K0 data pairs in figures 2B1 and 2B2, respectively, which for comparison also replot the true data curves from panel A2 (filled circles). For the Cx36KO, the randomized and CS data curves are similar in value, whereas for the Wts, the CS data curve is significantly above the randomized curve. In addition, note that in both cases the randomized curves are flat in comparison to the Wt data curve, which decreases with distance.
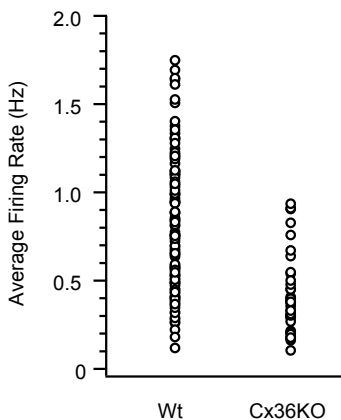
Figure 3. Average complex spike firing rates. Cx36KOs display lower CS firing rates than Wts. CS average firing rate distributions for the Wt and Cx36K0 cells. Each marker shows the value for one cell.

Wt and Cx36K0 mice show rhythmic ~10 Hz CS activity but have a lower average firing

To investigate the dependence of IO excitability and CS rhythmicity on coupling between IO neurons, we compared the firing rates and autocorrelogram characteristics of Wt and Cx36K0 CSs. The average CS firing rate in the Cx36K0 (0.41 ± 0.04 Hz) was half that observed in the Wt (0.82 ± 0.04 Hz; p = 2.5x10-1Z). Additionally, the Wt firing rates had a broader range than the Cx36K0 (Wt: 0.12-1.75 Hz; Cx36K0: 0.10-0.94 Hz; Figure 3).

Autocorrelograms of Wt and Cx36K0 CSs revealed that in 6 / 8 Wt experiments and 4 / 6 Cx36K0 experiments, rhythmic CS activity was present (Figure 4). The level of rhythmicity varied somewhat between experiments for both Wt and Cx36KOs, as shown by the examples in figure 4; however, the strongest rhythmicity was observed in Cx36KOs (compare Figure 4A2 and 4B2).

Wt oscillation frequencies had a slightly lower range than that of the Cx36K0 (Wt: 6.57-10.26 Hz; Cx36K0: 8.16-14.80 Hz), but the mean oscillation frequency for Wts and Cx36KOs were not statistically different (Wt, 9.19 ± 0.50; Cx36K0, 9.77 ± 0.71; p=0.51).
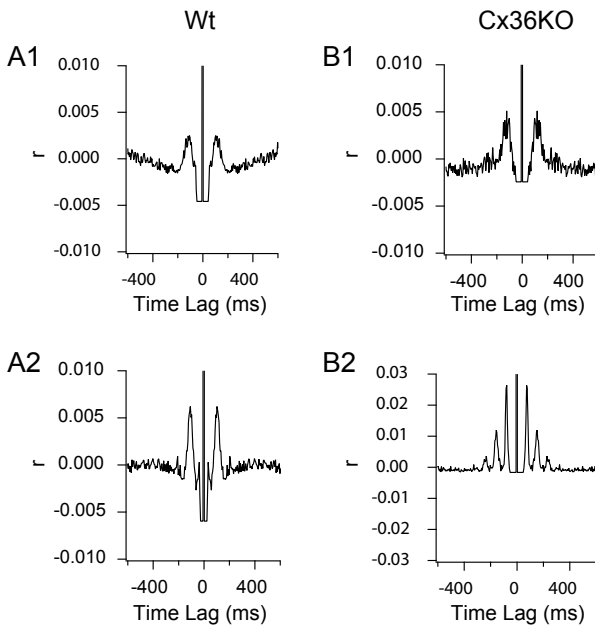
Figure 4. Rhythmic CS activity in Wt and Cx36K0 mice. Normalized population autocorrelograms of CS activity from two Wt mice (A1: n= 8 cells; A2: n= 13 cells) and two Cx36K0 mice (B1, 2: n= 5 cells each). Peaks in the autocorrelograms indicate the presence of 10 Hz rhythmic CS activity in both the Wt and Cx36K0.
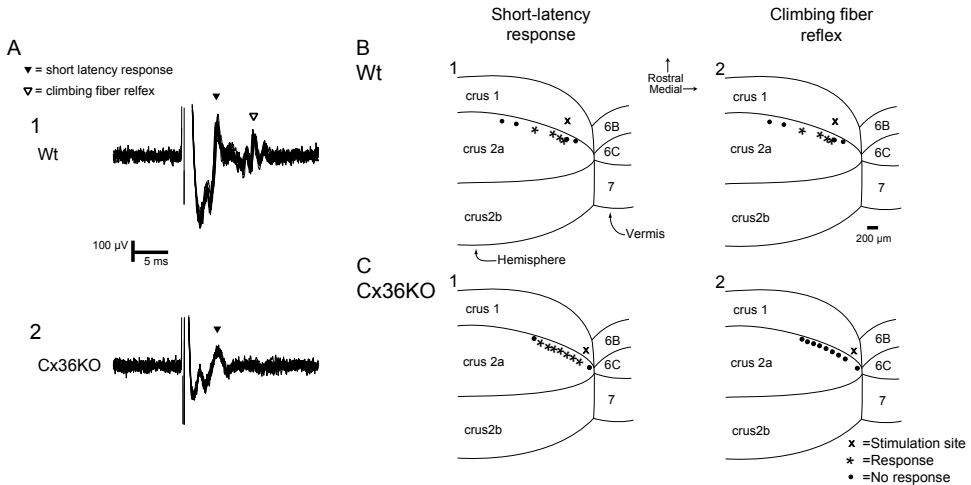
Figure 5. Climbing fiber reflex responses in Wt and Cx36K0 mice. A. Extracellular traces of evoked responses to cerebellar white matter stimulation. In the Wt (A1), cerebellar white matter stimulation elicits a reflex response at ~10 ms (open arrowhead), which is mediated by electrotonically coupled IO neurons; this response is absent in the Cx36K0 (A2). In contrast, botte populations exhibit short-latency responses (A1 and 2, filled arrowhead), which are mediated by climbing fiber collaterals and are independent of IO coupling. Ten overlapped traces each. **B, C.** Comparison of short latency and CF reflex distributions in the Wt and Cx36K0. In the Wt, short-latency (B1) and CF reflex responses (B2) co-occur in a limited area predominantly lateral to the stimulation site. A similar pattern of short-latency responses is observed in the Cx36K0 (C1), but the CF reflex response is absent in this animal (C2). Left column: *= short-latency response; • = no short-latency response. Right column: *= CF reflex response; • = no CF reflex response.

The climbing fiber reflex is mediated by olivary gap junctions

Stimulation of the cerebellar white matter elicits two CS responses in PCs: a short latency, direct response due to direct activation of the climbing fiber, and a longer latency, reflex response that is due to antidromic invasion of the IO (Eccles et al., 1966). Following demonstration of electrical coupling between IO neurons, this longer latency response has been presumed to be generated by current flow through gap junctions (Llinás et al., 1974). The Cx36K0 provides an opportunity to test this proposed mechanism because electrical coupling between IO neurons is nearly absent in these mice (Long et al., 2002).

Thus, responses evoked in Wt and Cx36KOs by cerebellar white matter stimulation were compared. In Wts, stimulation often evoked botte direct (filled triangle) and reflex (open triangle) responses (Fig 5A1). In contrast, in Cx36KOs only direct responses could be elicited (Figure 5A2), with a single exception. To verify that the absence of reflex responses in the Cx36KOs did not represent a sampling artifact, the spatial extent and overlap of the stimulus evoked responses in crus 2 were determined.

Figure 5B compares the response distributions in a Wt and Cx36K0 mouse to a similarly placed stimulation electrode (indicated by 'X'). In the Wt, direct and reflex responses botte occurred in a region starting at the parasagittal plane of the stimulus electrode and extending lateral for 600 μm (Figures 5B1, B2). In the Cx36K0, direct responses were elicited from similar sites to those in the Wt (Figure 5C1), but no reflex responses were observed (Figure 5C2). In different experiments the placement of the stimulus electrode was varied so as to test the response distribution across crus 2. In Wts, the reflex response distribution reflected the position of the stimulus electrode (Figure 6A, B). In the Cx36KOs, only one reflex response was detected (Figure 6C, indicated by '*') despite testing cortical areas that corresponded to those tested in Wts.
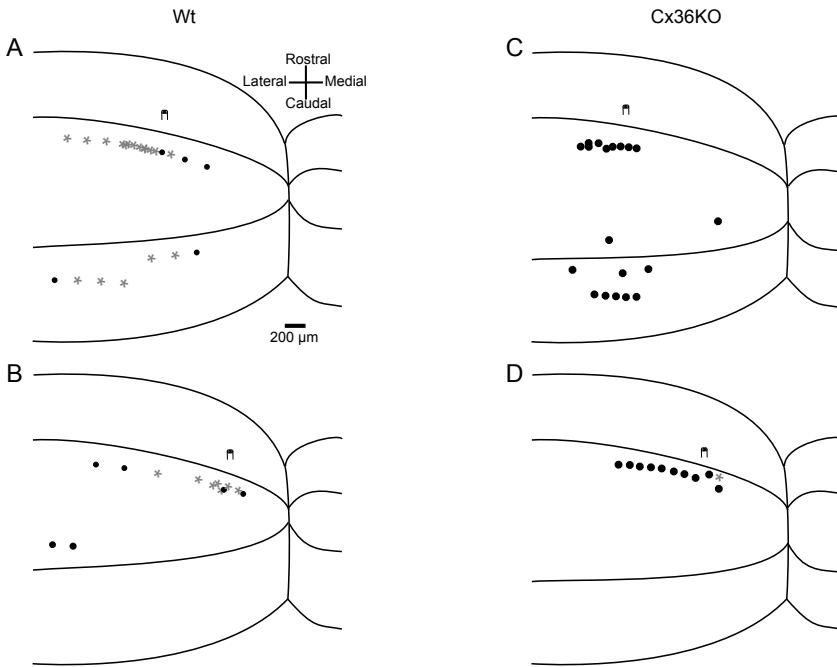
Figure 6. Climbing fiber reflex response distribution in the mouse. (A, B) CS responses to white matter stimulation in Wt mice are distributed witkin a parasagittal band positioned slightly lateral to the stimulation site. **A.** Distribution of recording sites in crus 2a and b from 3 Wts in which the stimulation electrode (P1) was placed at the same location, near the middle of crus 1. An asterisk indicates that CF reflex and short-latency responses were elicited at that recording site. • = no response. **B.** Same as A, except that recordings were from 3 additional animals in which the stimulation electrode was placed more medially on crus 1. **C.** Distribution of recording sites in crus 2a and b from two Cx36KOs in which the stimulation electrode was placed near the middle of crus 1. • =short-latency responses only. **D.** Same as C, except responses obtained for cells from two additional animals in which the stimulus electrode was placed more medially on crus 1. One cell showed botte short latency and reflex responses (indicated by the asterisk).

In total, Wts showed reflex responses in 56% of cells (n=35 / 62 cells, 10 animals), whereas in Cx36KOs only 3% of cells (n=1 /36 cells, 3 animals) showed a reflex response. In Wt mice, reflex responses were present witte (30 cells) or without (5 cells) direct responses. More-over, of the 31 cells that had direct responses, 30 (97 %) had reflex responses. In contrast, in the Cx36K0 mice, 12 cells showed direct responses, but only one cell showed a reflex response (8 %).
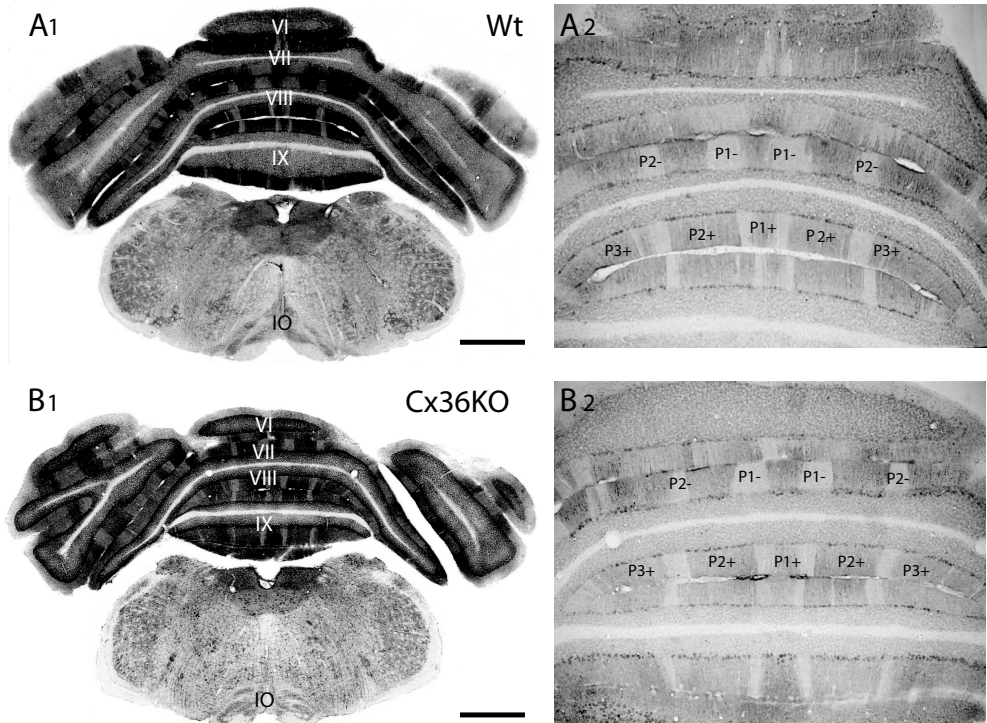
Figure 7. Cerebellar zonation patterns as revealed by zebrin II staining of Purkinje cells are indistinguishable among Wt and Cx36K0 mice. A. Zebrin stained Purkinje cell zones in a Wt mouse. A1. Coronal section showing the brainstem and the posterior lobe (vermis and hemispheres) of the cerebellum. Lobules 6 to 9 are indicated by VI-IX. A2. Higher magnification view of vermis portion. Zebrin II positive (P+) and negative (P-) zones are indicated. P1+ corresponds to the midline area. **B.** Overview of zebrin stained Purkinje cell zones in the posterior lobe and hemispheres of a Cx36K0. Similar levels of cerebellar cortex as veere shown for Wt in A. The similarity in labeling pattern to that of the Wt indicates that the zonal organization of the cerebellar Purkinje cells is not affected by a lack of Cx36 in the IO. Scale bars indicate 500 µm; IO indicates inferior olive.
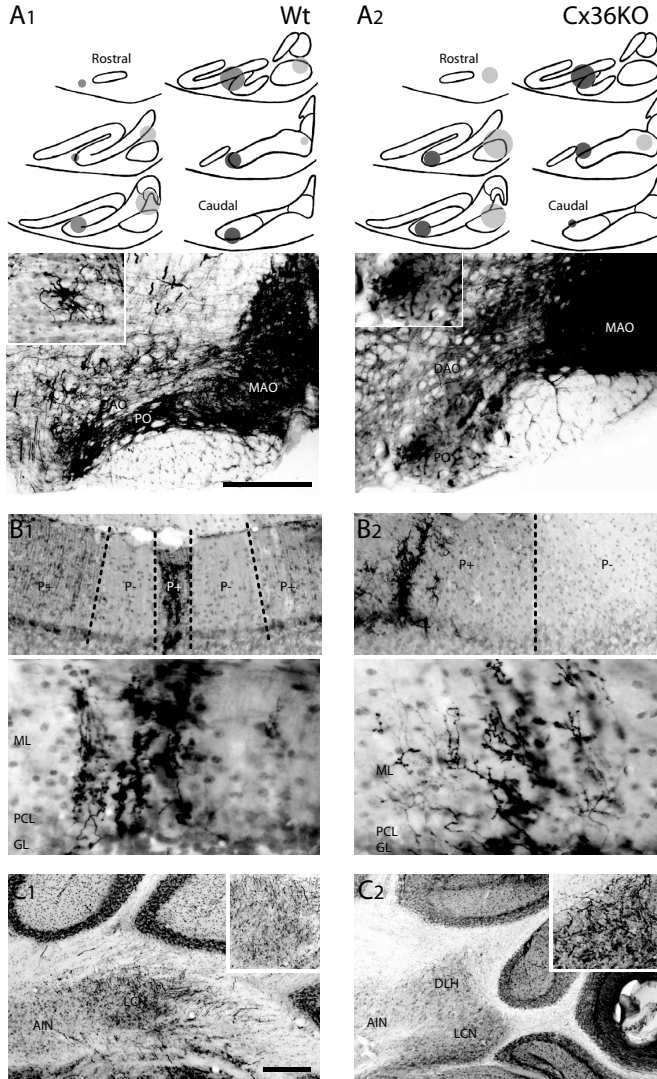
Figure 8. Cerebellar zonation patterns as revealed by anterograde tracing of olivary climbing fibers are indistinguishable among Wt and Cx36K0 mice. A. Top panels, schematic drawings of BDA injection sites in the inferior olive in Wt mice (A1) and Cx36K0 mice (A2). The diameters of the circles' areas reflect the size of the injection sites witkin the respective subnuclei. Each set of circles corresponds to one injection in one animal. Bottom panels, photographs of BDA injections in the medial accessory olive (MAO); insets show examples of individual olivary neurons that took up BDA in the areas bordering the core of the injection site. **B.** Anterograde labeling of climbing fibers in Wt mice (B1) and Cx36K0 mice (B2) at lower (top panels) and higher (lower panels) magnifications. In these examples the labeled climbing fibers are in botte wild types and Cx36K0 mice restricted to zones that are positively labeled for zebrin II. **C.** Lower and higher (insets) magnifications of BDA labeled climbing fiber collaterals in the cerebellar nuclei. Abbreviations: PO, principal olive; DAO, dorsal accessory olive; AIN, anterior interposed nucleus; LCN, lateral cerebellar nucleus; DLH, dorsolateral hump (Scale bar in Al indicates 100 μm; scale bar in C1 indicates 20 μm).

Zonal organization is not affected by elimination of gap junctions

The cerebellar cortex is divided into different cortical zones defined by olivo-cortico-nuclear-connections. This zonal organization can be determined by specific biochemical markers that correlate the organization of cortical zones to their distribution in the cerebellar cortex. One of these markers, Zebrin II (Aldolase C), is confined to a specific subset of Purkinje cells, resulting in a parasagittal pattern in the cerebellar cortex. Immunolabeling against Zebrin II provides a highly reproducible and consistent staining. Thus, we compared this labeling pattern in Wt (n = 2) and Cx36K0 (n = 2) mice to determine whether absence of gap junctions would affect this zonal organization. In Wt cerebellum, immunolabeling showed a distinctive strip-like pattern with labeled and non-labeled areas, which are called P+ and P- respectively. Labeling was restricted to the cerebellar cortex (Figure 7A). The same general labeling pattern was found in Cx36K0 cerebellum (Figure 7B). Moreover, the distribution of parasagittal bands in the cerebellar cortex of the Cx36K0 was identical to that in Wt. This similarity was confirmed for both vermal and hemispheric portions of all cerebellar lobules. This similarity in zebrin-positive and negative bands indicates that the zonal compartmentation is not affected in Cx36K0 mice.

Because the organization of cortical zones in Cx36K0 and Wt mice are equivalent, climbing fiber projections can be compared with the use of anterograde tracers such as BDA. Intra-olivary BDA injections were made in Wt (n = 3) and Cx36K0 (n=2) animals. One injection was made per animal, and the specific injection sites are superimposed on the schematics shown in figure 8A1-2. The extent of each injection is shown by one set of circles. Intra-olivary BDA injections result in labeling of contralateral climbing fibers which project to a specific area within the cerebellar cortex (Figures 8A and B). Groups of labeled climbing fibers arising from the same local IO region remain confined to essentially the same zebrin areas in Wt (Figure 8B) and Cx36K0 (Figure 8C) mice. This finding suggests that climbing fiber projections in Cx36K0 mice appear to hold the same zonal organization as in Wt mice. Therefore, it can be concluded that Cx36K0 mice show no obvious anatomical differences compared with Wt mice. Any physiological differences are thus likely the direct result of absent electrical coupling among IO neurons, rather than structural alterations witkin the olivocerebellar circuit.

DISCUSSION

The present study used a Cx36KO mouse model to investigate the importance of olivary gap junctions for the anatomical and physiological organization of the olivocerebellar system. The results indicate that Cx36KOs have a topographically normal olivocerebellar projection and a normai cerebellar cortical organization, bot that the activity of this system is significantly altered by the loss of electrical coupling between inferior olive neurons. In the Cx36K0, CS synchrony, which was observed in the Wt, was absent; average CS firing rates were reduced; and rhythmic CS activity was present. Lastly, the climbing fiber reflex was absent in the Cx36KOs. The implications of these findings are discussed below.

Electrical coupling of IO neurons onderlies CS synchrony

Synchronous CS activity kas been demonstrated in several species, including rat, guinea pig, and rabbit (Bell et al., 1972; Lang et al., 1999; Sasaki et al., 1989; Wylie et al., 1995). The present findings extend this list to include mice. In each case, CS synchrony levels are highest among Purkinje cells located witkin the same parasagittally oriented, 250-500 μm-wide strip of cortex. This spatial distribution, in part, reflects the fact that the neurons of each small region of the IO project to a specific longitudinally oriented strip of cerebellar cortex (Sugihara et al., 2006). There is, however, a large dynamic component to this distribution, as dramatic changes in this synchrony distribution result from blocking synaptic input to the IO (Lang, 2001; Lang et al., 1996; Lang, 2002), and synchrony distribution changes are also associated with voluntary movement (Welsh et al., 1995). The mechanism by which activity of olivary neurons is synchronized is the fundamental issue addressed in the present study. Ultrastructural studies indicate that the IO contains one of the richest neuronal gap junction networks in the adult CNS (Sotelo et al., 1974; De Zeeuw et al., 1989). Electrical coupling of IO neurons kas also been demonstrated (Llinás et al., 1974; Llinás and Yarom, 1981a). Moreover, olivary neurons are almost all projection cells that do not have local axon collaterals (Sugihara et al., 1993; Lang and Rosenbluth, 2003). These observations leave two major choices for the cause of synchronous CS activity: electrical coupling of IO neurons by gap junctions and synchronized activity in IO afferents. The latter possibility has been mostly ruled out by studies which demonstrated the continued presence of CS synchrony following block of the major excitatory (glutamate) and inhibitory (GABA) inputs to the IO (Lang, 2001; Lang et al., 1996; Lang, 2002).

In contrast, the present results support the first possibility, namely that synchronous CS activity requires electrical coupling of IO neurons. Our results are consistent with previ-

ous ones that investigated this issue. For example, the density of gap junctions, as judged by the presence of lamellar bodies, in the set of IO regions that project to the flocculus was correlated with the level of CS synchrony in corresponding parts of the flocculus (De Zeeuw et al., 1997). Also, *in vitro* studies of IO neurons from Cx36KO mice showed that subthreshold oscillations in neighboring cells, which are in phase in normai animals, are not so in the knockout (Long et al., 2002). Most recently, pharmacological block of IO gap junctions by local injections of carbenoxolone were shows to reduce or eliminate CS synchrony (Belnkinsop and Lang, 2006). While objections may be raised against each of these approaches, taken together they reinforce the common conclusion that CS synchrony is a result of IO gap junction coupling.

Given the demonstration of CS synchrony in several different species by several laboratories, as noted above, the finding of no significant CS synchrony in Wt mice reported in one previous study (Kistler et al., 2002) is surprising, and is contradicted by the present findings. We have no definitive explanation for the results of Kistler et al. (2002); however, we note that the study of Kistler et al. differed from this report in that the recordings were obtained using only pairs of electrodes, rather than arrays, and given the sampling procedure used by Kistler et al. and the narrowness of the synchrony bands, relatively few pairs would have been expected to show significant levels of synchrony. These pairs may have been missed in the small samples that were obtained. A second possible contributing factor is that CS synchrony levels in the mouse appear to be somewhat lower than is typically found in rats based on the present results. Whether this represents a true species difference, or simply a difference in the state of the preparation is not clear (mice tolerated the multiple electrode recording procedures less well than do rats). In this context, it is worth noting that any damage to the cerebellar cortex will likely lead to increased cerebellar nuclear activity, which in turn would increase GABA levels in the IO and a reduction in CS synchrony, which may have been a factor in the failure to observe synchrony previously in Wt mice (Ariel, 2005). At the least, the lower overall levels would make observation of synchronous CS activity witti electrode pairs more difficult and would require more precise alignment of electrodes for its detection.

Electrical coupling is a determinant of IO excitability and rhythmicity
The average CS spike firing rate of Cx36KOs was approximately half that of Wts, and roughly half that of the 1 Hz spontaneous rate typically reported for normai animals. This finding suggests that gap junction coupling plays a major role in setting the excitability of IO

neurons, and that current flow through gap junctions is responsible for about half of the spontaneous CS activity. This suggestion is consistent with several recent findings. Acute pharmacological block of gap junctions also led to a similar reduction in spontaneous CS firing rates (Blenkinsop and Lang, 2006). Moreover, spontaneous CS activity, while reduced, remains following block of major excitatory and inhibitory afferents to the inferior olive (Lang, 2001; Lang, 2002).

Our results also suggest that electrical coupling may not be necessary for oscillatory behavior, but this is an issue in which there is much conflicting data, and one which will require further study. Cx36KOs had CS activity that was at least as rhythmic as that found in Wts. This result is somewhat in contradiction to our previous result that acute pharmacological block of olivary gap junctions with carbenoxolone reduced or abolished rhythmic CS activity (Blenkinsop and Lang , 2006). Moreover, in that study, the degree of reduction in a cell's rhythmic activity was highly correlated with the loss of synchrony it experienced (Blenkinsop and Lang, 2006). One possible explanation of these divergent results is that carbenoxolone blocked ionic conductances in addition to blocking gap junctions; however, this possibility is unlikely, as two different groups have reported that carbenoxolone does not affect the major membrane conductances of IO neurons, most notably their Ca^{2+} conductances (Leznik, 2004; Leznik et al., 2003; Leznik and Llinás, 2005; Placantonakis et al., 2004). One alternative is that some compensatory changes in the IO neurons of Cx36KOs allows them to continue generating oscillatory activity, despite their lack of coupling (De Zeeuw et al., 2003). Other, mostly *in vitro*, studies have also reached divergent conclusions on the role of gap junctions in determining rhythmic inferior olive activity. These studies have primarily focused on the subthreshold oscillations that IO neurons can display in slices. Modeling, developmental, and physiological studies have led investigators to suggest that subthreshold oscillations are a population phenomena requiring gap junction coupling for its expression (Llinás and Yarom, 1986; Yarom, 1991; Bleasel and Pettigrew, 1992; Manor et al., 1997). However, consistent with our present results, *in vitro* recordings from Cx36KOs showed that IO neurons from these mice displayed subthreshold oscillations, suggesting that individual IO neurons could act as independent oscillators (Long et al., 2005). It was suggested, however, that subthreshold oscillations occur in Cx36K0 IO neurons, despite their lack of coupling, because the membrane properties of these cells are altered as a compensatory response to the mutation (De Zeeuw et al., 2003). But it is not clear that the observed changes, increased input resistance and generation of low threshold Ca^{2+} spikes during hyperpolarizing current pulses, are not simply the direct consequence of the loss of electrical coupling,

rather than compensatory changes in the composition or density of membrane channels. In fact, after application of gap junction blockers, normal rat IO neurons *in vitro* are still capable of generating subthreshold oscillations and of generating Ca^{2+} spikes that during a hyperpolarizing current pulse (Leznik, 2004; Leznik and Llinás, 2005). Other investigators, however, have found that subthreshold oscillations are greatly diminished by application of carbenoxolone or disruption of gap junctions using a lentiviral vector to cause expression of mutated nonfunctional Connexin36 (Placantonakis et al., 2006). In sum, while it seems clear that electrical coupling will act to constrain the oscillatory behavior of olivary neurons, it is difficult to reach a definite conclusion about their absolute requirement from the above data. A further complication is that CS rhythmicity appears to vary signiflcantly across the cerebellum, and that some regions of the inferior olive, most notably those projecting to lobules 9 and 10, do not appear to generate rhythmic CSs (Lang, Smith, McSheene, Blenkin-sop unpublished observations).

climbing fiber reflex responses are triggered by currents flowing through gap junctions

The climbing fiber reflex was first described by Eccles et al. (1966a), who reported that cer-ebellar white matter (juxtafastigial) stimulation could elicit not only a short latency CS re-sponse due to evoked action potentials traveling a purely axonal, intracerebellar route, but also a longer latency reflex CS response. Those authors speculated that the reflex response was due to a synaptic activation of IO cells either by climbing fiber or mossy fiber collater-als (Eccles et al., 1966). Subsequently, however, electrical coupling of IO cells, rather than synaptic excitation, was implicated as the most likely underlying mechanism for reflex re-sponses by botte the discovery of gap junctions between IO cells and the demonstration that juxtafastigial stimulation evoked a gap junction mediated, 'short-latency depolarization' in IO cells, which could trigger spikes in IO cells (Sotelo et al., 1974; Llinás et al., 1974).
The latter interpretation is also consistent witte the facts that there appear to be no intraIO collaterals from olivocerebellar axons (De Zeeuw et al., 1996), and that reflex responses still can be elicited following intra-IO injection of glutamate and GABA receptor antagonists (Lang, 2002; Lang, 2001). Moreover, reflex responses disappear following intra-olivary injec-tion of carbenoxolone (Blenkinsop and Lang, 2006).

In sum, it is clear that the climbing fiber reflex does not require chemical synaptic transmission. Thus, when the stimulus evokes only a reflex response in a Purkinje cell, the reflex response must be the result of the Purkinje cell's IO cell (i.e., the IO cell whose axon

synapses onto that Purkinje cell) being excited by current flowing through gap junctions from neighboring IO cells. That is, antidromic spikes elicited in the axons of other olivary cells result in a depolarization of these cells, which then spreads, via gap junctions, to non-antidromically excited cells and excites them to fire orthodromic spikes that return to the cerebellum and generate reflex responses. However, when both short-latency and reflex responses are observed, as is often the case, an alternative mechanism may be considered for the reflex response generation. Namely, the short-latency response implies that tke climbing fiber was antidromically activated, and when this spike reaches the IO cell it may produce a high-threshold Ca^{2+} spike in its dendrites that could in turn lead directly to orthodromic spikes returning to the cerebellum. That is, there is simply a reflection of the antidromic spike into an orthodromic spike witkin the same cell. Intracellular recording from olivary cells proefdes some evidence against this self-excitation possibility, and for the gap junction mechanism (Llinás et al., 1974). Juxtafastigial stimulation was used to evoke antidromic activation of an inferior olivary cell, but at the same time a depolarizing current was injected into the cell triggering an orthodromic spike, which collided with the antidromic one. By annihilating the antidromic spike a gap junction mediated depolarization was revealed, and was shown to be able to trigger orthodromic spikes. Thus, even in antidromically invaded IO cells, the reflex response can be driven via gap junction mediated excitation.

Nevertheless, the above results do not rule out the possibility that the antidromic spike could trigger reflex responses if allowed to backpropagate into the soma and dendrites. The present results, however, strongly indicate that this possibility occurs rarely, if at all. That is, in the Cx36KOs the short-latency response was found in many cells, but the reflex response was, with one exception, never found. Because electrical coupling among olivary neurons is not completely absent in the Cx36K0 (Long et al., 2002), this sole exception still likely represents excitation via gap junctions; however, the backpropagation mechanism may also be an explanation. Nevertheless, given the singularity of this exception, we conclude antidromic invasion does not normally lead to a secondary orthodromic response in IO cells from Cx36KOs. We may extend this conclusion to normai animals by noting that IO cells in Cx36K0 mice appear to have the same membrane conductances as normai inferior olive cells or may in fact be somewhat more excitable than normai because of their increased input resistance (Long et al., 2002; De Zeeuw et al., 2003), and thus should have exhibited reflex responses had backpropagation been a significant underlying mechanism.

ACKNOWLEDGMENTS

REFERENCES

Bennett MVL and Zukin RS. Electrical coupling and neuroval synchronization in the mammalian brain. Neuron. 2004;41:495-511.

Sotelo C, Llinás R and Baker R. Structural study of inferior olivary nucleus of the cat: morphological correlaten of electrotonic coupling. J Neurophysiol. 1974;37:541-59.

Llinás R, Baker R and Sotelo C. Electrotonic coupling between neurons in cat inferior olive. J Neurophysiol. 1974;37:560-571.

Llinás R. and Yarom Y. Oscillatory properties of guinea-pig inferior olivary neurones and their pharmacological modulation: an *in vitro* study. J Physiol (Zond). 1986;376:163-182.

Long MA, Deans MR, Paul DL and Connors BW. Rhythmicity without synchrony in the electrically uncoupled inferior olive. J Neurosci. 2002;22:10898-10905.

Bell CC and Kawasaki T. Relations among climbing fiber responses of nearby Purkinje cells. J Neurophysiol. 1972;35:155-169.

Llinás R and Sasaki K. The functional organization of the olivo-cerebellar system as examined by multiple Purkinje cell recordings. Eur J Neurosci. 1989;1:587-602.

Lang EJ, Sugihara I, Welsh JP and Llin s R. Patterns of spontaneous Purkinje cell complex spike activity in the awake rat. J Neurosci. 1999;19:2728-2739.

Welsh JP, Lang EJ, Sugihara I and Llin s R. Dynamic organization of motor control within the olivocerebellar system. Nature. 1995;374:453-457.

Lang EJ, Sugihara I and Llin s R. Olivocerebellar modulation of motor cortex ability to generate vibrissal movements in rats. J Physiol (Lond). 2006;571:101-120.

Llinás R and Yarom Y. Electrophysiology of mammalian inferior olivary neurones *in vitro*. Different types of voltage-dependent Tonic conductances. J Physiol (Lond). 1981a;315:549-567.

Lang EJ, Sugihara I and Llinás R. GABAergic modulation of complex spike activity by the cerebellar nucleoolivary pathway in rat. J Neurophysiol. 1996;76:255-275.

Lang EJ. Organization of olivocerebellar activity in the absence of excitatory glutamatergic input. J Neurosci. 2001;21:1663-1675.

Lang EJ. GABAergic and glutamatergic modulation of spontaneous and motor-cortex-evoked complex spike activity. J Neurophysiol.2002;87:1993-2008.

Blenkinsop TA and Lang EJ. Block of inferior olive gap junctional coupling decreases Purkinje cell complex spike synchrony and rhythmicity. J Neurosci. 2006;26:1739-1748.

Condorelli DF, Belluardo N, Trovato-Salinaro A and Mudo G. Expression of Cx36 in mammalian neurons. Brain Research Reviews. 2000;32:72-85.

Rash JE, Stafnes WA, Yasumura T, Patel D, Furman CS, Stelmack GL, et al. Immunogold evidence that neuroval gap junctions in adult rat brain and spinal Gord contain connexin-36 but not connexin-32 or connexin-43. Proc Natl Acad Sci USA. 2000;97:7573-7578.

De Zeeuw CI, Chorev E, Devor A, Manor Y, Van Der Giessen RS, De Jeu MT, et al. Deformation of network connectivity in the inferior olive of connexin 36-deficient mice is compensated by morphological and electrophysiological changes at the single neuron level. J Neurosci. 2003;23:4700-4711.

Güldenagel M, Ammerm lier J, Feigenspan A, Teubner B, Degen J, S hl G, et al. Visual transmission deficits in mice with targeted disruption of the gap junction gene Connexin36. J Neurosci. 2001;21:6036-6044.

Sasaki K, Bower JM and Llinás R. Multiple Purkinje cell recording in rodent cerebellar cortex. Eur J Neurosci. 1989;1:572-586.

Eccles JC, Llinás R and Sasaki K. The excitatory synaptic action of climbing fibers on the Purkinje cells of the cerebellum. J Physiol (Zond). 1966a;182:268-296.

Wylie DR, De Zeeuw CI and Simpson JI. Temporal relations of the complex spike activity of Purkinje cell pairs in the vestibulocerebellum of rabbits. J Neurosci. 1995;15:2875-2887.

Sugihara I, Marshall SP and Lang EJ. Relationship of complex spike synchrony bands and climbing fiber projection determined by reference to aldolase C compartments in crus IIa of the rat cerebellar cortex. J Comp Neurol. 2006:under review.

De Zeeuw CI, Holstege JC, Ruigrok TJH and Voogd J. Ultrastructural study of the GABAergic, cerebellar, and mesodiencephalic innervation of the cat medial accessory olive: anterograde tracing combined with immunocytochemistry. JComp Neurol. 1989a;284:12-35.

De Zeeuw CI, Lang EJ, Sugihara I, Ruigrok TJH, Eisenman LM, Mugnaini E, et al. Morphological correlaten of bilateral synchrony in the rat cerebellar cortex. J Neurosci. 1996;16:3412-3426.

Fredette BJ, Adams JC and Mugnaini E. GABAergic neurons in the mammalian inferior olive and ventral medulla detected by glutamate decarboxylase immunocytochemistry. JComp Neurol. 1992;321:501-514.

De Zeeuw CI, Koekkoek SKE, Wylie DRW and Simpson JI. Association between dendritic lamellar bodies and complex spike synchrony in the olivocerebellar system. J Neurophysiol. 1997;77:1747-1758.

Kistler WM, De Jeu MTG, Elgersma Y, van der Giessen RS, Hensbroek R, Luo C, et al. Analysis of Cx36 knockout does not support tenet that olivary gap junctions are required for complex spike synchronization and normal motor performance. Ann N Y Acad Sci. 2002;978:391-404.

Leznik E. Spatio-Temporal Characteristics of Oscillatory Patterns in the Inferior Olivary Nucleus. New York: New York University, School of Medicine; 2004.

Leznik E and Llinás R. Role of gap junctions in generating and synchronizing oscillations in the inferior olivary nucleus. Soc Neurosci Abstr. 2003:274.12.

Leznik E and Llinás R. Role of gap junctions in synchronized neuroval oscillations in the inferior olive. J Neurophysiol. 2005;94:2447-2456.

Placantonakis DG, Bukovsky AA, Zeng X-H, Kiem H-P and Welsh JP. Fundamental tule of inferior olive connexin 36 in muscle coherente during tremor. Proc Natl Acad Sci USA. 2004;101:7164-7169 .

Yarom Y. Rhythmogenesis in a hybrid system—interconnecting an olivary neuron to an analog network of coupled oscillators. Neuroscience. 1991;44:263-275.

Bleasel AF and Pettigrew AG. Development and properties of spontaneous oscillations of the membrane potential in inferior olivary neurons in the rat. Dev Brain Res. 1992;65:43-50.

Manor Y, Rinzel J, Segev I and Yarom Y. Low-amplitude oscillations in the inferior olive: a model based on electrical coupling of neurons with heterogeneous channel densities. J Neurophysiol . 1997;77:2736-2752.

Placantonakis DG, Bukovsky AA, Aicher SA, Kiem H-P and Welsh JP. Continuous electrical oscillations emerge from a coupled network: a study of the inferior olive using lentiviral knockdown of Connexin36. J Neurosci. 2006;26:5008-5016.

CHAPTER 4.3

Role of Olivary Coupling in Learning-Dependent Timing

R.S. van der Giessen[1]*, S.K. Koekkoek[1]*, S. Khosrovani[1]*, S. van Dorp[1]*, A. Cupido[1]*, B. Dortland[1], K. Wellershaus[2], J. Degen[2], J. Deuchars[4], E.C. Fuchs[5], H. Monyer[5], K. Willecke[2], M.T.G. De Jeu[1], and C.I. De Zeeuw[1,6]

[1]Department of Neuroscience, Erasmus MC, 3000 DR Rotterdam, The Netherlands
[2]Institute of Genetics, Division of Molecular Genetics, University of Bonn, 53117, Germany
[3]Department of Physiology & Neuroscience, NYU Medical Center, New York, USA
[4]Institute of Membrane and Systems Biology, University of Leeds, UK
[5]Department of Clinical Neurobiology, Interdisciplinary Center for Neuroscience, 69120 Heidelberg, Germany
[6]Netherlands Institute for Neuroscience, Royal Academy of Arts & Sciences (KNAW), Amsterdam, The Netherlands

* These authors contributed equally

ABSTRACT

Neurons in the mammalian brain communicate extensively with each other through chemical neurotransmission. However, many brain regions also contain neurons that are coupled by electrical synapses allowing signals to traverse directly from one neuron to the other with minimal delay. The level of coupling in the inferior olive is higher than in any other brain region. Yet, the functional role of this phenomenon in cerebellar motor control remains to be determined. Here, we subjected mice that lack coupling among their olivary neurons to paradigms that require learning-dependent timing. Cx36-deficient mice showed impaired timing of both locomotion and eyeblink responses that were conditioned to a tone. The timing of spike activities generated in the olive of coupling-deficient mice was abnormal in that their latencies in response to the unconditioned stimulus were inconsistent and that their overall synchrony was reduced. Whole cell recordings of olivary neurons *in vivo* showed that these different spiking activities over time result at least in part from altered interactions with their subthreshold oscillations. These results, combined with analysis of olivary activities in a computer simulation of the cerebellar system, suggest that electrotonic coupling among olivary neurons is necessary for proper synchronous oscillations in the inferior olive, which in turn determine the pace of the olivary responses necessary for learning-dependent timing in cerebellar motor control.

INTRODUCTION

More than a century ago in 1906 Santiago Rámon y Cajal received the Nobel Prize for the neuron doctrine stating that neurons operate as anatomically and functionally distinct cellular units in the mammalian brain. This tenet still holds to a large extent, but over the past decade the neuron doctrine is increasingly challenged by new discoveries about the constitution, distribution and cell physiological functions of neuronal gap junctions that can provide cytoplasmic continuity among large ensembles of neurons (Bullock et al., 2005). Importantly, in 1998 groups led by Condorelli (Condorelli et al., 1998) and Willecke (Söhl et al., 1998) cloned the first gap junction protein, i.e. Connexin36 (Cx36), that is predominantly expressed by neurons. The identification of this protein allowed several groups to study the distribution of Cx36 and/or to create mouse mutants to investigate the cellular consequences of a lack of Cx36 in the brain (Bennett and Zukin, 2004; Connors and Long, 2004). To date, Cx36 and neuronal gap junctions are widely distributed in regions such as the olfactory bulb, hippocampus, cerebral cortex, (hypo)thalamus and inferior olive, and

for most of these regions the possible role of neuronal gap junctions has been determined at the cell physiological level (Deans et al., 2001; Landisman et al., 2002; Long et al., 2002). In these *in vitro* studies a lack of Cx36 generally leads to an absence of electrotonic coupling and changes in subthreshold activities (Buhl et al., 2003; De Zeeuw et al., 2003; Long et al., 2002). Yet, for all brain systems investigated so far a clear phenotype remains to be determined at the behavioural level and/or systems electrophysiological level. Previous behavioural studies on Cx36-/- mutants showed no ataxia and virtually normal motor performance (Kistler et al., 2002). Here we show that although Cx36-/- mutants have no general motor deficits, they do show problems when challenged to a learning-dependent motor task such as conditioning their locomotion pattern or eyeblink response to a tone. In these learning tasks the timing of the motor responses is modified by conditioning the movement to a conditioned stimulus (CS) that starts before, but co-terminates with, an unconditioned stimulus (US) (Garcia and Mauk, 1998; Koekkoek et al., 2003; Perrett et al., 1993). The CS is conveyed by the mossy fiber - parallel fiber system to the Purkinje cells in the cerebellar cortex, while the US is probably conveyed by their climbing fibers originating from the inferior olive (De Zeeuw and Yeo, 2005; Hesslow et al., 1999; Jirenhed et al., 2007). Thus, it is our hypothesis that appropriate timing of conditioned motor responses critically depends on the precise temporal coding of the activities of coupled neurons in the inferior olive (De Zeeuw et al., 1998; Leznik et al., 2002; Placantonakis et al., 2004).

MATERIAL AND METHODS

Knockout animals

Global Cx36-/- mutants and wild type mice were generated and characterized as described by (Guldenagel et al., 2001). The mutants that lacked Cx36 in their cerebellar nuclei neurons were cross-breedings of floxed-Cx36 mutants and Parvalbumin-Cre mice. In contrast to the mouse published in (Degen et al., 2004), the current conditional Cx36 deficient mouse has the 5' loxP site inserted in the 5'UTR of Cx36 and not in the intron, leading to functional expression of the floxed Cx36 allele. Furthermore, after Cre mediated deletion a cyan fluorescent protein (CFP) was expressed instead of the floxed Cx36 allele (Figure 2B). Transfection of embryonic stem cells, creation of cell cultures, screening for homologously recombined HM-1 cell clones, and injections of blastocyst were performed as described by (Theis et al., 2000). Subsequently Cx36+/flox(CFP) mice were mated to Cx36+/del (lacZ) : Parvalbumin-

Cre mice to obtain cerebellum deleted offspring with the genotype Cx36del(lacZ)/flox(CFP) : Parvalbumin-Cre. For the experiments described in the present study offspring from a Parvalbumin-Cre founder with multicopy integration of the transgene was used.

Immunofluorescence

Cx36-/flox : Parvalbumin-Cre mice and Cx36-/flox(CFP) littermate controls were anesthetized and perfused with 4% paraformaldehyde in PBS. The brains were removed and cut on a vibratome (Leica, U.K.), and the sections were immersed in rabbit anti-GFP (1:1000, Invitrogen, U.K). Sections were washed in PBS and incubated in donkey anti-rabbit Cy3 (1:1000, Jackson ImmunoResearch, USA) prior to mounting (Vector Labs, U.K). Cy3 was viewed with a custom filter set and Alexa488 with FITC filters (Nikon E600 microscope) and images were captured directly from the slide using an Acquis Image Capture system (Synoptics, U.K).

Erasmus Ladder

The Erasmus Ladder is a fully automated system to screen both motor performance and motor learning capabilities of mutant mice in a non-invasive manner at a high-throughput level. It consists of a horizontal ladder in between two shelter boxes, which are equipped with two pressurized air outlets (Pneumax, 171E2B.T.A.0009) to control the moment of departure and speed of the mouse. The ladder has 2 x 37 rungs for the left and right side, which are separated 2 mm apart. The rungs are 12 mm long and 3 mm in diameter, and the distance between two rungs on one side is 15 mm. All rungs are equipped with pressure sensors (produced in our own facilities), which are continuously monitored and which can be used to register and analyse the walking pattern of the mouse instantaneously. Moreover, based upon the prediction of the walking pattern the rungs can be moved up or down by a high-speed pneumatic slide (Pneumax, 2141.52.00.36.91) with a maximum of 13 mm at any moment in time. The computer system (National Instruments, PXI-1000B) that runs the real-time system to record sensor data, adjust air pressure, predict future touches, calculate interventions, reposition slides and store data, operates in a time fixed cycle of 2 ms. In the conditioning procedures a 15 kHz tone (Voltcraft 7202), which gradually increased over 20 ms to 100 dB and which lasted 300 ms, was used as the CS, while a rising rung, which ascended 12 mm, was used as the US. The trials were separated by a random inter-trial interval ranging from 9 to 11 sec.

Eyeblink conditioning

Wild type and mutant mice were prepared for eyeblink conditioning according the MDMT procedure (Koekkoek et al., 2002; Koekkoek et al., 2005). Mice were anaesthetized using

nitrous oxide and isoflurane, and a dental acrylic pedestal was placed on the skull. On each day the MDMT measurement system was attached to the pedestal, while a magnet was glued on the lower eyelid. Mice were subjected to either a paired or a randomly paired procedure; both procedures lasted 4 days during each of which 1 session (64 trials grouped in 8 blocks) was conducted. The trials were separated by a random inter-trial interval ranging from 20 to 40 sec. Eyelid movements were considered as a significant eyelid response when its amplitude was greater than the mean +3 SD's of the amplitude of the movements that occurred in the 500 ms period before the onset of the CS.

Extracellular recordings

To investigate the temporal aspects of climbing fiber activities (i.e. complex spikes) mice were prepared by placing a pedestal on the head and by placing a recording chamber above the simplex lobule and adjacent areas. During experiments the animals were immobilized using a restrainer. Extracellular Purkinje cell activities were recorded in the eyeblink region of awake animals with glass micro-electrodes using a Multiclamp 700A and Digidata 1322A from Axon Instruments. Complex spike responses were recorded during 1Hz air puff stimulation to the eye and analyzed off-line. A voltage threshold was used to detect complex spikes, and the time and waveform of the voltage records were used for off-line analysis (IGOR analysis software; WaveMetrics, OR). All experiments were conducted in accordance with the European Communities Council Directive (86/609/EEC) and approved by the Dutch national ethics committee.

Whole cell recordings in vivo

Mice were prepared for experiments under isoflurane or ketamine/xylazine anesthesia. The head was fixed by bolting a pedestal to a metal bar, the neck area was opened, and the dura was removed. Glass patch pipettes (OD 1.5 mm, ID 1.2 mm, 4-6 MW) containing standard intracellular solution (in mM: KCl 9, KOH 10, $MgCl_2$ 3.48, NaCl 4, KGluconate 120, HEPES 10, sucrose 17.5, Na_2ATP 4, Na_3GTP 0.4, pH 7.2, osmolarity 290-310 mOsm/kg) were advanced into the inferior olive in 1-5 μm steps (SM IV, Luigs & Neumann, Ratingen, Germany). The exposed area was covered with artificial fluid (NaCl 148, KCl 3.0, $CaCl_2 \cdot 2H_2O$ 1.4, $MgCl_2 \cdot 6H_2O$ 0.8, $Na_2HPO_4 \cdot 7H_2O$ 0.8, $NaH_2PO_4 \cdot H_2O$ 0.2). Recordings were amplified with the use of a MultiClamp 700A and DIGIDATA 1322A (Axon Instr.). All membrane potentials were corrected for the junction potential (8 mV). In current-clamp experiments, we measured voltage responses to a series of negative current steps (100 nA). Cells expressing I_h-current were determined by the presence of an increasing depolarizing sag in more than three sequential

hyperpolarization steps. Likewise, rebound depolarizations were only counted if present following more than three hyperpolarization steps. Correlations between the STO frequencies and preferred spiking frequencies were determined by analyzing autocorrelograms (clampfit 9.0 software, Axon Instruments, CA). Bursts with a significant poisson surprise value (> 5) were correlated to the corresponding STO frequency extracted from the power spectrum of the recordings. All experiments were conducted in accordance with the European Communities Council Directive (86/609/EEC) and approved by the Dutch national ethics committee.

Computer simulation

Simulation scripts were written in Matlab 7.1 (MathWorks) and simulations were done on an AMD64 3200+ machine running Gentoo Linux. The model is created top-down and provides a descriptive view of the underlying predefined principle. It is organized according to the circuitry of the cerebellum and incorporates basic characterizations of the activity of five groups of neurons including olivary neurons (# 80), neurons providing the mossy fibers (# 100), granule cells (# 2000), Purkinje cells (# 400), and cerebellar nuclei neurons (# 200). Each connection is characterized by a specific time delay and synaptic strength. Details of the model are presented as supplementary material.

RESULTS

Deficits in locomotion conditioning

To quantify their general level of motor performance Cx36-/-mutants (C57BL/6 background; n = 9) and wild type littermates (n = 10) were trained to walk over the Erasmus ladder. The Erasmus Ladder is formed by 2 x 37 rungs positioned between a start- and end-box across which the mice can run back and forth (Figure 1A, left panel). Each rung on both the left and right side is equipped with a pressure sensor, which is continuously monitored. Based on instantaneous analysis of the activities of these sensors, the walking pattern of the mice can be predicted in the millisecond range, and, if wanted, interrupted by moving each individual rung up or down. Initially, the mice were trained with the even numbered rungs on the left side and the odd numbered rungs on the right side in a descended position so as to create an alternated stepping pattern with 30 mm gaps (Figure 1A, right panel). In this paradigm the Cx36-/-mutants and wild type littermates showed a comparably low number of missteps, which were identified by touches on the descended rungs (p > 0.10 for each session; t-test; Figure 1B).

For comparison we also tested Lurcher mice (C57BL/6 background; n = 9), which lack Purkinje cells and which are known to show cerebellar ataxia (Porras-Garcia et al., 2005; Van Alphen et al., 2002) Indeed, these spontaneous mouse mutants showed 3 to 4 times more missteps than the Cx36-/- mutants or their wild type littermates (p < 0.0001 and p < 0.0001 for each session; t-test).
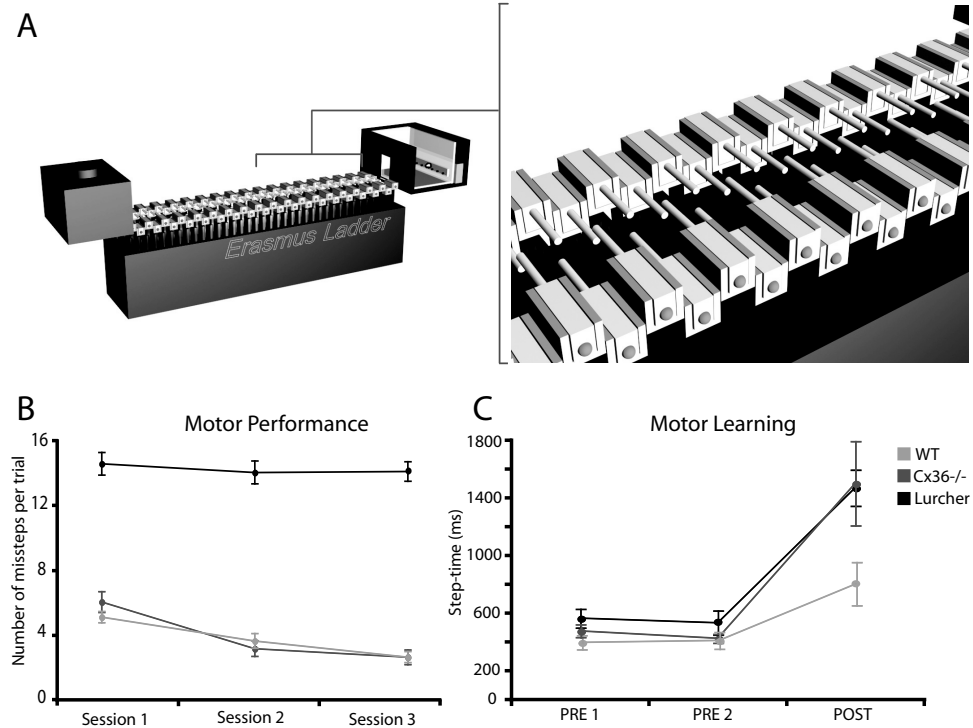
Figure 1. Erasmus Ladder test for detecting performance and learning deficits in locomotion. A. The Ladder consists of 2 x 37 horizontal rungs placed in between 2 shelter-boxes. Mice are trained to walk from one side to the other using air pressure devices placed in the bottom of the boxes. The rungs, which are all equipped with pressure sensors, can be moved up or down under the control of a linked computer system that can analyze the walking pattern instantaneously during locomotion. B. Motor performance level is revealed by the amount of descended rungs touched, i.e. number of missteps. Cx36-/- mutants (red) and wild type littermates (blue) show normal motor performance, while Lurcher mice (black) show deficits in performance during all sessions. C. Motor learning level is revealed by the change in step-time after the conditioning starts (i.e. post re pre). During conditioning trials a randomly selected rung rises 12 mm above the walking level to create a perturbation; this unconditioned stimulus occurs at a fixed moment after the onset of the conditioned stimulus (a 15 kHz tone). Both Cx36-/- mutants and Lurcher mice reveal difficulties in motor learning as compared to wild types.

Thus, in line with previous rotarod tests (Frisch et al., 2005; Kistler et al., 2002), we conclude from this test on the Erasmus Ladder that Cx36-/- mutants show, in contrast to lurcher mice, a normal motor performance.

To find out whether the ability for motor learning is affected in Cx36-/- mice, we subjected them to a conditioning paradigm in which they were trained to make a new loco-motion movement using a 15 kHz tone as the CS (300 ms) and a rising rung as the US (starting 55 ms after the moment the mouse has touched the preceding rung). A training session consisted of 8 blocks of 8 trials, which were separated by an inter-trial interval of 8 to 12 s. During the preconditioning sessions the time needed to place the front paw from one rung to the other ('step-time') was not different among Cx36-/- mutants and wild-type litter-mates ($p > 0.25$; t-test). However, as soon as the conditioning procedure started the front paw step-time in the mutants increased significantly compared to that of the wild types ($p < 0.05$; t-test). In fact, this increase in step-time was comparable to that observed in lurch-ers (Figure 1C). Thus, taken together, these experiments show that motor performance is not affected in Cx36-/- mutants, while their ability in motor learning is affected in that this process is slowed down.

Deficits in eyeblink conditioning

Analysis of the locomotion conditioning process described above suggests that learning-dependent timing is affected in Cx36-/- mice, but in this paradigm the movements are analysed in discrete steps and it is virtually impossible to identify the exact deficits over time during continuously recorded ongoing locomotion movements. Thus, to further inves-tigate the potential role of Cx36-/- in learning-dependent timing, we subjected the Cx36-/- mutants to an eyeblink conditioning paradigm. For this paradigm, the motor responses can be continuously measured using the magnetic distance measurement technique (MDMT; Koekkoek et al., 2002). We subjected adult Cx36-/- mutants (n = 8) and wild type litter-mates (n = 8) to a conditioning paradigm using a tone as the CS and an air puff as the US at interstimulus intervals (ISIs) of 350 ms. Here too, the 8 daily training blocks consisted of 8 trials (1 US-alone, 6 paired, and 1 CS-alone). After four paired training sessions (T-1 to T-4) the percentage of conditioned responses and their average peak amplitude in wild types reached levels of 77 % and 0.48 mm, respectively, while those in Cx36-/- mice had values of 78 % and 0.56 mm. These values were not significantly different ($p > 0.9$ and $p > 0.5$; MANOVA for repeated measures; adjusted for multiple comparisons via Bonfer-roni correction). In contrast, the timing properties of the conditioned responses differed dramatically among the wild types and Cx36-/- mutants as the training proceeded. While the average latency to peak amplitude of the conditioned eyelid responses was appro-priately fixed in wild types at the moment when the US occurs, that in the mutants got
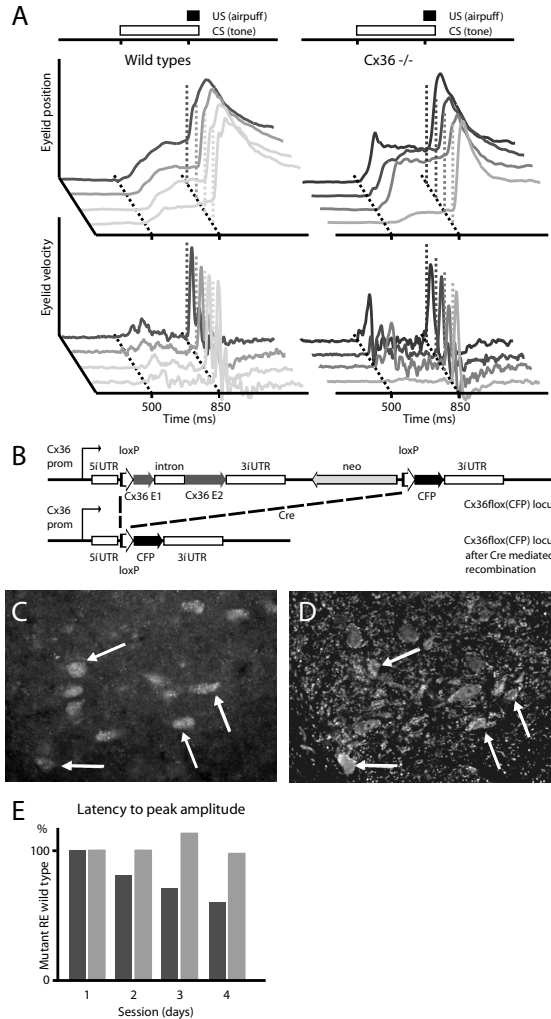
Figure 2. A lack of coupling by Cx36 gap junction proteins in the inferior olive, but not in the cerebellar nuclei, results in impaired learning-dependent timing. A. Both wild types and global Cx36-/- mutants show conditioned eyeblink responses after 4 training sessions using a tone as the conditioned stimulus (CS) and an air puff as the unconditioned stimulus (US). However, while the timing of the learned response in wild types improves over the sessions, that in the mutants gets worse. B. Genetic design of floxed-Cx36 mutants cross-bred with Parvalbumin-Cre mice, which were used as controls. C. The Cx36del(lacZ)/flox(CFP) : Parvalbumin-Cre control mice showed CFP staining in their cerebellar nuclei neurons demonstrating that Cx36 has been floxed in these neurons. D. Immunostaining for parvalbumin of the same sections showed that most of the cerebellar nuclei neurons indeed normally express both Cx36 and parvalbumin (arrows). Thus, the Cx36del(lacZ)/flox(CFP) : Parvalbumin-Cre control mice do not express Cx36 in their cerebellar nuclei, while their expression in the relevant olivary subnuclei is normal (data not shown). E. While the latency to peak amplitude in the global knock outs of Cx36 (red) got worse during the training sessions, that in the Cx36del(lacZ)/flox(CFP) : Parvalbumin-Cre control mice (blue) was indistinguishable from that in their unaffected littermates.

worse during the four training sessions (Figure 2A). At the end of the training the average latency to peak amplitude in the mutants preceded the moment of the US by 196 ms (9.7 SEM), which was significantly different from that in wild types ($p < 0.005$; t-test). Similarly, the average latency to peak velocity in the mutants also significantly preceded that in wild types ($p < 0.01$; t-test). These data indicate that coupling deficient mutants cannot appropriately time their movements when demanded in a challenging conditional task.

Still, these experiments on the global Cx36 null-mutants do not directly demonstrate that the behavioural phenotype can be attributed solely to a lack of coupling in the inferior olive. Neurons in the cerebellar nuclei also show a prominent expression of Cx36 (Degen et al., 2004; Van Der Giessen et al., 2006), and a lack of this expression may therefore in principle also affect any cerebellar conditioning paradigm (Bengtsson and Hesslow, 2006). To circumvent this possibility, we generated mutant mice in which the expression of Cx36 is ablated in the cerebellar nuclei, while that in the relevant olivary subnuclei is normal (Figures 2B, 2C and 2D). These mutants (n = 4), which were cross-breedings of floxed-Cx36 mutants and Parvalbumin-Cre mice, showed the same conditioned eyeblink responses as the wild types, i.e. without any deficits in their timing (Figure 2E). Another potential bias in the interpretation of the Cx36-/- mutants could have been formed by a disruption of the coupling between the stellate cells in the cerebellar cortex (Mann-Metzer and Yarom, 1999). We therefore investigated the constitution of the gap junctions between these cells. It turned out that the vast majority of these interneuronal gap junctions is formed by Connexin45 rather than Cx36 (Van Der Giessen et al., 2006). Thus, we conclude that Cx36-/- mutants indeed show deficits in learning-dependent timing and that these behavioural deficits are likely due to an impairment of electrotonic coupling in the inferior olive.

Abnormal temporal pattern of climbing fiber responses

If the deficits in learning-dependent timing are due to a lack of coupling between the olivary neurons, one expects that the timing properties of the activities in these neurons are disrupted in Cx36-/- mutants. To investigate these properties we recorded the climbing fiber activities of Purkinje cells in the cerebellar cortex that reveal the olivary signals of the US during eyeblink conditioning (Hesslow, 1994; Mauk et al., 1986). The climbing fiber activities of Purkinje cells generally reflect the temporal coding of olivary neurons rather precisely, because they are generated in an all-or-none fashion (Thach, 1967). Purkinje cells that responded well to the air puff stimulation used in the eyeblink paradigm described above were situated in an area covering lobulus simplex in the hemisphere and the adjacent
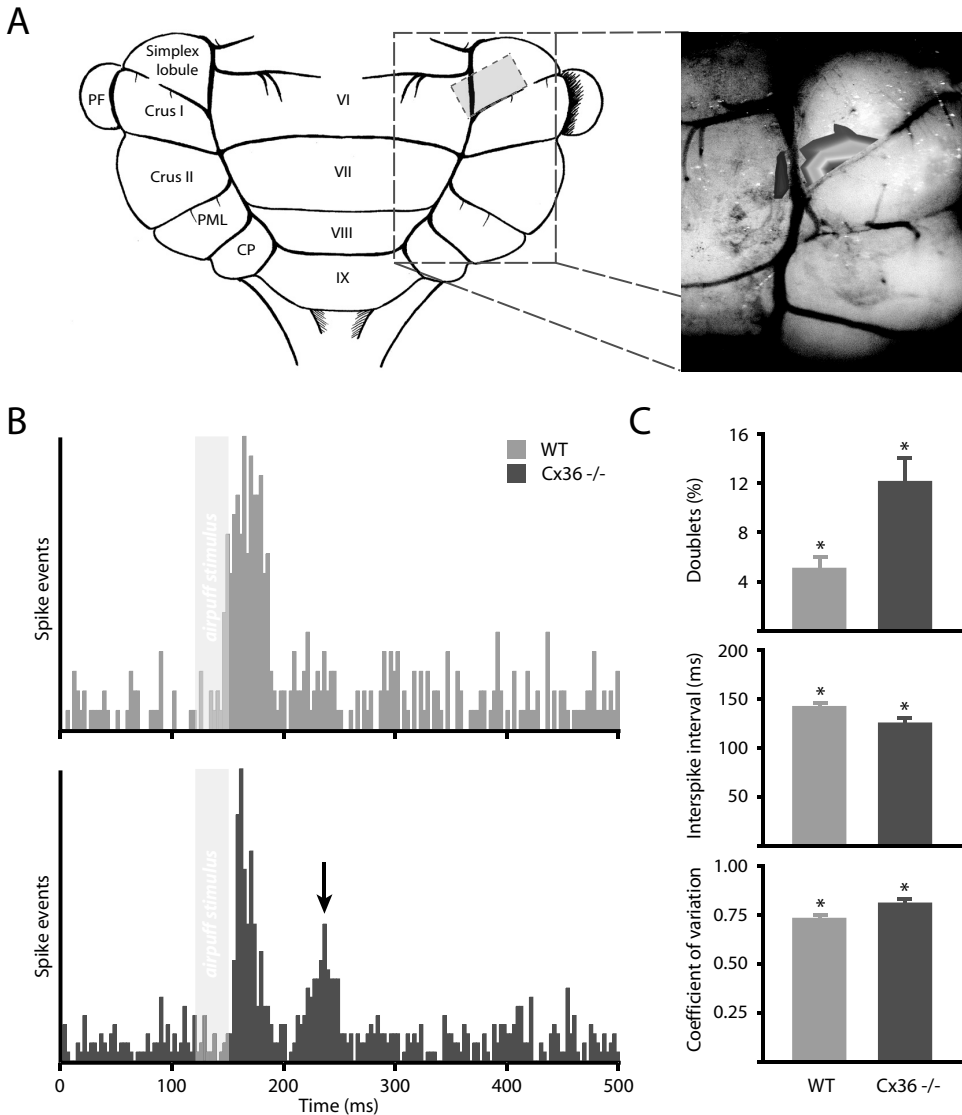
Figure 3. A lack of coupling of inferior olivary neurons results in altered timing of climbing fiber activities in the cerebellar cortex. A. Purkinje cells that responded well to air puff stimulation (i.e. US) were situated in an area covering the lobulus simplex in the hemisphere and the adjacent part of lobule VI in the anterior lobe. **B.** Air puff stimulation evoked only short-latency climbing fiber responses in awake wild types (blue) (latency of 29 ± 9 ms), while in the Cx36-/- mutants (red) the same peri-oribital stimulation evoked both short-latency (30 ± 7 ms) and long-latency responses (101 ± 17 ms). Note that the scales of the top and bottom panel are not the same so that the difference is even greater than indicated. **C.** During spontaneous activity in the awake state the Cx36-/- mutants showed significantly more doublets of two or three complex spikes occurring within 200 ms (p < 0.01; t-test), a significantly smaller mean interspike interval within these doublets (p < 0.01; t-test), and a general increased coefficient of variation for spike intervals (p < 0.02; t-test).

part of lobule VI in the anterior lobe (Figure 3A). In awake wild types (n = 9) the air puff stimulation evoked virtually only short-latency climbing fiber responses; these responses had an average peak latency of 29 ± 9 ms (SD) over 879 successful stimulations. In contrast, in all Purkinje cells recorded in the Cx36-/- mutants (n = 10) the same peri-oribital stimulation evoked both short-latency responses (average to peak of 30 ± 7 ms) and long-latency responses (101 ± 17 ms) (Figure 3B). Of all successful stimulations (n = 1036) in the mutants 60% and 34% resulted in pure short-latency and pure long-latency responses, respectively, while 6% resulted in both a short-latency and long-latency response. These differences in the temporal distribution patterns following peripheral stimulation were highly significantly different among wild types and mutants (p < 0.001; t-tests). Similarly, during spontaneous activity the Cx36-/- mutants showed significantly (p < 0.01; t-test) more doublets of two or three climbing fiber responses occurring within 200 ms (12 ± 6 %, SD) than wild types (5 ± 2 %, SD) (Figure 3C, upper panel), while the mean interspike interval within a doublet was significantly smaller (123 ± 11 ms in Cx36-/- mutants re 140 ± 12 ms in wild types; p < 0.01; t-test) (Figure 3C, middle panel). This difference was also reflected by a general increased coefficient of variation for spike intervals (p < 0.02; t-test) (Figure 3C, bottom panel). All these differences were not influenced by the average firing frequencies, because these were not significantly different (0.94 ± 0.19 in wild types re 1.00 ± 0.26 in Cx36-/- mutants; p > 0.4; t-test). Thus, mice lacking Cx36 show robust differences in the temporal pattern of their climbing fiber activities, but not in absolute firing frequency.

Altered correlation between spiking activities and subthreshold oscillations

To explain the differences in latencies and spiking patterns following peri-orbital stimulation described above, we investigated the activities of olivary neurons using whole cell recordings *in vivo* in anaesthetized animals (Table 1). The majority of the neurons in wild types showed pronounced subthreshold oscillations that either had a clear sinusoidal appearance, a more complex rhythmic shape, which probably corresponds to the activation of low threshold calcium conductances (Llinás and Yarom, 1981), or both types of subthreshold activities (Figure 4A). In the mutants the same types of oscillating cells were observed, but they showed significantly more cells that did not oscillate (p < 0.01; c2-test) (Figure 4B). Power spectra of the oscillating subthreshold activities showed that the frequencies of the oscillations occurred in both wild types and mutants mostly in the range of 1 to 3 Hz or in the range of 6 to 8 Hz (Figure 4C).

Table 1. Properties of olivary neurons in wild types and Cx36 -/- mutants following whole cell recordings *in vivo*

Parameter	Wild type	n	Cx36 -/-	n	Statistics
All neurons					
Resting membrane potential (mV)	-55.0±0.7	59	-55.1±0.8	28	0.46
Input resistance (GΩ)	40.9±3.3	61	47.3±4.1	27	0.15
Membrane capacitance (pF)	206.5±24.6	61	208.1±32.7	27	0.49
Firing rate (Hz)	0.65±0.05	57	0.58±0.10	28	0.24
Coefficient of variation for spike intervals	0.72±0.03	57	0.82±0.04	28	0.03
% Cells expressing depolarizing sag	16	51	50	27	0.01
% Cells expressing rebound depolarization	63	54	93	25	0.03
% Cells expressing afterhyperpolarization	24	47	31	24	0.65
% Cells expressing spontaneous STO's	87	59	88	28	0.87
STO frequency (Hz)	2.8±0.3*	59	3.1±0.6*	28	0.30
STO amplitude (mV)	6.0±0.6*	59	7.0±1.0*	28	0.21
% Cells expressing spontaneous no STO's	13	59	12	28	0.87
Cells expressing spontaneous STO's					
Resting membrane potential (mV)	-55.3±0.7	53	-54.6±0.9	16	0.31
Input resistance (GΩ)	40.1±3.8	53	45.2±4.3	14	0.24
Membrane capacitance (pF)	188.7±11.8	53	233.0±37.0	14	0.07
Firing rate (Hz)	0.64±0.05	50	0.54±0.09	14	0.15
Coefficient of variation for spike intervals	0.72±0.02	50	0.83±0.05	14	0.02
STO frequency (Hz)	3.1±0.3*	53	3.4±0.6*	16	0.32
STO amplitude (mV)	7.5±0.6*	53	7.7±0.9*	16	0.44
% Cells expressing depolarizing sag	24	58	62	14	0.01
% Cells expressing rebound depolarization	62	58	92	14	0.05
% Cells expressing afterhyperpolarization	19	45	45	12	0.26
Cells expressing no spontaneous STO's					
Resting membrane potential (mV)	-52.3±2.1	9	-57.5±0.5	12	0.11
Input resistance (GΩ)	42.3±5.2	9	48.3±15.5	12	0.32
Membrane capacitance (pF)	159.6±19.1	9	100.6±3.9	12	0.07
Firing rate (Hz)	0.54±0.11	9	0.92±0.35	12	0.10
Coefficient of variation for spike intervals	0.68±0.13	9	0.68±0.04	12	0.49
% Cells expressing depolarizing sag	0	8	0	12	1.00
% Cells expressing rebound depolarization	60	8	100	12	0.29
% Cells expressing afterhyperpolarization	40	8	0	12	0.29

Statistics: t-test or X^2-test
* All measured STO's (subthreshold oscillations); a single cell can have multiple STO frequencies.

Still, the olivary activities differed in that the oscillations of the wild type neurons often showed dynamic crescendo amplitudes starting directly after the generation of an action potential, while those in the mutants showed relatively constant amplitudes (Figure 4A). Moreover, the correlation between the preferred frequencies of the subthreshold oscillations and those of the olivary spiking activities was significantly smaller in the Cx36 null-mutant (mean residual scores of 1.33 re 0.63; p < 0.01; t-test). Interestingly, this reduced correlation is in line with the observation that the olivary spikes occurred significantly more often on the peak of an oscillation in wild types than in mutants (p < 0.05; t-tests) (Figure 4D; see also arrows in Figure 4A).
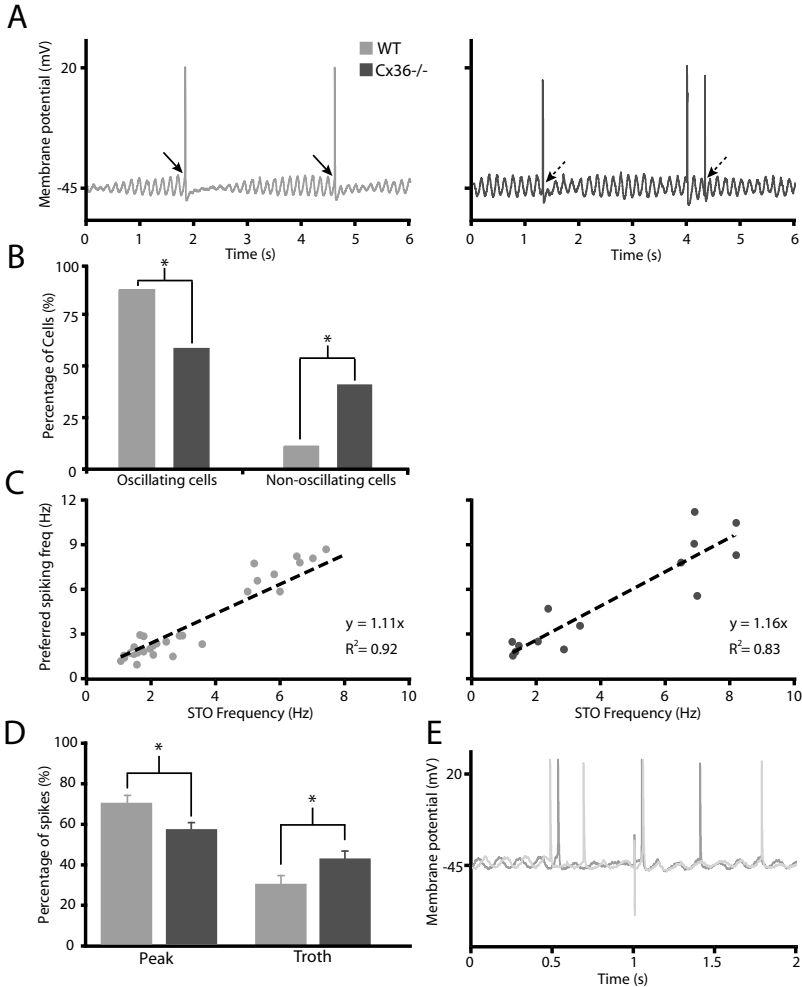
Figure 4. A lack of electrotonic coupling in the inferior olive results in altered interactions between subthreshold oscillations and generation of spiking activities. A. Examples of whole cell recordings of olivary neurons in a wild type (blue) and Cx36-/-mutant (red) *in vivo*. Most of the olivary spikes in the wild type occurred around the peak of the oscillations (solid arrows), while those in the mutant could also occur in the troth area (dashed arrows). B. Percentages of oscillating and non-oscillating cells differ significantly among wild types and Cx36-/-mutants; asterisks indicate significance level p < 0.01 (c2-test). **C.** Power spectra showed that the frequencies of both the oscillations and spikes occurred in both wild types and mutants mostly in the range from 1 to 3 Hz and from 6 to 8 Hz. However, the correlation between the preferred frequency of the oscillations and that of the spiking activities was significantly stronger in the wild types (p < 0.01; t-test). **D.** Percentage of spikes that occurred on the peak of an oscillation was significantly lower in Cx36-/- mutants, while that in the troth was significantly higher (p < 0.05; t-tests). **E.** Examples of action potentials and subthreshold oscillations in wild types before and after peripheral stimulation. Note that the peripheral stimulation had a resetting effect in that the oscillations after the occurrence of the stimulus were in phase with each other, while they were out of phase before the oscillations. Stimulus artefact is set at 1.

Figure 5. Impact of olivary coupling on learning-dependent timing in a network simulation. The model shows the activities of simulated olivary neurons (top panels), granule cells and Purkinje cells (second row of panels), as well as cerebellar nucleus cells (two bottom rows of panels) during eyeblink conditioning in wild types (blue) and Cx36-/-mutants (red). The top panel shows the spiking activities of olivary neurons before, during and after presentation of the unconditioned stimulus (i.e. the air puff). Note that the olivary activities correspond to the data presented in Figure 3 in that the number of doublets is higher. The middle panel of the second row shows that the granule cells are activated by the mossy fibers, which convey the conditioned stimulus (i.e. the tone); these granule cells
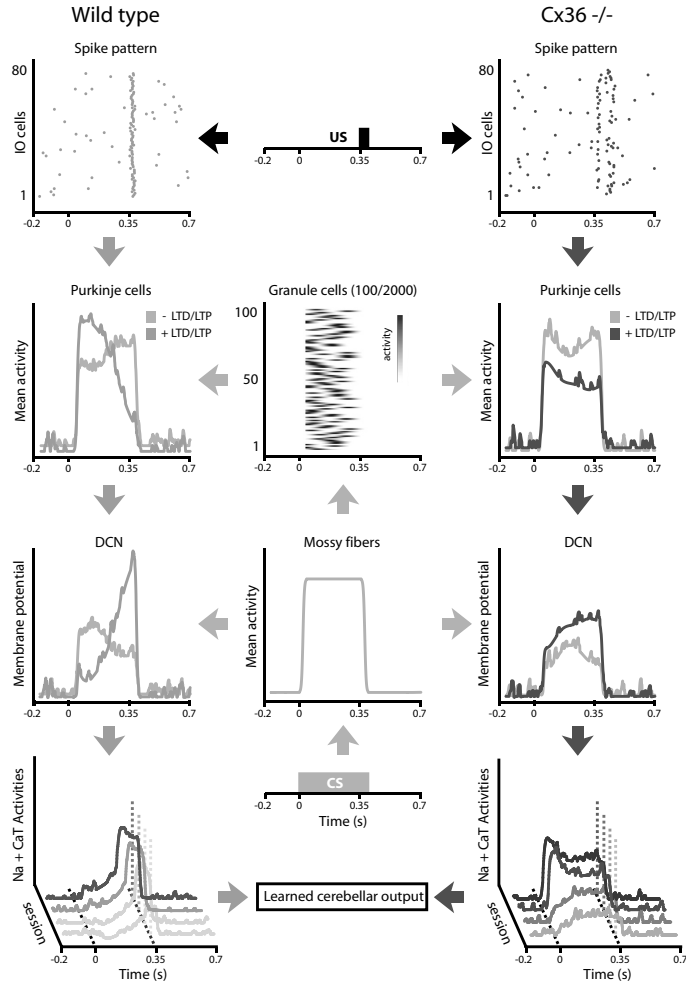
are presumed to operate as 'delayed ringers' in that each of them responds with its own delay and activity rise time. The left and right panels of the second row show the simple spike activities of the Purkinje cells in the wild types and mutants in rest (grey) and during acquisition (in blue and red). Due to differences in the timing of their climbing fiber activities and the consequences for the induction of LTD and LTP at the parallel fiber to Purkinje cell synapse, the block shaped configuration of the simple spike activities in the wild types in rest is converted into an asymmetric profile during acquisition, while that in the mutants is largely left unchanged. The membrane potential of the deep cerebellar nuclei neurons (DCN) does not only depend on the inhibitory signals from the Purkinje cells, but also on the input from the mossy fiber collaterals as well as their capacity for plasticity. When presynaptic activity in the mossy fiber collateral is combined with calcium induced rebound depolarization followed by sodium spiking activity LTP will be induced in the cerebellar nuclei neurons. These dynamic changes in the membrane potential will ultimately lead to sodium and Ca-T current activities in cerebellar nuclei neurons (bottom panels) that in wild types are close to the moment when the US is about to take place, whereas in mutants they occur a few hundred milliseconds too early.

These differences in interactions between spike generation and subthreshold oscillations also occurred following peripheral stimulation as used in the conditioning paradigms described above (see e.g. Figure 4E). Thus, peripheral sensory stimulation can indeed induce and modify the subthreshold activities and such modulation can influence the timing of subsequent spiking activities of olivary neurons when they are appropriately coupled. Therefore, the altered timing of the climbing fiber signals mediating the US in the coupling deficient Cx36-/-mutants can at least in part be explained by altered interactions with their subthreshold oscillations.

How may altered spiking patterns lead to changes in learning-dependent timing?

To find out as to how the abnormally timed climbing fiber responses may lead to deficits in learning-dependent motor timing, we created and tested a model of the olivocerebellar system controlling conditioned eyeblink responses (Figure 5). The model we created is focused on the olivo-cerebellar modular loops consisting of coupled olivary neurons, Purkinje cells in the cerebellar cortex, and the inhibitory and excitatory neurons in the cerebellar nuclei that provide feedback to the olive and control the eyeblink output, respectively (De Zeeuw and Yeo, 2005). The following assumptions and constraints were included: 1) The CS activates during its time course consecutively different sets of granule cells (Medina and Mauk, 2000); 2) the US normally activates the climbing fibers at fixed moments in time and the timing of these climbing fiber activities depends on the level of electrotonic coupling among olivary neurons (see results presented above); 3) the strengths of the parallel fiber to Purkinje cell synapse depend for each activated granule cell on the width of the time interval to the climbing fiber stimulus (Coesmans et al., 2004; Wang et al., 2000); 4) a fast release form inhibition drives cerebellar nuclei neurons effectively through post inhibitory rebound (Aizenman and Linden, 1999; Aizenman and Linden, 2000); 5) the strength of the response of a cerebellar nucleus neuron will not only be determined by instantaneous changes in firing rate of the afferent Purkinje cells but also by the steady-state level of the activity of cerebellar nuclei neurons (Koekkoek et al., 2005); and 6) the motor response during a conditioned response is determined by the instantaneous firing rate of a subpopulation of neurons in the cerebellar nuclei (Gruart et al., 1997). The details of the model and simulations are presented as supplementary data. The model demonstrates that a change in electrotonic coupling can alter the timing of the climbing fiber activities evoked by the US, which in turn will alternate the plastic changes and simple spike activities in Purkinje cells, and thereby the timing of the conditioned activities in the cerebellar nuclei neurons and

eyeblink responses. In particular, an increase in complex spike doublets and a reduction in complex spike synchrony in response to the US will lead to insufficient compensatory long-term potentiation at the parallel fiber to Purkinje cell synapse and thereby to insufficient reshaping of the activities in the cerebellar nuclei and to a rectangular eyeblink response, which prevents an optimal closure of the eyelid at the moment when the US is about to take place. Thus, the current model provides a possible explanation as to how altered timing of the climbing fiber signals mediating the US can lead to deficits in learning-dependent timing as observed in the Cx36 null-mutants (compare bottom panels of Figure 5 to panels in Figure 2A).

DISCUSSION

So far systems analyses of Cx36-deficient animals that lack neuronal coupling have revealed only minor behavioural phenotypes and/or did not reveal a clear electrophysiological mechanism that may explain these phenotypes (Bennett and Zukin, 2004; Buhl et al., 2003; Connors and Long, 2004; Deans et al., 2001; Frisch et al., 2005; Kistler et al., 2002; Landisman et al., 2002; Placantonakis et al., 2004). Here, we showed that a lack of electrotonic coupling in the inferior olive leads to abnormal firing patterns of its neurons, which in turn can contribute to deficits in the timing of conditioned motor responses. These behavioural deficits were robust despite secondary compensations that may occur in the Cx36-/-mutant (De Zeeuw et al., 2003). They could be prominently revealed in different paradigms in which either a locomotion response or an eyeblink response was conditioned to a tone. In both cases conditioned responses occurred, but the timing that had to be learned to make the response optimal was aberrant. In the locomotion test on the Erasmus Ladder Cx36-/-mutants were impaired in learning to avoid a bar that rose after a fixed period after the onset of the tone. Likewise, in the eyeblink test the coupling-deficient mutants showed after four training sessions a mismatch in their latency to peak amplitude of approximately 200 ms with respect to the onset of an air-puff. This period stands in marked contrast to the 10 to 20 ms delay that can be observed in the basic eye movement responses of Cx36 null-mutants to optokinetic stimulation (Kistler et al., 2002) or in the tremorgenic, limb and body movements of coupling deficient rats treated with replication-incompetent lentiviral vectors (Placantonakis et al., 2004). Together, these findings indicate that the role of coupling between inferior olivary neurons becomes apparent when the olivocerebellar system is challenged in a cerebellar motor learning task and that this role is to facilitate learning-dependent timing in response to unexpected events rather than timing of movements per se.

In combination with the modelling study our electrophysiological recordings demonstrated that a lack of precision in the timing of the climbing fiber activities mediating the US signals is probably responsible for the behavioural deficits in the coupling-deficient Cx36-/-mutants. This lack of precision in timing is due to an increased number of long-latency responses after the US, which adds to a reduced synchrony of climbing fiber activities (see also Marshall et al., 2007). The long-latency responses probably result from altered interactions with the subthreshold oscillations in the Cx36-/- mutants. Our whole cell recordings of olivary neurons *in vivo* did not only demonstrate that intact animals have more subthreshold oscillations than Cx36-/-mutants, but also that the incidence of spikes occurring in the troth of their oscillations is significantly higher in Cx36-/-mutants while the correlation between their preferred spiking pattern and the frequency of their oscillations is generally weaker. The robust appearance of subthreshold oscillations of olivary neurons has recently also been shown *in vivo* in rats with the use of sharp electrode recordings (Chorev et al., 2007), while the contribution of electrotonic coupling to the occurrence of subthreshold oscillations in olivary cells has recently also been shown in rats with the use of lentiviral knockdown of Cx36 or pharmacological blockage of gap junctions (Leznik and Llinás, 2005; Placantonakis et al., 2006). Thus, together with the current findings we conclude that coupling supports the oscillations in the inferior olive *in vivo* and that oscillations in uncoupled olivary neurons have less effect on spiking patterns, which results in a more random timing of their spikes in relation to the oscillations.

The question remains as to how dynamic regulation of electrotonic coupling in the olive may contribute to learning-dependent timing (Bengtsson and Hesslow, 2006; De Zeeuw et al., 1998; Llinás and Sasaki, 1989; Schweighofer et al., 1999). Llinás and colleagues have provided strong evidence that the GABAergic input from the cerebellar nuclei, which terminates strategically at the coupled dendrites in olivary glomeruli (De Zeeuw et al., 1998), can uncouple the olivary neurons (Lang et al., 1996; Llinás and Sasaki, 1989). According to the simulations in our model such a mechanism would counteract learning-dependent timing of the conditioned responses, because it desynchronizes the climbing fiber inputs that mediate the signals of the US. Interestingly, Mauk and colleagues recently demonstrated that the GABAergic projection to the olive is necessary for extinction of the conditioned responses by reducing the firing rate of the relevant olivary neurons below resting level (Medina et al., 2002). Thus, in this respect the mechanism of uncoupling and the mechanism of reducing the firing rate of olivary neurons may serve the same effect in that they both actively counteract the conditioning process.

ACKNOWLEDGMENTS

REFERENCES

Aizenman, C. D., and Linden, D. J. (1999). Regulation of the rebound depolarization and spontaneous firing patterns of deep nuclear neurons in slices of rat cerebellum. J Neurophysiol 82, 1697-1709.

Aizenman, C. D., and Linden, D. J. (2000). Rapid, synaptically driven increases in the intrinsic excitability of cerebellar deep nuclear neurons. Nat Neurosci 3, 109-111.

Bengtsson, F., and Hesslow, G. (2006). Cerebellar control of the inferior olive. Cerebellum 5, 7-14.

Bennett, M. V., and Zukin, R. S. (2004). Electrical coupling and neuronal synchronization in the Mammalian brain. Neuron 41, 495-511.

Buhl, D. L., Harris, K. D., Hormuzdi, S. G., Monyer, H., and Buzsaki, G. (2003). Selective impairment of hippocampal gamma oscillations in connexin-36 knock-out mouse *in vivo*. J Neurosci 23, 1013-1018.

Bullock, T. H., Bennett, M. V., Johnston, D., Josephson, R., Marder, E., and Fields, R. D. (2005). Neuroscience. The neuron doctrine, redux. Science 310, 791-793.

Chorev, E., Yarom, Y., and Lampl, I. (2007). Rhythmic episodes of subthreshold membrane potential oscillations in the rat inferior olive nuclei *in vivo*. J Neurosci 27, 5043-5052.

Coesmans, M., Weber, J. T., De Zeeuw, C. I., and Hansel, C. (2004). Bidirectional parallel fiber plasticity in the cerebellum under climbing fiber control. Neuron 44, 691-700.

Condorelli, D. F., Parenti, R., Spinella, F., Trovato Salinaro, A., Belluardo, N., Cardile, V., and Cicirata, F. (1998). Cloning of a new gap junction gene (Cx36) highly expressed in mammalian brain neurons. Eur J Neurosci 10, 1202-1208.

Connors, B. W., and Long, M. A. (2004). Electrical synapses in the mammalian brain. Annu Rev Neurosci 27, 393-418.

De Zeeuw, C. I., Chorev, E., Devor, A., Manor, Y., Van Der Giessen, R. S., De Jeu, M. T., Hoogenraad, C. C., Bijman, J., Ruigrok, T. J., French, P., et al. (2003). Deformation of network connectivity in the inferior olive of connexin 36-deficient mice is compensated by morphological and electrophysiological changes at the single neuron level. J Neurosci 23, 4700-4711.

De Zeeuw, C. I., Simpson, J. I., Hoogenraad, C. C., Galjart, N., Koekkoek, S. K., and Ruigrok, T. J. (1998). Microcircuitry and function of the inferior olive. Trends Neurosci 21, 391-400.

De Zeeuw, C. I., and Yeo, C. H. (2005). Time and tide in cerebellar memory formation. Curr Opin Neurobiol 15, 667-674.

Deans, M. R., Gibson, J. R., Sellitto, C., Connors, B. W., and Paul, D. L. (2001). Synchronous activity of inhibitory networks in neocortex requires electrical synapses containing Connexin36. Neuron 31, 477-485.

Degen, J., Meier, C., Van Der Giessen, R. S., Söhl, G., Petrasch-Parwez, E., Urschel, S., Dermietzel, R., Schilling, K., De Zeeuw, C. I., and Willecke, K. (2004). Expression pattern of lacZ reporter gene representing Connexin36 in transgenic mice. J Comp Neurol 473, 511-525.

Frisch, C., De Souza-Silva, M. A., Söhl, G., Guldenagel, M., Willecke, K., Huston, J. P., and Dere, E. (2005). Stimulus complexity dependent memory impairment and changes in motor performance after deletion of the neuronal gap junction protein Connexin36 in mice. Behav Brain Res 157, 177-185.

Garcia, K. S., and Mauk, M. D. (1998). Pharmacological analysis of cerebellar contributions to the timing and expression of conditioned eyelid responses. Neuropharmacology 37, 471-480.

Gruart, A., Pastor, A. M., Armengol, J. A., and Delgado-Garcia, J. M. (1997). Involvement of cerebellar cortex and nuclei in the genesis and control of unconditioned and conditioned eyelid motor responses. Prog Brain Res 114, 511-528.

Güldenagel, M., Ammermuller, J., Feigenspan, A., Teubner, B., Degen, J., Söhl, G., Willecke, K., and Weiler, R. (2001). Visual transmission deficits in mice with targeted disruption of the gap junction gene Connexin36. J Neurosci 21, 6036-6044.

Hesslow, G. (1994). Correspondence between climbing fibre input and motor output in eyeblink-related areas in cat cerebellar cortex. J Physiol 476, 229-244.

Hesslow, G., Svensson, P., and Ivarsson, M. (1999). Learned movements elicited by direct stimulation of cerebellar mossy fiber afferents. Neuron 24, 179-185.

Jirenhed, D. A., Bengtsson, F., and Hesslow, G. (2007). Acquisition, extinction, and reacquisition of a cerebellar cortical memory trace. J Neurosci 27, 2493-2502.

Kistler, W. M., De Jeu, M. T., Elgersma, Y., Van Der Giessen, R. S., Hensbroek, R., Luo, C., Koekkoek, S. K., Hoogenraad, C. C., Hamers, F. P., Güldenagel, M., et al. (2002). Analysis of Cx36 knockout does not support tenet that olivary gap junctions are required for complex spike synchronization and normal motor performance. Ann N Y Acad Sci 978, 391-404.

Koekkoek, S. K., Den Ouden, W. L., Perry, G., Highstein, S. M., and De Zeeuw, C. I. (2002). Monitoring kinetic and frequency-domain properties of eyelid responses in mice with magnetic distance measurement technique. J Neurophysiol 88, 2124-2133.

Koekkoek, S. K., Hulscher, H. C., Dortland, B. R., Hensbroek, R. A., Elgersma, Y., Ruigrok, T. J., and De Zeeuw, C. I. (2003). Cerebellar LTD and learning-dependent timing of conditioned eyelid responses. Science 301, 1736-1739.

Koekkoek, S. K., Yamaguchi, K., Milojkovic, B. A., Dortland, B. R., Ruigrok, T. J., Maex, R., De Graaf, W., Smit, A. E., VanderWerf, F., Bakker, C. E., et al. (2005). Deletion of FMR1 in Purkinje cells enhances parallel fiber LTD, enlarges spines, and attenuates cerebellar eyelid conditioning in Fragile X syndrome. Neuron 47, 339-352.

Landisman, C. E., Long, M. A., Beierlein, M., Deans, M. R., Paul, D. L., and Connors, B. W. (2002). Electrical synapses in the thalamic reticular nucleus. J Neurosci 22, 1002-1009.

Lang, E. J., Sugihara, I., and Llinás, R. (1996). GABAergic modulation of complex spike activity by the cerebellar nucleoolivary pathway in rat. J Neurophysiol 76, 255-275.

Leznik, E., and Llinás, R. (2005). Role of gap junctions in synchronized neuronal oscillations in the inferior olive. J Neurophysiol 94, 2447-2456.

Leznik, E., Makarenko, V., and Llinás, R. (2002). Electrotonically mediated oscillatory patterns in neuronal ensembles: an *in vitro* voltage-dependent dye-imaging study in the inferior olive. J Neurosci 22, 2804-2815.

Llinás, R., and Sasaki, K. (1989). The Functional Organization of the Olivo-Cerebellar System as Examined by Multiple Purkinje Cell Recordings. Eur J Neurosci 1, 587-602.

Llinás, R., and Yarom, Y. (1981). Electrophysiology of mammalian inferior olivary neurones *in vitro*. Different types of voltage-dependent ionic conductances. J Physiol 315, 549-567.

Long, M. A., Deans, M. R., Paul, D. L., and Connors, B. W. (2002). Rhythmicity without synchrony in the electrically uncoupled inferior olive. J Neurosci 22, 10898-10905.

Mann-Metzer, P., and Yarom, Y. (1999). Electrotonic coupling interacts with intrinsic properties to generate synchronized activity in cerebellar networks of inhibitory interneurons. J Neurosci 19, 3298-3306.

Mauk, M. D., Steinmetz, J. E., and Thompson, R. F. (1986). Classical conditioning using stimulation of the inferior olive as the unconditioned stimulus. Proc Natl Acad Sci U S A 83, 5349-5353.

Marshall, S.P., Van Der Giessen, R.S., De Zeeuw, C.I., and Lang E.J. (2007). Altered olivocerebellar activity patterns in the Connexin36 knockout mouse. The Cerebellum 6(2), 4209-4222.

Medina, J. F., and Mauk, M. D. (2000). Computer simulation of cerebellar information processing. Nat Neurosci 3 Suppl, 1205-1211.

Medina, J. F., Nores, W. L., and Mauk, M. D. (2002). Inhibition of climbing fibres is a signal for the extinction of conditioned eyelid responses. Nature 416, 330-333.

Perrett, S. P., Ruiz, B. P., and Mauk, M. D. (1993). Cerebellar cortex lesions disrupt learning-dependent timing of conditioned eyelid responses. J Neurosci 13, 1708-1718.

Placantonakis, D. G., Bukovsky, A. A., Aicher, S. A., Kiem, H. P., and Welsh, J. P. (2006). Continuous electrical oscillations emerge from a coupled network: a study of the inferior olive using lentiviral knockdown of Connexin36. J Neurosci 26, 5008-5016.

Placantonakis, D. G., Bukovsky, A. A., Zeng, X. H., Kiem, H. P., and Welsh, J. P. (2004). Fundamental role of inferior olive connexin 36 in muscle coherence during tremor. Proc Natl Acad Sci U S A 101, 7164-7169.

Porras-Garcia, E., Cendelin, J., Dominguez-del-Toro, E., Vozeh, F., and Delgado-Garcia, J. M. (2005). Purkinje cell loss affects differentially the execution, acquisition and prepulse inhibition of skeletal and facial motor responses in Lurcher mice. Eur J Neurosci 21, 979-988.

Schweighofer, N., Doya, K., and Kawato, M. (1999). Electrophysiological properties of inferior olive neurons: A compartmental model. J Neurophysiol 82, 804-817.

Söhl, G., Degen, J., Teubner, B., and Willecke, K. (1998). The murine gap junction gene Connexin36 is highly expressed in mouse retina and regulated during brain development. FEBS Lett 428, 27-31.

Thach, W. T., Jr. (1967). Somatosensory receptive fields of single units in cat cerebellar cortex. J Neurophysiol 30, 675-696.

Theis, M., Magin, T. M., Plum, A., and Willecke, K. (2000). General or cell type-specific deletion and replacement of connexin-coding DNA in the mouse. Methods 20, 205-218.

Van Alphen, A. M., Schepers, T., Luo, C., and De Zeeuw, C. I. (2002). Motor performance and motor learning in Lurcher mice. Ann N Y Acad Sci 978, 413-424.

Van Der Giessen, R. S., Maxeiner, S., French, P. J., Willecke, K., and De Zeeuw, C. I. (2006). Spatiotemporal distribution of Connexin45 in the olivocerebellar system. J Comp Neurol 495, 173-184.

Wang, S. S., Denk, W., and Hausser, M. (2000). Coincidence detection in single dendritic spines mediated by calcium release. Nat Neurosci 3, 1266-1273.

CHAPTER 5

General Discussion

GENERAL DISCUSSION

Accurate motor behavior is required for animals in order to function efficiently during daily life. For accurate motor behavior appropriate timing and appropriate force are demanded. The inferior olive may play an important role in regulating these two (motor) components. The inferior olive has two intriguing properties that might be important for these components. First, olivary neurons exhibit subthreshold oscillations in their membrane potential. These intrinsically generated subthreshold oscillations affect the excitability of olivary neurons in a very unique manner. Second, the inferior olive contains a lot of gap junctions resulting in a high degree of electrical coupling between olivary neurons. Due to this electrical coupling, olivary cells are or can become part of a network ensemble. These two major olivary properties and their functional role will be discussed in the following sections.

Subthreshold oscillations in the inferior olive

Subthreshold oscillations are assumed to be a general phenomenon of all olivary neurons. However, the first intracellular recordings *in vitro* of olivary neurons already showed that these oscillations are not present in every olivary cell. One study stated that 90% of the recorded cells were oscillators nevertheless it also admits that this can be biased by their methodology. Once they found oscillatory activity in a specific area, recordings were continued in that region (Benardo and Foster, 1986). Other *in vitro* studies reported spontaneous subthreshold oscillations in only 10% of the slice preparations (Lampl and Yarom, 1997; Llinás and Yarom, 1986; Yarom, 1991), strangely enough most cells in such a slice show oscillatory activity. Techniques were developed to improve the viability of slices resulting in an increased presence of subthreshold oscillations (For example incubation in cold sucrose solution; (Aghajanian and Rasmussen, 1989); incubation sequences with several solutions or ice-cold perfusion of the brain). These new methods reported enhanced occurrences of spontaneous oscillations in 50% of the slices with 80% of oscillating cells within these slices (Devor and Yarom, 2002b; Leznik and Llinás, 2005; Long et al., 2002). Bal and McCormick' preparations (1997), using a sucrose treatment, revealed silent olivary neurons that started oscillating only after gross electrical stimulation. This study describes olivary cells with a non-oscillatory resting state that possess all the necessary currents required to endogenously oscillate. Except for this report, most *in vitro* studies neglect non-oscillating neurons because they presumed that these cells are in an unhealthy or functionally less intriguing state. Furthermore, these studies do not give a clear view on the exact distribution of oscillating and non-oscillating cells and stability of oscillatory activity in olivary neurons.

The reason that olivary neurons do not oscillate in the *in vitro* condition can be due to damage of the cells, loss of input and outputs or decreased general health of slices. The advantage of obtaining an *in vivo* preparation is that all circuits are still intact and the general condition of neurons is more natural. However not all cells show oscillations in our *in vivo* studies. Only 85% of the cells do show subthreshold activity (merely 13% shows real sine-wave oscillations which are usually described in literature). Apparently, non-oscillating cells do exist even in the *in vivo* situation and are not a sign of deterioration. Of course, the question remains whether non-oscillating cells can be activated into oscillating cells by specific stimuli or that these cells cannot activate subthreshold activity at all.

Different types of oscillations

Since the demonstration of spontaneous subthreshold oscillations of the membrane potential in olivary cells, oscillations are described by a range of 3-10 Hz and an amplitude of 0.3-10 mV (Lampl and Yarom, 1997; Yarom, 1991). Some studies recognize two distinctive groups of oscillations while others even acknowledge different kinds of oscillators (Manor et al., 1997). It has also been reported that NMDA receptors can influence oscillatory activity dividing them in two oscillatory states (Placantonakis and Welsh, 2001). Thus far, oscillations are grouped together with a certain range of frequencies. However, our *in vivo* studies show different types of oscillations, but these types of oscillations are very stable and rarely switch from one type to another. So cells can either express 1-3 Hz oscillations, 4-8 Hz oscillations or both frequency ranges. *In vitro* studies showed that the frequency and amplitude of oscillations can be modified by drug application and massive stimulus (Yarom, 1991). Massive stimulation does not change the type of oscillations *in vivo*. Although, we cannot exclude that this persistent stability is artificially induced by anesthetics or a washout of signaling molecules. An early study of Benardo and Foster reported that the continuous rhythmic fluctuations in a cell occurred with great regularity and although the oscillations varied from 3-10 Hz for a given neuron the rate was quite regular (Benardo and Foster, 1986). However, a study by Devor and Yarom exhibited variations in amplitude as well as frequency of the subthreshold oscillations (Devor and Yarom, 2002b). Other studies have divided olivary neurons into different categories based on the stability of the oscillatory behavior such as: continuously, intermittently oscillating cells and a silent group (Devor and Yarom, 2000). The continuously oscillating and the silent cells are found in the *in vivo* condition, the intermittently oscillating cells are not.

The possibility of anesthetics having a stabilizing effect on the oscillations cannot be excluded, but the intact olivocerebellar circuitry might also be able to generate this stabilizing effect. *In vivo* experiments show that oscillations are more stable then previously thought, but we cannot exclude that all olivary cells may still posses all properties for every type of oscillation. Specific cellular processes may underlie the activation of certain ion channels. When a specific frequency of oscillation is required activation or deactivation of specific ion channels might be necessary to switch from one type to another. The subthreshold oscillations provide temporal windows of opportunity for action potentials. These temporal windows of opportunity depend on the frequency of oscillations. Not only oscillations can influence the timing of spikes by alternating the spiking probability also action potentials themselves (either spontaneous or evoked by somatosensory stimulation) can reset the phase of the subthreshold oscillation and thereby shifting the temporal windows opportunity. This mechanism has been observed *in vitro* (Leznik et al., 2002) as well as *in vivo* (See Chapter 3.2). In this way subthreshold oscillatory activity determines the chance of spiking whereas spikes determine the phase, thereby generating an autoregulatory system. Furthermore, it has been suggested that different type of oscillations can be included in the ensembles of olivary neurons (See Chapter 3.2). This recruitment of different frequencies might also reflect the overall frequency found in the ensemble. Different oscillatory frequency domains can implicate different functions in timing. For instance several experiments have shown that olivary cells in different areas show an increased probability of firing during certain phases of a walking cycle (Andersson and Armstrong, 1987; Lou and Bloedel, 1992). Multiple frequencies of subthreshold oscillations can be combined for specific firing patterns during movements.

Gap junctions in the inferior olive

The neuronal specific gap junction protein Connexin36 is abundantly expressed in the inferior olive (Condorelli et al., 2000), therefore it is assumed that olivary gap junctions are mainly made up by these proteins. Not only Connexin36 but also two other connexins are expressed in neurons; namely Connexin45 and Connexin30.2 (data not shown). Connexin45 is expressed in the inferior olive, but mostly during development. Mouse mutants revealed that a lack of Connexin45 did not have any effect on the gap junctions, whereas a lack of Connexin36 disrupted the gap junctions (See Chapter 2.2). Therefore Connexin36 can be considered to be the essential connexin for gap junctions, while Connexin45 may serve as a modifier of the electrical properties of the olivary gap junctions. Since deletion of Con-

nexin36 alone is enough for uncoupling olivary neurons Connexin36 knockout mice provide a suitable opportunity to investigate the role of gap junctional coupling in the inferior olive. Although it seems that electrotonic coupling has a central role in the circuitry of the inferior olive, the exact role of gap junctions is still a matter of debate. The hypothesis that electrical synapses are necessary for generating subthreshold oscillations was primarily supported by the observation that oscillations emerge in the inferior olive when gap junctions develop (Pettigrew et al., 1988). In rat inferior olive for example oscillations arise between 10-15 days postnatally and consistently with the ultrastructural appearance of olivary gap junctions (Bleasel and Pettigrew, 1992). Besides this merely indirect evidence, some models suggest that gap junctions are needed to produce continuous oscillations instead of instable episodic oscillations (Manor et al., 1997; Yarom, 1991). By using lentiviral knockdown technique for Connexin36 (Placantonakis et al., 2006) showed that continuous oscillations emerge from a population of weak and episodic single cell oscillators. Nevertheless olivary neurons lacking Connexin36 as described in chapter 3 are electrically uncoupled but still show continuous oscillations. These findings suggest that oscillations are generated by intrinsic properties of olivary neurons. This discrepancy is according to placantonakis et al. due to compensatory processes that might be responsible for this oscillatory behavior and that conclusions cannot be drawn from such a permanent Connexin36 deletion. Although some alterations might have occurred during development without Connexin36, the generation of oscillations does not seem to be an olivary network property. Though it is possible that some cells need the network to sustain their oscillatory behavior or that, they need inputs from other oscillating cells to start oscillate themselves.

Our *in vivo* study shows that there is a significant increase of more silent cells (Cluster IV) in Connexin36 mutants and neurons lacking Connexin36 during development do indeed show compensatory ionic changes on a single cell level. However, our *in vivo* study also revealed that uncoupled cells can still generate stable oscillations and non-oscillating cells can be forced to oscillate by application of Harmaline, which proves that all cells have at least the necessary properties to oscillate (unpublished data). Additionally, Leznik et al. (2005) showed that pharmacologically uncoupled cells continue to oscillate with similar frequency and amplitude proving again the intrinsic nature of the oscillations.

Synchrony

Several *in vitro* studies suggested the involvement of gap junctions for the synchronization of oscillations. Using mice that lack olivary gap junctions provided an opportunity to investi-

gate this synchronization mechanism. In our first study on complex spike synchronization we used dual-electrode approach to detect synchrony. This study showed that complex spikes were only loosely synchronized found (See Chapter 4.1). The degree of synchrony that was found did not significantly differ between knockout and wild type animals. This loose synchronization can be ascribed to chemical synaptic input or to a locking phenomena generated by reverberating loops in the olivocerebellar circuit and does not need the fast dynamics of electrotonic coupling. Nevertheless, this study was in conflict with previous studies that described synchrony at a millisecond timescale. The dual electrode method that was used may not have detected this synchrony because the synchrony parameters used in mice were based on earlier studies done in other animals (Aggelopulos et al., 1995; Keating and Thach, 1995; Wylie et al., 1995). The most obvious explanation of this discrepancy is that in mice the synchrony band is narrower then in rat. Consequently, it is much more difficult to find synchrony between Purkinje cells in mice, which explains the lower synchrony index values that we find in mice compared to rat (Lang et al., 1996; Lang et al., 1999). By having narrow synchrony bands, more alignment errors can occur. It has been shown that the Zebrin II pattern found in the cerebellar cortex is closely related to the synchrony bands (Sugihara et al., 2007). Zebrin bands are 30% smaller in mice compared to rat which confirms that synchrony bands in mice might indeed be narrower. Thus the discrepancy that was seen between the two studies might be due to such an alignment error. The alignment of electrodes is more accurate with the multielectrode recording technique than with the dual electrode technique. The multi-electrode technique is, therefore, just good enough to detect "significant" synchrony levels, whereas the dual electrode technique is not. It is noteworthy, that the synchrony levels in mice measured by multi-electrodes dropped to a level in which the observed millisecond synchrony can be explained by synchronization of olivary subthreshold oscillations. Subthreshold oscillations generate a window of firing opportunity of approximately 25 ms. Two olivary cells that spike with 1 Hz and have synchronized oscillations of 6 Hz have by chance a synchrony level of (1/25 *1/6=) 0.007. This is very close to the measured SI of 0.008 (See Chapter 4.2).

Synchronization of olivary neurons was proposed in 1974 by Rodolfo Llinás. Despite that several studies demonstrated, thus far, synchronous complex spike activity in different species (Bell and Kawasaki, 1972) and that olivary gap junctional coupling seems to underlie this phenomenon, the levels of synchrony between Purkinje cells remained rather low. Perhaps synchronized spiking that occurs at a millisecond level is to some degree a result of synchronized subthreshold activity. The fact that bidirectional coupling between olivary neurons is

not very strong and has low-pass filter properties, the coupling might be only sufficient to support synchronization of low frequency subthreshold oscillations and not of action potentials (Devor and Yarom, 2000; Devor and Yarom, 2002b). Olivary neurons that do oscillate in the same phase with a 6 Hz oscillations also synchronize their windows of firing opportunity. Since subthreshold oscillations only allow firing in their rising phase the occasion of firing can be brought down to a 25 ms windows in which a majority of spikes occur. If action potentials occur at the same point in the oscillation they can be synchronized at a millisecond level with a reasonable chance. In this way the observed millisecond synchrony is created by synchronized subthreshold oscillations. It is noteworthy that olivary neurons without gap junctional coupling tend to firing also outside this window (See Chapter 4.3), suggesting an inappropriate timing of their spikes.

Gap junctional coupling not only enables olivary cells to become synchronized it also determines the number of cells in the ensemble. Since the size of the network can have important implication for the function of the inferior olive it is substantial to determine the number of cells *in vivo*. Through internalization or specific phosphorylation mechanisms of gap junction proteins the degree of coupling can be regulated (Urschel et al., 2006) and although there have been several estimates on the size of the ensemble it is still unknown how many cells are involved in an *in vivo* ensemble. Dye coupling experiments demonstrates a network of around 9 cells (Chapter 3.1) whereas experiments based on physiological data estimated that each cell is coupled a number of cells ranging from 6 to 115 (De Zeeuw et al., 1996; Devor and Yarom, 2002a; Ruigrok et al., 1990). Most results are not consistent with each other which maybe due to the technique that is used or the kind of species. Therefore, the exact size of a coupled network *in vivo* remains to be elucidated and the functional implication of differences in ensembles can only be hypothesized. One may suggest that in case of complex movements more olivary cells are needed for adjusting perturbations, whereas less complicated movements require a smaller amount of cells within an ensemble.

Gap junctions also enable intercellular, bidirectional transport of metabolites, second messengers and other signaling molecules. In non-excitable cells gap junctions generally are thought to be biochemically important (Karpen and Crawford, 1999; Zhang et al., 2005). Therefore neuronal gap junctions may also have an important biochemical function. It is possible that second messengers travel via gap junctions from one synapse to another in a glomerulus of coupled cells and that synaptic plasticity can be spread within such a glomerulus.

FUNCTIONAL IMPLICATIONS

Olivary neurons are able to function as pacemakers by an interplay between different ionic conductances resulting in subthreshold fluctuations at two different frequencies. Sinusoidal subthreshold oscillations can form a mechanism for rhythmic firing of olivary neurons. The depolarized periods within the sine wave provide a window for firing because the membrane potential will be substantially closer to the firing threshold. Additionally, individual synaptic inputs combined with the oscillating membrane potential can generate an output at a specific time. Although each cell can fire in a "non rhythmic" pattern, a network of neurons will generate regular rhythmic firing if all oscillations are synchronized (Lampl and Yarom, 1993). Gap junctions are able to synchronize this oscillatory activity of these neurons. The inferior olive gives an important signal to the cerebellar cortex about incoming sensory information. In order to give an appropriate adjustment of the motor behavior, gap junctions in the inferior olive may be involved in both appropriate timing and recruitment of olivary cells.

If the inferior olive considered as a network of coupled cells and all gap junctions would be static every single cell would oscillate in the same phase (Figure 1A). As a result of these synchronized oscillations the multiple windows of firing will also occur at the same time. This sequence of firing windows as also been proposed as a neuronal clock with a 100 ms time scale. Subthreshold oscillations are regarded as providing time windows of opportunity of 100 ms. Spike patterns that evolve represent information about what happened and when it happened simultaneously (Kistler and De Zeeuw, 2002). By synchronizing the firing opportunities gap junctions can synchronize large ensembles of cells that results in synchronized firing of complex spikes. Stimulation of a single cell within this network resets the oscillations in this cell and through electrical coupling oscillations the entire network might reset (Figure 1B). The synchronized resetted oscillations provide a synchronized spike output with a different time pattern. In this way, the timing of spikes make sure the fine-tuning of motor commands occur at the correct time. These time patterns can represent a population coding or alternating sensory input of muscle activity (Kistler and De Zeeuw, 2002; Welsh, 2002). Other studies recognize subthreshold activity as a central gating mechanism (Devor, 2002; Velarde et al., 2004). In Connexin36 knockout mice where oscillations cannot be synchronized, synchrony levels of spiking will only occur by chance (Figure 1A and B). Furthermore when a single cell in Cx36 knockout mice is stimulated only this cell will show a reset in oscillations while other cells oscillate in random phases.

In general, gap junctional coupling is not considered to be a static but rather dynamic process. Therefore certain ensembles can be generated by recruiting cells through gap junctions. If a movement demands a small adjustment only limited groups of inferior olive cells need to be involved (Figure 1C).
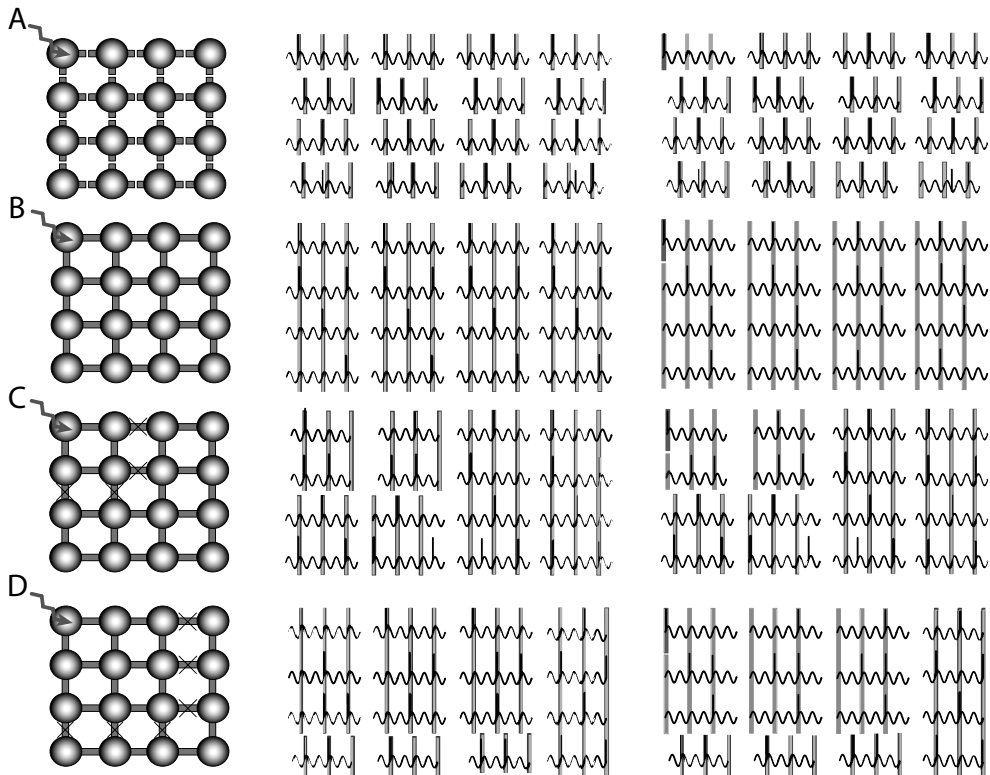
Figure 1. Schematic model of the inferior olive involving gap junction and subthreshold oscillations. A. Uncoupled olivary neurons oscillate out of phase with respect to adjacent cells. After stimulation only the stimulated cells resets its oscillation. **B.** Olivary neurons within a network of 16 cells. All cells show synchronized oscillations and after stimulation all cells respond by resetting their oscillations. **C** and **D.** Gap junctions between olivary neurons determine the size of the network. By increasing or decreasing the subset of synchronized cells, the number of neurons that are involved in adjusting the motor output can be regulated.

However when a larger adjustment has to take place an expansion in the number of cells will lead to an increased number of cells involved in the motor output (Figure 1C and D). Electrotonic coupling can be adjusted by shunting or by opening and closing of gap junctions. The opening and closing of gap junctions by phosphorylation is much slower and the uncoupling or coupling state would be relatively long term. This coupling mechanism can also be achieved by the presence of strategically positioned GABAergic terminals in the

vicinity of the gap junctions. When activated they can bypass the current flow between the olivary cells. In this way inferior olivary networks can dynamically be formed and adjusted to specific motor tasks that require certain timing and adjustments in force. Other studies assert the GABAergic input as solely inhibitory and involved in the gating of sensory input to the inferior olive (Bengtsson and Hesslow, 2006). After stimulation of the nucleo-olivary pathway it shows a delayed strong inhibition of the inferior olive (Garifoli et al., 2001; Svensson et al., 2006). A large number of studies do recognize the role of GABAergic terminals of a coupling/uncoupling mechanism (De Zeeuw et al., 1996; Lang et al., 1996; Leznik and Llinás, 2005; Yamamoto et al., 2001). By decreasing or increasing the number of cells within an ensemble the number of indirectly adjusted motoneurons is also changed and thereby the force. So in this model gap junctional coupling does not only influence the timing of muscle adjustment but also the amount of force that is used to modify certain movements. An interesting point is that after uncoupling through GABAergic terminals the biochemical exchange can still take place while after uncoupling due to phosphorylation the gap junctions are closed for both electrical current as well as passage of small molecules. This difference may be of great importance for the function of olivary gap junctional coupling. When for example uncoupling occurs through GABAergic inputs synchrony cannot occur while spreading of synaptic plasticity still can occur. Therefore it is plausible that both mechanisms can be active at the same time to let the inferior olive work optimally.

FUTURE PERSPECTIVE

Our studies show an important role for gap junctional coupling within the inferior olive, however recruitment of olivary neurons has not been shown yet *in vivo*. Future experiments of *in vivo* imaging using Calcium or voltage sensitive dyes are needed to prove recruitment of olivary cells within ensembles of cells and to confirm whether oscillations occur as distinctive clusters. Since Connexin36 knockout mice show an inappropriate timing in their eyeblink conditioning and impaired Erasmus ladder performance, these results could also be obtained in further research on humans. Lariam, an antimalarial drug, provides a great opportunity for such a study since it contains mefloquine that is known to be a gap junction blocker with specific affinity for Connexin36. Using an eyeblink paradigm in humans this phenotype could then also confirm the function of gap junctions in humans.

REFERENCES

Aggelopulos, N. C., Duke, C., and Edgley, S. A. (1995). Non-uniform conduction time in the olivocerebellar pathway in the anaesthetized cat. J Physiol 486 (Pt 3), 763-768.

Aghajanian, G. K., and Rasmussen, K. (1989). Intracellular studies in the facial nucleus illustrating a simple new method for obtaining viable motoneurons in adult rat brain slices. Synapse 3, 331-338.

Andersson, G., and Armstrong, D. M. (1987). Complex spikes in Purkinje cells in the lateral vermis (b zone) of the cat cerebellum during locomotion. J Physiol 385, 107-134.

Bal, T., and McCormick, D. A. (1997). Synchronized oscillations in the inferior olive are controlled by the hyperpolarization-activated cation current I(h). J Neurophysiol 77, 3145-3156.

Bell, C. C., and Kawasaki, T. (1972). Relations among climbing fiber responses of nearby Purkinje Cells. J Neurophysiol 35, 155-169.

Benardo, L. S., and Foster, R. E. (1986). Oscillatory behavior in inferior olive neurons: mechanism, modulation, cell aggregates. Brain Res Bull 17, 773-784.

Bengtsson, F., and Hesslow, G. (2006). Cerebellar control of the inferior olive. Cerebellum 5, 7-14.

Bleasel, A. F., and Pettigrew, A. G. (1992). Development and properties of spontaneous oscillations of the membrane potential in inferior olivary neurons in the rat. Brain Res Dev Brain Res 65, 43-50.

Condorelli, D. F., Belluardo, N., Trovato-Salinaro, A., and Mudo, G. (2000). Expression of Cx36 in mammalian neurons. Brain Res Brain Res Rev 32, 72-85.

De Zeeuw, C. I., Lang, E. J., Sugihara, I., Ruigrok, T. J., Eisenman, L. M., Mugnaini, E., and Llinás, R. (1996). Morphological correlates of bilateral synchrony in the rat cerebellar cortex. J Neurosci 16, 3412-3426.

Devor, A. (2002). The great gate: control of sensory information flow to the cerebellum. Cerebellum 1, 27-34.

Devor, A., and Yarom, Y. (2000). GABAergic modulation of olivary oscillations. Prog Brain Res 124, 213-220.

Devor, A., and Yarom, Y. (2002a). Electrotonic coupling in the inferior olivary nucleus revealed by simultaneous double patch recordings. J Neurophysiol 87, 3048-3058.

Devor, A., and Yarom, Y. (2002b). Generation and propagation of subthreshold waves in a network of inferior olivary neurons. J Neurophysiol 87, 3059-3069.

Garifoli, A., Scardilli, G., and Perciavalle, V. (2001). Effects of cerebellar dentate nucleus GABAergic cells on rat inferior olivary neurons. Neuroreport 12, 3709-3713.

Karpen, S. J., and Crawford, J. M. (1999). Cellular and molecular biology of the liver. Curr Opin Gastroenterol 15, 184-191.

Keating, J. G., and Thach, W. T. (1995). Nonclock behavior of inferior olive neurons: interspike interval of Purkinje cell complex spike discharge in the awake behaving monkey is random. J Neurophysiol 73, 1329-1340.

Kistler, W. M., and De Zeeuw, C. I. (2002). Dynamical working memory and timed responses: the role of reverberating loops in the olivo-cerebellar system. Neural Comput 14, 2597-2626.

Lampl, I., and Yarom, Y. (1993). Subthreshold oscillations of the membrane potential: a functional synchronizing and timing device. J Neurophysiol 70, 2181-2186.

Lampl, I., and Yarom, Y. (1997). Subthreshold oscillations and resonant behavior: two manifestations of the same mechanism. Neuroscience 78, 325-341.

Lang, E. J., Sugihara, I., and Llinás, R. (1996). GABAergic modulation of complex spike activity by the cerebellar nucleoolivary pathway in rat. J Neurophysiol 76, 255-275.

Lang, E. J., Sugihara, I., Welsh, J. P., and Llinás, R. (1999). Patterns of spontaneous pur-kinje cell complex spike activity in the awake rat. J Neurosci 19, 2728-2739.

Leznik, E., and Llinás, R. (2005). Role of gap junctions in synchronized neuronal oscilla-tions in the inferior olive. J Neurophysiol 94, 2447-2456.

Leznik, E., Makarenko, V., and Llinás, R. (2002). Electrotonically mediated oscillatory patterns in neuronal ensembles: an *in vitro* voltage-dependent dye-imaging study in the inferior olive. J Neurosci 22, 2804-2815.

Llinás, R., and Yarom, Y. (1986). Oscillatory properties of guinea-pig inferior olivary neu-rones and their pharmacological modulation: an *in vitro* study. J Physiol 376, 163-182.

Long, M. A., Deans, M. R., Paul, D. L., and Connors, B. W. (2002). Rhythmicity without synchrony in the electrically uncoupled inferior olive. J Neurosci 22, 10898-10905.

Lou, J. S., and Bloedel, J. R. (1992). Responses of sagittally aligned Purkinje cells during perturbed locomotion: synchronous activation of climbing fiber inputs. J Neurophysiol 68, 570-580.

Manor, Y., Rinzel, J., Segev, I., and Yarom, Y. (1997). Low-amplitude oscillations in the inferior olive: a model based on electrical coupling of neurons with heterogeneous channel densities. J Neurophysiol 77, 2736-2752.

Pettigrew, A. G., Crepel, F., and Krupa, M. (1988). Development of ionic conductances in neurons of the inferior olive in the rat: an *in vitro* study. Proc R Soc Lond B Biol Sci 234, 199-218.

Placantonakis, D., and Welsh, J. (2001). Two distinct oscillatory states determined by the NMDA receptor in rat inferior olive. J Physiol 534, 123-140.

Placantonakis, D. G., Bukovsky, A. A., Aicher, S. A., Kiem, H. P., and Welsh, J. P. (2006). Continuous electrical oscillations emerge from a coupled network: a study of the inferior olive using lentiviral knockdown of Connexin36. J Neurosci 26, 5008-5016.

Ruigrok, T. J., de Zeeuw, C. I., van der Burg, J., and Voogd, J. (1990). Intracellular labeling of neurons in the medial accessory olive of the cat: I. Physiology and light microscopy. J Comp Neurol 300, 462-477.

Sugihara, I., Marshall, S. P., and Lang, E. J. (2007). Relationship of complex spike synchrony bands and climbing fiber projection determined by reference to aldolase C compartments in crus IIa of the rat cerebellar cortex. J Comp Neurol 501, 13-29.

Svensson, P., Bengtsson, F., and Hesslow, G. (2006). Cerebellar inhibition of inferior olivary transmission in the decerebrate ferret. Exp Brain Res 168, 241-253.

Urschel, S., Hoher, T., Schubert, T., Alev, C., Söhl, G., Worsdorfer, P., Asahara, T., Dermietzel, R., Weiler, R., and Willecke, K. (2006). Protein kinase A-mediated phosphorylation of Connexin36 in mouse retina results in decreased gap junctional communication between AII amacrine cells. J Biol Chem 281, 33163-33171.

Velarde, M. G., Nekorkin, V. I., Makarov, V. A., Makarenko, V. I., and Llinás, R. R. (2004). Clustering behavior in a three-layer system mimicking olivo-cerebellar dynamics. Neural Netw 17, 191-203.

Welsh, J. P. (2002). Functional significance of climbing-fiber synchrony: a population coding and behavioral analysis. Ann N Y Acad Sci 978, 188-204.

Wylie, D. R., De Zeeuw, C. I., and Simpson, J. I. (1995). Temporal relations of the complex spike activity of Purkinje cell pairs in the vestibulocerebellum of rabbits. J Neurosci 15, 2875-2887.

Yamamoto, T., Fukuda, M., and Llinás, R. (2001). Bilaterally synchronous complex spike Purkinje cell activity in the mammalian cerebellum. Eur J Neurosci 13, 327-339.

Yarom, Y. (1991). Rhythmogenesis in a hybrid system--interconnecting an olivary neuron to an analog network of coupled oscillators. Neuroscience 44, 263-275.

Zhang, Y., Tang, W., Ahmad, S., Sipp, J. A., Chen, P., and Lin, X. (2005). Gap junction-mediated intercellular biochemical coupling in cochlear supporting cells is required for normal cochlear functions. Proc Natl Acad Sci U S A 102, 15201-15206.

SUMMARY

The olivocerebellar system regulates movement indirectly by adjusting output of the motor cortex. To coordinate movement it receives information from the motor cortex and spinal cord. The cerebellum can be divided into three functional regions with regard to the different parts of the body. The central segment of the cerebellum is involved in the execution of limb movement, whereas the lateral parts of the cerebellum are involved in planning and initiation of movement. The third part, the flocculonodular lobe, is involved in posture, balance and eye movements.

Although lesions in the cerebellum do not cause paralysis, the execution of movement is severely disturbed. Since the cerebellum provides important information to the motor output to adjust movements, cerebellar deficits result in disorders in equilibrium, posture, timing of movements and motor learning. The main symptoms of cerebellar lesions are classified as hypotonia, ataxia and intention tremor. Hypotonia is defined as a decreased tone of skeletal muscles that is caused by a disbalance in the circuitry. This state restores usually within a certain time after the lesioning. Ataxia is a condition in which the body shows a loss of ability to coordinate muscular movement. This results in unsteady movements and staggered walking. Intention tremor is an involuntary movement or shaking of a body part specifically during excution of movement or when reaching for a target.

As a part of the olivocerebellar system, the inferior olive projects to the cerebellar cortex. A lesion of the inferior olive is as effective, at least in the initial phase, as a complete cerebellectomy. Therefore the inferior olive is considered as the major input to the cerebellum. The inferior olive complex is located in the ventral part of the brainstem and olivary neurons have two distinctive properties. First, olivary cells exhibit subthreshold oscillations that can have a shape of a sine-wave which provides a timing signal and a gating mechanism. Second, olivary neurons are coupled through gap junctions that provide a direct pathway between olivary neurons that allows olivary neurons to synchronize their subthreshold activity. These two properties play a central role in the processing of the inferior olive and therefore this thesis mainly focuses on these features.

Despite the fact that Connexin36 is a major junction protein the exact expression pattern of Connexin36 in the olivocerebellar system has not been described yet, therefore we investigated in Chapter 2.1 the distribution of Connexin36 using a reporter protein that was expressed instead of Connexin36. Besides the expression in the olivocerebellar system, Connexin36 is also expressed in the retina, insulin producing b-cells of the pancreas and in the medulla of the adrenal gland. In the olivocerebellar system, expression was present in GABAergic neurons of the cerebellar nuclei. Additionally, Connexin36 was abundantly ex-

pressed in neurons of the inferior olive.

Although Connexin36 is highly expressed in neuronal gap junctions of the inferior olive, it is not clear whether these electrical synapses can develop without Connexin45. In Chapter 2.2 we describe the development and spatiotemporal distribution of Connexin45 in relation to that of Connexin36 in the olivocerebellar system. During development Connexin45 is expressed in virtually all neurons of the inferior olive and cerebellar nuclei. During (later) postnatal development and adulthood there is a considerable overlap of expression of both connexins in subpopulations of all main olivary nuclei and cerebellar nuclei as well as in the stellate cells in the cerebellar cortex. Despite the expression of Connexin45, ultrastructural analysis of neuronal gap junctions in Connexin45 knockout mice show that their formation appears normal in contrast to that in knockouts of Connexin36. The morphological data suggest that Connexin45 may play a modifying role in the widely distributed, coupled neurons of the olivocerebellar system, but that it is not essential for the creation of olivary gap junctions. To investigate the effect of uncoupling on the cellular level, we investigated olivary neurons *in vitro* in the absence of Connexin36. In contrast to wildtype, we found in Connexin36 knockouts gap junction-like structures with an abnormally wide interneuronal space while other gap junction characteristics were unaffected. Also dye coupling was absent in the Connexin36 knockouts. This points out that Connexin36 is essential for the proper functioning of the neuronal gap junctions in the inferior olive. This chapter further shows that uncoupled neurons still have the ability to oscillate, although it seems that single neurons also compensate for changes in the network connectivity by retuning their intrinsic electrical properties.

In Chapter 3.2 we describe the properties of olivary neurons *in vivo*. This report shows that inferior olivary neurons do oscillate in an intact neuronal circuitry. Furthermore, the oscillations tend to be rather stable and can be subdivided into four clusters based on the level of subthreshold activity. These *in vivo* recordings also show that action potentials only occur on the peak of an oscillation and that these action potentials can reset the oscillation towards 90 degrees. On the other hand the oscillations maintain a preferred spiking pattern. So the interactions between action potential and oscillation is bi-directional.

Chapter 4.1 describes motor performance of mice that lack gap junctions. These mice show a normal performance on the accelerating rotarod and have a regular walking pattern. Also after application of a tremorgenic drug called Harmaline, which specifically excites olivary neurons, these mice show similar amplitude and frequency of tremor. Additionally, complex spike synchronization was not detected in both knockout and wildtype mice, although a

dual electrode measurement was used. In contrast to the dual electrode measurements in chapter 4.2 the multiple electrode measurements did show synchrony of complex spikes although the bands of synchrony in mice might be more narrow compared to other species.

In Chapter 4.3 we describe the consequences on the more complex behavior such eye blink conditioning and Erasmusladder. Cx36 deficient mice show impaired learning-dependent timing in that they were not able to fix the timing of their conditioned responses at the moment when the unconditioned stimulus is about to occur. Furthermore, the timing of spike activities generated in the olive of coupling-deficient mice was abnormal in that their latencies in response to the unconditioned stimulus were inconsistent. Whole-cell patch clamp recordings of olivary neurons *in vivo* show that different spiking activities result from changed interactions with their subthreshold oscillations. These results, were combined with a computer simulation of the cerebellar systeem which suggests that electrotonic coupling among olivary neurons is necessary for proper synchronous oscillations in the inferior olive and consequently for learning-dependent timing of cerebellar motor control.

SAMENVATTING

Het olivocerebellaire systeem reguleert bewegingen van het lichaam indirect door uitgaande signalen van de motorische schors aan te passen. Om de motoriek te coördineren ontvangt het informatie van zowel de motorische schors (motorische informatie) als het ruggenmerg (sensorische informatie). De kleine hersenen (het cerebellum) kunnen worden verdeeld in drie functionele gebieden met betrekking tot de verschillende delen van het lichaam. Het centrale segment van het cerebellum is betrokken bij bewegingen van de ledematen, terwijl de laterale delen betrokken zijn bij het plannen en initiëren van bewegingen. Het laatste deel, het vestibulocerebellum, is betrokken bij lichaamshouding, evenwicht en oogbewegingen.

Hoewel beschadigingen aan het cerebellum geen verlammingen veroorzaken, raakt het uitvoeren van bewegingen ernstig verstoord. Omdat het cerebellum belangrijke informatie verstrekt resulteert cerebellaire schade in stoornissen van het evenwicht, lichaamshouding en timing van bewegingen, maar ook het leren van bewegingen. De belangrijkste symptomen veroorzaakt door cerebellaire beschadigingen worden geklassificeerd als hypotonie, ataxie en intentietremor. Hypotonie wordt gedefinieerd als een verminderde spanning van de skeletspieren en wordt veroorzaakt door een disbalans in het zenuwcircuit. Dit symptoom verdwijnt gewoonlijk enige tijd na de beschadiging. Ataxie is een conditie waarin het lichaam een verlies laat zien van de mogelijkheid om spierbewegingen te coördineren. Dit leidt tot onzekere bewegingen en een wankelend looppatroon. Een intentietremor is een onwillekeurige beweging en wordt gekenmerkt door het schudden van een lichaamsdeel met name tijdens de uitvoering van een beweging of tijdens het uitstrekken naar een doel.

Als onderdeel van het olivocerebellaire systeem, projecteert de onderste olijf (de oliva inferior) naar de schors van het cerebellum. Een beschadiging in dit hersengebied is even effectief, in ieder geval in de beginfase, als een complete verwijdering van de kleine hersenen. Daarom wordt de onderste olijf beschouwd als een van de belangrijkste toevoeren naar de kleine hersenen. Het onderste olijf complex is gelegen in het ventrale gedeelte van de hersenstam. Olijfcellen hebben twee karakteristieke eigenschappen. Ten eerste hebben de olijfcellen laagdrempelige oscillaties van 1-10 Hz die een sinusvorm kunnen aannemen en die fungeren als een kloksignaal, maar ook als poortwachterfunctie van signalen die de olijf binnenkomen. Ten tweede zijn olijfcellen gekoppeld door middel van directe verbindingen, gap junctions genaamd, die synchronisatie van deze oscillaties bewerkstelligen.

Deze twee eigenschappen hebben een centrale rol in de verwerkingsprocessen van de onderste olijf en daarom richt dit proefschrift zich met name op deze eigenschappen.

Hoewel Connexin36 een belangrijk gap junction eiwit is, werd het exacte expressie patroon van Connexin36 in het olivocerebellaire systeem nog niet eerder beschreven. Daarom beschrijft hoofdstuk 2.1 de distributie met behulp van een reporter eiwit dat tot expressie komt in plaats van Connexin36. Naast de expressie in het olivocerebellaire systeem, komt Connexin36 ook tot expressie in de retina, de insuline producerende beta-cellen in de pancreas en in het bijniermerg. In het olivocerebellaire systeem is expressie aanwezig in GABAerge neuronen van de cerebellaire kernen. Daarnaast komt Connexin36 sterk tot expressie in neuronen van de onderste olijf.

Ondanks het feit dat Connexin36 sterk aanwezig is in de neuronale gap junctions van de onderste olijf, is het niet duidelijk of deze electrische synapsen zich ook kunnen ontwikkelen zonder de aanwezigheid van Connexin45. In hoofdstuk 2.2 wordt de ontwikkeling en de distributie van Connexine45 in relatie tot die van Connexin36 in het olivocerebellaire systeem beschreven. Tijdens de ontwikkeling komt Connexin45 tot expressie in bijna alle neuronen van de onderste olijf en cerebellaire kernen. Tijdens de postnatale ontwikkeling en in het volwassenstadium is er een aanzienlijke overlap van de expressie van beide connexines in subpopulaties in zowel alle belangrijke olijfkernen, cerebellaire kernen als in de stellate cellen in de cerebellaire schors. Ondanks de expressie van Connexin45 in het olivocerebellaire systeem, laat een analyse van de ultrastructuur van gap junctions zien dat afwezigheid van Connexin45 de vorming van gap junctions niet verstoord terwijl de afwezigheid van Connexin36 dat wel doet. Deze morfologische data suggereert dat Connexin45 vermoedelijk een modificerende rol speelt in gekoppelde neuronen van het olivocerebellaire systeem, maar niet essentieel is voor de formatie van deze gap junctions.

Om het effect van ontkoppeling te bestuderen op het cellulaire niveau, werden olijfcellen *in vitro* onderzocht in afwezigheid van Connexin36. In tegenstelling tot gekoppelde cellen, werden er in de cellen zonder Connexin36 gap junction-achtige structuren gevonden met abnormaal verwijde ruimtes tussen de neuronen, terwijl alle andere gap junction karakteristieken onaangetast bleven. Daarnaast bleek het aankleuren van neuronen door middel van gap junctions via omringende cellen niet mogelijk in afwezigheid van Connexin36. Deze experimenten laat zien dat Connexin36 essentieel is voor het correct functioneren van neuronale gap junctions in de onderste olijf. Dit hoofdstuk laat verder zien dat ontkoppelde neuronen nog steeds de mogelijkheid hebben om te oscilleren.

Desalniettemin blijken afzonderlijke cellen ook te compenseren voor veranderingen in het verlies van de netwerkverbindingen met andere olijfcellen door hun intrinsieke elektrische eigenschappen aan te passen.

In hoofdstuk 3.2 worden de eigenschappen van olivaire neuronen *in vivo* beschreven. Dit onderzoek toont aan dat olijfcellen inderdaad oscilleren in een intact neuronaal circuit. Verder zijn de oscillaties aanzienlijk stabiel en kunnen onderverdeeld worden in vier clusters op basis van het niveau van hun activiteit. Deze data laten ook zien dat actiepotentialen van olijfcellen alleen plaatsvinden op de piek van een oscillatie en dat deze actiepotentialen gereset kunnen worden naar 90 graden. Aan de andere kant beïnvloeden de oscillaties omgekeerd het vuurgedrag van de olijfcellen. Dus de interactie tussen actiepotentialen en oscillaties is een tweerichtingsverkeer.
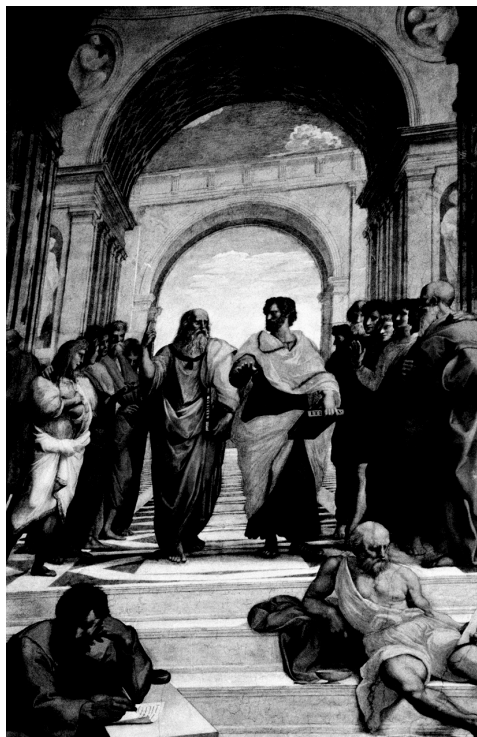
Hoofdstuk 4.1 beschrijft het motorische gedrag van muizen die geen functionele gap junctions hebben. Deze muizen vertonen een normaal motorisch gedrag en hebben een regulair looppatroon. Ook na toediening van een tremorgene stof (Harmaline), die specifiek olijcellen activeert, wordt eenzelfde tremor gezien als in muizen met normale gap junctions. Verder wordt er geen synchronisatie gevonden in zowel wildtype muizen als in muizen zonder gap junctions. Hierbij werd echter wel een duale elektrode meettechniek gebruikt.

In tegenstelling tot deze duale elektrode metingen laten de multiple elektrode metingen in hoofdstuk 4.2 wel synchroniciteit zien bij aanwezigheid van normale gap junctions en een reductie in synchroon vuurgedrag bij afwezigheid van gap junctions. In hoofdstuk 4.3 beschrijven we de consequenties van het meer complexe motorische gedrag zoals de conditionering van oogknipperbewegingen en een barricade-looptest (de Erasmusladder). Muizen zonder gap junctions laten een verstoorde timing van hun bewegingen zien doordat ze niet in staat zijn hun knipperresponsen te fixeren op het moment dat de ongeconditioneerde stimulus zou gaan moeten plaatsvinden en doordat zij het ontwijken van een barricade op de Erasmusladder niet kunnen timen. Op cellulair niveau is ook de timing van het vuurgedrag in de olijf abnormaal doordat de latentietijd van de responsen ten op zichte van de ongeconditioneerde stimulus inconsistent was. Olijfcellen *in vivo* laten zien het veranderde vuurgedrag veroorzaakt wordt door een veranderde interactie met de laagdrempelige oscillaties. Deze resultaten werden in een computersimulatie van het olivocerebellaire systeem geïncorporeerd en de uitkomst hiervan suggereert dat gap junction koppeling tussen olijfcellen verantwoordelijk is voor correcte synchrone oscillaties in de onderste olijf en daardoor dus noodzakelijk is voor een juiste timing van motoriek.

DANKWOORD

Rome, juli 2002. Terwijl de wind af en toe door de pijnbomen waait en zorgt dat de hete zomerzon door de bomen heen glinstert, schuift de rij gestaag door naar de ingang van het museum. Eenmaal binnengekomen weet ik precies waar we heen moeten en lopen we in snel tempo het gebouw door naar de juiste hal. In de hal aangekomen blijkt de mensenstroom in de richting van de Sixtijnse kapel te zijn gegaan, want de zaal is nog zo goed als leeg.

Ik maak snel foto's van het doek voordat er mensen voor gaan staan en daarna neem ik de tijd om er eens goed naar te kijken. Als je namelijk veel over iets leest krijgt het meer waarde om het in het echt te zien en nu zie ik voor het eerst het schilderij in levende lijve. '*De School van Athene*' door Rafaello Sanzio in de Stanza della Segnatura. Bijna ieder zelfrespecterend filosofieboek beschrijft dit schilderij vanwege de vele griekse filosofen die hierop te zien zijn. Bovendien heeft Rafaël elke filosoof weergegeven door een van zijn tijdgenoten zoals onder andere Leonardo da Vinci, Michelangelo, Bramante en daarnaast ook zichzelf. Op het doek heeft de kunstenaar naast een opsomming van alle griekse filosofen ook symbolisch de filosofie en zijn geschiedenis uitgebeeld. Met name door middel van de twee personen in het midden van het kunstwerk. Wie namelijk goed kijkt naar het schilderij ziet Plato en zijn leerling Aristoteles in gesprek. Hun gesprek gaat over het hier en het daar, de aarde en de hemel. Plato beweert dat wat de mens in deze wereld met zijn zintuigen ervaart, slechts 'schaduwen' zijn van een andere werkelijkheid. Deze werkelijkheid neemt het bestaan aan van een andere wereld met reële begrippen (εἶδος) die onafhankelijk is van de wereld waarin de mens leeft. De mens heeft hier geen invloed op en is afhankelijk van een hogere macht. Aristoteles wijst dit metafysische denken af en redeneert alleen via de logica, het wetenschappelijk denken. Aristoteles gelooft in een natuurlijke werkelijkheid en dat begrippen slechts bestaan in ons denken. De mens kan dus bepalen wat de werkelijkheid is en zijn eigen mogelijkheden creëren. Aristoteles wijst naar beneden, Plato naar boven.

Ook al is het alweer enkele jaren geleden dat ik dit meesterwerk van Rafaël gezien heb, moet ik hier toch weer aan denken nu ik als laatste van mijn proefschrift het dankwoord moet gaan schrijven. De discussie die hier wordt weergegeven symboliseert voor mij namelijk het leven van ieder persoon. Er zijn veel zaken die je zelf kan regelen en gelegenheden die je kan creëren. Wetenschappelijk onderzoek doen, de experimenten uitvoeren kan men zelf voorbereiden en uitvoeren. Het analyseren van data, publicaties schrijven en wetenschappelijke kennis vergaren heeft men zelf in de hand. Als je daar hard aan werkt en een beetje slim handelt heb je vaak wel resultaten. Deze 'logica' zoals Aristoteles zegt heb je zelf in de hand. Maar waar je echter geboren wordt, wie je ouders zijn, je broers of zussen en familie zijn, wie je collega's zijn dat zijn zaken waar je geen invloed op hebt. Het is zoals Plato aanwijst: het komt van boven. Het is iets waar je alleen maar dankbaar voor kan zijn.

Allereerst gaat mijn dank uit naar mijn promotor Prof.dr. Chris de Zeeuw. Beste Chris, Jouw enthousiasme en ambitie voor het onderzoek hebben altijd aanstekelijk op mij gewerkt. Ik herinner me bijvoorbeeld nog goed toen ik nog stagaire was en ik je belde terwijl ik achter de EM zat en de afwijkende gap junctions had gevonden. Je was binnen 2 microseconden boven om te kijken. Dat enthousiasme heeft mij altijd gestimuleerd om verder onderzoek te blijven doen. Ik ben blij dat ik ooit dat telefoontje gepleegd heb om te vragen of ik stage mocht lopen op jouw afdeling. Sindsdien ben ik blijven plakken en heb in de loop van de jaren veel ervaring opgedaan en heel veel geleerd wat tot deze promotie heeft geleidt. Bedankt voor de vrijheid die je me altijd hebt gegeven om te werken op mijn eigen manier en met mijn eigen ideeën.

Mijn co-promotor Dr. Marcel De Jeu. Beste Marcel, hartelijk dank voor al je begeleiding op de werkvloer in de laatste jaren van mijn promotietraject. Je heb altijd alle geduld van de wereld om iets uit te leggen en je hebt altijd wel suggesties over hoe we het beste iets konden onderzoeken (natuurlijk wel na eerst een marathon te hebben gerend:-)). Ook onze "discussies" over het olivocerebellaire systeem, allerhande wetenschappelijke feitjes en de wetenschap in het algemeen heb ik altijd als zeer prettig ervaren. Ik had me geen betere begeleider voor deze promotie kunnen wensen.

Beste Elize, natuurlijk val je onder de noemer "het histolab", maar omdat je ook mijn begeleidster was toen ik voor het eerst als laborant-guppie op de afdeling kwam, wil ik je speciaal bedanken naast al het histologische werk en EM-werk wat je hebt gedaan.

Mandy, ook jij bedankt voor al het histologie- en bestelwerk en natuurlijk alle gezellige praatjes op z'n tijd.

Erika, bedankt voor het verwerken van de talloze BDA en neurobiotine-injecties, je adviezen en tips over histologie, maar ook over welke landen de moeite waard zijn om naar toe te reizen.

Edith, je bent altijd behulpzaam, geïnteresseerd en zeker sfeerbepalend voor de afdeling geweest en nog steeds. Bedankt voor je hulp en natuurlijk alle snoepjes uit de legendarische snoeppot.

Loes, bedankt voor al je administratieve werk en uitleg over alle formulieren die ik regelmatig moest invullen.

Eddie, bedankt voor het vele scanwerk (De plaatjes zijn goed gelukt, niet waar?), al je computerondersteuning en tevens je adviezen over soft- en hardware.

Hans, bedankt voor al je technische assistentie, je grappen, je ideeën voor experimenten en je uitleg over elektronica. Dankzij jou zijn er niet alleen heel veel experimenten geslaagd, maar is ook het klussen thuis veel makkelijker geworden. Bovendien zijn je adviezen over auto's of een huis kopen altijd erg handig geweest. Bedankt!

Annette en Kenneth, bedankt voor al jullie bestelwerk!

Dear Sara, I enjoyed our talks during the patch-clamp experiments about life in general and your homeland Iran. I learned a lot about it's history, culture and language. Of course I will always remember the 'high-five'-moments when we patched a nice oscillating cell (without any 50 Hz noise!!). Thanks for our nice collaboration and for being my paranimf!

Beste Corina, ik ga dit toch maar in het Nederlands schrijven, want met een staatsexamen op zak heb ik natuurlijk weinig keuze. Bedankt voor alle gesprekken die hebben gehad, het was altijd fijn om tegenover je te zitten (misschien was ik voor jou alleen een betere alternatief??!;-)) en zo af en toe eens wat frustaties over en weer te luchten. Bedankt voor alle

sinaasappels die ik van je kreeg (voor de vitaminen!) en het boekje over Roemenië, wat nog steeds bij mij in de kast staat (en op een dag ga ik echt een keer naar Roemenië en kan ik je wel precies vertellen wat voor beroemde Roemeense personen of uitvindingen er zijn!) Bedankt dat je mijn paranimf wilt zijn en ik hoop dat jij ook snel je promotie kan afronden.

Tom, bedankt voor al je uitleg over de anatomie van de olijf. Altijd kon ik even bij je aankloppen voor wat uitleg over projecties van en naar de olijf of andere anatomische vragen. Natuurlijk ook bedankt voor het lezen van mijn manuscript.
Verder wil ik ook de andere leden van de kleine commissie bedanken voor het lezen van mijn proefschrift. Christian, Joan, bedankt dat jullie de moeite wilde nemen om mijn manuscript door te lezen.

I would like to thank my collegues at the university of Bonn (Prof.dr. Klaus Willecke, Stephan Maxeiner, Joachim Degen, Kerstin Wellerhaus) Thank you for the great collaboration and your hospitality during the many times I visited your department. I specially would like to thank you, Stephan, for the time staying at your place and the nice guiding tour with Martha and me through Bonn. I really enjoyed working with you and I appreciate our friendship.

Verder een aantal personen met wie ik een keer experimenten deed:
Pim French, bedankt voor je begeleiding tijdens mijn uitstapje in het moleculaire lab. Hoewel ik uiteindelijk toch weer van het moleculaire werk af ben gegaan is jouw uitleg over de (radioactieve) *in situ* hybridisaties onmisbaar geweest voor mijn eerste publicaties. Het is ook al weer een tijd geleden dat ik de dye-coupling experimenten deed met Jan Bijman. Beste Jan, bedankt voor al onze literaire besprekken en je lessen over de soevereiniteit van de mens naast/tijdens de experimenten die we deden. Freek Hoebeek, helaas dat de olijf-injecties met virus niet echt wilde werken, ik vond het in ieder geval wel altijd gezellig beneden in het EDC (met de radio aan op een hele foute rotterdamse zender). Martijn, Ik hoop dat we de BDA-injecties nog een keer goed kunnen afronden. Het was mij in ieder geval een waar genoegen kamergenoot van je te zijn in een klein goedkoop italiaans hoteltje. Bas, bedankt voor je uitleg over Adobe indesign (je ziet het resultaat!!) en verder je werk met de eyeblink conditionering. Alexander, bedankt voor al je ladder-experimenten en je luidruchtige, maar toch vrolijke aanwezigheid op het lab. En ook Bjorn voor alle eyeblink-proeven, de breedings van het Connexin36-project.

David, bedankt voor je interesse in mijn onderzoek en mijn studie. Ik waardeer alle gesprekken die we hebben gehad tijdens onze lange marsen en ook na die tijd. Bedankt voor je advies om altijd uit te blinken.

Beste Yair en Karen, jullie wil ik bedanken voor de lessen vanuit jullie studiehuis. Het heeft mij doen beseffen dat er meer is dan alleen het griekse denken. !תודה רבה

Naast mijn collega's en vrienden wil ik ook mijn familie en schoonfamilie bedanken. Iedereen die betrokken is geweest tijdens mijn onderzoek en ondanks de vaak lastige en specialistische begrippen toch probeerde interesse te tonen. In het bijzonder wil ik iedereen bedanken van de "familie Wit" (Ik ga niet de hele lijst noemen). We hebben het laatste jaar een aantal hoogte- en dieptepunten (van bruiloft tot begrafenis) gehad. Gelukkig hebben we altijd een hechte band met elkaar gehouden en ik kijk met veel plezier terug naar alle barbeques, verjaardagen, film- en computeravonden. Ik hoop dat er nog veel zullen komen! Jag vill också inte glömma mina släkter i Sverige: Daniël, Linda, Elin och Enar Wit. Fastän att ni bor utomlands, ni känslor alltid med oss i Holland. Tack so mycket!

Mijn broers, Nathan en Thomas, bedankt voor al jullie interesse naar mijn onderzoek, maar ook voor de gezellige jeugd die we samen hebben gehad. Als kinderen hebben we altijd met z'n drietjes lopen ravotten, maar ook nu kan ik nog steeds bij jullie terecht voor een goeie ouderwetse discussie, een knipbeurt, een rolletje in een film of als er wat anders is.

Mijn ouders, Lieve papa, bedankt dat ik altijd op je kon terugvallen als dat nodig was. Alleen al die zekerheid was/is voor mij vaak al voldoende om vol zelfvertrouwen in het leven te staan. Lieve mama, bedankt voor al je wijze levenslessen en visie op het leven/mensen. Je hebt mij vanaf mijn jeugd al gestimuleerd om dingen te ontdekken en om op onderzoek uit te gaan. Bedankt dat jullie mij niet alleen als kind willen zien, maar ook als gelijke. Ik zal jullie altijd dankbaar zijn voor de manier waarop jullie mij in het leven hebben gezet.

En natuurlijk mijn lieve Martha, jouw vrolijkheid, zorgzaamheid en onvoorwaardelijke liefde hebben er voor gezorgd dat ik alle ruimte en gelegenheid heb gehad om dit allemaal te kunnen doen. Ik ben blij dat ik met jou al zoveel van de wereld heb mogen zien en dat ik ook dit hoogtepunt met jou samen mag beleven!

CURRICULUM VITAE

First names: Ruben Simon

Family name: Van der Giessen

Date of Birth   April 7th, 1979

Place of Birth   Hendrik Ido Ambacht, the Netherlands

Education

Sept. 1991-June 1997:   HAVO at Develsteincollege, Zwijndrecht

Sept. 1997-July 2001:   Laboratory highschool, Medical biology
                                        Hogeschool of Rotterdam en Omstreken (HLO), Rotterdam
                                        Bachelor of Applied Sciences degree (*Cum laude*)

Sept. 2001-July 2002:   Propaedeuse Medicine study (*Cum Laude*)
                                        Erasmus University of Medicine, Rotterdam

Sept. 2001-Mar. 2005:   Medicine study at Erasmus University of Medicine, Rotterdam

Feb. 2002-Feb. 2005:   Master of Neuroscience degree (*Cum Laude*)
                                        Department of Neuroscience, Erasmus University, Rotterdam

Aug. 2007-Present   Clinical internships

Research training

Oct. 2000-July 2001:   Undergraduate student under supervision of Prof.C.I. De Zeeuw
                                        Department of Anatomy. Erasmus University, Rotterdam

Mar. 2005-Aug. 2007:   PhD research
                                        Promotor: Prof.dr. C.I. De Zeeuw, Co-promotor: Dr.M.T.J. De Jeu
                                        Department of Neuroscience, Erasmus University, Rotterdam

LIST OF PUBLICATIONS

R.S. van der Giessen*, S.K. Koekkoek*, S. Khosrovani*, S. van Dorp*, B. Dortland, K. Wellershaus, J. Degen, S.P. Marshall, J. Deuchars, E.C. Fuchs, H. Monyer, K. Willecke, E.J. Lang, M.T.G. De Jeu, and C.I. De Zeeuw (2007). Role of Olivary Coupling in Learning-Dependent Timing. *Submitted*

R.S. Van Der Giessen*, S. Khosrovani*, C.I. De Zeeuw and M.T.G. De Jeu (2007). Whole cell recordings of mouse inferior olivary neurons in vivo: heterogeneity in subthreshold oscillations and spiking patterns. PNAS 2007 Oct 2;104(40):15911-6

Marshall SP, **Van Der Giessen RS**, De Zeeuw CI, and Lang EJ (2007). Altered olinocerebellar patterns in the connexin36 knockout mouse. The Cerebellum 6(2):4209-4222.

van Hagen JM, van der Geest JN, **van der Giessen RS**, Lagers-van Haselen GC, Eussen HJ, Gille JJ, Govaerts LC, Wouters CH, de Coo IF, Hoogenraad CC, Koekkoek SK, Frens MA, van Camp N, van der Linden A, Jansweijer MC, Thorgeirsson SS, De Zeeuw CI (2007). Contribution of CYLN2 and GTF2IRD1 to neurological and cognitive symptoms in Williams Syndrome. Neurobiology of Disease 26(1):112-24.

Van Der Giessen RS, Maxeiner S, French PJ, Willecke K, De Zeeuw CI (2006).Spatiotemporal distribution of Connexin45 in the olivocerebellar system. Journal of Comparative Neurology 495(2):173-84.

van Looij MA, van der Burg H, **van der Giessen RS**, de Ruiter MM, van der Wees J, van Doorninck JH, De Zeeuw CI, van Zanten GA (2005). GATA3 haploinsufficiency causes a rapid deterioration of distortion product otoacoustic emissions (DPOAEs) in mice. Neurobiology of Disease 20(3):890-7.

Degen J, Meier C, **Van Der Giessen RS**, Söhl G, Petrasch-Parwez E, Urschel S, Dermietzel R, Schilling K, De Zeeuw CI, Willecke K (2004). Expression pattern of lacZ reporter gene repre-senting connexin36 in transgenic mice. Journal of Comparative Neurology 473(4):511-25.

De Zeeuw CI, Chorev E, Devor A, Manor Y, **Van Der Giessen RS**, De Jeu MT, Hoogenraad CC, Bijman J, Ruigrok TJ, French P, Jaarsma D, Kistler WM, Meier C, Petrasch-Parwez E, Dermietzel R, Söhl G, Güldenagel M, Willecke K, Yarom Y (2003). Deformation of network connectivity in the inferior olive of connexin 36-deficient mice is compensated by morpho-logical and electrophysiological changes at the single neuron level. Journal of Neuroscience 23(11):4700-11.

Kistler WM*, De Jeu MT*, Elgersma Y, **Van Der Giessen RS**, Hensbroek R, Luo C, Koekkoek SK, Hoogenraad CC, Hamers FP, Güldenagel M, Söhl G, Willecke K, De Zeeuw CI (2002) Analysis of Cx36 knockout does not support tenet that olivary gap junctions are required for complex spike synchronization and normal motor performance. Annals of New York Academy of Sci-ence 978:391-404.

*Authors contributed equally